SPECTROSCOPIC INVESTIGATIONS OF INTER- AND INTRAMOLECULAR PROCESSES IN CRYSTALLINE BENZENE

Thesis by

Donald Maxwell Burland

In Partial Fulfillment of the Requirements
For the Degree of
Doctor of Philosophy

California Institute of Technology
Pasadena, California
1970
(Submitted December 4, 1969)

for Jan

with love and squalor.

ACKNOWLEDGMENTS

I am deeply indebted to all of my fellow students here at the California Institute of Technology and at Dartmouth College where I was an undergraduate. They have provided an atmosphere within which it has been a real pleasure to work. Those colleagues who have made specific contributions to the work reported here are acknowledged at the appropriate place in the text of the thesis. I would like to reserve this section to particularly recognize and express my gratitude to five people who have contributed immeasurably to my educational development.

First and really foremost I would like to thank my parents who have in so many ways both tangible and intangible helped to provide the educational foundation on which this thesis rests.

The advice, criticism and encouragement of my research advisor, Professor G. Wilse Robinson, has been of immeasurable value. From him I have learned the importance of describing complicated physical processes in visualizable terms, a lesson that I hope always to remember in my future scientific work.

Professor J. F. Hornig, my undergraduate research advisor at Dartmouth College, first introduced me to the study of organic molecular crystals. His personal hospitality and guidance made my years at Dartmouth enjoyable and fruitful and his attitude convinced me, at a time when I needed convincing, of the correctness of my choice of chemistry as a profession.

My interest in spectroscopy and a great many other aspects of

science was first kindled by a junior high school science teacher, Mr. Kenneth Gramsted. He more than any one person was responsible for my turning down the road of science and I will always be grateful for his direction.

Finally I would like to express my gratitude to the California Institute of Technology, the Shell Companies Foundation and the National Science Foundation for financial support.

ABSTRACT

I. Introductory Remarks

A brief discussion of the overall organization of the thesis is presented along with a discussion of the relationship between this thesis and previous work on the spectroscopic properties of benzene.

II. Radiationless Transitions and Line Broadening

Radiationless rates have been calculated for the $^3B_{1u} \rightsquigarrow {}^1A_{1g}$ transitions of benzene and perdeuterobenzene as well as for the $^1B_{2u} \rightsquigarrow {}^1A_{1g}$ transition of benzene. The rates were calculated using a model that considers the radiationless transition as a tunneling process between two multi-dimensional potential surfaces and assuming both harmonic and anharmonic vibrational potentials. Whenever possible experimental parameters were used in the calculation. To this end we have obtained experimental values for the anharmonicities of the carbon-carbon and carbon-hydrogen vibrations and the size of the lowest triplet state of benzene. The use of the breakdown of the Born-Oppenheimer approximation in describing radiationless transitions is critically examined and it is concluded that Herzberg-Teller vibronic coupling is 100 times more efficient at inducing radiationless transitions.

The results of the radiationless transition rate calculation are used to calculate line broadening in several of the excited electronic states of benzene. The calculated line broadening in all

cases is in qualitative agreement with experimental line widths.

III. $^3B_{1u} \leftarrow {}^1A_{1g}$ Absorption Spectra

The $^3B_{1u} \leftarrow {}^1A_{1g}$ absorption spectra of C_6H_6 and C_6D_6 at 4.2° K have been obtained at high resolution using the phosphorescence photoexcitation method. The spectrum exhibits very clear evidence of a pseudo-Jahn-Teller distortion of the normally hexagonal benzene molecule upon excitation to the triplet state. Factor group splitting of the 0–0 and 0–0 + ν exciton bands have also been observed. The position of the mean of the 0 – 0 exciton band of C_6H_6 when compared to the phosphorescence origin of a C_6H_6 guest in a C_6D_6 host crystal indicates that the "static" intermolecular interactions between guest and host are different for C_6H_6 and C_6D_6. Further investigation of this difference using the currently accepted theory of isotopic mixed crystals indicates that there is a 2 cm^{-1} shift of the ideal mixed crystal level per host deuterium atom. This shift is observed for both the singlet and triplet states of benzene.

IV. $^3E_{1u} \leftarrow {}^1A_{1g}$, Absorption Spectra

The $^3E_{1u} \leftarrow {}^1A_{1g}$ absorption spectra of C_6H_6 and C_6D_6 at 4.2° K have been obtained using the phosphorescence photoexcitation technique. In both cases the spectrum is broad and structureless as would be expected from the line broadening calculations.

TABLE OF CONTENTS

PART I

INTRODUCTORY REMARKS

This thesis is divided into two conceptually distinct parts, one a theoretical calculation of radiationless transition rates and line broadening in benzene (Part II) and the other an experimental investigation of the two lowest energy triplet states of benzene (Parts III and IV).

The theoretical section is an extension of an earlier investigation of radiationless transitions by Robinson and Frosch.[1] These workers developed a theory of radiationless transition processes in "large" molecules which has had considerable success in qualitatively accounting for many of the experimental results; but until the work described in this thesis, no quantitative attempt to compare theoretical and experimental radiationless transition rates had been made. Benzene was chosen for this comparison because, of all the simple aromatics, it has the most completely studied vibrational structure in both ground and excited states. A detailed knowledge of this vibrational structure is essential to any quantitative calculation of radiationless transition rates using the theory developed by Robinson and Frosch. The results of this theoretical calculation are discussed in Sections IIA and IIB.

Intimately related to the radiationless transition problem is the problem of line broadening in electronic states other than the lowest state of a given multiplicity. In Section IIC we have attempted to use the results of the radiationless transition calculation to estimate vibronic line-widths in several of the excited electronic states of benzene. These estimated linewidths have also been compared with experimental results.

The experimental investigation, described in the remainder of the thesis, is a natural outgrowth of earlier work on crystalline benzene by G. C. Nieman, S. D. Colson, E. R. Bernstein and D. S. Tinti.[2] Their work along with the results discussed here make crystalline benzene one of the most, if not the most, thoroughly understood of the molecular crystals, although many unsolved problems still remain. In Section IIIA the $^3B_{1u} \leftarrow {}^1A_{1g}$ absorption spectrum of benzene is presented and in Section IIIB the results of the previous section (IIIA) are used to investigate the applicability of the theory of isotopic mixed crystals first developed by Koster and Slater[3] to benzene. Finally in Part IV the second triplet absorption spectrum ($^3E_{1u} \leftarrow {}^1A_{1g}$) is presented and discussed.

Many of the theoretical and experimental details are contained in the Appendices. These Appendices have been written in the hope that they will enable the reader to check or refine any of the results (particularly where calculations are involved) presented in this thesis. In many cases they contain information which is of interest for its own sake. In this regard the complete list of benzene phosphorescence lines in Appendix A and the $^3B_{1u}$ and $^1B_{2u}$ density of exciton states in Appendix E are of particular note.

REFERENCES

1. G. W. Robinson and R. P. Frosch, J. Chem. Phys. 37, 1962 (1962); 38, 1187 (1963).
2. G. C. Nieman, Ph. D. Thesis, California Institute of Technology, 1965; S. D. Colson, ibid., 1968; E. R. Bernstein, ibid., 1968; D. S. Tinti, ibid., 1968.
3. G. F. Koster and J. C. Slater, Phys. Rev. 95, 1167 (1954); 96, 1208 (1954).

PART II

RADIATIONLESS TRANSITIONS AND LINE BROADENING IN THE EXCITED STATES OF BENZENE AND DEUTEROBENZENE

A. CALCULATED RADIATIONLESS TRANSITION RATES FOR BENZENE AND DEUTEROBENZENE

1. Introduction

We will be concerned in this section with molecular electronic radiationless transitions, that is, those transitions by which the energy of electronic excitation is redistributed among the various electronic states of a molecule without the emission of radiation. The excess energy after redistribution goes into vibrational energy for an isolated molecule and vibrational and lattice energy for a molecule in a condensed medium. We will not be concerned with the subsequent vibrational relaxation processes except to assume that they are rapid compared to the electronic processes. If the radiationless redistribution is among states of like multiplicity, the process is called internal conversion and if among states of different multiplicity, intersystem crossing.

A theory, which has had success in at least qualitatively describing these transitions in "large" molecules, was outlined by Robinson and Frosch[1] and formulated in a somewhat different way by Hunt, McCoy, and Ross.[2] Siebrand[3] has recently used this theory to derive a relationship between triplet energy, triplet lifetime and the relative number of hydrogen atoms per molecule. The form of this relationship is in good agreement with the experimental lifetimes and energies for a large number of aromatic hydrocarbons. In addition Lin[4] and Bixon and Jortner,[5] along with Siebrand,[3] have attempted to amplify the theory by being more explicit about the coupling mechanism

that is responsible for the radiationless process. They have attributed the non-stationary character of the excited electronic states to a coupling between vibrational and electronic motion brought about by a breakdown of the Born-Oppenheimer approximation.[6]

In this section we calculate the radiationless transition rate for the transition from the lowest triplet state of benzene to the ground singlet state ($^3B_{1u} \rightsquigarrow {}^1A_{1g}$) and for the transition from the lowest singlet to the ground singlet ($^1B_{2u} \rightsquigarrow {}^1A_{1g}$). In this way we hope to show that the theory gives reasonable quantitative results for these radiationless processes.

2. Mechanism of Radiationless Relaxation

Figure 1 schematically represents the processes involved in the radiationless relaxation from an initial vibronic state Ψ_f^n. The initial state Ψ_i, for the purpose of our discussion here, is assumed to represent a molecular vibronic state with all normal mode oscillators in their zero-quantum levels. Similarly, Ψ_f represents the zero-quantum vibronic level of the final electronic state. The states labelled Ψ_f^j, where $j = 1, \ldots, n$, are final vibronic levels nearly degenerate with the initial state Ψ_i.

The final and initial states are all eigenstates of a certain incomplete Hamiltonian for the molecule plus its environment. When the neglected terms in the Hamiltonian are included, these states become non-stationary. We can denote these neglected terms in the Hamiltonian by H′ and consider the subsequent time development of a system initially prepared in a state Ψ_i. (The exact meaning of "the

Figure 1. Schematic energy level diagram for the radiationless transition process. Ψ_i is the initial state that is coupled by the matrix element β to a state Ψ_f^1 in the manifold of final states. The final states are all presumed to be coupled to each other by a matrix element α. The rate-controlling process is the transfer of energy from Ψ_i to Ψ_f^1. The distribution of the vibrational energy among lattice and molecular modes in the final state occurs rapidly.

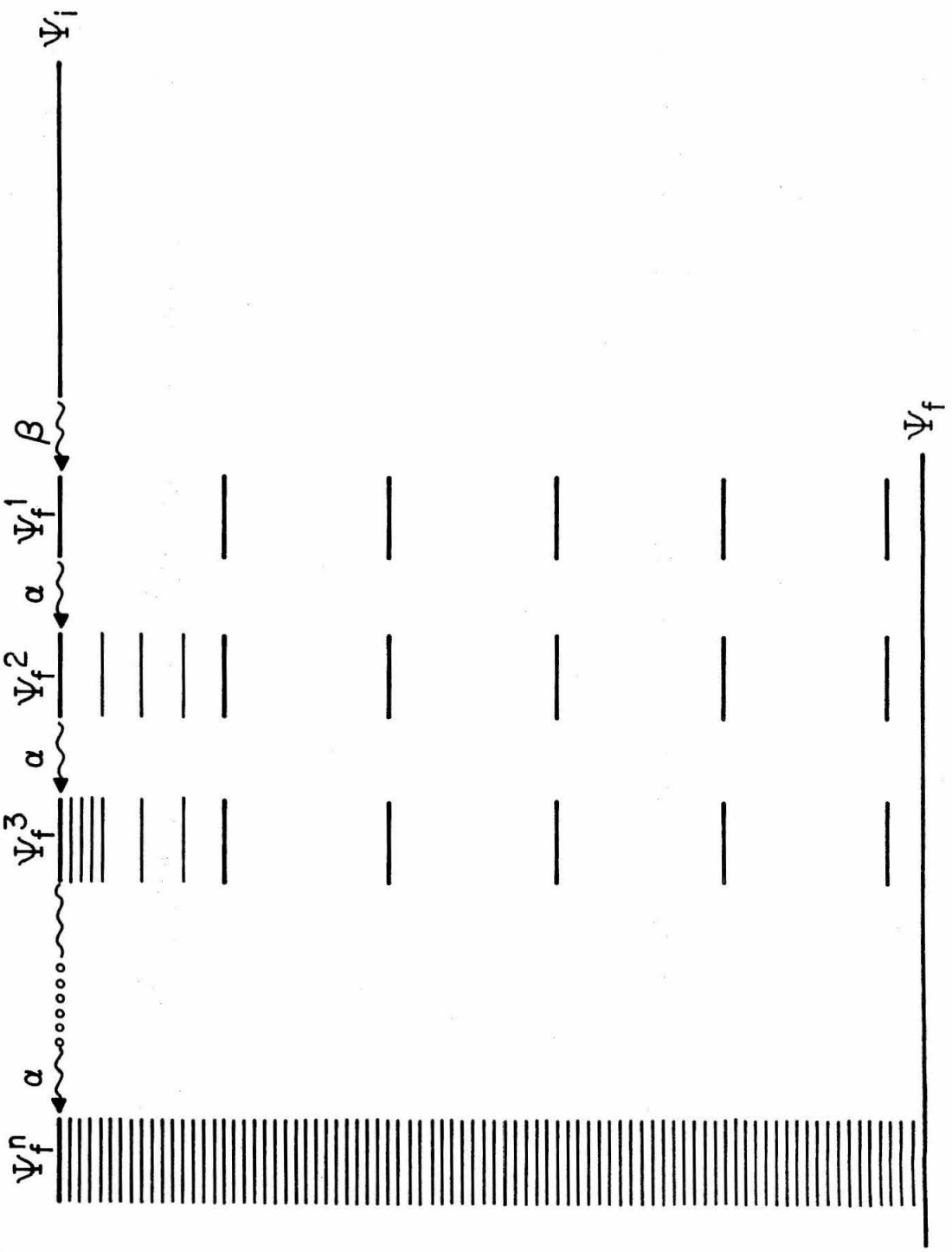
Ψ_i
β
Ψ_f^1
α
Ψ_f^2
α
Ψ_f^3
α
Ψ_f^n
Ψ_f

preparation of a system in a given state" is discussed in detail by Bixon and Jortner.[5]) A certain number, but not all, of the states in the final system Ψ_f^j are "directly coupled" to Ψ_i by the perturbing Hamiltonian H′ (i.e., coupled in first order by H′ rather than in higher order by the combined effect of H′ and purely vibrational coupling--the division of states into directly and indirectly coupled states naturally depends upon the choice of zero-order states). The relevant matrix element for this coupling is $\beta = \langle \Psi_f^j | H' | \Psi_i \rangle$. In Fig. 1 we have represented only one of these directly coupled states by Ψ_f^1. In addition, the directly doubled states are even more strongly coupled to other states in the final system of states Ψ_f^n by the vibrational mixing matrix element α. If the vibrationally unexcited states Ψ_i and Ψ_f are sufficiently separated in energy and if the molecule and environment are sufficiently complex, then the number of vibrational or lattice levels in Ψ_f nearly degenerate with Ψ_i will be large enough to make the transition from Ψ_i to Ψ_f practically speaking irreversible. The rate-determining step in the process is the initial transfer of excitation from Ψ_i to Ψ_f^1. This represents a conversion of electronic energy to vibrational energy. The subsequent vibrational relaxation is assumed to be rapid, i.e., it is assumed that $\alpha \gg \beta$.

Using simple perturbation theory and the assumption that $\Delta E \gg \alpha \gg \beta$ where ΔE is the energy separation of Ψ_i and Ψ_f, Robinson and Frosch obtained the expression

$$k = (2\pi/\alpha\hbar)\beta^2 \sum_n |\langle \phi_f^n | \phi_i^o \rangle|^2 \quad , \tag{1}$$

where the sum is over all "directly coupled states." The Born-Oppenheimer separation has been assumed for those states involved in the vibrational overlap sum so that $\Psi_i = \psi_i \phi_i^o$ and $\Psi_f^n = \psi_f \phi_f^n$, where the ψ's are purely electronic and the ϕ's purely vibrational wavefunctions. Thus the individual terms in the sum are products of Franck-Condon factors.

In the work of Robinson and Frosch, H′ is not specified in detail. It is merely defined as the difference between a zero-order Hamiltonian and the complete Hamiltonian of molecule and environment. Actually there are no restrictions on the origin of H′. It depends, as was stated in the earlier work,[1] on the particular radiationless transition under discussion, providing of course that there is a clear separation in magnitude between H′ and other parts of the Hamiltonian.

In writing ψ_i and ψ_f as purely electronic states and thereby separating vibrational and electronic wavefunctions, we have made two assumptions. First we have assumed that the electrons see a static potential due to nuclei fixed at their equilibrium positions. When this assumption is removed, we get Herzberg-Teller vibronic coupling.[7] In this case the perturbing Hamiltonian to first order in Q becomes

$$H' = \sum_i \left(\frac{\partial V}{\partial Q_i}\right)_0 Q_i \quad , \tag{2}$$

where V is the electronic-nuclear Coulomb potential, Q_i is the $i^{\underline{th}}$ normal coordinate, and the partial derivative is evaluated about the equilibrium nuclear configuration. We have also assumed that the nuclei move very slowly compared to the electrons, and thus that the

electrons 'see' the nuclear positions but not the nuclear motion, that is we ignore the nuclear kinetic energy in calculating the electronic energy. This is the Born-Oppenheimer approximation. The form of the radiationless rate expression for processes in which the Born-Oppenheimer approximation is inadequate has been discussed by Bixon and Jortner.[5] Their expression differs from (1) in certain important details, but the overall form, i.e., a product of a matrix element squared and Franck-Condon factors, remains the same.[6]

The removal of either of these restrictions can mix electronic and vibrational terms in (1) in which case the matrix element β cannot be described as purely electronic. Assuming that only one of the normal coordinates is effective in mixing the purely electronic states ψ_i and ψ_f, as is often the case for radiative transitions, we can still use Eq. (1) for the radiationless rate if we define β in the Herzberg-Teller coupling case to be,

$$\beta = \langle \psi_i \left| \left(\frac{\partial V}{\partial Q_j} \right)_o \right| \psi_f \rangle \langle \Phi_f^j | Q_j | \Phi_i^o \rangle \quad , \tag{3}$$

and if we restrict the sum in (1) to $\underline{n}$'s not involving the $j^{\underline{th}}$ normal mode. Here Φ_f^j is the vibrational wave function for the $j^{\underline{th}}$ normal mode.

We will rewrite Eq. (1) in an approximate form that makes calculation easier. First we note that the matrix element α, which is related to the vibrational relaxation time, can be eliminated since, in addition to appearing in the denominator, it also determines the number of accessible directly coupled states.[8] We then have for the

radiationless transition rate

$$k = (2\pi/\hbar)\rho\beta^2 \overline{F} \quad , \tag{4}$$

where ρ is the density of final states nearly degenerate with the initial state and $\overline{F}$ is an average Franck-Condon factor for the directly coupled states.

To calculate the radiationless transition rate from Eq. (4), we need to know β, ρ and $\overline{F}$. The matrix element β will be determined by assuming a Herzberg-Teller type of vibronic coupling along with spin-orbit coupling where necessary.[9] The density of states ρ can be calculated from a knowledge of the ground state vibrational frequencies for benzene. Since the distribution of intensities among the various members of a vibrational progression in phosphorescence or fluorescence depends on the Franck-Condon factors, an experimental measurement of the phosphorescence and fluorescence intensities enables us to determine the parameters necessary for a calculation of $\overline{F}$.

In the next section we describe the experimental measurements that were made. In Sec. 4 we use these experimental results to calculate the Franck-Condon factors for both harmonic and anharmonic oscillators. Section 5 discusses the calculation of the density of states ρ for harmonic and anharmonic oscillators. We then combine in Sec. 6 the results of Secs. 4 and 5 with an estimate of the coupling matrix element β to yield the radiationless transition rates.

3. Experimental Results

a. Intensity Measurements

The phosphorescence transition $^3B_{1u} \rightarrow {}^1A_{1g}$ in benzene is both orbitally and spin forbidden and some combination of spin-orbit and vibronic coupling is necessary to introduce allowed character into the transition. Thus the most intense vibrational progressions observed are built on e_{2g} base vibrations. The progressions built on these vibronic origins involve totally symmetric a_{1g} vibrations.[10b]

By far the most intense progression in the benzene phosphorescence involves $\nu_8(e_{2g}) + n \cdot \nu_1(a_{1g})$ where $n = 0, 1, 2, \cdots$.[11] This progression is however in Fermi resonance with the progression $\nu_6(e_{2g}) + (n+1) \cdot \nu_1$ and thus is not suitable for intensity measurements. We have chosen in this work to measure the intensity of the somewhat weaker vibrational progression $\nu_9(e_{2g}) + n \cdot \nu_1$. The vibration ν_1 is a totally symmetric carbon-carbon stretching mode and yields parameters related to the carbon-carbon bond. We also need information on the carbon-hydrogen stretching modes since they presumably play an important role in the radiationless process.[1c] The totally symmetric carbon-hydrogen mode in benzene is ν_2. The only progressions in this vibration that were observed involved the two Fermi doublet progressions (ν_8 and $\nu_6 + \nu_1$) $+ n \cdot \nu_2$ and ($\nu_8 + \nu_1$ and $\nu_6 + 2 \cdot \nu_1$) $+ n \cdot \nu_2$.

The positions of these C_6H_6 phosphorescence lines for a mixed crystal of approximately 1% C_6H_6 in C_6D_6 were measured photographically on a 2.0-m Czerny-Turner spectrograph with a 15,000 line/in. grating blazed at 1.0 μ. The measurements were made at 4.2° K

using a 200 W xenon arc lamp as an excitation source. All of the spectra were taken in the second order using Kasha liquid filters,[12] Corning glass filters and 0.1 m-atm. Cl_2 and Br_2 filters to excite preferentially the first singlet state of the C_6D_6. The C_6H_6 then acted as a low energy excitation trap from which phosphorescence was observed. The method of purifying the benzene and growing the crystals has been described elsewhere.[10] Exposure times with 50 μ slits ranged from 5 min for the high energy region of the spectra near the 0-0 to 2 h for the very weak long wavelength lines.

Because of the complexity of the spectrum in the region investigated, it was possible to make vibrational assignments only for those lines that appeared as definite members of a progression. The frequencies and assignments of the phosphorescence lines used in this work are listed in Table I. (Additional measured phosphorescence lines are reported in Appendix A.) Each progression involving the C-H vibration was assigned on the basis of its position and the fact that it belonged to a distinctive Fermi-doublet series identified as a progression of doublets separated by 3060 cm^{-1}. Since long progressions in the C-H vibration ν_2 are not observed, their assignment is in more doubt than the series involving ν_1. However the intensity and anharmonicity measurements seem to support the assignments given. (The doublet $\nu_8 + 2 \cdot \nu_2$ plus $\nu_6 + \nu_1 + 2 \cdot \nu_2$ is anomalously intense. This may be due to a misassignment but is more likely due to Fermi coupling with $3 \cdot \nu_8 + 3 \cdot \nu_1$, which is expected to be strong.[13])

The relative intensities of the phosphorescence lines were measured photoelectrically in the second and third orders of a

TABLE I. C_6H_6 phosphorescence lines used for intensity measurements (all vibrations have e_{2g} symmetry in D_{6h}).

ν_{vac} (cm^{-1})	$\Delta\nu$ (cm^{-1} from 0-0)	Assignment[d]
28,484[a]	1175	ν_9
27,494[a]	2164	$\nu_9 + \nu_1$
26,503[b]	3154	$\nu_9 + 2 \cdot \nu_1$
25,520[b]	4138	$\nu_9 + 3 \cdot \nu_1$
24,533[b]	5125	$\nu_9 + 4 \cdot \nu_1$
27,090[a]	2568	$\nu_8 + \nu_1$
27,064[a]	2594	$\nu_6 + 2 \cdot \nu_1$
24,047[b]	5611	$\nu_8 + \nu_1 + \nu_2$
24,032[b]	5626	$\nu_6 + 2 \cdot \nu_1 + \nu_2$
28,074[a]	1584	ν_8
28,055[a]	1603	$\nu_6 + \nu_1$
25,030[b]	4628	$\nu_8 + \nu_2$
25,015[b]	4643	$\nu_6 + \nu_1 + \nu_2$
22,015[b, c]	7643	$\nu_8 + 2 \cdot \nu_2$ (?)
22,004[b, c]	7654	$\nu_6 + \nu_1 + 2 \cdot \nu_2$ (?)

[a]Ref. 10b. [b]This work.

[c]These lines may be in Fermi resonance with $3 \cdot \nu_8 + 3 \cdot \nu_1$.

[d]Ref. 11.

Jarrell-Ash 1.8-m Ebert spectrometer with a 600 line/mm grating blazed at 9000 Å. An EMI 6256 phototube cooled with dry ice was used as a detector. A 150 W xenon arc lamp was used with a Bausch and Lomb ultraviolet monochromator as an excitation source. The 1% C_6H_6 in C_6D_6 crystals were purified and grown as before and the intensity measurements were made at 4.2° K.

Both the phototube and the spectrograph have a spectral response that varies appreciably over the wavelength range of interest. To obtain meaningful relative intensities, it was thus necessary to calibrate the spectrograph and phototube. The easiest way to calibrate a system such as this is to measure the spectrum of a sample whose intensity distribution is already very precisely known. Then, by comparing the known and experimental spectra a calibration curve can be drawn that represents the spectral response of the system (spectrograph plus phototube). For this purpose we used the fluorescence of a 5×10^{-3} M solution of quinine bisulfate in 1N H_2SO_4[14] and the fluorescence of a 2×10^{-4} M solution of β-naphthol in a 0.020 N acetate buffer.[15] The quinine bisulfate was used to calibrate the system in the region 3800-5000 Å and the β-naphthol in the region 3300-4500 Å. Calibrations were made in both second and third orders of the spectrograph.

Intensity measurements were made on five different crystals of approximately 1% C_6H_6 in C_6D_6. The results of these measurements are listed in Table II. The deviation quoted is the average deviation from the mean for the five different crystals. Each intensity entry in Table II represents an average of three or more intensity measure-

TABLE II. Experimental relative intensities of C_6H_6 phosphorescence lines.

Phosphorescence Line	Crystal Number 1	2	3	4	5[a]	Average	Deviation
ν_9	1.0	1.0	1.0	1.0	1.0	1.0	--
$\nu_9 + \nu_1$	0.94	1.2	1.1	1.0	1.2	1.1	0.1
$\nu_9 + 2 \cdot \nu_1$	0.37	0.57	0.47	0.47	0.56	0.49	0.06
$\nu_9 + 3 \cdot \nu_1$	0.12	0.18	0.15	0.16	--	0.15	0.02
$\nu_9 + 4 \cdot \nu_1$	--	--	0.045	0.038	--	0.042	0.004
$\nu_8 +$ $\nu_6 + \nu_1$		1.0		1.0		1.0	--
$\nu_8 + \nu_2$ $\nu_6 + \nu_1 + \nu_2$		0.042		0.036		0.039	0.003
$\nu_8 + 2 \cdot \nu_2$ $\nu_6 + \nu_1 + 2 \cdot \nu_2$		0.0096		0.0083		0.0090	0.0007
$\nu_8 + \nu_1$ $\nu_6 + 2 \cdot \nu_1$				1.0			
$\nu_8 + \nu_1 + \nu_2$ $\nu_6 + 2 \cdot \nu_1 + \nu_2$				0.020			

[a]Measured in the third order.

ments on each crystal. The slits on the spectrograph were opened to 200 μ allowing a spectral band pass much wider than the phosphorescence line width. This was inferred from the fact that the measured linewidth at half-height for all of the lines was essentially constant. The intensities of the spectral lines could thus be determined from the peak height alone, and line-shape problems were avoided in measuring intensities.[16] One of the crystals was measured in the third order of the spectrograph as a means of checking the intensity calibration of the system.

b. Anharmonicity Measurements

Three different C-C ν_1 progressions and two different C-H ν_2 progressions were used to determine the anharmonicities. If we assume that the energy of an anharmonic oscillator may be written

$$\omega_n = \omega_e(n + \tfrac{1}{2}) - x_e\omega_e(n + \tfrac{1}{2})^2 \quad , \tag{5}$$

then the difference between successive levels is

$$\Delta\omega = \omega_n - \omega_{n-1} = \omega_e - 2nx_e\omega_e \quad . \tag{6}$$

In Fig. 2 we have plotted the difference $\Delta\omega$ as a function of $\underline{n}$ for the ν_1 vibration of the $^1A_{1g}$ states of benzene in both gas and crystal phases. The gas-phase frequency measurements are from the fluorescence measurements of Garforth and Ingold.[17] The crystal measurements are from the present work. The crystal phase anharmonicities were determined from line position measurements on the ν_1 progressions $\nu_9 + n\cdot\nu_1$, $\nu_4 + n\cdot\nu_1$ and $\nu_5 + n\cdot\nu_1$. The values of ω_e

Figure 2. Anharmonicity plot for the totally symmetric carbon-carbon vibration of benzene in the $^1A_{1g}$ electronic state. The gas phase frequency values are from Ref. 17 for the progression $\nu_8 + n \cdot \nu_1$. The crystal phase values are averages of values for $\nu_9 + n \cdot \nu_1$, $\nu_4 + n \cdot \nu_1$ and $\nu_5 + n \cdot \nu_1$ determined in this work.

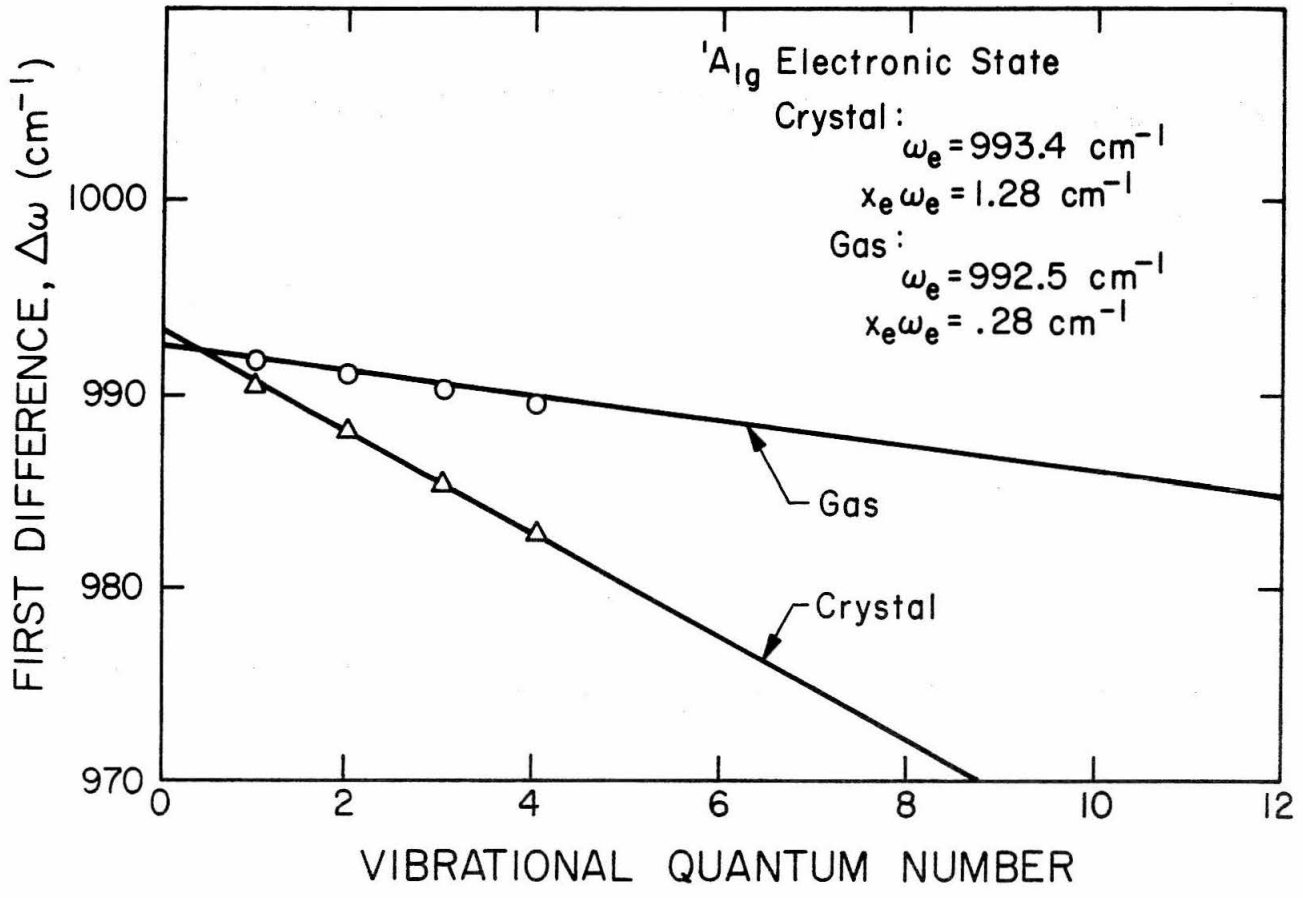
$^1A_{1g}$ Electronic State
Crystal:
$\omega_e = 993.4\ cm^{-1}$
$x_e\omega_e = 1.28\ cm^{-1}$
Gas:
$\omega_e = 992.5\ cm^{-1}$
$x_e\omega_e = .28\ cm^{-1}$
Gas
Crystal
FIRST DIFFERENCE, $\Delta\omega$ (cm^{-1})
1000
990
980
970
0
2
4
6
8
10
12
VIBRATIONAL QUANTUM NUMBER

and $x_e\omega_e$ calculated from the graph using Eq. (6) are also shown in Fig. 2. The anharmonicity of ν_1 in the crystal is considerably larger than the corresponding gas phase value.

The anharmonicity of ν_2 is more difficult to estimate. Since the longest progression observed for ν_2 only extends to n = 2, we have just two points with which to draw an anharmonicity plot. If we draw a straight line through the two available experimental points, we get values of 3063.4 cm^{-1} for ω_e and 12.6 cm^{-1} for $x_e\omega_e$.

Ellis[18] has observed a long series of CH-stretching overtones in the infrared spectrum of liquid benzene. Extracting anharmonicity constants from these data is complicated however by the severe mixing among the four CH-stretching normal modes. Martin and Kalantar[19] explained these infrared results by assuming that the observed series corresponded to $\nu_{20}(e_{1u}) + n \cdot \nu_2$. They thus obtained an anharmonicity $x_e\omega_e$ of 57.5 cm^{-1} for the ν_2 vibration. Henry and Siebrand[20] obtained even better agreement with experiment by abandoning the normal mode picture altogether and explaining the CH-stretching overtones in terms of local vibrational modes, that is vibrations of each individual CH bond. They found that the infrared spectrum could be explained by a local mode anharmonicity of 55.2 cm^{-1}. Of course these local modes can be expressed as linear combinations of normal modes and the anharmonicity of the ν_2 mode extracted. Henry and Siebrand's value for the ν_2 anharmonicity $x_e\omega_e$ is 9.2 cm^{-1}.

Symmetry requires that the CH progressions observed in the phosphorescence spectrum involve the totally symmetric ν_2 mode only. From our results we thus obtain the ν_2 anharmonicity directly and the

severe mixing that complicates the infrared analysis appears only as a shift in ω_e but does not affect $x_e\omega_e$. Our value of 12.6 cm^{-1} for the ν_2 anharmonicity is in good agreement with the local mode picture of Henry and Siebrand. It is interesting to note that, as for the ν_1 normal mode, the ν_2 anharmonicity seems to increase on going from in this case liquid to crystal.

4. Franck-Condon Factor Calculations

a. Harmonic Normal Modes

We will initially assume that the benzene normal modes may be treated as independent harmonic oscillators. The wave function for a harmonic oscillator with m quanta of excitation, an angular frequency ω and a normal coordinate Q is given by[21]

$$\Phi_m(Q) = N_m e^{-\gamma^2 Q^2/2} H_m(\gamma Q) \quad , \tag{7}$$

where the normalization constant N_m is

$$N_m = \left[\left(\frac{\omega}{\pi\hbar} \right)^{\frac{1}{2}} \left(\frac{1}{m!\, 2^m} \right) \right]^{\frac{1}{2}}$$

and

$$\gamma = \left(\frac{\omega}{\hbar} \right)^{\frac{1}{2}} \quad .$$

H_m is a Hermite polynomial of order m. The vibrational overlap integral we wish to calculate may be written

$$I = \int_{-\infty}^{\infty} \Phi^*_m(Q)\Phi_{m'}(Q')dQ \quad , \tag{8}$$

where the primed quantities refer to the excited state and the unprimed quantities to the ground state. The Franck-Condon factor $\overline{F}$ is the square of the absolute value of this expression.

We can perform the integration in Eq. (8) in a closed form if we assume that the ground and excited state normal coordinates differ only by a small additive constant; that is, if we assume that the normal coordinates appropriate for describing the ground state are also appropriate for the excited state except perhaps for a small change in equilibrium position. We then define the quantities

$$\delta = Q' - Q$$

and

$$f = \frac{\omega'}{\omega} \quad ,$$

where the prime refers in all cases to the excited state. Equation (8) can now be integrated[22] to give

$$I = \frac{1}{\gamma}\left(\frac{2\pi}{1+f}\right)^{\frac{1}{2}} \exp\left[-\frac{f\gamma^2\delta^2}{2(1+f)}\right] N_m N_{m'}$$
$$\times \sum_{\ell=0}^{m' \text{ or } m} \frac{1}{\ell!}\,\frac{m!}{(m-\ell)!}\,\frac{m'!}{(m'-\ell)!}\left[\frac{4\sqrt{f}}{1+f}\right]^{\ell}\left[\frac{f-1}{f+1}\right]^{(m-\ell)/2}$$
$$\times \left(\frac{1-f}{f+1}\right)^{(m'-\ell)/2} H_{m-\ell}\left[\frac{-f\gamma\delta}{(f^2-1)^{\frac{1}{2}}}\right] H_{m'-\ell}\left[\frac{\gamma\sqrt{f}\,\delta}{(1-f^2)^{\frac{1}{2}}}\right] . \tag{9}$$

The sum in Eq. (9) is over the smaller of $\underline{m}$ or $\underline{m'}$.

For a radiative or radiationless transition $^3B_{1u} \rightarrow {}^1A_{1g}$ or $^1B_{2u} \rightarrow {}^1A_{1g}$, Eq. (9) can be considerably simplified by noting that at low temperatures and assuming rapid vibrational relaxation most of the molecules of a benzene crystal in the $^3B_{1u}$ or $^1B_{2u}$ electronic state will be in zero-quantum vibrational levels. We can thus set $m' = 0$ in Eq. (9) and get the much simpler equation:

$$I = \left(\frac{1}{m!}\right)^{\frac{1}{2}} \left[\frac{f(f-1)^{2m}}{(f+1)^{2m+2}\, 2^{2m-2}}\right]^{\frac{1}{4}} \exp\left[\frac{-f\gamma^2\delta^2}{2(1+f)}\right] H_m\left[\frac{-f\gamma\delta}{(f^2-1)^{\frac{1}{2}}}\right] . \qquad (10)$$

Equations (9) and (10) apply only to a one-dimensional harmonic oscillator. The benzene molecule also has ten doubly-degenerate normal modes. The overlap integral for these two-dimensional vibrations has been derived by Bell and Warsop[23] for the special case where $\delta = 0$. In this case with $m' = 0$

$$I = \frac{2f^{\frac{1}{2}}}{f+1} \left\{\frac{(1-f)}{(1+f)}\right\}^{m/2} . \qquad (11)$$

We now turn to an analysis of the benzene phosphorescence spectrum in terms of these expressions for the vibrational overlap integrals. The most prominent features of the phosphorescence spectrum involve excitation of e_{2g} vibrations and long progressions of a_{1g} vibrations built on these e_{2g} base vibrations. In addition, weaker a_{1g} progressions are found built on b_{2g} base vibrations. No other long progressions are observed. From this qualitative consideration of the benzene phosphorescence spectrum, we can conclude that the major

difference between the benzene molecule in the $^1A_{1g}$ state and in the $^3B_{1u}$ state is an increase or decrease in the size of the molecule with no appreciable change in symmetry. This means that δ, for a particular vibration, is appreciably different from zero only for the a_{1g} modes. Within the accuracy of the above analysis no other distortions are present. Were a distortion present other than the one described, a progression in the vibration whose motion corresponded to the distortion would be observed. It should be noted that de Groot and van der Waals[24] and Nieman and Tinti[25] have recently advanced evidence in support of a distortion away from hexagonal symmetry for the triplet state benzene molecule in the condensed phase. This distortion, however, does not seem to affect the phosphorescence intensity distribution and it will be ignored in what follows.

The magnitude of the change in the a_{1g} normal coordinates for the ν_1 and ν_2 vibrations can be determined from the relative intensities of the members of phosphorescence vibrational progressions involving ν_1 and ν_2. Such calculations have actually been carried out by Craig[26] for the $^1B_{2u}$ state of benzene by analyzing the fluorescence intensities. In our calculation we use the square of Eq. (10), i.e., the Franck-Condon factor, to fit the experimental intensities by varying the two parameters δ and $\underline{f}$.

In Table III we compare the computed intensities for various combinations of δ and $\underline{f}$ with the experimentally observed intensities. These calculations and all subsequent ones were carried out on an IBM 7094 computer. For the ν_1 normal mode, we obtain values of

TABLE III. Computed phosphorescence intensities for the ν_1 benzene vibration.

Average Experimental Intensity	Computed intensity (f = 0.980)					Computed intensity ($\delta = 2.65 \times 10^{-9}$)				
	$\delta(g^{\frac{1}{2}}\ cm \times 10^{9}) =$ 2.55	2.60	2.65	2.70	2.72	f = 1.000	0.990	0.980	0.970	0.960
1.00	1.00	1.00	1.00	1.00	1.00	1.00	1.00	1.00	1.00	1.00
1.10	0.94	0.98	1.02	1.06	1.07	1.04	1.03	1.02	1.01	1.00
0.49	0.43	0.47	0.51	0.55	0.56	0.54	0.52	0.51	0.49	0.48
0.15	0.13	0.15	0.16	0.18	0.19	0.19	0.18	0.16	0.15	0.14
0.04	0.03	0.03	0.04	0.05	0.05	0.05	0.04	0.04	0.04	0.03

$(2.65 \pm .05) \times 10^{-9}$ amu$^{\frac{1}{2}}$ cm for δ_{ν_1} and $0.98 \pm .02$ for $\underline{f}$. Because of the limited amount of intensity data available for the ν_2 carbon-hydrogen vibration, we chose a value for $\underline{f}$ of 1.02, the correct value for ν_2 in the $^1B_{2u} \rightsquigarrow {}^1A_{1g}$ transition,[27] and then varied δ_{ν_2} to fit the experimental intensities. In this way we obtain a δ_{ν_2} value of 2.80×10^{-10} amu$^{\frac{1}{2}}$ cm.

To transform these two values for the normal coordinate changes into carbon-carbon (ΔR) and carbon-hydrogen (Δr) bond length changes, the normal coordinate analysis of Whiffen[28] as revised by Albrecht[29] is used. The results are[30]

$$\Delta R = (0.0286 \pm 0.005)\,\text{Å}$$

$$\Delta r = -(0.0136 \pm 0.01)\,\text{Å}.$$

The sign of ΔR and Δr cannot be determined from our experimental data. We have assigned a sign to these two quantities by analogy with the singlet state values of Craig.[26] In Table IV our values for ΔR and Δr are compared with previous determinations of these quantities for both the $^3B_{1u}$ and $^1B_{2u}$ states.

From our phosphorescence measurements we have thus obtained δ and $\underline{f}$ for the two totally symmetric vibrations ν_1 and ν_2. We have also noted that δ for all other normal modes is zero. The only remaining parameters to be determined are the $\underline{f}$'s for the non-totally symmetric modes. The values that depend on the triplet state vibrational frequencies are unfortunately not experimentally available. We will assume that the $\underline{f}$ values for the $^1B_{2u}$ state are also appropriate for the $^3B_{1u}$ state.[27] In Table V we have listed the frequencies

TABLE IV. Carbon-carbon and carbon-hydrogen bond length changes upon excitation for the benzene molecule.

	$^3B_{1u}$			$^1B_{2u}$
	a	b	c	d
ΔR	0.029 Å	0.036 Å	0.030 Å	0.037 Å
Δr	-0.014 Å	--	--	-0.01 Å

[a]This work; pure crystal.

[b]A. Grabowska, J. Mol. Spectry. 20, 96 (1966); O_2 perturbed gas phase.

[c]E. F. McCoy and I. G. Ross, Australian J. Chem. 15, 573 (1962); theoretical calculation.

[d]Ref. 26; gas phase.

TABLE V. Vibrational frequencies for the $^1A_{1g}$ and $^1B_{2u}$ electronic states of benzene and perdeuterobenzene.

Vibration	Class	Symmetry	Frequency				f	
			C_6H_6		C_6D_6			
			$^1A_{1g}$ [a]	$^1B_{2u}$ [b]	$^1A_{1g}$ [c]	$^1B_{2u}$ [b]	C_6H_6	C_6D_6
1	C-stretching	a_{1g}	990	923	945	879	0.932	0.930
2	H-stretching	a_{1g}	3063	3130	2303	2340	1.022	1.016
3	H-bending	a_{2g}	[1340]	1210	1059	940	0.903	0.888
4	Out-of-plane	b_{2g}	705	365	599	306	0.518	0.511
5	Out-of-plane	b_{2g}	1005	775	829	663	0.771	0.800
6	C-bending	e_{2g}	606	521	579	499	0.860	0.862
7	H-stretching	e_{2g}	3042	3080	2278	2320	1.012	1.020
8	C-stretching	e_{2g}	1584	1470	1558	1403	0.928	0.901
9	H-bending	e_{2g}	1174	1130	868	830	0.963	0.956
10	Out-of-plane	e_{1g}	863	585	659	454	0.678	0.689
11	Out-of-plane	a_{2u}	697	513	496	382	0.736	0.770
12	C-bending	b_{1u}	1011	985	970	940	0.974	0.969

TABLE V. (Continued)

Vibration	Class	Symmetry	Frequency				f	
			C_6H_6		C_6D_6			
			$^1A_{1g}$ [a]	$^1B_{2u}$ [b]	$^1A_{1g}$ [c]	$^1B_{2u}$ [b]	C_6H_6	C_6D_6
13	H-stretching	b_{1u}	[3069]	3130	2285	2340	1.020	1.024
14	C-stretching	b_{2u}	1313	1510	1282	1440	1.150	1.123
15	H-bending	b_{2u}	1147	1010	824	750	0.881	0.910
16	Out-of-plane	e_{2u}	405	243	345	208	0.600	0.603
17	Out-of-plane	e_{2u}	978	706	787	590	0.722	0.750
18	H-bending	e_{1u}	1035	940	814	740	0.908	0.909
19	C-deformation	e_{1u}	[1478]	1470	1333	1320	0.995	0.990
20	H-stretching	e_{1u}	[3063]	3130	2288	2300	1.022	1.010

[a]Ref. 10b; values in brackets are from R. D. Mair and D. F. Hornig, J. Chem. Phys. 17, 1237 (1949).

[b]F. M. Garforth, C. K. Ingold, and H. G. Poole, J. Chem. Soc. 1948, 491

[c]S. Brodersen and A. Langseth, Kgl. Danske Videnskab. Selskab Mat.-Fys. Skrifter 1, No. 7, 1 (1959).

of the vibrations in both the $^1A_{1g}$ and $^1B_{2u}$ states for both benzene and deuterobenzene. In addition values for $\underline{f}$ are listed. We have also divided the vibrations in Table V into six classes according to the physical nature of the normal modes.

Average values of $\underline{f}$, ν and δ for each vibrational class are included in Table VI. We have listed the two totally symmetric a_{1g} modes separately. Using these parameters and Eqs. (10) and (11), we have calculated Franck-Condon factors for all eight classes and for both degenerate and non-degenerate normal modes of benzene and deuterobenzene. A similar set of calculations for the $^1B_{2u}$ state was also done. We have listed the results of a few of the calculations for the triplet state in Table VII. A more complete list of these Franck-Condon factors is given in Appendix B.

b. Anharmonic Normal Modes

The anharmonicity is restricted to either cubic or quartic terms in the potential energy. We retain the assumption that the normal modes behave as independent oscillators. For the cubic case the vibrational part of the Hamiltonian is

$$\mathcal{H} = \mathcal{H}_0 + aQ^3 \quad , \tag{12}$$

where $\mathcal{H}_0$ is the zeroth order harmonic oscillator Hamiltonian. A straightforward application of perturbation theory[31] gives us for the energy

TABLE VI. Summary of parameters used in Franck-Condon factor calculation.

Vibrational Class	No. of Vibrations in Class	$\nu(cm^{-1})$		f		$\delta(g^{\frac{1}{2}}\ cm)$	
		C_6H_6	C_6D_6	C_6H_6	C_6D_6	$^1B_{2u}$	$^3B_{1u}$
C-stretching	3	1494	1466	1.002	0.975	0	0
H-stretching	5	3056	2285	1.018	1.017	0	0
H-bending	6	1151	875	0.921	0.921	0	0
Out-of-plane	9	766	612	0.669	0.685	0	0
C-bending	3	741	709	0.898	0.898	0	0
C-deformation	2	1478	1333	0.995	0.990	0	0
C-totally symmetric	1	990	945	0.932	0.930	3.06×10^{-9}	2.65×10^{-9}
H-totally symmetric	1	3063	2303	1.022	1.016	3.45×10^{-10}	2.80×10^{-10}

TABLE VII. Calculated Franck-Condon factors for benzene triplet state.

Ground State Vibrational Quantum Number n	Franck-Condon Factor					
	Non-Degenerate			Degenerate		
	Out-of-plane	C-Ts[a]	H-Ts	Out-of-plane	C-St[b]	H-St
0	9.80×10^{-1}	3.61×10^{-1}	9.65×10^{-1}	7.63×10^{-1}	1.00	1.00
1	0.00	3.64×10^{-1}	3.49×10^{-2}	1.91×10^{-1}	9.99×10^{-4}	8.91×10^{-3}
2	1.93×10^{-2}	1.80×10^{-1}	3.85×10^{-4}	3.78×10^{-2}	9.98×10^{-7}	7.96×10^{-5}
3	0.00	5.82×10^{-2}	8.88×10^{-7}	7.48×10^{-3}	9.97×10^{-10}	7.09×10^{-7}
4	5.69×10^{-4}	1.38×10^{-2}	2.04×10^{-9}	1.49×10^{-3}	9.96×10^{-13}	6.33×10^{-9}
5	0.00	2.57×10^{-3}	1.11×10^{-10}	2.95×10^{-4}	9.95×10^{-16}	5.64×10^{-11}
6	1.87×10^{-5}	3.88×10^{-4}	2.41×10^{-13}	5.84×10^{-5}	9.94×10^{-19}	5.03×10^{-13}
7	0.00	4.91×10^{-5}	1.77×10^{-15}	1.16×10^{-5}	9.93×10^{-22}	4.49×10^{-15}
8	6.41×10^{-7}	5.31×10^{-6}	4.19×10^{-17}	2.30×10^{-6}	9.92×10^{-25}	4.01×10^{-17}
9	0.00	4.97×10^{-7}	9.06×10^{-21}	4.56×10^{-7}	9.91×10^{-28}	3.57×10^{-19}
10	2.27×10^{-8}	4.08×10^{-8}	1.85×10^{-21}	9.04×10^{-8}	9.90×10^{-31}	3.19×10^{-21}
11	0.00	2.96×10^{-9}	1.02×10^{-23}	1.79×10^{-8}	9.89×10^{-34}	2.84×10^{-23}

TABLE VII. (Continued)

Ground State Vibrational Quantum Number n	Franck-Condon Factor					
	Non-Degenerate			Degenerate		
	Out-of-plane	C-Ts[a]	H-Ts	Out-of-plane	C-St[b]	H-St
12	8.19×10^{-10}	1.91×10^{-10}	2.31×10^{-26}	3.56×10^{-9}	9.88×10^{-37}	2.54×10^{-25}
13	0.00	1.11×10^{-11}	1.04×10^{-27}	7.05×10^{-10}	9.87×10^{-40}	2.26×10^{-27}
14	2.99×10^{-11}	5.76×10^{-13}	2.31×10^{-31}	1.40×10^{-10}	9.86×10^{-43}	2.02×10^{-29}
15	0.00	2.71×10^{-14}	5.02×10^{-32}	2.77×10^{-11}	9.85×10^{-46}	1.80×10^{-31}

[a] Ts = carbon or hydrogen totally symmetric stretching mode.

[b] St = carbon or hydrogen stretching mode.

$$E_m = \hbar\omega(m + \tfrac{1}{2}) - \frac{a^2}{8}\left(\frac{\hbar}{\omega}\right)^3 \left(\frac{30m^2 + 30m + 11}{\hbar\omega}\right) \tag{13}$$

and for the wave function

$$\Phi'_m = \Phi_m + \frac{a}{3\hbar\omega_0 8^{\frac{1}{2}}}\left(\frac{\hbar}{\omega}\right)^{3/2}\Big[\sqrt{(m-2)(m-1)m}\ \Phi_{m-3}$$

$$- \sqrt{(m+1)(m+2)(m+3)}\ \Phi_{m+3} + 9\sqrt{m^3}\ \Phi_{m-1}$$

$$- 9\sqrt{(m+1)^3}\ \Phi_{m+1}\Big] \quad , \tag{14}$$

where Φ_m is the harmonic oscillator wave function of order $\underline{m}$ given by Eq. (7).

Alternatively, we may assume that the anharmonicity is due entirely to quartic terms. The Hamiltonian is then

$$\mathcal{H} = \mathcal{H}_0 + bQ^4 \quad , \tag{15}$$

and the energy is

$$E_m = \hbar\omega(m + \tfrac{1}{2}) + \frac{3b\hbar^2}{4\omega^2}\ [2m^2 + 2m + 1] \quad . \tag{16}$$

The wave function for the quartic oscillator is

$$\Phi'_m = \Phi_m + \frac{b\hbar}{4\omega^3}[(2m+1)\ \sqrt{(m-1)m}\ \Phi_{m-2}$$

$$- (2m+1)\ \sqrt{(m+1)(m+2)}\ \Phi_{m+2}] \quad . \tag{17}$$

Since we have assumed that all transitions come from the zero-point vibrational level of the $^3B_{1u}$ electronic state, the effect of

anharmonicity on the excited state wave functions will not be as important as its effect on the more highly excited ground state vibrational functions. We thus have assumed in our calculation of the anharmonic Franck-Condon factors that the upper state is harmonic. The values of a and b, the anharmonicity parameters, for the ground state can be determined from the values of $x_e\omega_e$ discussed in Sec. 3b. We then use Eq. (14) or (17) for the ground state wave function and Eq. (7) for the excited state and evaluate the integral (8). Table VIII contains the results of this calculation of cubic and quartic anharmonic Franck-Condon factors for the benzene totally symmetric carbon-hydrogen vibration. From the table we see that for n = 10, that is for a purely carbon-hydrogen vibrational excitation energy nearly degenerate with the $^3B_{1u}$ state, cubic and quartic anharmonicities may increase the Franck-Condon factor by as much as a factor of 50. Similar calculations were carried out for the carbon-carbon totally symmetric vibrations. Although these vibrations are more harmonic, the quantum number n is much larger (n = 25) and the anharmonicity increases the Franck-Condon factor by a factor of about 100. However, these carbon-carbon vibrations, even including anharmonicity, contribute only negligibly to the average Franck-Condon factor in Eq. (4).

5. Density-of-States Calculation

The density of states ρ can be calculated from a knowledge of the vibrational frequencies and the form of the energy expression. In our calculations we have used an extremely rapid program kindly provided to us by Professor E. W. Schlag[32] for calculating ρ. This

TABLE VIII. Anharmonic Franck-Condon factors for benzene triplet state (carbon-hydrogen vibrations).

n	Franck-Condon Factor		
	Harmonic	Quartic	Cubic
0	9.65×10^{-1}	9.65×10^{-1}	9.65×10^{-1}
1	3.49×10^{-2}	3.49×10^{-2}	3.42×10^{-2}
2	3.84×10^{-4}	3.56×10^{-4}	3.47×10^{-4}
3	8.88×10^{-7}	3.58×10^{-7}	6.01×10^{-8}
4	2.05×10^{-9}	1.23×10^{-8}	6.32×10^{-8}
5	1.11×10^{-10}	2.40×10^{-10}	1.72×10^{-9}
6	2.41×10^{-13}	2.11×10^{-14}	5.57×10^{-12}
7	1.77×10^{-15}	2.31×10^{-14}	3.89×10^{-14}
8	4.19×10^{-17}	1.73×10^{-16}	2.04×10^{-15}
9	9.06×10^{-21}	4.01×10^{-19}	4.29×10^{-18}
10	1.85×10^{-21}	3.29×10^{-20}	8.16×10^{-20}
11	1.02×10^{-23}	3.19×10^{-23}	1.84×10^{-21}
12	2.31×10^{-26}	2.18×10^{-24}	1.03×10^{-25}
13	1.04×10^{-27}	2.18×10^{-26}	1.54×10^{-25}
14	2.31×10^{-31}	3.48×10^{-29}	8.11×10^{-28}
15	5.02×10^{-32}	3.18×10^{-30}	3.77×10^{-30}

program divides the 30 normal modes of benzene into five groups of six-fold degenerate vibrations whose frequencies are the geometric mean of the true vibrational frequencies of the normal modes included in each group. The density of states is then calculated using these five frequencies, their degeneracy and the anharmonic or harmonic energy expressions. In Appendix C the density of states calculations are discussed in more detail.

We have calculated values of ρ for both harmonic and anharmonic oscillators. The carbon-hydrogen modes were assumed to have an anharmonicity $x_e\omega_e$ of 12.6 cm^{-1}. For all of the other modes we assumed an anharmonicity of 1.28 cm^{-1}. The anharmonicity had very little effect on the density of states. For example, the harmonic density of states for the $^1A_{1g}$ electronic state of benzene with 30,000 cm^{-1} of vibrational energy is, according to our calculations, 5.23×10^{12} states/cm^{-1}. By comparison, the anharmonic density of states using the parameters mentioned above is 5.32×10^{12} states/cm^{-1}. We have concluded that, <u>while anharmonicities may be important in calculating the Franck-Condon factors, they may be ignored in the calculation of the density of states</u>.

If there are selection rules governing the radiationless transition rate, only a fraction of the total number of states will have the proper symmetry to contribute to this rate. There are 12 irreducible representations of the D_{6h} symmetry group for the benzene molecule. Eight of these representations are one-dimensional; the other four are two-dimensional. If we divide the irreducible representations of benzene into 16 one-dimensional representations, then at sufficiently

high state density each of these one-dimensional representations should have the same density of states. Thus if a selection rule demands that only states that belong to a particular one-dimensional irreducible representation of the group contribute to a transition rate, then the total density must be divided by 16. If a two-dimensional representation is involved, we must divide by 8 since each two-dimensional representation includes two one-dimensional representations. We have verified this result by a direct computer calculation using benzene's exact vibrational frequencies and find that it holds quite well for vibrational energies greater than 5000 cm^{-1}. This result can be extended to other molecules provided that the distribution of molecular vibrations among the symmetry representations of the molecular point group is uniform enough so that all irreducible representations can be generated from direct products of the representations of the fundamental vibrations and provided that the vibrational frequencies are sufficiently spread in energy so that the density-of-states function approaches a continuous function.

6. Benzene Radiationless Transition Rates

a. $^3B_{1u} \rightsquigarrow {}^1A_{1g}$--Benzene

We assume that H′ involves a spin-orbit coupling of the triplet and singlet manifolds with a subsequent Herzberg-Teller vibronic coupling in the singlet manifold. The treatment follows that of Albrecht.[33] The Hamiltonians involved in this coupling scheme are

$$\left.\begin{aligned} H(1) &= H^0_{so} && \text{pure spin orbit} \\ H(2) &= \sum_a (\partial H_0/\partial Q_a)_0 \, Q_a && \text{vibronic} \end{aligned}\right\} \quad , \tag{18}$$

where H_0 is the zero-order Hamiltonian and H^0_{so} is a spin-orbit Hamiltonian. The derivatives are evaluated at the equilibrium nuclear configuration and the sums are over all the normal modes a.

The interaction energy for the coupling scheme outlined above may be written

$$\beta = \left\{ \frac{\langle {}^1A_{1g} | H(2) | {}^1B_{2u} \rangle \langle {}^1B_{2u} | H(1) | {}^3B_{1u} \rangle}{E^0_{{}^3B_{1u}} - E^0_{{}^1B_{2u}}} \right\} \quad , \tag{19}$$

The matrix element $\langle {}^1B_{2u} | H(1) | {}^3B_{1u} \rangle$ has been calculated by Hameka and Oosterhoff[35] to be 0.33 cm^{-1}, and we will choose a value of 4000 cm^{-1} for the quantity $\langle {}^1A_{1g} | H(2) | {}^1B_{2u} \rangle$. This last value is midway between the highest and lowest values for matrix elements of the type $\langle X | H(2) | Y \rangle$ estimated by Albrecht.[33] We take the energy denominator to be 8000 cm^{-1}. Using these values we get

$$\beta = 0.16 \text{ cm}^{-1} \quad .$$

We then have, from Eq. (4), the expression

$$k = 3.10 \times 10^{10} \rho \overline{F} \text{ sec}^{-1} \quad , \tag{20}$$

for the rate of intersystem crossing ${}^3B_{1u} \rightsquigarrow {}^1A_{1g}$.

The ${}^1A_{1g}$ and ${}^3B_{1u}$ states are separated by 29,658 cm^{-1}.[10b] The density of vibronic levels in the ${}^1A_{1g}$ state at this distance from

the zero-point vibrational level of the $^1A_{1g}$ state is, from the calculation in Sec. 5, 4.40×10^{12}. In the coupling mechanism we have assumed that vibronic coupling occurs by way of a b_{2u} vibrational mode. Thus only states of this symmetry are effective in the direct coupling process. Since our selection rule for the radiationless process demands that only states belonging to a particular one-dimensional irreducible representation of the D_{6h} symmetry group be counted in the density of states, we must divide the above value of ρ by 16, which gives 2.75×10^{11}.

The calculation of an average Franck-Condon factor $\overline{F}$ for these 2.75×10^{11} states is a bit more difficult. Ideally one would calculate the Franck-Condon factor for each of these states individually and then average their sum. This is impractical however and we have instead selected a smaller number of representative states and averaged over this reduced set. We divide the benzene vibrations into six classes as discussed earlier and calculate the Franck-Condon factors for vibrational levels of the $^1A_{1g}$ state nearly degenerate with the zeroth level of the $^3B_{1u}$ state consisting exclusively of one class of vibrations. For example, we calculate the Franck-Condon factor for 20 quanta of carbon-stretching mode with a frequency of 1494 cm^{-1}. There are three such carbon-stretching modes for benzene. We can thus calculate the number of states of this type by considering the number of levels in a three-fold degenerate oscillator excited with 20 quanta of vibrational energy using the expression

$$N = \binom{n + g - 1}{n} \quad , \tag{21}$$

where N is the number of levels, g the degeneracy and n the number of quanta excited.

We do the same calculation for each of the other five classes of vibrations and then obtain an average value for the Franck-Condon factor from the expression

$$\overline{F} = \sum_{i=1}^{6} N_i F_i \Big/ \sum_{i=1}^{6} N_i \qquad (22)$$

where N_i is the value of N for the $i^{\underline{th}}$ vibrational class and F_i is the Franck-Condon factor for that class. Mixed vibrational levels, that is levels in which more than one normal mode is excited, have not been treated in our averaging process. We have calculated F for several of these mixed levels and find that they are all within the range of values of the F_i used in Eq. (22). On this basis we conclude that the neglect of mixed modes in calculating $\overline{F}$ does not lead to significant errors.

Only two of the classes contribute significantly to $\overline{F}$ in the approximation that all normal modes are harmonic, the out-of-plane and hydrogen-stretching modes, with the latter making the dominant contribution. The value of $\overline{F}$ obtained in this way is 1.06×10^{-26}. Combining the harmonic value of $\overline{F}$ with ρ using Eq. (20) we have,

$$k = 9.04 \times 10^{-5} \text{ sec}^{-1} \quad .$$

The experimental value of k for the $^3B_{1u} \rightsquigarrow {}^1A_{1g}$ radiationless transition has been estimated to be 0.024 sec^{-1}.[1a] This estimate is based on the assumption that the phosphorescence lifetime of the perdeuterated

molecule is equal to the true radiative lifetime for the perprotonated molecule.

The difference between experiment and theory here is considerable, a factor of 200. But this difference is enlightening when we consider the approximations we have made in our calculation. It is, of course, possible that our estimate of β is inaccurate especially if Herzberg-Teller coupling is not the cause of the radiationless transition. A more reasonable explanation for this discrepancy, however, seems to us to be that it is due to anharmonicities. Since we do not know the exact form of the anharmonicity we can only roughly predict the magnitude of its effect. If we assume that anharmonicity increases the Franck-Condon factor by a factor of 50 (see Table VIII for n = 10), then $\underline{k}$ for the radiationless transition $^3B_{1u} \rightsquigarrow {}^1A_{1g}$ has a value of $0.005\ sec^{-1}$. Siebrand has also found it necessary in his analysis of the radiationless process to introduce anharmonicities into his calculation in order to obtain agreement between theory and experiment.[3b]

If anharmonicities are important in explaining the radiationless transition rate as the above analysis indicates, at least a partial contribution to the experimentally observed environmental effect on the radiationless transition rate[36] may also have been found. As we have seen, the anharmonicity of both the carbon-carbon and carbon-hydrogen totally symmetric modes increases upon going from gas or liquid to crystal. The environment thus acts on the molecule to change the anharmonicity of the carbon-hydrogen modes and indirectly the relaxation rates, since these rates are dependent on anharmonicity.

Hirota and Hutchison[36] have found, from an analysis of the exponential decay of the magnetic resonance signal, that deuteration of the host increases the triplet lifetime of the guest for various deuteronaphthalenes in durene and durene-d_{14}. Their results cannot be explained in terms of thermal activation and subsequent triplet-triplet annihilation. Watts and Strickler[37] have recently observed a similar solvent effect for naphthalene-d_8 in ethanol and perdeuteroethanol. These lifetime effects can perhaps be explained in terms of differences between the anharmonicities of CD modes in deuterated and undeuterated solvents. A part of the temperature effect on radiationless transition rates may also be attributable to this effect.[38]

b. $^3B_{1u} \rightsquigarrow {}^1A_{1g}$--Perdeuterobenzene

We expect from experimental results[39] that $\underline{k}$ will decrease upon deuteration. We assume that β does not substantially change. The $^1A_{1g} - {}^3B_{1u}$ separation for deuterobenzene is 29,850 cm^{-1}.[10a] This change in singlet-triplet separation along with changes in the frequencies of the carbon-hydrogen stretching modes causes changes in both ρ and $\overline{F}$. The value of ρ appropriate to deuterobenzene is 1.12×10^{13} and the harmonic $\overline{F}$ is 3.41×10^{-34}. The harmonic radiationless rate is then

$$k = 1.18 \times 10^{-10} \text{ sec}^{-1} \quad .$$

For C_6D_6 the only modes that contribute significantly to the average Franck-Condon factor are the carbon-deuterium modes. The out-of-plane vibrations are no longer even minimally important. The

theoretical rate for C_6D_6 is a factor of 10^6 slower than the corresponding rate for C_6H_6! This result lends credence to the assumption that the phosphorescence lifetime of perdeuterated benzene is essentially the true radiative lifetime, that is, compared to the radiative rate, the radiationless rate is negligible. Even if we include anharmonicities, which in this case increase $\underline{k}$ by a factor of about 100, the radiationless rate is still much smaller than that for benzene. The radiationless rate for C_6D_6 corrected for anharmonicity is

$$k = 1.2 \times 10^{-8} \text{ sec}^{-1} \quad .$$

c. $^1B_{2u} \rightsquigarrow {}^1A_{1g}$--Benzene

For the case of internal conversion from the lowest excited singlet state to the ground state, the density of states ρ and the average Franck-Condon factor $\overline{F}$ are calculated as before, this time for an energy separation of 37,853 cm^{-1} [10b] and for frequencies appropriate for the $^1B_{2u}$ electronic state. The only parameter that needs to be evaluated in a different manner is the matrix element β, since we are now dealing with a spin-allowed singlet-singlet radiationless transition.

We will again use 4000 cm^{-1} as a typical value for a purely vibronic β. Our expression for $\underline{k}$ in this case becomes

$$k = 1.89 \times 10^{19} \rho \overline{F} \quad .$$

The ground state density of states at 37,850 cm^{-1} is 2.72×10^{13} and the harmonic value of $\overline{F}$ is 6.30×10^{-32}; therefore

$$k = 32.4 \text{ sec}^{-1} \quad .$$

The radiative transition rate for the $^1B_{2u} \rightarrow {}^1A_{1g}$ fluorescence transition is 1.59×10^6 sec^{-1}.[1b] Thus the radiationless internal conversion process is negligible when compared to the radiative process. Within the rather large error limits, the experimental data indicate that the $^1B_{2u}$ state loses its energy primarily by fluorescence and intersystem crossing[40, 8] in support of our theoretical conclusion.

7. Conclusions

The results of these radiationless rate calculations are summarized in Table IX. We have shown that the Robinson and Frosch mechanism for radiationless transitions using Herzberg-Teller vibronic coupling does in fact yield transition rates that are of the right order of magnitude to explain the experimental results if one includes anharmonicities in the calculation. It should be emphasized that we expect only order-of-magnitude agreement between our calculations and experiment primarily because of the uncertainties in β and the form of the anharmonicity. The introduction of anharmonicity into the calculation in order to explain the observed radiationless transition rate also provides a mechanism by which one can explain at least a portion of the effects of environment and temperature on the triplet lifetime. Both the deuterium effect on phosphorescence lifetime and the apparent insignificance of the $^1B_{2u} \rightsquigarrow {}^1A_{1g}$ radiationless process are explained by these calculations. In addition it is interesting to note that the out-of-plane modes make a small but significant contribution to the $^3B_{1u} \rightsquigarrow {}^1A_{1g}$ radiationless rate for C_6H_6 but not for C_6D_6. The fact that these low frequency modes contribute at all to the

TABLE IX. Summary of calculated radiationless transition rates.

Transition	Harmonic Rate (sec^{-1})	Anharmonic Rate (sec^{-1})	Experimental Rate (sec^{-1})
$^3B_{1u} \rightsquigarrow {}^1A_{1g}$ (C_6H_6)	9.0×10^{-5}	4.5×10^{-3}	2.4×10^{-2} [a]
$^3B_{1u} \rightsquigarrow {}^1A_{1g}$ (C_6D_6)	1.2×10^{-10}	1.2×10^{-8}	--
$^3B_{2u} \rightsquigarrow {}^1A_{1g}$ (C_6H_6)	32.4	--	--

[a] Ref. 1a.

Franck-Condon factors is due to their number, nine out-of-plane modes compared with six carbon-hydrogen stretching modes, and the large difference between the potential surfaces of these modes in the ground and excited states as expressed by the parameter f.

Several quantities have been obtained that are of importance independent of the context in which they are discussed in this thesis. We have obtained values for the crystal phase anharmonicities for the C-C and C-H totally symmetric stretching modes and have cited evidence that indicates that both anharmonicities change on going from gas or liquid to crystal phases. We also have calculated the C-H and C-C bond length changes on excitation from the ground state to the $^3B_{1u}$ state.

Acknowledgments

We would like to thank Professor E. W. Schlag of Northwestern University for providing us with a copy of his computer program for the calculation of the density of states, and Dr. W. G. Valance for his help in explaining this program to us.

REFERENCES

1. (a) G. W. Robinson, J. Mol. Spectry. 6, 58 (1961); (b) G. W. Robinson and R. P. Frosch, J. Chem. Phys. 37, 1962 (1962); (c) ibid. 38, 1187 (1963).
2. G. R. Hunt, E. F. McCoy, and I. G. Ross, Australian J. Chem. 15, 591 (1962).
3. (a) W. Siebrand, J. Chem. Phys. 46, 440 (1967); (b) ibid. 47, 2411 (1967); (c) W. Siebrand and D. F. Williams, J. Chem. Phys. 49, 1860 (1968).
4. S. H. Lin, J. Chem. Phys. 44, 3759 (1966).
5. M. Bixon and J. Jortner, J. Chem. Phys. 48, 715 (1968).
6. We make a distinction between Herzberg-Teller vibronic coupling and the breakdown of the Born-Oppenheimer approximation. This distinction is quite often not explicitly made and can lead to confusion. For more details on the exact nature of this distinction the reader is referred to Sec. IIB of this thesis and to H. Sponer and E. Teller, Rev. Mod. Phys. 13, 75 (1941).
7. (a) G. Herzberg and E. Teller, Z. Physik Chem. B21, 410 (1933); (b) A. C. Albrecht, J. Chem. Phys. 33, 156 (1960).
8. G. W. Robinson, J. Chem. Phys. 47, 1967 (1967).
9. We have discussed two possible mechanisms that may be responsible for the electronic-vibrational coupling necessary for the occurrence of radiationless transitions. There are others [for a mechanism involving a coupling due to the oscillating phonon field in solids see M. Gouterman, J. Chem. Phys. 36, 2846

(1962)]. The choice of the Herzberg-Teller coupling mechanism for the present calculation is supported by the results of the present calculation, the utility of Herzberg-Teller coupling in describing vibronically induced radiative transitions and a calculation (see Sec. IIB of this thesis) that indicates that the matrix element resulting from the Born-Oppenheimer breakdown is several orders of magnitude too small to describe radiationless processes.

10. (a) S. D. Colson and E. R. Bernstein, J. Chem. Phys. 43, 2661 (1965); (b) E. R. Bernstein, S. D. Colson, D. S. Tinti, and G. W. Robinson, J. Chem. Phys. 48, 4632 (1968).
11. The convention for numbering the vibrations is due to E. B. Wilson, Phys. Rev. 45, 706 (1934).
12. M. Kasha, J. Opt. Soc. Am. 38, 929 (1948).
13. J. H. van der Waals, A. M. D. Berghuis, and M. S. de Groot, Mol. Phys. 13, 301 (1967).
14. W. H. Melhuish, J. Phys. Chem. 64, 762 (1960).
15. E. Lippert, W. Nagele, I. Seibold-Blankenstein, U. Staiger, and W. Voss, Z. Anal. Chem. 170, 1 (1959).
16. L. de Galan and J. D. Winefordner, Spectrochim. Acta 23B, 277 (1968).
17. F. M. Garforth and C. K. Ingold, J. Chem. Soc. 1948, 427
18. J. W. Ellis, Trans. Faraday Soc. 25, 888 (1929).
19. T. E. Martin and A. H. Kalantar, J. Chem. Phys. 49, 235 (1968).
20. B. R. Henry and W. Siebrand, J. Chem. Phys. 49, 5369 (1968).

21. E. B. Wilson, J. C. Decius, and P. C. Cross, Molecular Vibrations (McGraw-Hill Book Co., Inc., New York, 1955), p. 37.

22. R. P. Forsch (unpublished results).

23. S. Bell and P. A. Warsop, J. Mol. Spectry. 20, 425 (1966).

24. M. S. de Groot and J. H. van der Waals, Mol. Phys. 6, 545 (1963).

25. G. C. Nieman and D. S. Tinti, J. Chem. Phys. 46, 1432 (1967).

26. D. P. Craig, J. Chem. Soc. 1950, 2146.

27. The $^3B_{1u}$ and $^1B_{2u}$ states are alike in many ways. They have similar amounts of electronic excitation, the carbon-carbon bond length changes upon excitation are similar and the change of the electronic energy levels upon deuteration is similar for both states. Thus it seems reasonable, in the absence of experimental information for the triplet state, to assume that the vibrational frequencies in the $^3B_{1u}$ and $^1B_{2u}$ states are the same.

28. D. H. Whiffen, Phil. Trans. Roy. Soc. London A248, 131 (1955).

29. A. C. Albrecht, J. Mol. Spectry. 5, 236 (1960).

30. The error limits here and in the reported values of δ and f are related to the average deviation reported in Table II. They bracket those values of δ and f that yield calculated intensities that agree with the average experimental intensities within the limits set by the average deviation.

31. See, for example, L. I. Schiff, Quantum Mechanics (McGraw-Hill Book Co., Inc., New York, 1955), p. 151f.

32. E. W. Schlag and R. A. Sandsmark, J. Chem. Phys. 37, 168 (1962); E. W. Schlag, R. A. Sandsmark, and W. G. Valance, ibid. 40, 1461 (1964); J. Phys. Chem. 69, 1431 (1965).

33. A. C. Albrecht, J. Chem. Phys. 38, 354 (1963).

34. As indicated earlier, the choice of a coupling Hamiltonian depends on our choice of zero-order Hamiltonians. In the present case the zero-order Hamiltonian includes the spin-orbit coupling terms. β may then be viewed as a first-order direct coupling matrix element, since it is first order in the vibronic Hamiltonian H(2).

35. H. F. Hameka and L. J. Oosterhoff, Mol. Phys. 1, 358 (1958).

36. N. Hirota and C. A. Hutchison, J. Chem. Phys. 46, 1561 (1967).

37. R. J. Watts and S. J. Strickler, J. Chem. Phys. 49, 3867 (1968).

38. G. F. Hatch, M. D. Erlitz, and G. C. Nieman, J. Chem. Phys. 49, 3723 (1968); P. F. Jones and S. Siegel, J. Chem. Phys. 50, 1134 (1969).

39. M. R. Wright, R. P. Frosch, and G. W. Robinson, J. Chem. Phys. 33, 934 (1960).

40. W. A. Noyes and D. A. Harter, J. Chem. Phys. 46, 674 (1967).

B. A CRITICAL ANALYSIS OF THE USE OF THE FAILURE OF THE BORN-OPPENHEIMER APPROXIMATION IN DESCRIBING RADIATIONLESS TRANSITIONS

1. Introduction

A radiationless transition from one electronic state to another lower in energy, necessarily involves a conversion of the excess electronic energy into vibrational, rotational, or translational energy. For large molecules the energy almost certainly goes initially into vibrational channels. We have shown earlier[1] that Herzberg-Teller vibronic coupling[2] gives radiationless transition rates in good agreement with the experimental results. We wish to consider here an alternative mechanism of coupling between vibrational and electronic motion, coupling that is due to a breakdown of the Born-Oppenheimer approximation. This mechanism has recently been invoked by several authors[3] to account for the electronic radiationless transition process. We will determine below the circumstances under which the matrix elements due to the Born-Oppenheimer breakdown exceed the Herzberg-Teller vibronic coupling matrix elements.

In the next section the two matrix elements will be considered in some detail. It appears that a clear distinction between the breakdown of the Born-Oppenheimer approximation and Herzberg-Teller vibronic coupling has not always been made. One of the purposes of Sec. 2 is to make this distinction clear. In Sec. 3 we calculate the ratio between the two matrix elements in a form that enables us to determine quite simply those circumstances under which the Born-

Oppenheimer breakdown is the dominant mechanism of vibronic coupling. Whenever numerical values must be used, we employ values appropriate for the $^3B_{1u} \rightsquigarrow {}^1A_{1g}$ radiationless transition in benzene.

2. Theory

The Born-Oppenheimer approximation[5] involves the assumption that the total molecular wave-function may be written as a product of electronic and vibrational parts

$$\Psi_{kr}(q, Q) = \varphi_k(q, Q)\chi_{kr}(Q) \quad , \tag{1}$$

where q represents the set of electronic coordinates and Q the nuclear coordinates. φ_k is the $k^{\underline{th}}$ electronic wave function and χ_{kr} is the $r^{\underline{th}}$ vibrational wave function for the $k^{\underline{th}}$ electronic state.

We require that the wave function (1) be the best possible product wave function of this form and using a variational approach[6] arrive at the following Schrödinger equations for φ and χ:

$$[T(q) + U(q, Q)]\varphi_k(q, Q) = E_k(Q)\varphi_k(q, Q) \tag{2}$$

$$[E_k(Q) + V(Q) + T(Q) + \langle \varphi_k | T(Q) | \varphi_k \rangle]\chi_{kr}(Q) = W_{kr}\chi_{kr}(Q) \quad . \tag{3}$$

Here, T(q) and T(Q) are the electronic and nuclear kinetic energies, respectively. U(q, Q) is a sum of the nuclear-electronic and electronic-electronic Coulomb potentials and V(Q) is the nuclear-nuclear Coulomb repulsion. $E_k(Q)$ is the energy of the $k^{\underline{th}}$ electronic state, while W_{kr} is the total vibronic energy for a molecule in the $k^{\underline{th}}$ electronic and $r^{\underline{th}}$ vibrational level.

In solving the vibrational Schrödinger Eq. (3), the "harmonic approximation"[7] is usually made:

$$\mathcal{V}(Q) \equiv E_k(Q) + V(Q) + \langle \varphi_k | T(Q) | \varphi_k \rangle \approx \tfrac{1}{2} \sum_\alpha \left[\frac{\partial^2 \mathcal{V}(Q)}{\partial Q_\alpha^2} \right]_0 Q_\alpha^2 , \quad (4)$$

where the Q_α are normal coordinates, the derivative is evaluated at an equilibrium point Q_0 defined by

$$\left(\frac{\partial \mathcal{V}}{\partial Q_\alpha} \right)_0 = 0 \quad (5)$$

for all normal coordinates α, and the zero of energy is chosen such that $\mathcal{V}(Q_0) = 0$. The total vibrational wave function then becomes a product of harmonic oscillator wave functions for each normal coordinate

$$\chi_{kr}^{\text{harm.}}(Q) = \prod_\alpha x_{kr}^\alpha(Q_\alpha) \quad . \quad (6)$$

The electronic Schrödinger Eq. (2) is solved in a similar way.[8] $U(q, Q)$ is expanded about the point Q_0 defined in (5)

$$U(q, Q) \approx U(q, Q_0) + \sum_\alpha \left[\frac{\partial U(q, Q)}{\partial Q_\alpha} \right]_0 Q_\alpha + \ldots \quad . \quad (7)$$

The solutions of (2) using only the first term in (7) are treated as zero-order wave functions and denoted $\varphi_k(q, Q_0)$. These zero-order functions give rise to what Longuet-Higgins[6] has described as the "crude Born-Oppenheimer approximation". A better Born-Oppenheimer

approximation can be obtained by considering the higher terms in (7) as perturbations. For example, to first order in Q_α,

$$H' = \sum_\alpha \left[\frac{\partial U(q, Q)}{\partial Q_\alpha}\right]_0 Q_\alpha \quad . \tag{8}$$

This perturbing Hamiltonian H′ gives rise to first-order Herzberg-Teller vibronic coupling.[2] A straightforward application of perturbation theory then yields the following first-order wave function

$$\varphi_k(q, Q) = \varphi_k(q, Q_o) + \sum_{\ell \neq k} \frac{\langle \varphi_k(q, Q_o) | H' | \varphi_\ell(q, Q_o) \rangle}{E^o_\ell - E^o_k} \varphi_\ell(q, Q_o) \ , \tag{9}$$

where $E^o_k = E_k(Q_o)$ is the energy of a zeroth-order <u>electronic</u> wave-function. If this Herzberg-Teller expansion is carried out to all orders in Q, one obtains the exact Born-Oppenheimer wave function. It is important to remember that <u>the entire treatment of the problem to this point has been carried out within the framework of the Born-Oppenheimer approximation</u>. With the above expressions for χ [Eq. (6)] and φ [Eq. (9)], we can proceed with the evaluation of the coupling between Born-Oppenheimer states.

A derivation of the matrix element connecting two different Born-Oppenheimer states Ψ_{kr} and Ψ_{js} $(k \neq j)$ has recently been outlined by Bixon and Jortner.[3a] Their final result is[9]

$$\beta_{B.O.} = \langle \Psi_{kr} | \hat{H} | \Psi_{js} \rangle$$

$$-2 \sum_{\alpha} \frac{\hbar^2}{2} \int \chi^*_{kr} \langle \varphi_k | \frac{\partial}{\partial Q_\alpha} | \varphi_j \rangle \frac{\partial}{\partial Q_\alpha} \chi_{js} dQ$$

$$+ \int \chi^*_{kr} \langle \varphi_k | T(Q) | \varphi_j \rangle \chi_{js} dQ \quad , \tag{10}$$

where $T(Q) = -\frac{\hbar^2}{2} \sum_{\alpha} \frac{\partial^2}{\partial Q_\alpha^2}$ and $dQ = dQ_1 dQ_2 \cdots$. The Hamiltonian $\hat{H}$ is the complete molecular Hamiltonian.

We will consider two electronic states, φ_1 and φ_2, given by the expressions

$$\left.\begin{aligned} \varphi_1 &= \varphi_1^0 + \sum_{\ell \neq 1} \sum_{\alpha} \frac{a_\alpha^{\ell 1} Q_\alpha}{\Delta E_{1\ell}} \varphi_\ell^0 \\ \varphi_2 &= \varphi_2^0 + \sum_{i \neq 2} \sum_{\beta} \frac{a_\beta^{i2} Q_\beta}{\Delta E_{2i}} \varphi_i^0 \end{aligned}\right\} \tag{11}$$

where

$$a_\beta^{ij} = \langle \varphi_i^0 | (\partial U / \partial Q_\beta)_0 | \varphi_j^0 \rangle$$

$$\Delta E_{ij} = E_i^0 - E_j^0 \quad ,$$

and E_i^0 is the energy of a zero-order state φ_i^0. Later, when we wish to obtain a numerical value for (10), state 1 will become the benzene $^1A_{1g}$ ground state and state 2 the $^3B_{1u}$ state.

The evaluation of (10) will be carried out only to first order in the normal coordinates Q. The second term in (10), which involves a

second derivative with respect to Q, will be neglected. The first term involves the matrix element $\langle \varphi_1 | (\partial/\partial Q_\alpha) | \varphi_2 \rangle$, which can be evaluated by using φ_1 and φ_2 from (11). The lowest order non-zero term then becomes

$$\langle \varphi_1 | \frac{\partial}{\partial Q_\alpha} | \varphi_2 \rangle = \frac{a_\alpha^{12}}{\Delta E_{21}} \quad . \tag{12}$$

Substituting (6) and (12) into (10) we finally have[10]

$$\beta_{B.O.} = -\hbar^2 \sum_\alpha \frac{a_\alpha^{12}}{\Delta E_{21}} \langle x_\alpha^{1r} | \frac{\partial}{\partial Q_\alpha} | x_\alpha^{2s} \rangle \prod_{\gamma \neq \alpha} \langle x_\gamma^{1r} | x_\gamma^{2s} \rangle \quad . \tag{13}$$

In practice the sum in (13) over all normal coordinates α can usually be considerably simplified by symmetry and energy considerations.

The Herzberg-Teller coupling matrix element to first order in Q is familiar from studies of vibronically induced radiative transitions.[2b] The Hamiltonian H′ of Eq. (8) is used to connect the two zero-order electronic states φ_1^0 and φ_2^0. The matrix element is then

$$\beta_{H.T.} = \langle \varphi_1^0 \chi_{1r} | \sum_\alpha \left(\frac{\partial U}{\partial Q_\alpha} \right)_0 Q_\alpha | \varphi_2^0 \chi_{2s} \rangle \quad . \tag{14}$$

This becomes upon using Eq. (6) and the definition of a_α^{1a}

$$\beta_{H.T.} = \sum_\alpha a_\alpha^{12} \langle x_\alpha^{1r} | Q_\alpha | x_\alpha^{2s} \rangle \prod_{\gamma \neq \alpha} \langle x_\gamma^{1r} | x_\gamma^{2s} \rangle \quad . \tag{15}$$

The ratio of the two matrix elements (13) and (15) is then

$$\frac{\beta_{B.O.}}{\beta_{H.T.}} = \frac{-\hbar^2}{\Delta E_{21}} \frac{\langle x_\alpha^{1r} | \frac{\partial}{\partial Q_\alpha} | x_\alpha^{2s} \rangle}{\langle x_\alpha^{1r} | Q_\alpha | x_\alpha^{2s} \rangle} \quad , \tag{16}$$

where we are considering only one normal mode α. This ratio has the nice feature that it is independent of the electronic matrix element a_α^{12} and the Franck-Condon factors $\prod_{\gamma \neq \alpha} \langle x_\gamma^{1r} | x_\gamma^{2s} \rangle$.

3. Calculations

In this section we will calculate the ratio in Eq. (16), using as a numerical example the $^3B_{1u} \rightsquigarrow {}^1A_{1g}$ radiationless transition of benzene. This transition is known to occur experimentally[11] and a rough estimate of its rate is available.[12] In addition a calculation of the radiationless rate for this transition using the Herzberg-Teller coupling scheme has been completed and agrees quite well with experiment.[1]

To calculate the ratio in (16), we first need to know the form of the vibrational matrix elements $\langle x_\gamma^{1r} | \frac{\partial}{\partial Q_\gamma} | x_\gamma^{2s} \rangle$ and $\langle x_\gamma^{1r} | Q_\gamma | x_\gamma^{2s} \rangle$. The vibrational wave functions x_γ^{1r} are harmonic oscillator wave functions in a first-order approximation. The numerical superscript indicates the electronic state (1 = $^1A_{1g}$ and 2 = $^3B_{1u}$) and the letters $\underline{r}$ or $\underline{s}$ denote the number of vibrational quanta used. The Greek subscript refers to the particular normal mode under discussion. The harmonic oscillator wave functions may be written[13]

$$x_{\gamma}^{1r}(Q_{1\gamma}) = N_{\gamma}^{1r} e^{-\alpha_{1\gamma}^2 Q_{1\gamma}^2/2} H_r(\alpha_{1\gamma} Q_{1\gamma}) \quad , \tag{17}$$

where

$$\alpha_{1\gamma} = (\omega_{1\gamma}/\hbar)^{\frac{1}{2}} \quad ,$$

and the normalization constant is

$$N_{\gamma}^{1r} = \left[\left(\frac{\omega_{1\gamma}}{\pi\hbar}\right)^{\frac{1}{2}} \left(\frac{1}{r!\,2^r}\right)\right]^{\frac{1}{2}} \quad ,$$

where $\omega_{1\gamma}$ is the angular frequency of the $\gamma^{\underline{\text{th}}}$ normal mode in electronic state 1, and $H_r(\alpha_{1\gamma}Q_{1\gamma})$ is a Hermite polynomial of order $\underline{r}$.

The matrix elements we wish to evaluate become

$$\langle x_{\gamma}^{1r} | \hat{A}_{\gamma} | x_{\gamma}^{2s} \rangle = N_{\gamma}^{1r} N_{\gamma}^{2s} \int_{-\infty}^{\infty} e^{-\alpha_{1\gamma}^2 Q_{1\gamma}^2/2} H_r(\alpha_{1\gamma} Q_{1\gamma})$$

$$\hat{A}_{\gamma} e^{-\alpha_{2\gamma}^2 Q_{2\gamma}^2/2} H_s(\alpha_{2\gamma} Q_{2\gamma}) dQ_{1\gamma} \quad , \tag{18}$$

where $\hat{A}_{\gamma}$ is either $\partial/\partial Q_{\gamma}$ or Q_{γ}. This integration can be performed in a closed form by making the following substitutions

$$\alpha_{2\gamma} = (f_{\gamma})^{\frac{1}{2}} \alpha_{1\gamma}$$

$$Q_{2\gamma} = Q_{1\gamma} + \delta_{\gamma}$$

for all normal coordinates γ, and by using simple relationships between derivatives of Hermite polynomials[14] along with the mathematical results from a previous paper.[1] In radiationless processes

at low temperatures ($kT < 200\ cm^{-1}$), all of the normal mode oscillators may be considered to be in their lowest zero quantum levels prior to the transition. In our case this means that $s = 0$ for all γ of the $^3B_{1u}$ initial electronic state. In addition we have shown[1] from an analysis of the phosphorescence spectra that $\delta_\gamma = 0$ for all but the totally symmetric vibrational modes. This means that the normal coordinate origin is undisplaced upon excitation. In our calculations only non-totally symmetric modes at low temperatures will be considered and for these modes Eq. (18) for $\hat{A} = \partial/\partial Q_\gamma$ becomes

$$\langle x_\gamma^{1r} | \frac{\partial}{\partial Q_\gamma} | x_\gamma^{20} \rangle$$

$$= \frac{-2rf_\gamma N_\gamma^{1r} N_\gamma^{20}}{(1+f_\gamma)} \left(\frac{2\pi}{1+f_\gamma}\right)^{\frac{1}{2}} \left(\frac{f_\gamma - 1}{f_\gamma + 1}\right)^{(r-1)/2} H_{r-1}[0] \quad \text{for } \underline{r} \text{ odd}$$

$$= 0 \quad \text{for } \underline{r} \text{ even} \quad . \qquad (19)$$

When $\hat{A} = Q_\gamma$ the integral is

$$\langle x_\gamma^{1r} | Q_\gamma | x_\gamma^{20} \rangle$$

$$= \frac{2rN_\gamma^{1r} N_\gamma^{20}}{(1+f_\gamma)\alpha_\gamma^2} \left(\frac{2\pi}{1+f_\gamma}\right)^{\frac{1}{2}} \left(\frac{f_\gamma - 1}{f_\gamma + 1}\right)^{(r-1)/2} H_{r-1}[0] \quad \text{for } \underline{r} \text{ odd}$$

$$= 0 \quad \text{for } \underline{r} \text{ even} \quad . \qquad (20)$$

The ratio for odd $\underline{r}$ given by Eq. (16) becomes simply

$$\frac{\beta_{B.O.}}{\beta_{H.T.}} = \frac{f_\gamma E_\gamma}{\Delta E_{21}} \quad , \tag{21}$$

where we have replaced α^2 by $\omega/\hbar$ and where $E_\gamma = \hbar\omega_\gamma$ is the vibrational energy quantum.

Equation (21) exhibits several intereating features. First it is independent of the level of excitation $\underline{r}$ of the normal mode γ. This is a consequence of our assumptions that the normal modes are harmonic and that $\delta_\gamma = 0$. When these restrictions are relaxed, a slight $\underline{r}$ and δ dependence results. The exact form of $\beta_{B.O.}/\beta_{H.T.}$ is discussed in Appendix D. If f = 1, Eq. (21) is valid no matter what the value of δ_γ. In practice the mode γ, called the "promoting mode" by Lin and Bersohn,[15] will be excited to a low vibrational level ($\underline{r}$ small) where the assumptions we have made are valid. The remainder of the vibrational energy is taken up by all of the other normal modes (the so-called "accepting modes"), but their contribution to the radiationless rate through the Franck-Condon factors conveniently cancels out of Eq. (21).

The quantity f_γ in Eq. (21) is defined in Eq. (18) as the ratio of the α_γ's for the two states involved in the radiationless process. These α_γ's for harmonic oscillators are the reciprocal of the classical zero-point vibrational amplitudes for the normal modes γ. f_γ is thus a measure of the change in the width of the harmonic well upon going from one electronic state to another. For benzene these f's range in size from 1.1 to 0.6 with most modes having an f less than but very near 1.0.[1]

In Table I values of the ratio $\beta_{B.O.}/\beta_{H.T.}$ are calculated for various values of f_γ and E_γ appropriate for the $^3B_{1u} \rightsquigarrow {}^1A_{1g}$ transition. The energy separation between these two states ΔE_{21} is taken to be 29,650 cm^{-1}.[16] In all cases the Born-Oppenheimer matrix element is at least ten times smaller than the Herzberg-Teller matrix element. When calculating radiationless transition rates, it is the square of these matrix elements that is proportional to the rate. This means that considered by itself the breakdown of the Born-Oppenheimer approximation is less than 1% as effective as Herzberg-Teller coupling at inducing the $^3B_{1u} \rightsquigarrow {}^1A_{1g}$ radiationless transition.

4. Discussion

From Eq. (21), we can deduce a criterion for determining when the breakdown of the Born-Oppenheimer approximation will be important for radiationless processes. Since the factor involving f_γ is near unity for most vibrations (at least for benzene), the Herzberg-Teller mechanism will be the dominant mechanism provided the zero-order electronic energy difference is larger than the vibrational frequency of the "accepting mode",

$$\Delta E_{21} > E_\gamma \quad ,$$

and the Born-Oppenheimer breakdown will be dominant whenever

$$\Delta E_{21} < E_\gamma \quad .$$

One is not free to choose any normal mode γ to accomplish the vibronic coupling. Symmetry usually restricts γ to a few vibrations

TABLE I. Ratio of Born-Oppenheimer and Herzberg-Teller matrix elements for the $^3B_{1u} \rightsquigarrow {}^1A_{1g}$ transition.[a]

Vibration Type	E_γ (cm^{-1})	f_γ	$\lvert\beta_{B.O.}/\beta_{H.T.}\rvert$
Hydrogen-stretching	3056	1.018	0.1049
Carbon-stretching	1494	1.002	0.0505
Carbon-deformation	1478	0.995	0.0496
Hydrogen-bending	1151	0.921	0.0358
Carbon-bending	741	0.898	0.0224
Out-of-plane	766	0.669	0.0173

[a]The parameters E_γ and f_γ are from Ref. 1.

and of these few, one often has an electronic matrix element a_γ^{12} that is large enough to dominate the others. For example in the radiative process $^3B_{1u} \rightarrow {}^1A_{1g}$, the 1584 cm^{-1} carbon-stretching normal mode is known from theory[17] and experiment[18] to dominate the vibronic coupling due to its large a_γ^{12}. For comparison we have extracted several values of a_γ^{12} for various normal modes γ from calculations by Albrecht[19] and listed them in Table II. These values are for vibronic coupling in benzene between the E_{1u} or E_{2g} state and B_{1u} or B_{2u} state. For the process we are considering ($^3B_{1u} \rightsquigarrow {}^1A_{1g}$) an additional spin-orbit coupling would be necessary but this type of coupling does not usually involve any additional vibronic interactions. From Table II we can see that the high frequency hydrogen-stretching modes are the least effective in all cases at mixing electronic levels even though the ratio $\beta_{B.O.}/\beta_{H.T.}$ is largest for this type of vibration. If on this basis we ignore the hydrogen-stretching modes, we can then say that for benzene the Born-Oppenheimer breakdown dominates the vibronic coupling only when the electronic energy levels being coupled are closer than 1500 cm^{-1}.

The ratio in Eq. (21) does not guarantee that either the Born-Oppenheimer breakdown or Herzberg-Teller coupling will be able to couple two electronic states together strongly enough so that experimentally observable radiationless transitions will occur. It merely enables us to determine which of the two mechanisms is dominant. They may in fact both be insignificant. For the $^3B_{1u} \rightsquigarrow {}^1A_{1g}$ transition, we have shown[1] that Herzberg-Teller coupling is sufficiently strong to account for the observed radiationless transition and our present

TABLE II. Electronic matrix elements for vibronic coupling with the benzene E_{1u} state.[a]

Vibration and Symmetry[b]	Frequency (cm^{-1})[c]	Type[d]	Matrix element (eV/amu$^{\frac{1}{2}}$ Å)	
			B_{1u}	B_{2u}
6 (e_{2g})	606	C-bending	1.00098	2.28565
7 (e_{2g})	3042	H-stretching	-0.20006	-0.47322
8 (e_{2g})	1584	C-stretching	-3.55368	1.73488
9 (e_{2g})	1174	H-bending	0.85590	0.00762
			$E_{2g\gamma}$[e,f]	$E_{2g\delta}$
18 (e_{1u})	1035	H-bending	-1.48190	-1.66090
19 (e_{1u})	[1478]	C-deformation	1.52208	-2.56052
20 (e_{1u})	[3063]	H-stretching	0.55910	0.16350

[a]The matrix elements were calculated from data presented in A. C. Albrecht, J. Chem. Phys. 33, 156, 169 (1960); J. Mol. Spectry. 5, 236 (1960).

[b]The convention for numbering the vibrations is due to E. B. Wilson, Phys. Rev. 45, 706 (1934).

[c]E. R. Bernstein, S. D. Colson, D. S. Tinti, and G. W. Robinson, J. Chem. Phys. 48, 4632 (1968). Values in brackets are from R. D. Mair and D. F. Hornig, J. Chem. Phys. 17, 1236 (1949).

[d]For a diagram of the normal mode motions for benzene, see G. Herzberg, Molecular Spectra and Molecular Structure. II. Infrared and Raman Spectra of Polyatomic Molecules (D. Van Nostrand, Co., Inc., Princeton, New Jersey, 1945), p. 118.

[e]The states γ and δ are defined by J. N. Murrell and J. A. Pople, Proc. Phys. Soc. (London) A69, 245 (1956).

[f]From symmetry one would expect b_{1u} and b_{2u} modes also to be effective in mixing E_{2g} and E_{1u} states. In Albrecht's calculation, however, the integrals involving these modes are identically zero.

calculations show that the breakdown of the Born-Oppenheimer approximation is insignificant for this transition. For radiationless transitions between higher, more densely spaced electronic states, quite the opposite conclusion could result.[20]

5. Conclusions

On the basis of our earlier calculation,[1] the utility of Herzberg-Teller coupling in describing vibronically-induced radiative transitions[2b] and the results of this paper, we conclude that the Born-Oppenheimer breakdown is unimportant in the description of the $^3B_{1u} \rightsquigarrow {}^1A_{1g}$ radiationless transition. In fact it is unimportant in all radiationless processes for benzene where the electronic states being coupled are separated by more than 1500 cm^{-1}. Our results show that the Born-Oppenheimer breakdown is unimportant in all molecules where the coupled electronic states are further apart than the vibrational frequency of the normal mode responsible for the coupling. Sponer and Teller[5c] reached analogous conclusions for radiative transitions in molecules many years ago.

REFERENCES

1. D. M. Burland and G. W. Robinson, "Calculated Radiationless Transition Rates for Benzene and Deuterobenzene", J. Chem. Phys. 51, 0000 (1969) and Sec. IIA of this thesis.
2. (a) G. Herzberg and E. Teller, Z. Physik Chem. B21, 410 (1933); (b) A. C. Albrecht, J. Chem. Phys. 33, 156 (1960).
3. (a) M. Bixon and J. Jortner, J. Chem. Phys. 48, 715 (1968); J. Jortner and R. S. Berry, J. Chem. Phys. 48, 2757 (1968); D. P. Chock, J. Jortner, and S. A. Rice, J. Chem. Phys. 49, 610 (1968); (b) W. Siebrand, J. Chem. Phys. 46, 440 (1967); ibid. 47, 2411 (1967); W. Siebrand and D. F. Williams, J. Chem. Phys. 49, 1860 (1968); (c) S. H. Lin, J. Chem. Phys. 44, 3759 (1966); (d) B. R. Henry and M. Kasha, Ann. Rev. Phys. Chem. 19, 161 (1968).
4. G. W. Robinson and R. P. Frosch, J. Chem. Phys. 38, 1187 (1963); ibid. 37, 1962 (1962); G. R. Hunt, E. R. McCoy, and I. G. Ross, Australian J. Chem. 15, 591 (1962).
5. (a) M. Born and R. Oppenheimer, Ann. Physik 87, 457 (1927); (b) M. Born and K. Huang, Dynamical Theory of Crystal Lattices (Oxford University Press, New York, 1954); (c) H. Sponer and E. Teller, Rev. Mod. Phys. 13, 75 (1941); this last reference quite explicitly makes the distinction between Herzberg-Teller coupling and the Born-Oppenheimer breakdown.
6. H. C. Longuet-Higgins, Advan. Spectry. 2, 428 (1961).
7. E. B. Wilson, J. C. Decius, and P. C. Cross, Molecular Vibrations (McGraw-Hill Book Co., Inc., New York, 1955), p. 14.

8. See, for example, R. L. Fulton and M. Gouterman, J. Chem. Phys. 35, 1059 (1961).

9. This expression is identical to the corresponding equation of Bixon and Jortner [Ref. 3a, Eq. (8b)] with one exception. Q_α in our case is a normal coordinate and thus contains the nuclear mass (cf. Ref. 8, p. 20). Therefore the nuclear mass does not appear in our equation as it does in that of Bixon and Jortner.

10. We have tacitly assumed, in the derivation of Eq. (13), that the normal coordinates Q_α do not change upon excitation, that is the normal coordinates for the state φ_1 are also the normal coordinates for φ_2. This assumption is treated in more detail in the discussion preceding Eq. (19).

11. E. H. Gilmore, G. E. Gibson, and D. S. McClure, J. Chem. Phys. 20, 829 (1952); T. E. Martin and A. H. Kalantar, J. Chem. Phys. 48, 4996 (1968).

12. G. W. Robinson, J. Mol. Spectry. 6, 58 (1961).

13. Ref. 7, p. 37.

14. H. Margenau and G. M. Murphy, The Mathematics of Physics and Chemistry (D. Van Nostrand Co., Inc., Princeton, 1956), p. 123.

15. S. H. Lin and R. Bersohn, J. Chem. Phys. 48, 2732 (1968).

16. D. M. Burland and G. Castro, J. Chem. Phys. 50, 4107 (1969); and Sec. IIIA of this thesis.

17. A. D. Liehr, Z. Naturforsch. 13a, 311 (1958).

18. S. Leach and R. Lopez-Delgado, J. Chim. Phys. 61, 1636 (1964).

19. A. C. Albrecht, J. Chem. Phys. 33, 169 (1960). Actually Albrecht does not explicitly list these matrix elements in this

reference. However, using his formulae along with the values he gives for the parameters involved one can easily calculate the electronic matrix elements mentioned.

20. Our treatment has assumed that all normal modes are harmonic and that the electronic wavefunctions depend linearly on the normal coordinates. The relaxation of these restrictions will effect both matrix elements. The emphasis here is on the matrix element ratio, which will be less sensitive to these higher order effects than the individual matrix elements themselves.

C. LINE BROADENING IN SOME EXCITED STATES OF BENZENE

1. Introduction

Radiationless transitions and line broadening in excited electronic states are intimately related as a moments reflection will reveal. The excited state lifetime $\Delta\tau$ and the spectral line width ΔE are linked via the uncertainty principle so that

$$\Delta E = \frac{\hbar}{\Delta\tau} \quad . \tag{1}$$

The lifetime $\Delta\tau$ may in general be divided into two parts, τ_{rad} due to the radiative depletion of the excited state and τ_{nonrad} due to all of the radiationless processes:[1]

$$\frac{1}{\Delta\tau} = \frac{1}{\tau_{rad}} + \frac{1}{\tau_{nonrad}} \quad . \tag{2}$$

In most cases one of the two terms in Eq. (2) will dominate and the measured line-broadening or lifetime may be spoken of as purely radiative or purely non-radiative. For example, the emission lines from an excited atom isolated in space will exhibit pure radiative broadening since the only possible radiationless process for this system, that of collisional deactivation, cannot occur in isolated atoms.

For the upper non-emitting excited states of large molecules on the other hand the line broadening is dominated by nonradiative processes. These radiationless processes in molecular electronic excited states other than the lowest one of a given multiplicity are so

rapid that one may state as a general rule that emission is only observed from the lowest state of a given multiplicity.[2] Only three possible exceptions to this rule are known at present.[3] Along with this rule concerning the possible emitting and non-emitting electronic states of large molecules, necessarily goes another rule about line broadening in excited states. This second rule states that the absorption lines of a non-emitting electronic state are broad.[4] It can be seen to be a natural consequence of the first rule and Eq. (1).

Here we wish to discuss line broadening processes in some of the excited states of benzene. In the next section we discuss the theory of line broadening in large molecules as it has recently been developed. In Section 3 the results of calculations on four excited states of benzene are presented and in Section 4 these calculated values for the excited state line broadening are discussed and compared with experiment.

2. The Theory of Line Broadening

As was emphasized in the introduction the theory of line broadening and the theory of radiationless transitions are intimately connected. The presently accepted theory of radiationless transitions in large molecules[5, 6] envisions the nonradiative process as a conversion of excitation from an initially prepared vibrationless excited electronic state to the quasi-continuum of states formed by the vibrational sublevels of some lower excited electronic state. The subsequent vibrational relaxation is rapid and does not enter into the

discussion. The line broadening is consequently due to the interaction of the initially prepared discrete state and the quasi-continuum. We ignore any contributions to the radiationless transition rate from predissociation or photoreaction of the excited state. This is not necessary and these additional processes can very easily be fit into the formalism developed below.

In developing an expression for the half-width of a non-radiatively broadened line, we will follow very closely the treatment of Fano[7] as adapted by Bixon and Jortner.[6] Consider two sets of states:

a) a single discrete state φ

b) a quasi-continuum of states ψ_i

and assume that these states have been normalized so that

$$\left.\begin{aligned} \langle \varphi | \varphi \rangle &= 1 \\ \langle \varphi | \psi_i \rangle &= 0 \\ \langle \psi_i | \psi_j \rangle &= \delta_{ij} \end{aligned}\right\} \qquad (3)$$

Also assume that the states φ and ψ_i have been chosen to be eigenstates of some zero-order Hamiltonian

$$\left.\begin{aligned} \langle \varphi | H^o | \varphi \rangle &= E^o_{\varphi} \\ \langle \psi_i | H^o | \psi_j \rangle &= E^o_i \delta_{ij} \\ \langle \varphi | H^o | \psi_j \rangle &= 0 \end{aligned}\right\} \qquad (4)$$

where the total Hamiltonian for the system may be written

$$H = H^0 + H_{INT} \quad . \tag{5}$$

The interaction term H_{INT} mixes the discrete state with the quasi-continuum states:

$$\left.\begin{aligned} \langle \varphi | H_{INT} | \varphi \rangle &= E_{\varphi}^{INT} \\ \langle \psi_i | H_{INT} | \psi_j \rangle &= E_{ij}^{INT} \\ \langle \varphi | H_{INT} | \psi_i \rangle &= V_i^{INT} \end{aligned}\right\} \tag{6}$$

The eigenvectors of the coupled system, i.e., eigenvectors of H given by Eq. (5), may be written

$$\Psi_m = a_m \varphi + \sum_{i=0}^{\infty} b_m^i \psi_i \quad . \tag{7}$$

Multiplying Eq. (7) through by $\varphi^* H$ and integrating gives

$$a_m (E_{\varphi}^0 + E_{\varphi}^{INT}) + \sum_{i=0}^{\infty} b_m^i V_i^{INT} = E_m a_m \quad . \tag{8a}$$

Similarly multiplying by $\psi_i^* H$ and integrating yields

$$a_m V_i^{INT*} + b_m^i (E_i^0 + E_{ii}^{INT}) + \sum_{j \neq i} b_m^j E_{ij}^{INT} = E_m b_m^i \quad . \tag{8b}$$

The two Eq. (8) are a set of coupled equations for the coefficients a_m and b_m^i. To make the solution of Eq. (8) simpler without any real loss of generality, we will assume that H^{INT} does not connect different states in the quasi-continuum, that is that $E_{ij}^{INT} = 0$. This simplification requires only that the set of states $\{\psi_i\}$ be a complete set. In

addition we will define

$$E_i \equiv E_i^0 + E_{ii}^{INT}$$

$$E_\varphi \equiv E_\varphi^0 + E_\varphi^{INT} \quad .$$

Solving Eq. (8b) for b_m^i we then obtain

$$b_m^i = \frac{a_m V_i^{INT*}}{E_m - E_i} \quad . \tag{9}$$

This equation blows up if $E_i = E_m$ and at this point we will assume for simplicity that for no $\underline{i}$ are the two energies equal. Actually one does not have to worry about this problem.[8]

Using Eq. (9) in Eq. (8a), we finally obtain

$$E_m = E_\varphi + \sum_{i=0}^{\infty} \frac{|V_i^{INT}|^2}{E_m - E_i} \quad . \tag{10}$$

The coefficient a_k which factors out of Eq. (11) (or rather its modulus, the phase is arbitrary for our purposes) is determined by normalization of the Ψ_m. This normalization yields

$$|a_m|^2 = \frac{1}{1 + \sum_{i=0}^{\infty} \frac{|V_i^{INT}|^2}{(E_m - E_i)^2}} \quad . \tag{11}$$

Equation (11) is the exact expression for $|a_m|^2$, but as it stands it is impossible to evaluate. To simplify Eq. (11) we make the

assumptions (1) that all of the interaction matrix elements are equal

$$|V_{INT}|^2 = |V_i^{INT}|^2$$

for all $\underline{i}$, and (2) that the quasi-continuum states are equally spaced so that

$$E_i = E_\varphi + \frac{i}{\rho}$$

where $\underline{i}$ is an integer ranging from $-\infty$ to ∞. The separation between quasi-continuum states is given by $1/\rho$ and ρ is thus the density of quasi-continuum states. With these assumptions and a little algebra[6] one arrives at the following expression for the coefficient a_m

$$|a_m|^2 = \frac{|V_{INT}|^2}{\{|V_{INT}|^2 + |V_{INT}|^4 \rho^2\pi^2 + (E_m - E_\varphi)^2\}} \quad . \tag{12}$$

Equation (12) describes a Lorentzian lineshape as a function of E_m with half-width

$$\Delta E_{\frac{1}{2}} = [\,|V_{INT}|^2 + (\pi |V_{INT}|^2 \rho)^2\,]^{\frac{1}{2}} \tag{13}$$

which simplifies to

$$\Delta E_{\frac{1}{2}} = \pi |V_{INT}|^2 \rho \tag{14}$$

if $|V_{INT}| \gg 1/\rho$.

Equations (13) and (14) are the ultimate goals of the above derivation and it is these expressions that will be used in what follows to calculate the nonradiatively broadened half-widths. Before we

proceed, however, it might be instructive to consider an alternative derivation of Eq. (14). If we go all the way back to Eq. (11) and at this point make the assumption that $|V_{INT}| \gg 1/\rho$, then the sum in Eq. (11) becomes an integral

$$|a_m|^2 = \frac{1}{1 + \int_{-\infty}^{\infty} \frac{|V_i^{INT}|^2 \rho}{(E - E_i)^2} dE} \quad . \tag{15}$$

This is equivalent to assuming that the set of states $\{\psi_i\}$ forms a true continuum. Fano's method[7] can at this point be directly used to arrive at Eq. (14) since his method specifically treats the interaction of a discrete state and a continuum.

To emphasize the unity of the treatment of line broadening given above and the treatment of radiationless transitions outlined in Secs. IIA and B and presented in more detail in Ref. 5 and 6, we can obtain the radiationless rate $\underline{k}$ from the uncertainty principle Eq. (1) and our expression for $\Delta E_{\frac{1}{2}}$ given by Eq. (14). Replacing ΔE by $2\Delta E_{\frac{1}{2}}$ and $1/\Delta\tau$ by $\underline{k}$ in Eq. (1) we have for $\underline{k}$

$$k = \frac{2\Delta E_{\frac{1}{2}}}{\hbar} = \frac{2\pi |V_{INT}|^2 \rho}{\hbar} \tag{16}$$

which is exactly the expression given in Eq. (4) of Sec. IIA. The limits of validity of Eq. (16) are also the same as in these earlier discussions, namely:

a) $|V_{INT}| = \text{const.}$ for all $\{\psi_i\}$

b) $|V_{INT}| \ll 1/\rho$

c) $\Delta\tau \ll \hbar\rho$.

This last criterion although not necessary for the derivation of Eq. (14), is necessary in deriving Eq. (16) from Eq. (14). Limit (c) is merely a restatement of the criterion for the validity of the uncertainty principle.[9]

The separation of the system into a discrete state φ and a set of quasi-continuum states $\{\psi_i\}$ is not arbitrary. If $|a_m|^2$ given by Eq. (12) is to represent the absorption lineshape, then the zero-order state φ must be chosen in such a way that the transition dipole matrix element between the excited state Ψ_m and the ground state Ψ_G must be equal to

$$\vec{\mu}_{mG} = \langle \Psi_m | \vec{\mu} | \Psi_G \rangle = a_m \langle \varphi | \vec{\mu} | \Psi_G \rangle \qquad (17)$$

which implies that

$$\langle \psi_i | \vec{\mu} | \Psi_G \rangle = 0$$

for all i. Here $\vec{\mu}$ is the electric dipole moment operator. In words Eq. (17) requires that the discrete state φ be the only zero-order state in the energy region being considered that bears any appreciable oscillator strength with the ground state. We thus have a very specific criterion for the separation of our system into φ and $\{\psi_i\}$.

3. Calculations

In this section, we calculate the line broadening in some of the excited electronic states of benzene due to interaction with other lower energy electronic states. In Fig. 1 we list the positions of a few of the lower electronic levels. The position of all of the levels in Fig. 1 are accurately known except for the third triplet $^3B_{2u}$. The indicated position of this level is the one obtained from very recent low energy electron impact studies.[10] Its experimental position is in reasonable agreement with theoretical calculations.[11]

The line-broadening Eq. (14) will be used in these calculations and we will verify its validity for each electronic level by making sure that $|V_{INT}|\rho \gg 1$. In those cases where Eq. (14) is not valid, Eq. (13) will be used. To make the calculation of $\Delta E_{\frac{1}{2}}$ possible and to provide a connection between the present calculation and the calculation of radiationless transition rates presented in Sec. IIA, we will rewrite the interaction matrix element

$$|V_{INT}|^2 = \beta^2 \overline{F} \tag{18}$$

where β is an electronic coupling matrix element and $\overline{F}$ is an average Franck-Condon factor. Both β and $\overline{F}$ are very thoroughly described in Sec. IIA. Using Eq. (15) the expression for the half-width $\Delta E_{\frac{1}{2}}$ becomes

$$\Delta E_{\frac{1}{2}} = \pi\beta^2 \overline{F}\, \rho \tag{19}$$

To calculate the Franck-Condon factor $\overline{F}$ for two electronic

Figure 1. Electronic energy levels of benzene. (a) G. Scheibe, F. Povenz and C. Linstrom, Z. Phys. Chem. B20, 283 (1933); L. W. Pickett, M. Muntz, and E. M. McPherson, J. Am. Chem. Soc. 73, 4862 (1951); T. M. Dunn and C. K. Ingold, Nature 176, 65 (1955); (b) E. R. Bernstein, S. D. Colson, D. S. Tinti, and G. W. Robinson, J. Chem. Phys. 48, 4632 (1968); (c) J. P. Doering, manuscript to be published; the position in the figure is 2000 cm^{-1} less than the Franck-Condon maximum determined in Doering's low energy electron impact experiments; (d) S. D. Colson and E. R. Bernstein, J. Chem. Phys. 43, 2661 (1965); Part IV of this thesis.

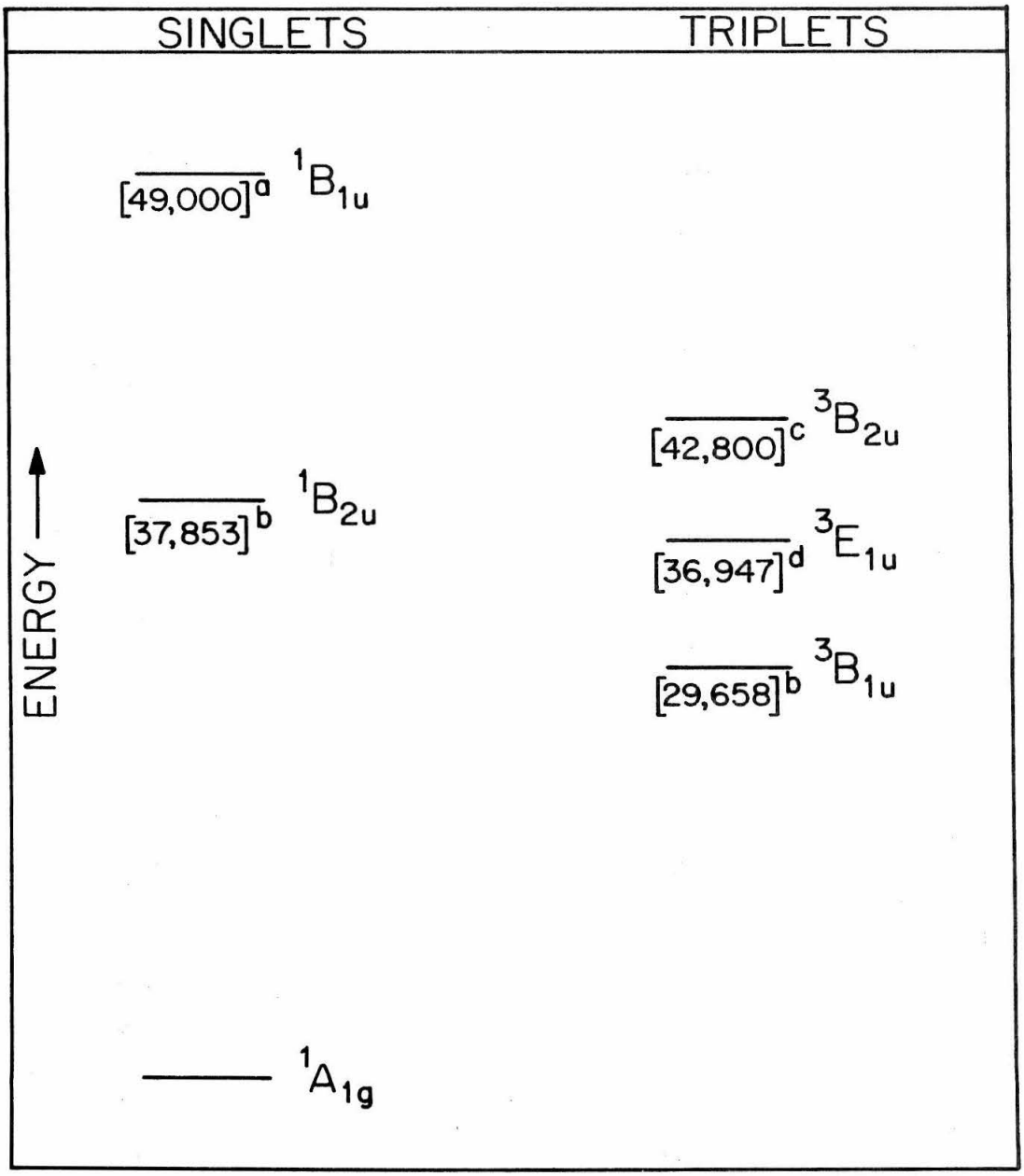
SINGLETS
TRIPLETS
ENERGY
[49,000]a
1B1u
[37,853]b
1B2u
[42,800]c
3B2u
[36,947]d
3E1u
[29,658]b
3B1u
1A1g

states one needs to know the bond lengths of the molecule in each state as well as all of the vibrational frequencies in both states. We do not know these experimental parameters for all of the benzene excited states. In fact the $^1B_{2u}$ states is the only excited state for which the necessary vibrational frequencies[12] and bond lengths[13] are known. We will therefore assume in calculating $\overline{F}$ that these parameters for any two interacting states are the same as they are for the $^1B_{2u}$ - $^1A_{1g}$ states. This means that we can directly use the Franck-Condon factors calculated in Section IIA. In using the results of Section IIA, we will make the approximation that the differences in bond lengths δ between two excited states of benzene are equal for all pairs of excited states. That this is not too unreasonable can be seen from Table I. In Table I we have listed theoretically calculated values for the increase in carbon-carbon bond length upon going from the $^1A_{1g}$ level to a number of excited state levels. In all cases these changes fall within the narrow range $.032 \pm .008$ Å.

The assumption that the excited state vibrational frequencies change from state to state in exactly the same ratio as the change found for the $^1A_{1g}$ - $^1B_{2u}$ states is probably the worst of the many simplifying assumptions that are made in these line broadening calculations. Even this assumption for excitation levels less than 10 quanta/normal mode will introduce inaccuracies in $\overline{F}$ of less than a factor of 10.[14]

For calculating ρ we will use the ground state vibrational frequencies and the method described in Sec. IIA and Appendix C.[15] The energy difference between any two states can be determined from the energy level values collected in Fig. 1. The electronic matrix elements are chosen from the theoretical calculation of Albrecht.[16]

TABLE I. Bond length changes in several excited states of Benzene.[a]

State	Bond Length Change (Å)
$^1A_{1g}$	Reference Level
$^1B_{2u}$	.038
$^1B_{1u}$	.027
$^1E_{1u}$	.033
$^3B_{1u}$	.030
$^3E_{1u}$	.039
$^3B_{2u}$	.024

[a]From a calculation by E. F. McCoy and I. G. Ross, Austral. J. Chem. 15, 533 (1962).

The results of the calculation of $\Delta E_{\frac{1}{2}}$ are listed in Table II along with the various parameters that were used. Whenever $|V_{INT}|\rho \ll 1$ does not apply Eq. (13) has been used in addition to Eq. (14) for calculating $\Delta E_{\frac{1}{2}}$.

4. Discussion and Comparison with Experiment

The line-broadening calculations summarized in Table II indicate that of the benzene levels treated only the $^3E_{1u}$ and $^1B_{1u}$ levels will be noticeably broadened by interaction with other lower lying electronic states. In Fig. 2 a comparison of the $^1B_{2u} \leftarrow {}^1A_{1g}$ and $^1B_{1u} \leftarrow {}^1A_{1g}$ gas phase absorptions is made. The line broadening of the $^1B_{1u}$ level is quite apparent when compared with the instrument limited $^1B_{2u}$ line-widths. Similarly in Fig. 3 we present the crystal phase absorptions $^3B_{1u} \leftarrow {}^1A_{1g}$ and $^3E_{1u} \leftarrow {}^1A_{1g}$ as determined in Sections III and IV of this thesis. Again the increased line broadening is quite apparent. In fact no structure at all is observed in the $^3E_{1u}$ spectra consistent with the predicted 440 cm^{-1} half-width of each absorption line.

For benzene, these calculations reveal that the second excited electronic state of a given multiplicity is broadened only by the nearest lower state of the same multiplicity. Lower states of different multiplicity have no effect on the line-width. Furthermore, as Table II indicates the lowest singlet and triplet states are not significantly broadened by interaction with the ground $^1A_{1g}$ level. One might expect this for the $^3B_{1u}$ level because of the spin prohibition factor in β_{el}, but the $^1B_{2u} - {}^1A_{1g}$ result although not surprising is quite interesting and points the way towards a theoretical explanation of the general

TABLE II. Calculated line broadening values for several benzene excited states.

Interacting States	Energy Gap (cm^{-1})	ρ (cm^{-1})	$\beta_{el.}$ (cm.)	$\overline{F}$	$\Delta E_{\frac{1}{2}}$ [Eq. (14)] (cm^{-1})	$\lvert V_{INT} \rvert \rho$	$\Delta E_{\frac{1}{2}}$ [Eq. (13)] (cm^{-1})
$^3B_{1u}$ - $^1A_{1g}$	29,658	2.7×10^{11}	.16	1.06×10^{-26}	2.3×10^{-17}	4.3×10^{-3}	1.6×10^{-14}
$^1B_{2u}$ - $^1A_{1g}$	37,853	2.7×10^{13}	4000	6.30×10^{-32}	8.7×10^{-11}	27	--
$^1B_{2u}$ - $^3B_{1u}$	8,195	1.5×10^{3}	.23	1.79×10^{-8}	4.4×10^{-6}	4.5×10^{-2}	3.1×10^{-5}
$^3B_{1u}$ - $^3E_{1u}$	7,289	2.4×10^{2}	2178	1.26×10^{-7}	440	190	--
$^1B_{1u}$ - $^1B_{2u}$	11,147	6.0×10^{4}	4000	2.84×10^{-11}	87	1300	--
$^1B_{2u}$ - $^3E_{1u}$	906	0	--	--	0	--	--

Figure 2. A comparison of the $^1B_{2u} \leftarrow {}^1A_{1g}$ and $^1B_{1u} \leftarrow {}^1A_{1g}$ gas phase absorption spectra. The $^1B_{2u}$ spectrum was obtained by M. Bertolucci and the $^1B_{1u}$ spectrum by J. H. Smith. I am indebted to both of them for allowing me to use their spectra.

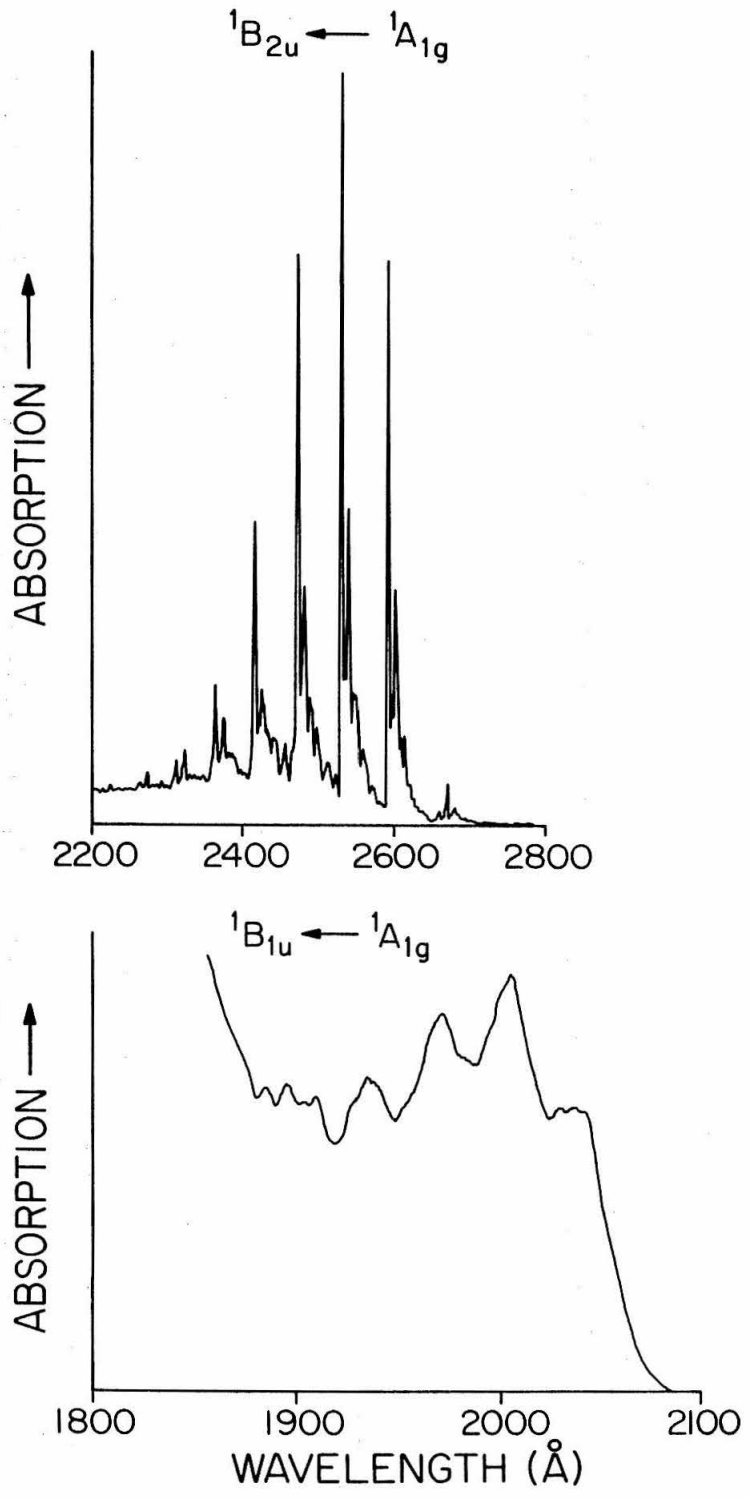
$^1B_{2u} \leftarrow {}^1A_{1g}$
ABSORPTION
2200
2400
2600
2800
$^1B_{1u} \leftarrow {}^1A_{1g}$
ABSORPTION
1800
1900
2000
2100
WAVELENGTH (Å)

Figure 3. A comparison of the $^3B_{1u} \leftarrow {}^1A_{1g}$ and $^3E_{1u} \leftarrow {}^1A_{1g}$ absorption spectra of crystalline benzene.

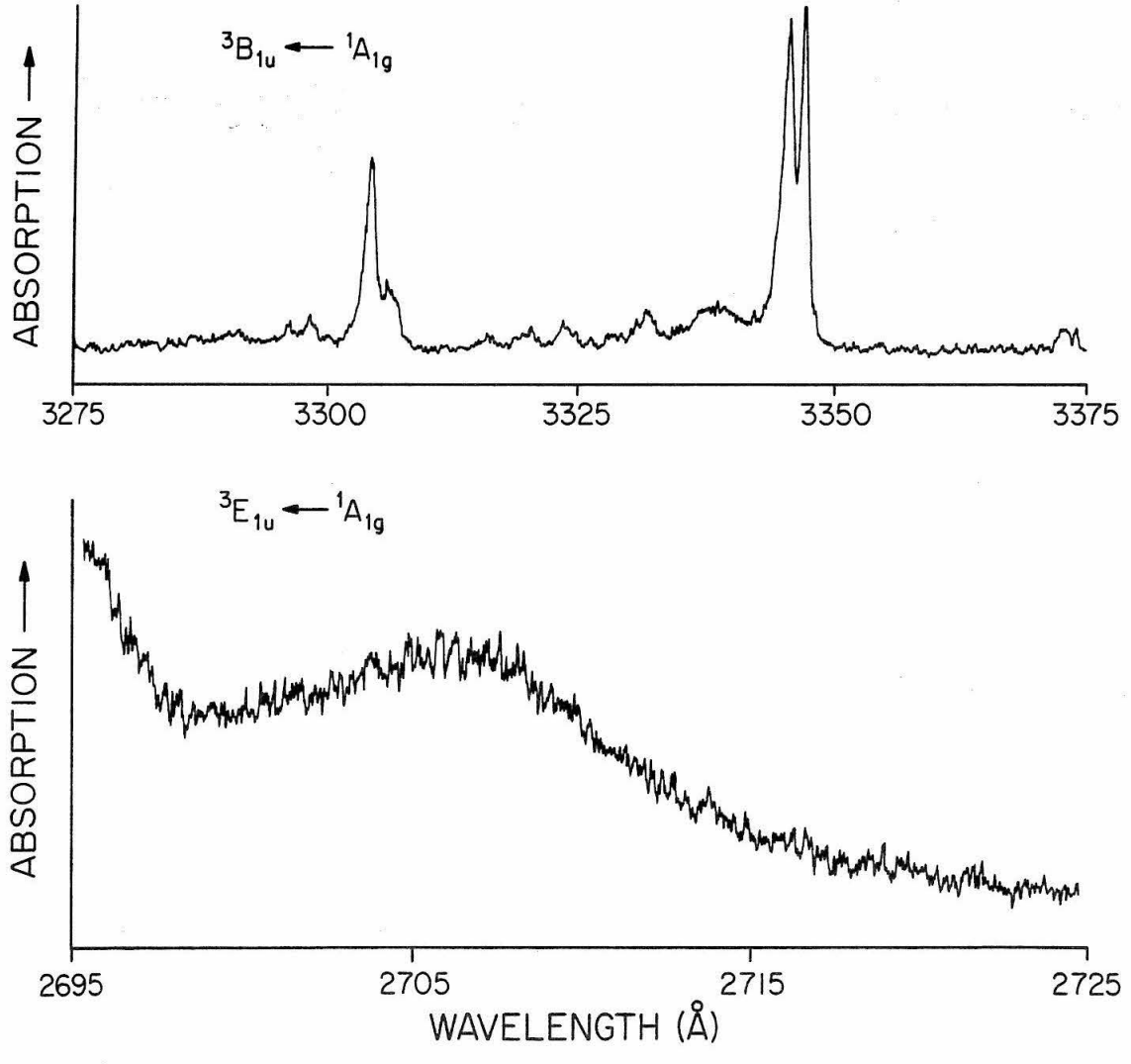
$^3B_{1u} \leftarrow {}^1A_{1g}$
ABSORPTION
3275
3300
3325
3350
3375
$^3E_{1u} \leftarrow {}^1A_{1g}$
ABSORPTION
2695
2705
2715
2725
WAVELENGTH (Å)

rules given in the introduction. The linewidth given by Eq. (14) involves two factors that depend on the magnitude of the energy gap, the average Franck-Condon factor $\overline{F}$ and the density of states ρ. The Franck-Condon factor $\overline{F}$ decreases much more rapidly with energy than the density of states increases. This means of course that there is a net decrease in the line broadening due to a lower state of the same multiplicity as the distance between the two interacting states increases. From the calculated linewidths $\Delta E_{\frac{1}{2}}$ it can be seen that the line broadening is negligible for states separated by more than about $20,000\ cm^{-1}$. This conclusion should apply to all benzene levels and in a more qualitative way to other molecules. As a rule the lowest excited singlet state of an aromatic molecule has an energy greater than $20,000\ cm^{-1}$ and consequently the lines of the absorption spectrum are sharp. The spacing between excited states of the same multiplicity on the other hand are in the $10,000\ cm^{-1}$ region which means that these states will have several hundred cm^{-1} broad absorption lines. To the extent that these results can be applied to molecules other than benzene we thus have an explanation of the general rule that excited states other than the lowest one of a given multiplicity have broad absorption spectra.

The extension of the conclusions drawn from these calculations on benzene to other molecules should be done with some caution. The density of states function ρ and the average Franck-Condon $\overline{F}$ depend on the number and types of normal modes present in the particular molecule under consideration. Furthermore, β_{el} can vary significantly from molecule to molecule and within a given molecule from

transition to transition.

Finally, we will consider the implications of the present calculations for the $^1B_{2u} \rightsquigarrow {}^3B_{1u}$ radiationless process. Fluorescence quantum yield measurements indicate that at low pressures in the gas phase about 61% of the excitation energy absorbed by the singlet reaches the lowest triplet.[17] There are two possible paths for this triplet population process:

$$^1B_{2u} \xrightarrow{k_1} {}^3E_{1u} \xrightarrow{k_2} {}^3B_{1u} \qquad \text{(a)}$$

$$^1B_{2u} \xrightarrow{k_3} {}^3B_{1u} \qquad \text{(b)}$$

The rate constant k may be calculated from Eq. (16).[18] Using Table II these values are

$$k_1 = 0$$

$$k_2 = 7.2 \times 10^{13} \text{ sec}^{-1}$$

$$k_3 = 1.2 \times 10^{7} \text{ sec}^{-1}$$

The calculated rates imply that process (b) is the most important means of depleting the excited singlet. The radiative rate k_f for the process $^1B_{2u} \rightarrow {}^1A_{1g}$ is 1.5×10^6 sec^{-1} in the gas phase.[19] Process (b) can thus easily compete with fluorescence.

The indirect process (a) should not be completely ruled out by these calculations however. The $^3E_{1u}$ density of states ρ is zero at an energy equal to that of the $^1B_{2u}$ only if the states are discrete. Our calculations (Table II) and the experimental results[20] indicate that the

$^3E_{1u}$ lines are actually quite broad. If these broad lines should overlap the $^1B_{2u}$ state, it is possible for $k_1 \neq 0$.

5. Conclusions

The line broadening calculations presented in this section are in very good agreement with the experimentally observed linewidths for benzene. This agreement provides very convincing evidence that line broadening in the excited states of large molecules involves a coupling with equi-energetic vibronic levels of lower electronic states. We have also indicated the very close connection between radiationless transitions and line broadening. A study of one necessarily yields important information about the other. In this context we have used the line broadening calculations to illucidate the radiationless intersystem crossing process $^1B_{2u} \rightsquigarrow {}^3B_{1u}$.

REFERENCES

1. The limits within which it is appropriate to separate radiative and non-radiative lifetimes are discussed by D. P. Chock, J. Jortner, and S. A. Rice, J. Chem. Phys. 49, 610 (1968).
2. M. Kasha, Disc. Fara. Soc. 9, 14 (1950).
3. These three possible exceptions are azulene [M. Beer and H. C. Longuet-Higgins, J. Chem. Phys. 23, 1390 (1955); M. Kasha and G. Viswanath, J. Chem. Phys. 24, 574 (1956)]; ferrocene [D. R. Scott and R. S. Becker, J. Chem. Phys. 35, 516 (1961)]; and Hafner's hydrocarbons [R. C. Dhingra and J. A. Poole, J. Chem. Phys. 48, 4829 (1968)].
4. R. M. Hochstrasser and C. Marzzacco, J. Chem. Phys. 49, 971 (1968); R. M. Hochstrasser, Acct. Chem. Res. 1, 266 (1968).
5. G. W. Robinson and R. P. Frosch, J. Chem. Phys. 37, 1962 (1962); ibid. 38, 1187 (1963); G. R. Hunt, E. F. McCoy, and I. G. Ross, Australian J. Chem. 15, 591 (1962).
6. M. Bixon and J. Jortner, J. Chem. Phys. 48, 715 (1968).
7. U. Fano, Phys. Rev. 124, 1866 (1961).
8. It can be shown that the new eigenvalues E_m will always fall between two old eigenvalues E_i so that the denominator in Eq. (9) will never be zero. See Ref. 6 for a further discussion of this point.
9. To be able to speak of a meaningful radiationless lifetime $\Delta\tau$, the decay of the excited state must be exponential. Restriction (c) indicates the time range within which the decay may be considered

exponential. For transitions satisfying this condition the uncertainty principle accurately describes the relationship between lifetimes and linewidth. If criterion (c) is not satisfied, we may still determine the line broadening from Eq. (13) or (14) but one cannot simply relate this linewidth to the radiationless lifetime.

10. J. P. Doering, to be published.

11. Theoretically it has been predicted that the distance from the $^3E_{1u}$ level to either of the other two triplets should be equal [R. Pariser, J. Chem. Phys. 24, 250 (1956)]. This prediction is in good agreement with the experimental results summarized in Fig. 1.

12. See Table V of Section IIA.

13. D. P. Craig, J. Chem. Soc. 1950, 2146; J. H. Callomon, T. M. Dunn, and I. M. Mills, Phil, Trans. Roy. Soc. London A259, 499 (1966).

14. The dependence of the Franck-Condon factors on the vibrational frequency change is treated in Appendix B.

15. Not all of the states ρ contribute to the radiationless transition rate. Symmetry restricts the number of states in benzene to $1/16^{\underline{th}}$ of ρ (see Sec. IIA). When we speak of ρ in this section we mean the total density of states divided by 16.

16. A. C. Albrecht, J. Chem. Phys. 38, 354 (1963).

17. E. M. Anderson and G. B. Kristiakowsky, J. Chem. Phys. 48, 4787 (1968); 51, 182 (1969); A. E. Douglas and C. W. Matthews, J. Chem. Phys. 48, 4788 (1968).

18. The rate k_3 calculated in this section should be viewed with some caution since $\hbar\rho \approx 10^{-9}$ sec. Strictly speaking, this means that Eq. (16) is only valid for calculating rates for processes that occur faster than 10^{-9} sec. The process described by k_3 occurs in 10^{-7} sec. We will assume, however, that k_3 calculated from Eq. (16) is appropriate for describing the $^1B_{2u} \rightsquigarrow {}^3B_{1u}$ process. One reason for apparently ignoring the criterion $\Delta\tau \ll \hbar\rho$ is the uncertainty in the exact value to use for ρ. It is not necessarily true that the value of ρ to be used in this situation is the same value as the one used in calculating $\Delta E_{\frac{1}{2}}$. It is quite likely that the ρ appropriate for use in the irreversibility criterion for the validity of Eq. (16) includes lattice modes for a solid and translational and rotational degrees of freedom for a gas or liquid.

19. J. W. Donovan and A. B. F. Duncan, J. Chem. Phys. 35, 1389 (1961).

20. Section IV of this thesis and S. D. Colson and E. R. Bernstein, J. Chem. Phys. 43, 2661 (1965).

PART III

THE $^3B_{1u} \leftarrow {}^1A_{1g}$ ABSORPTION SPECTRA OF BENZENE AND PERDEUTEROBENZENE

A. EXPERIMENTAL OBSERVATION OF SINGLET-TRIPLET ABSORPTION IN PURE CRYSTALLINE BENZENE

1. Introduction

Spin-orbit coupling is extremely inefficient in aromatic molecules like benzene, naphthalene, and anthracene.[1] Experimentally, this results in relatively long lifetimes for aromatic hydrocarbon triplet states in solid matrices[2] and extremely weak singlet-triplet absorptions.[3] Direct singlet-triplet absorptions have recently been observed for anthracene[3a] and naphthalene.[3b] However, prior to this work no absorption attributable to the lowest singlet-triplet transition ($^3B_{1u} \leftarrow {}^1A_{1g}$) has been observed for pure benzene although it has been searched for in 5-cm thick crystals at 4.2° K[4a] and in 22.5 m of liquid at 298° K.[4b] The $^3B_{1u} \leftarrow {}^1A_{1g}$ absorption has been observed for oxygen-perturbed benzene in both crystal[4a] and gas phases.[5] The oxygen perturbation technique however has the disadvantage of broadening the absorption and thus masking any detailed structure.

Direct singlet-triplet absorption measurements are more difficult for benzene than for naphthalene or anthracene not only because of the less ideal spectral region but also because the oscillator strength for the transition in benzene is weaker than in the other materials, being both spin and symmetry forbidden in the free molecule. Furthermore, as the present experiments will show, the singlet-triplet absorption spectrum in benzene is broader than the corresponding naphthalene[6b] and anthracene[3a] spectra making detection even more difficult.

An extremely sensitive indirect technique, the photoexcitation

method, has recently been used to obtain the singlet-triplet absorption spectra of a variety of aromatic hydrocarbons.[6,7] Instead of attempting to detect a small change in a very strong signal, as in the direct absorption method, the photoexcitation technique involves monitoring the delayed emission (phosphorescence or delayed fluorescence) that results from absorption. The problem of observing weak absorptions using the photoexcitation method thus reduces to one of detecting very weak emission. This problem is much easier to solve instrumentally than the problems that arise in the direct absorption method.

The success that the method of photoexcitation has had with anthracene[6a] and naphthalene[6b] encouraged us to attempt to observe the $^3B_{1u} \leftarrow {}^1A_{1g}$ transition in benzene at 4.2° K by this method. This transition is of interest for several reasons. An analysis of the factor-group splitting in the spectrum can yield valuable information on the nature of intermolecular interactions in these crystals. In addition the $^3B_{1u}$ state of benzene is distorted from hexagonal symmetry by a pseudo-Jahn-Teller interaction.[8,9] It is of interest to see how this distortion affects the absorption spectrum since the frequencies and intensities of the molecular vibrations of the triplet state itself are obtained, in contrast to the phosphorescence measurements that give direct information about the vibrationless triplet level only.

In this section we report the $^3B_{1u} \leftarrow {}^1A_{1g}$ high resolution absorption spectra of pure benzene and benzene-d_6 crystals using the phosphorescence photoexcitation technique.[7,10] We have observed factor-group splitting in the $^3B_{1u}$ state and have also obtained further evidence that the lowest triplet of benzene is non-hexagonal.

2. Experimental

a. Apparatus

The apparatus used in these experiments is shown schematically in Fig. 1. The light source is a high-intensity dc xenon lamp (an Osram XBO-6500 lamp operated at 4500 w). The exciting light from this lamp passes through the fused-quartz collimating Lens A and through two preliminary filters A and B. Filter A is a 10-cm path-length H_2O filter that removes much of the infrared radiation from the excitation beam, protecting subsequent parts of the system from damage due to excessive heating. Filter B is a 7-54 Corning glass filter which narrows the exciting bandwidth to the region 2400-4000 Å.[11] Lens B is a fused-quartz lens placed so that the grating in the spectrometer is completely filled for maximum instrumental resolving power. A Jarrell-Ash 1.8-m Ebert scanning spectrometer is used in the third order as a monochromator. The large dispersion of this instrument allows excitation of the sample with light of from 0.1 to 0.3 Å bandwidth for spectrometer slits between 50 and 150 μ. In the region of the benzene triplet (3300 Å) the optimum energy resolution of our system with 50 μ slits is about 1 cm^{-1}.

It is very important that Lenses C and D, which focus the monochromatic light on the sample, be Pyrex so that they can act as a final filtering stage to remove the 2500 Å light that comes through the spectrometer in fourth order. Without this final filtering the fourth-order light can excite the benzene singlet. Singlet excitation can cross to the triplet state resulting in unwanted phosphorescence

Figure 1. Diagram of experimental apparatus. Lenses A, B, E and F are fused quartz, lenses C and D Pyrex. Filter A is an H_2O filter, B a Corning glass 7-54 filter and C p-dimethyl-aminobenzaldehyde in methanol.

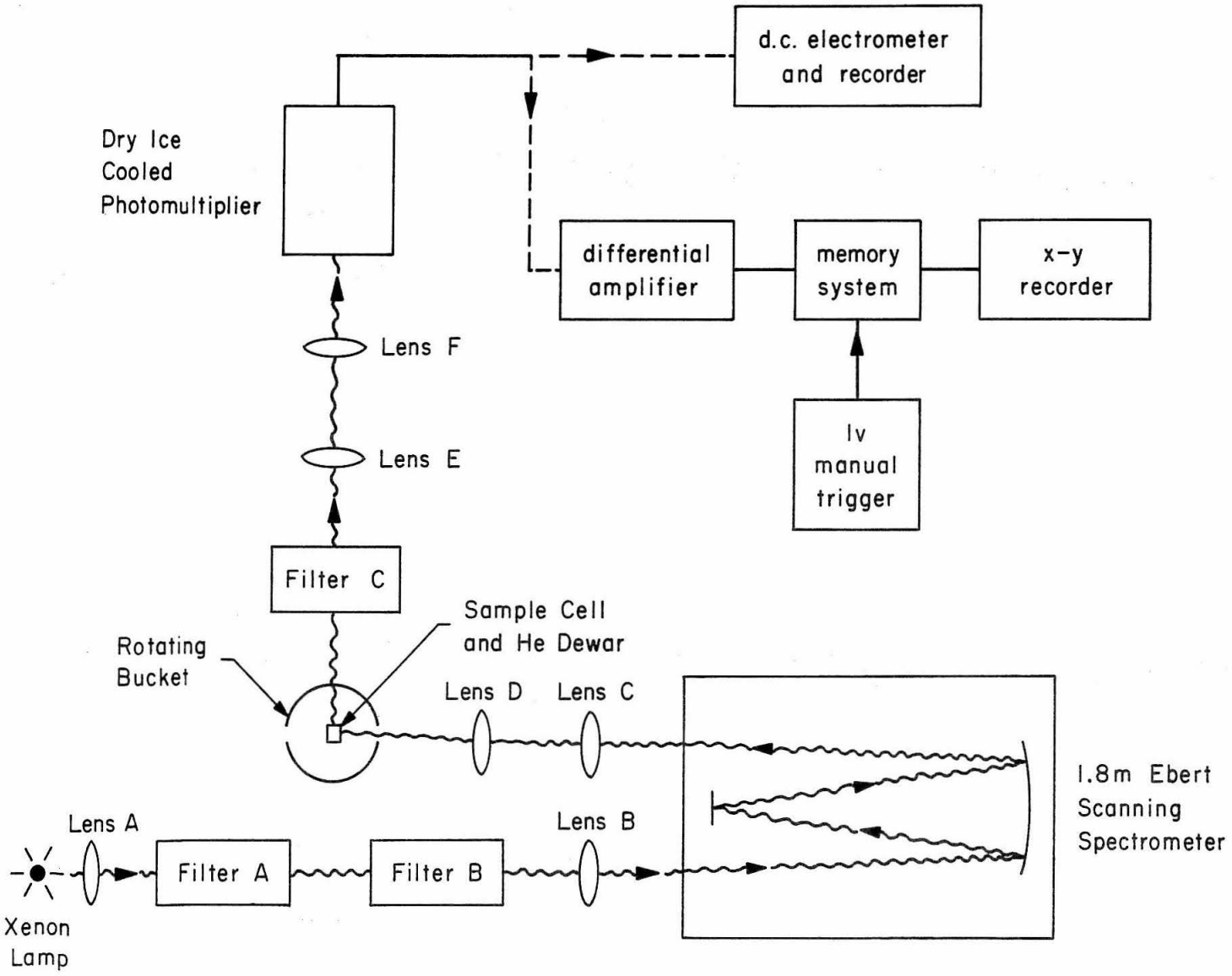
d.c. electrometer and recorder
Dry Ice Cooled Photomultiplier
differential amplifier
memory system
x-y recorder
Lens F
Lens E
Iv manual trigger
Filter C
Sample Cell and He Dewar
Rotating Bucket
Lens D
Lens C
1.8m Ebert Scanning Spectrometer
Lens A
Lens B
Filter A
Filter B
Xenon Lamp

that cannot be distinguished from the phosphorescence due to direct excitation of the triplet state with third-order light.

The benzene crystal is placed inside a liquid helium dewar and the dewar is mounted in a 1200 rpm rotating can with two slots 180° apart permitting the sample to view alternately the exciting light and the photocathode. The delayed emission from the sample passes through Filter C which eliminates any scattered exciting light. Filter C is a 1-cm pathlength cell filled with a solution of 0.025 g/liter of p-dimethylaminobenzaldehyde in methanol.[12] Fused-quartz Lenses E and F together focus the emission from the sample on the photocathode.

The photomultiplier tube is an EMI 6256S selected for low dark current and cooled to dry-ice temperature. Signals from the photomultiplier were treated in two ways. For general surveys of the absorption spectra (resolution 3-7 cm^{-1}) with slitwidths of 75 μ or greater the signal was fed into a dc electrometer and displayed on a strip-chart recorder. For higher resolution scans (50 μ slits and a resolution of 1 cm^{-1}) of narrow and weak regions of the spectrum, the signal was fed into a differential amplifier and then into a memory system (Nuclear Data-180ITB and -180 FM) operating in a multichannel scaling mode. The spectrometer was scanned through the region of interest at 1 Å/min. The memory was simultaneously scanned through 512 channels at 1 channel/sec so that the wavelength range of each scan through the memory was 8.5 Å. The memory scan was initiated by a manual trigger. Most of the weak absorption lines observed in this way could be resolved with a signal/noise ratio of

3:1 or better after 15-20 scans of the memory. The contents of the memory were displayed on an x-y recorder.

b. Purification and Growth of Crystals

The method of purifying the benzene crystals has been described in detail before.[4a] For the initial experiments on C_6H_6, Phillips Petroleum Company research grade benzene, refluxed twice over Cs metal at 100° C for 6 h, was used. The pure benzene was transferred under vacuum to a crystal-growing tube. It was found with subsequent samples that this double Cs-purification was unnecessary and consequently most of the work reported here was done on C_6H_6 and C_6D_6 samples that were refluxed only once over Cs. The C_6D_6 (99.5% deuterium) was obtained from Merck, Sharp and Dohme of Canada, Ltd. The crystals were grown across a sharp temperature gradient into liquid nitrogen as described previously.[13] The sample cells were modified "Bridgman type" tubes of 0.5-cm thickness.

c. The Phosphorescence System

Benzene-$\underline{h}_6$ crystals grown and purified as described in Section IIB are free of impurity absorption throughout the ultraviolet down to 2700 Å for 5-cm thick crystals at 4.2° K.[4a] At this low temperature these crystals do however exhibit delayed emission due to the trapping of excitation by residual impurities.[14a] This emission has a lifetime of about 5 sec and is undoubtedly phosphorescence from an impurity (probably toluene).[14b] The low oscillator strength of the impurity transition evidenced by its long lifetime accounts for the

absence of impurity absorption in the long crystal-absorption experiments. We use this naturally occurring impurity emission to monitor the pure crystal absorption spectrum of C_6H_6.[15] The photoexcitation technique used here is thus similar to that used by Castro and Robinson to obtain the singlet-triplet absorption spectrum of naphthalene.[6b]

For the C_6D_6 crystals the dominant emitting impurities are partially deuterated benzenes, $C_6H_2D_4$ and $C_6H_3D_3$. These partially deuterated impurities act as excitation traps in the C_6D_6 crystal. The C_6D_6 pure crystal absorption is monitored by detecting the phosphorescence from these isotopic traps.

3. Results

a. Analysis of the Spectra

(1) C_6H_6.

The C_6H_6 phosphorescence excitation spectrum is displayed in Fig. 2 and the measured line positions are given in Table I. The tabulated line positions are averages of measurements on three different crystals. Comparison of this spectrum with the C_6H_6 phosphorescence spectrum[13] reveals the absence of the approximate "mirror-image" relationship between absorption and emission that is so useful in assigning excited-state vibrational levels. This makes analysis of the $^3B_{1u}$ absorption spectrum difficult but at the same time extremely interesting.

The most prominent feature of the spectrum is the intense doublet located about 250 cm^{-1} from the origin. Both theory[16] and

Figure 2. C_6H_6 excitation spectrum. Intensity scale is the same for all three traces.

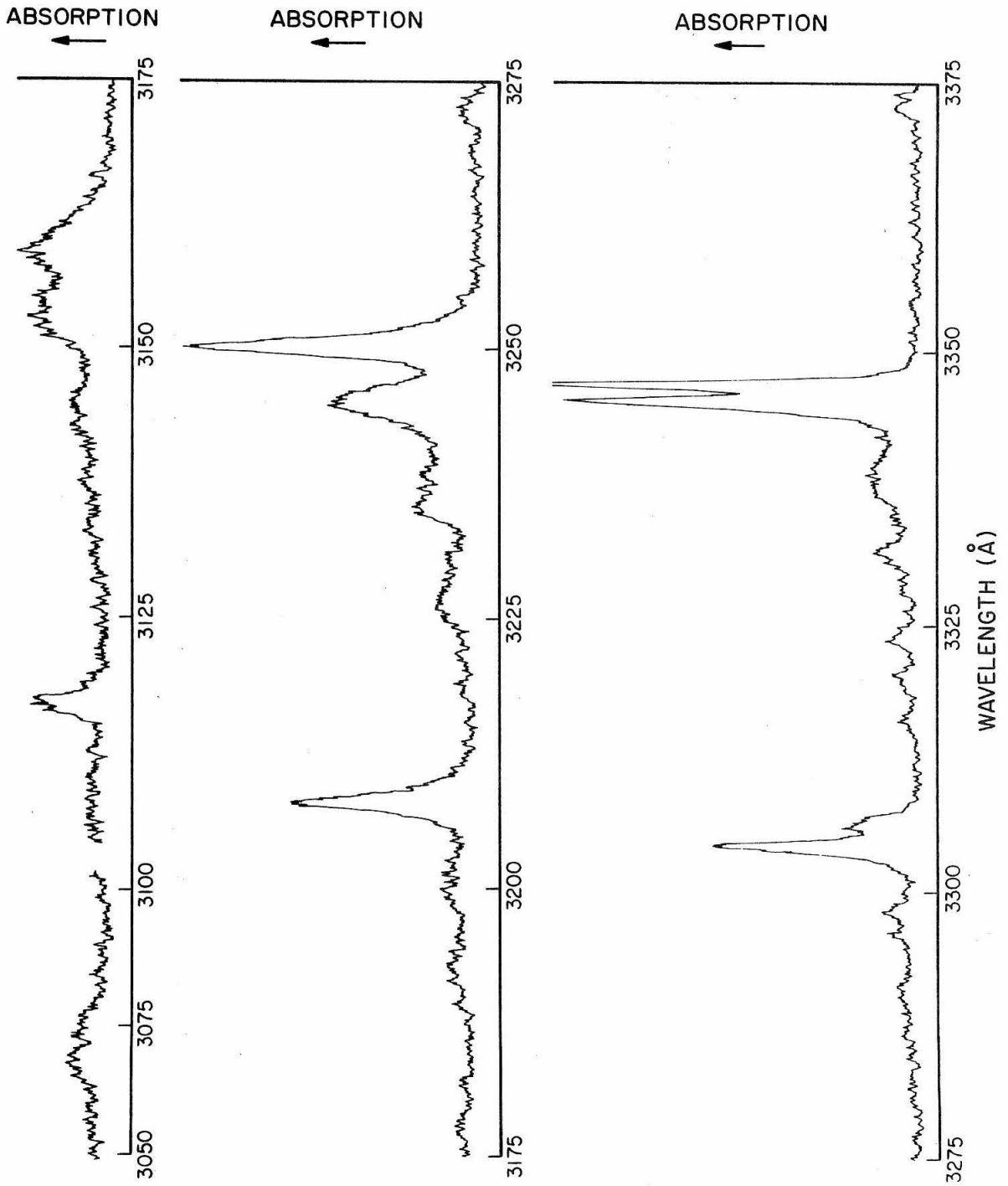
ABSORPTION
3050
3075
3100
3125
3150
3175
ABSORPTION
3175
3200
3225
3250
3275
ABSORPTION
3275
3300
3325
3350
3375
WAVELENGTH (Å)

TABLE I. Analysis of the $^3B_{1u} \leftarrow {}^1A_{1g}$ spectrum of C_6H_6.

Position λ_{air} (Å)	Position ν_{vac} (cm^{-1})	Distance from origin (cm^{-1})	Intensity[a]	Assignment[b]
3372.0	29,647 ± 5	0	VW	0-0
3345.1	29,886	239	VS	ν_8
3343.6	29,899	252	VS	
3336.5	29,963	316	W	ν_8 + phonon
3329.1	30,029	382	W	ν_4 (?)
3321.1	30,102	455	VW	
3317.6	30,134	487	VW	$2 \cdot \nu_{16}$ (?)
3313.4	30,172	525	VW	
3303.9	30,259	612	W	ν_5 (?)
3302.1	30,275	628	S	ν_6
3295.7	30,334	687	VW	ν_5 + phonon
3293.9	30,350	703	VW	ν_6 + phonon
3288.7	30,398	751	VW	
3270.0	30,572	925	VW	ν_1
3247.2	30,787	1140	VS	$\nu_8 + \nu_1$
3242.1	30,835	1188	M	ν_9
3232.0	30,932	1285	W	$\nu_8 + \nu_1$ + phonon
3222.9	31,019	1372	W	$2 \cdot \nu_{16} + \nu_1$ (?)
3204.6	31,196	1549	S	$\nu_6 + \nu_1$
3197.2	31,268	1621	VW	$\nu_6 + \nu_1$ + phonon
3190.4	31,335	1688	VW	?

TABLE I (Continued)

Position		Distance from origin (cm^{-1})	Intensity[a]	Assignment[b]
λ_{air} (Å)	ν_{vac} (cm^{-1})			
3177.9	31,458 ± 5	1811	VW	?
3174.1	31,496	1849	VW	$2 \cdot \nu_1$
3155.2	31,685	2038	W	$\nu_8 + 2 \cdot \nu_1$
3149.2	31,745	2098	W	$\nu_9 + \nu_1$
3112.7	32,117	2470	W	$\nu_6 + 2 \cdot \nu_1$
3068.8	32,577	2930	VW	$\nu_8 + 3 \cdot \nu_1$
3062.4	32,645	2998	VW	$\nu_9 + 2 \cdot \nu_1$

[a]VS = very strong, S = strong, M = moderate, W = weak, VW = very weak.

[b]Numbering of normal modes is due to E. B. Wilson, Phys. Rev. 45, 706 (1934).

experiment[13,17] indicate that the benzene normal mode most efficient at inducing the $^3B_{1u} \leftarrow {}^1A_{1g}$ transition is the doubly degenerate e_{2g} ν_8 mode[18] located at 1584 cm^{-1} in the ground state. If on this basis we assume that the 250 cm^{-1} doublet is in fact the ν_8 vibration of the triplet state we are presented with the problem of explaining why it has shifted so far from its ground state frequency. The ν_8 frequency in the lowest excited singlet ($^1B_{2u}$) state by comparison has shifted only to 1470 cm^{-1}.[19] However, van der Waals et al.[8b] have predicted just such a large shift in the ν_8 vibrational frequency due to the distortion of the $^3B_{1u}$ state (see Sec. IV). We believe that the intensity of this doublet, the fact that it is a doublet, and the agreement with the theoretical predictions all argue convincingly for the correctness of the assignment of this vibration to the doubly degenerate ν_8 mode. Although we cannot definitely rule out the possibility that the 250 cm^{-1} doublet may be due to an impurity, we believe that the available evidence makes this possibility improbable. Toluene is the only non-isotopic chemical impurity that we have been able to identify in our benzene samples,[14] and the concentration of toluene is much lower in the C_6D_6 samples than in the C_6H_6 samples. Yet the relative intensity of the 250 cm^{-1} doublet compared to absorption lines known to be due to benzene (see below) is the same for C_6H_6 and C_6D_6 contrary to what would be expected if the line were due to an impurity. The impurity content of C_6H_6 and C_6D_6 is discussed in detail in Appendix F.

The assignment of the origin and the ν_1 totally symmetric vibration have both been confirmed by observation of factor-group splitting of these lines (Sec. IIIB). The e_{2g} vibration $\nu_9 + n \cdot \nu_1$ in the $^3B_{1u}$

electronic state is in Fermi resonance[20] with $\nu_8 + (n+1)\cdot\nu_1$ where $n = 0, 1, 2, \cdots$. This Fermi resonance may obscure the expected splitting of the doubly degenerate $\nu_8 + \nu_1$ mode (but see Sec. IIIA. 2). The assignment of the line at 30, 835 cm^{-1} to the ν_9 vibration is consistant with the C_6D_6 spectrum (see Sec. IIIA. 2) where ν_9 and $\nu_8 + \nu_1$ are no longer in Fermi resonance.

As noted in the Table the assignments of the two b_{2g} vibrations ν_4 and ν_5 and the $2\cdot\nu_{16}$ vibration are tentative. It is possible that some of these lines correspond to phonon addition bands built on the ν_8 fundamental. The broad character of the absorption lines in the C_6H_6 spectrum compared with corresponding naphthalene and anthracene spectra[3, 6] may be further evidence for a significant coupling between lattice modes and vibronic levels.

In Table II we have listed the C_6H_6 $^3B_{1u}$ vibrational frequencies that are a consequence of our assignment of the absorption spectra. For comparison we have also given these vibrational frequencies in the ground ($^1A_{1g}$) state and the lowest ($^1B_{2u}$) singlet state. The O_2-perturbed gas phase $^3B_{1u}$ frequencies reported in the Table are from the work of King and Pinnington.[5] These workers observed a strong, totally symmetric progression built on the 0-0. Note that, even though the 0-0 is weak in the unperturbed transition, O_2 or heavy-atom perturbation is known to distort the relative vibronic intensities in a multiplicity forbidden transition.[21a] In addition a sideband appears associated with each of these a_{1g} bands 250 cm^{-1} from the main peak. King and Pinnington attributed this sideband to a b_{2g} mode. From our results it seems more likely that the e_{2g} ν_8 mode is responsible for

TABLE II. C_6H_6 vibrational frequencies.

Symmetry in D_{6h}	Vibration	Electronic State			
		$^3B_{1u}$		$^1A_{1g}$	$^1B_{2u}$
		Crystal (cm^{-1})[a]	Gas phase (O_2) (cm^{-1})[b]	(cm^{-1})[c]	(cm^{-1})[d]
a_{1g}	1	925	900	990	923
b_{2g}	4	382 (?)		705	365
	5	612 (?)		1005	775
e_{2g}	6	628		606	521
	8	239 252	250[e]	1584	1470
	9	1188		1174	1130
e_{2u}	16	244 (?)		405	243

[a]This work. [b]Ref. 5.

[c]Ref. 13. [d]Ref. 19.

[e]Attributed to b_{2g} in Ref. 5.

the sidebands.

(2) C_6D_6.

The C_6D_6 excitation spectrum is presented in Fig. 3. The line positions and assignments are listed in Table III. The resolution in the C_6D_6 spectrum is poorer because the delayed emission from these samples was weaker and longer-lived. The lifetime of the protonated benzene phosphorescence is 8 sec,[21b] and the spectrum in Fig. 3 was taken at a spectrometer scan speed of 5 Å/min. The longer phosphorescence lifetime in the C_6D_6 case thus cuts the resolution down to about 7 cm^{-1}.

The assignment of the C_6D_6 absorption spectrum follows in a straightforward way from the C_6H_6 assignments. One feature to note is that the two e_{2g} vibrations, ν_8 and ν_9, are no longer in Fermi resonance. The expected splitting of the $\nu_8 + (n+1)\cdot\nu_1$ levels ($n > 0$) is not clearly observed in the C_6D_6 spectrum, perhaps because of the low resolution and broad character of the spectrum. A weak, reproducible shoulder on the $\nu_8 + \nu_1$ line may be evidence of this splitting but this assignment is certainly open to question. The absence of splitting here is the one piece of experimental evidence that seems to be in conflict with our assignment of the intense features of the spectrum to the $\nu_8 + n\cdot\nu_1$ progression. Because of the generally broad character of the spectrum, the Fermi resonance in the C_6H_6 spectrum and the lower resolution in the C_6D_6 spectrum, we do not consider this conflict serious, particularly in view of the more serious problems that alternative assignments present. The C_6D_6 vibrational frequencies that result from these assignments are listed in Table IV.

Figure 3. C_6D_6 excitation spectrum. Intensity scale is the same for all three traces. There is a steady downward baseline drift with decreasing wavelength visible in the figure due to inadequate filtering of the exciting light. The sudden increase in signal around 3175 Å is an instrumental correction for this drift.

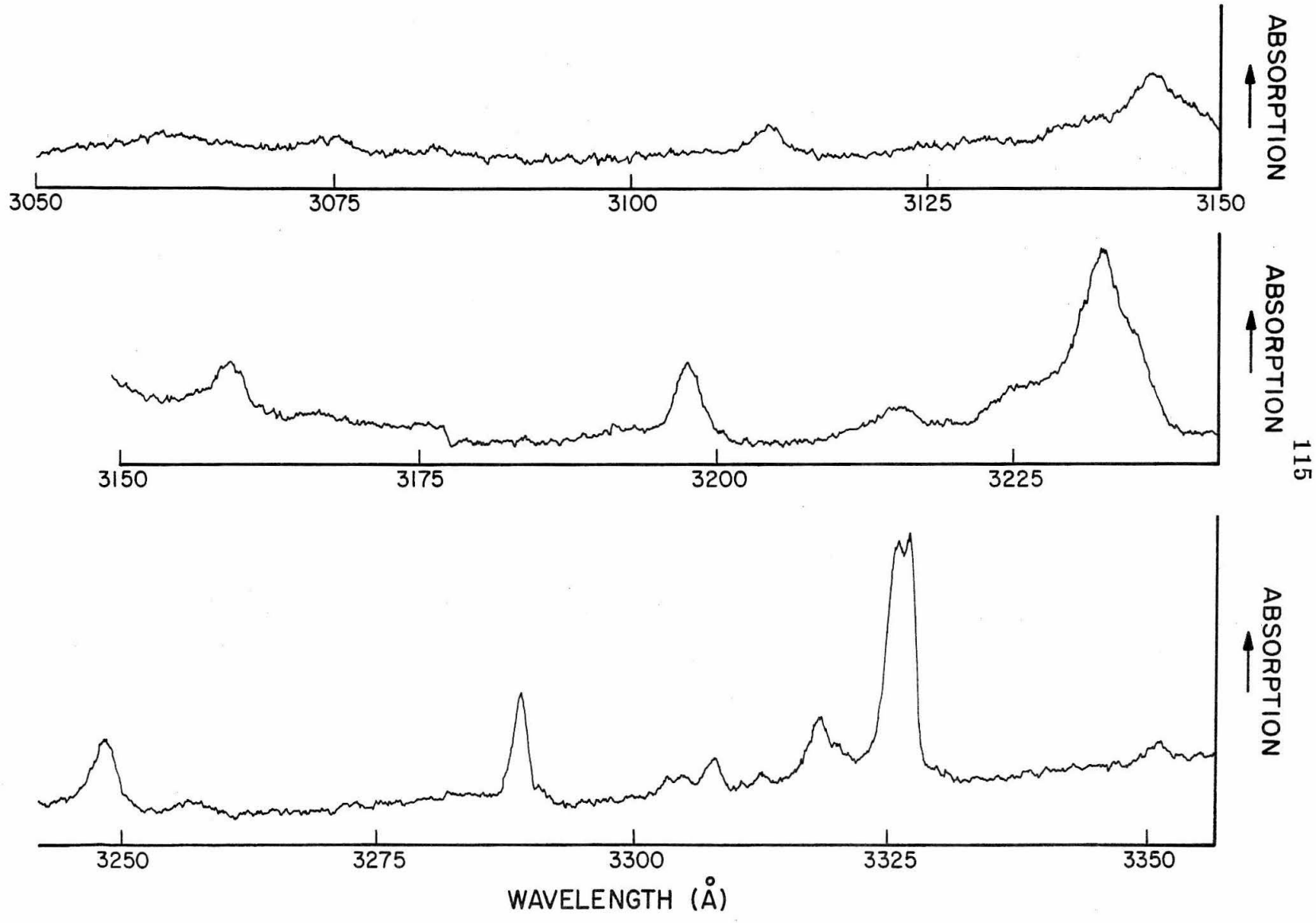
ABSORPTION
3050
3075
3100
3125
3150
ABSORPTION
3150
3175
3200
3225
ABSORPTION
3250
3275
3300
3325
3350
WAVELENGTH (Å)

TABLE III. Analysis of the $^3B_{1u} \leftarrow {}^1A_{1g}$ spectrum of C_6D_6.

Position		Distance from origin (cm^{-1})	Intensity[a]	Assignment[b]
λ_{air} (Å)	ν_{vac} (cm^{-1})			
3349.5	29,847 ± 5	0	VW	0-0
3324.2	30,074	227	VS	ν_8
3323.1	30,084	237	VS	
3315.2	30,155	308	W	ν_8 + phonon
3309.4	30,208	361	VW	ν_4 (?)
3304.8	30,250	403	VW	
3301.9	30,277	430	VW	$2 \cdot \nu_{16}$ (?)
3300.6	30,289	442	VW	
3287.9	30,406	559	VW	ν_5 (?)
3286.1	30,422	575	M	ν_6
3253.4	30,728	881	VW	ν_1
3245.0	30,808	961	W	ν_9
3231.1	30,940	1093	W	(?)
3228.9	30,961	1114	S	$\nu_8 + \nu_1$
3222.2	31,026	1179	VW	$\nu_8 + \nu_1$ + phonon
3211.8	31,126	1279	VW	$2 \cdot \nu_{16} + \nu_1$ (?)
3193.7	31,303	1456	W	$\nu_6 + \nu_1$
3155.3	31,684	1837	W	$\nu_9 + \nu_1$
3140.0	31,838	1991	W	$\nu_8 + 2 \cdot \nu_1$
3107.2	32,174	2327	VW	$\nu_6 + 2 \cdot \nu_1$

TABLE III. (Continued)

Position		Distance from origin (cm^{-1})	Intensity[a]	Assignment[b]
λ_{air} (Å)	ν_{vac} (cm^{-1})			
3070.0	32,564	2717	VW	$\nu_9 + 2 \cdot \nu_1$
3057.0	32,702	2855	VW	$\nu_8 + 3 \cdot \nu_1$

[a]VS = very strong, S = strong, M = moderate, W = weak, VW = very weak.

[b]Numbering of normal modes is due to E. B. Wilson, Phys. Rev. 45, 706 (1934).

TABLE IV. C_6D_6 vibrational frequencies

Symmetry in D_{6h}	Vibration	Electronic State			
		$^3B_{1u}$		$^1A_{1g}$	$^1B_{2u}$
		Crystal (cm^{-1})[a]	Gas phase (O_2) (cm^{-1})[b]	(cm^{-1})[c]	(cm^{-1})[d]
a_{1g}	1	881	870	945	879
b_{2g}	4	361 (?)		599	306
	5	559 (?)		829	663
e_{2g}	6	575		579	499
	8	227 237	230[e]	1558	1403
	9	961		868	830
e_{2u}	16	215 (?)		345	208

[a]This work. [b]Ref. 5.

[c]S. Brodersen and A. Langseth, Kgl. Danske Videnskab. Selskab, Mat.-Fys, Skrifter 1, No. 1 (1956).

[d]Ref. 19.

[e]Attributed to b_{2g} in Ref. 5.

b. Factor-Group Splitting

In Fig. 4 we present the factor-group splitting of the $^3B_{1u} \leftarrow {}^1A_{1g}$ 0-0 transitions of C_6H_6 and C_6D_6 and the 0-0 + ν_1 transition of C_6H_6. The benzene crystal has four molecules per unit cell[22] implying the presence of four factor-group components. A determination of the spin-orbit coupling selection rules for the $^3B_{1u} \leftarrow {}^1A_{1g}$ transition indicates that all four factor-group components should be observed in absorption.[23] These four components can be clearly seen in Fig. 4a. The splitting of the three closely spaced high energy components in Figs. 4b and 4c are not very obvious to say the least but can be observed upon close inspection of the spectra. The measured positions and splittings of all three bands are reported in Table V.

The fifth line in the 0-0 spectrum of C_6H_6 and C_6D_6 has been tentatively attributed to $^{13}C^{12}C_5H_6$ and its deuterated analog.[10] This isotopic impurity line should not be present in the 0-0 + ν_1 spectrum. The ν_1 vibration for $^{13}C^{12}C_5H_6$ is 7.6 cm^{-1} lower in energy than the corresponding C_6H_6 vibration.[24] This fact combined with the 11 cm^{-1} shift of the $^{13}C^{12}C_5H_6$ origin to higher energy means that the isotopic impurity line should be only 3 cm^{-1} from the center of the 0-0 + ν_1 exciton band. This places it well within the exciton band. Hanson[25] has shown for the benzene singlet that an isotopic impurity imbedded in the exciton band broadens and shifts the exciton components slightly but is not itself observed. The fifth line appears to be absent in Fig. 4b in agreement with our assignment of it, but the spectrum is in general of such poor quality that this evidence should not be considered too definitive.

Figure 4. Factor-group splitting in (a) the C_6H_6 0-0 band, (b) the C_6H_6 0-0 + ν_1 band, and (c) the C_6D_6 0-0 band. Four factor-group components have been observed for all three bands although in the figure only (a) shows the splitting clearly.

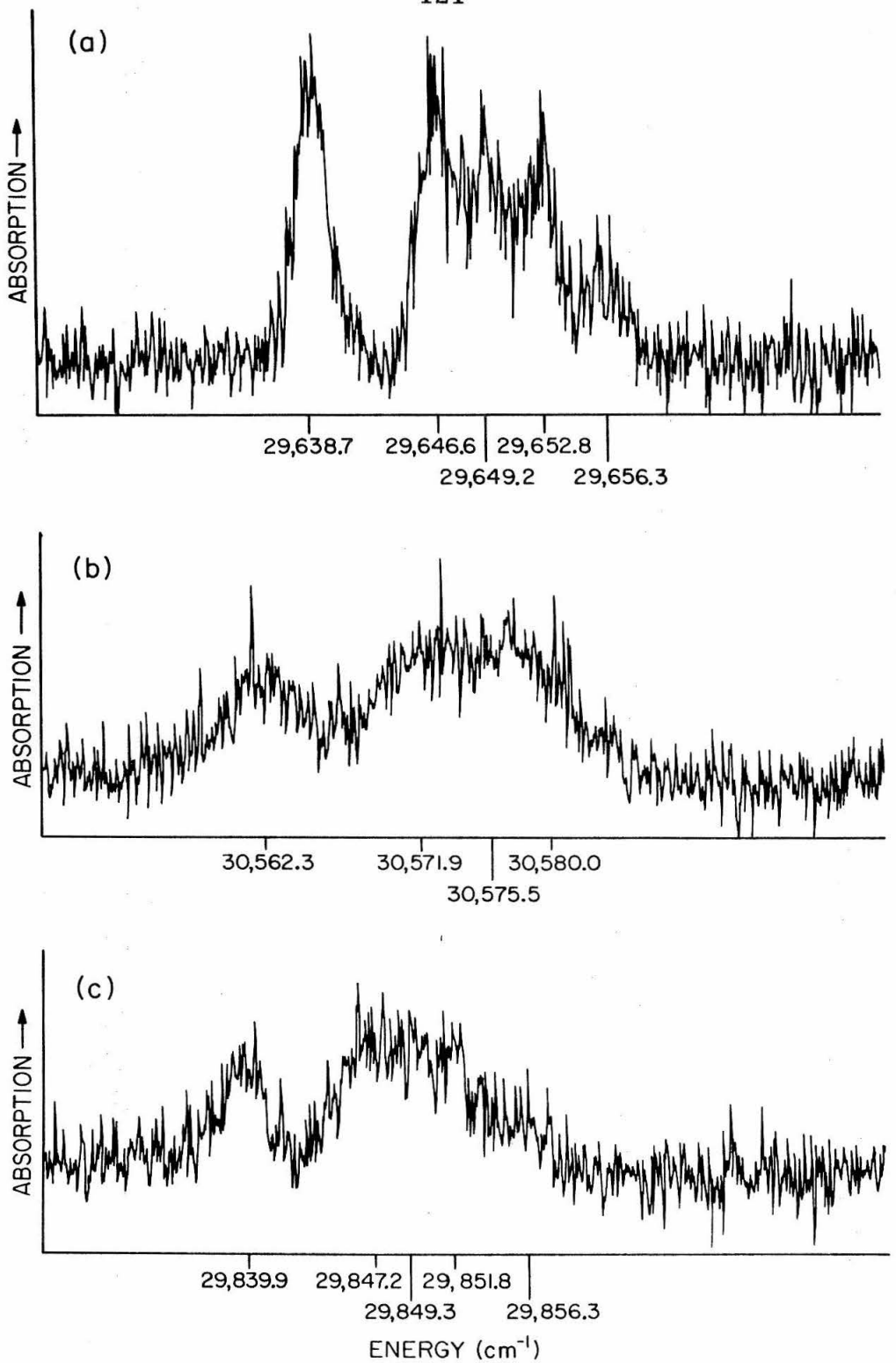
(a)
ABSORPTION
29,638.7
29,646.6
29,652.8
29,649.2
29,656.3
(b)
ABSORPTION
30,562.3
30,571.9
30,580.0
30,575.5
(c)
ABSORPTION
29,839.9
29,847.2
29,851.8
29,849.3
29,856.3
ENERGY (cm⁻¹)

TABLE V. Factor-group splitting in benzene.

Molecule and Energy Level	Position (cm^{-1})	Center of Band (cm^{-1})	Splitting from Center (cm^{-1})
C_6H_6 0-0	29,639 ± 2		- 8.1 ± 0.4
	29,647	29,647	- 0.2
	29,649		+ 2.4
	29,653		+ 6.0
0-0	30,562 ± 2		-10.1 ± 1.0
$+ \nu_1$	30,572	30,572	- 0.5
	30,576		+ 3.1
	30,580		+ 7.6
C_6D_6 0-0	29,840 ± 2		- 7.2 ± 1.0
	29,847	29,847	+ 0.1
	29,849		+ 2.2
	29,852		+ 4.7

For comparison we have listed in Table VI the $^3B_{1u} \leftarrow {}^1A_{1g}$ absorption origins for C_6D_6 and C_6H_6 in gas and crystal phases that other workers have obtained. The gas-to-crystal energy shift is $+ 131 \pm 11$ cm^{-1} for C_6H_6 and $+ 157 \pm 32$ cm^{-1} for C_6D_6. This implies that the average crystal-binding energy is smaller in the benzene triplet state than in the ground state. The shift is in the opposite direction from the shift for the $^1B_{2u} \leftarrow {}^1A_{1g}$ transition of C_6H_6, which is -248.0 ± 1 cm^{-1}.[26] The uncertainties in the gas-phase measurements make it difficult to tell if there is a real isotope effect on the gas-to-crystal shift as implied by the above two values. Actually such a shift, in the direction implied, is expected in view of the isotope effects on "static" crystal interactions to be discussed in the next section.

4. Discussion

a. Factor-Group Splitting

Within the framework of the Born-Oppenheimer approximation and weak vibronic coupling, the total factor-group splitting is distributed over the absorption origin and all totally symmetric vibrations built on this origin in a manner that is governed by the appropriate Franck-Condon factor.[27] The total exciton splitting is the quantity that should be compared with theoretical calculations. The Franck-Condon factor[28] for the C_6H_6 0-0 band in absorption is 0.367. It is 0.381 for the 0-0 + ν_1 band. The total exciton splittings are calculated by dividing the sum of the observed 0-0 and 0-0 + ν_1 splittings by 0.748, the sum of the corresponding Franck-Condon factors. The total

TABLE VI. $^3B_{1u} \leftarrow {}^1A_{1g}$ origin in absorption.

C_6H_6		C_6D_6	
Gas	Crystal	Gas	Crystal
29,516 ± 9[a]	29,674 ± 25[b]	29,690 ± 30[a]	29,851 ± 25[b]
	29,647 ± 2[c]		29,847 ± 2[c]
			29,855[d]

[a]Ref. 5. [b]Ref. 4a.

[c]This work. [d]Ref. 27b.

splittings referred to the band center[26] are then -24.3, -0.94, +7.35, and +18.2 cm^{-1}. The total splittings should be accurate to ± 2 cm^{-1} if the method[26] used for calculating them is correct. The Franck-Condon factor for the C_6D_6 band is 0.388 and the calculated total splittings are -18.5, +0.3, +5.7, and +12.1 ± 3 cm^{-1}. Due to experimental uncertainties and the uncertainties involved in the method of determining the total splitting, the apparent differences between the C_6H_6 and C_6D_6 factor-group splittings cannot be considered significant.

Silbey et al.[29] have recently completed a calculation of the triplet exciton splitting for benzene using the conventional neutral exciton formalism[30] and by using a formalism involving a mixing of ion-pair states with neutral exciton states.[31] The first mechanism predicts a total splitting for C_6H_6 (energy difference between highest and lowest factor-group components) of 7.2 cm^{-1}, much lower than the observed value of 42.5 cm^{-1}. The second method with the ion-pair state located at 5.7 eV yields a total splitting of 84 cm^{-1}, somewhat greater than the experimental value. In addition the ion-pair results were reported for only three of the four exciton components, making comparison of theory and experiment difficult.

The observed mean of the C_6H_6 triplet exciton band at 29,647 ± 2 cm^{-1} has important implications for mixed crystal theories[32] as they apply to benzene. If one compares this value with the phosphorescence origin for 0.1% C_6H_6 in a C_6D_6 crystal at 4.2° K (29,658.2 ± 0.1 cm^{-1}),[13] one notes an 11 cm^{-1} shift of the triplet level when the C_6H_6 triplet is removed from a C_6H_6 host crystal and placed in a C_6D_6 environment. In treating mixed crystals theoretically,

it is usually assumed that guest-host interactions do not change with isotopic substitution. Hanson et al.[33] have shown this assumption to be valid for naphthalene but Colson[34] has raised doubts about its validity for benzene. Our results strikingly support Colson's conclusion that for benzene isotopic mixed crystals guest-host "static" interactions[26] change with host isotopic composition. If there were no change in the guest-host interaction for the systems C_6H_6 in C_6H_6 and C_6H_6 in C_6D_6, then the 11 cm^{-1} shift that we observe would have to be caused by interaction of the C_6H_6 guest level with the C_6D_6 host exciton band. This obviously cannot be the case since the shift is in the wrong direction. Furthermore, a calculation of the quasiresonance shift using the experimentally observed exciton splitting and any of the various forms of mixed crystal theory[32] indicates that this "quasiresonance shift" for the C_6H_6 guest triplet in a C_6D_6 host is less than 1 cm^{-1} and certainly not near the observed shift of 11 cm^{-1}.

In summary then, it appears from our results and those of Colson[34] that deuteration of the host changes the guest-host "static" interaction for benzene. The application of the isotopic mixed crystal theories to benzene is described in detail in Section IIIB.

b. Pseudo-Jahn-Teller Distortion

Many years ago Lewis and Kasha[35] concluded after an investigation of the benzene phosphorescence spectrum that the molecule was contracted along the 1,4 axis of the triplet state. However, Shull[36] later showed that benzene phosphorescence in a rigid-glass solution can be completely understood in terms of a hexagonal D_{6h} configuration.

Recently Nieman[37] has reexamined the benzene phosphorescence intensity in detail and found evidence to support a very slight distortion away from hexagonal symmetry. Nieman's results also indicate that examination of the phosphorescence intensities alone is not a very sensitive way of determining the nature and extent of the distortion.

Perhaps the most cogent experimental evidence for a distorted triplet state comes from EPR[9b] and mixed-crystal phosphorescence studies.[9a] Both of these experiments indicate that the triplet state of C_6H_6 molecules in a C_6D_6 single crystal is distorted into a non-quinoidal structure (i. e., 2 long bonds and 4 short ones). This non-quinoidal structure has recently been confirmed by electron-nuclear double resonance results.[9c]

The fact that the lowest triplet state ($^3B_{1u}$) of benzene is susceptible to a pseudo-Jahn-Teller distortion due to vibronic coupling with the $^3E_{1u}$ level of the same Hückel parentage was predicted theoretically by Moffitt and Liehr[8a] long before these experimental results became available. Recently van der Waals et al.[8b] have considered in detail the effects of this distortion on the vibrational frequencies in the $^3B_{1u}$ state. These authors have concluded on the basis of a first-order calculation that the ν_8 normal mode, which is involved in the vibronic coupling, may decrease in frequency to as much as 1/3 of its value in the absence of coupling. Inclusion of higher-order terms is expected, according to these authors, to reduce the frequency even more and in addition to split the degenerate ν_8 vibration into a doublet.

These theoretical predictions are nicely confirmed by the present experimental results. The ν_8 frequency has shifted from an

expected value of about 1500 cm^{-1} to 250 cm^{-1} in the $^3B_{1u}$ state. In addition a 10 cm^{-1} splitting of the degenerate mode is observed.

5. Conclusions

Using the photoexcitation method we have obtained for the first time the $^3B_{1u} \leftarrow {}^1A_{1g}$ absorption spectra of crystalline C_6H_6 and C_6D_6 at 4.2° K. These results illustrate quite clearly the power of the photoexcitation method for observing weak absorptions. Benzene has an extremely small oscillator strength for its lowest singlet-triplet transition ($f \approx 10^{-10}$).[4a] In addition, as the results of this paper show, the absorption spectra for both C_6H_6 and C_6D_6 are quite broad compared for example to the corresponding spectra of naphthalene and anthracene.[3, 6a] Despite these complicating features we were able to see the spectra quite easily using the phosphorescence photoexcitation method. In fact a sharp transition as much as ten times weaker ($f \approx 10^{-11}$) could have been seen using this method and our apparatus. These results should be compared with the earlier direct absorption experiments where no absorption was observed in a 5-cm thick pure crystal[4a] or in 22.5 m of pure liquid.[4b]

Factor-group splitting of the 0-0 and the 0-0 + ν_1 exciton bands have been observed. The agreement between our experimental splittings and those calculated using various theoretical approaches was discussed in a preliminary report.[10] Benzene factor-group splitting is particularly sensitive to the distance and angle dependence of the molecular wavefunctions used in the calculation since, neglecting translationally equivalent interactions, three different molecule-

molecule interactions are involved as compared with one such interaction for naphthalene and anthracene. For this reason the benzene splitting provides a particularly severe test of the theoretical calculations.

The position of the mean of the exciton band of C_6H_6, when compared to the phosphorescence origin of a C_6H_6 guest in a C_6D_6 host crystal, indicates that the "static" intermolecular interactions between guest and host are different for a C_6H_6 triplet guest in C_6H_6 and C_6D_6 hosts. This result has important implications for the applicability of mixed crystal theories to benzene.

The $^3B_{1u} \leftarrow {}^1A_{1g}$ absorption spectrum of benzene exhibits very clear evidence of a pseudo-Jahn-Teller distortion of the $^3B_{1u}$ state. The ν_8 normal mode which corresponds in direction to the molecular distortion is shifted by the pseudo-Jahn-Teller interaction from about 1600 cm^{-1} in the ground state to 250 cm^{-1} in the excited triplet. All other lines in the spectrum can be understood on the basis of the hexagonal D_{6h} configuration of the triplet.

Acknowledgment

Much of the experimental work reported in this section was done in collaboration with Dr. George Castro.

REFERENCES

1. D. S. McClure, J. Chem. Phys. 20, 682 (1952); M. Mizushima and S. Koide, J. Chem. Phys. 20, 765 (1952).
2. For an extensive list of triplet lifetimes the reader is referred to W. Siebrand, J. Chem. Phys. 47, 2411 (1967).
3. (a) R. H. Clark and R. M. Hochstrasser, J. Chem. Phys. 46, 4532 (1967); C. -h. Ting, 23rd Symposium on Molecular Structure and Spectroscopy, The Ohio State University, Columbus, Ohio, 1968, Abstract Q10; (b) D. M. Hanson and G. W. Robinson, J. Chem. Phys. 43, 4174 (1965).
4. (a) S. D. Colson and E. R. Bernstein, J. Chem. Phys. 43, 2661 (1965); (b) D. P. Craig, J. M. Hollas, and G. W. King, J. Chem. Phys. 29, 974 (1958).
5. G. W. King and E. H. Pinnington, J. Mol. Spectry. 15, 394 (1965).
6. (a) P. Avakian, E. Abramson, R. G. Kepler, and J. C. Caris, J. Chem. Phys. 39, 1127 (1963); P. Avakian and E. Abramson, J. Chem. Phys. 43, 821 (1965); (b) G. Castro and G. W. Robinson, J. Chem. Phys. 50, 1159 (1969).
7. N. Hirota, J. Chem. Phys. 44, 2199 (1966); A. P. Marchetti and D. R. Kearns, J. Am. Chem. Soc. 89, 768 (1967).
8. (a) W. Moffitt and A. D. Liehr, Phys. Rev. 106, 1195 (1957); A. D. Liehr, Z. Naturforsch. 16a, 641 (1961); W. E. Donath, J. Chem. Phys. 42, 118 (1965); (b) J. H. van der Waals, A. M. D. Berghuis and M. S. de Groot, Mol. Phys. 13, 301 (1967).

9. (a) G. C. Nieman and D. S. Tinti, J. Chem. Phys. 46, 1432 (1967); (b) M. S. de Groot, I. A. M. Hesselmann, and J. H. van der Waals, Mol. Phys. 13, 583 (1967); 16, 45 (1969); (c) A. M. Ponte-Goncalves and C. A. Hutchison, J. Chem. Phys. 49, 4235 (1968).

10. D. M. Burland and G. Castro, J. Chem. Phys. 50, 4107 (1969).

11. Because of the spectral reponse to our phototube, we have not bothered to filter out light longer in wavelength than 6000 Å.

12. S. F. Pellicori, Appl. Opt. 3, 361 (1964); to duplicate the absorption spectra obtained by Pellicori we have had to use a 20:1 dilution of the solution he reported using. We have not investigated the reason for this discrepancy.

13. E. R. Bernstein, S. D. Colson, D. S. Tinti, and G. W. Robinson, J. Chem. Phys. 48, 4632 (1968).

14. (a) J. H. Smith, E. B. Priestley, and D. M. Burland (unpublished results); (b) The positions of the impurity emission lines agree reasonably well after correction for a "solvent" shift with the line positions reported for toluene in EPA glass [Y. Kanda and H. Sponer, J. Chem. Phys. 28, 798 (1958)] and in an unspecified alcohol glass [P. P. Dikun and B. Y. Sveshnikov, Zh. Eksp. Teor. Fiz. 19, 1000 (1949)] both at 77° K. In addition we have examined the emission and absorption spectra of toluene-doped samples of C_6H_6. The emission spectra of both "pure" and doped C_6H_6 are identical. The only absorption we observed in both doped and undoped samples that is attributable to toluene corresponds to absorption into the lowest singlet. This transition is much higher

in energy ($> 5000\ cm^{-1}$) than the $^3B_{1u} \leftarrow {}^1A_{1g}$ transition of benzene that we report here.

15. In a preliminary published report of this work (Ref. 10) we attributed the emission from the Cs-purified C_6H_6 crystal to delayed fluorescence. We now know that it is impurity phosphorescence. None of the conclusions in Ref. 10 is affected by this change, however.
16. W. Moffitt, J. Chem. Phys. 22, 320 (1954).
17. S. Leach and R. Lopez-Delgado, J. Chim. Phys. 61, 1636 (1964).
18. We represent the normal mode vibrations by ν_i, where the subscript i corresponds to the numbering of the modes by E. B. Wilson, Phys. Rev. 45, 706 (1934).
19. F. M. Garforth, C. K. Ingold, and H. G. Poole, J. Chem. Soc. 1948, 491
20. E. B. Wilson, J. C. Decius, and P. C. Cross, Molecular Vibrations (McGraw-Hill Book Co., Inc., New York, 1955), p. 198.
21. (a) See for example, G. W. Robinson, Methods of Experimental Physics, D. Williams, Ed. (Academic Press, New York, 1962), Vol. 3, Ch. 2.4, Fig. 19; (b) S. D. Colson and G. W. Robinson, J. Chem. Phys. 48, 2550 (1968).
22. E. G. Cox, D. W. J. Cruickshank, and J. A. S. Smith, Proc. Roy. Soc. (London) 247A, 1 (1958); E. G. Cox. Rev. Mod. Phys. 30, 159 (1958); G. E. Bacon, N. A. Curry, and S. A. Wilson, Proc. Roy. Soc. (London) 279A, 98 (1964).
23. R. M. Hochstrasser, J. Chem. Phys. 47, 1015 (1967).
24. A. R. Gee and G. W. Robinson, J. Chem. Phys. 46, 4847 (1967).

25. D. M. Hanson, J. Chem. Phys. 51, 653 (1969).

26. E. R. Bernstein, S. D. Colson, R. Kopelman, and G. W. Robinson, J. Chem. Phys. 48, 5596 (1968).

27. (a) D. P. Craig and S. H. Walmsley, Mol. Phys. 4, 113 (1961); (b) G. C. Nieman and G. W. Robinson, J. Chem. Phys. 39, 1298 (1963).

28. The method for calculating these factors is described in Section IIA of this thesis.

29. R. Silbey, S. A. Rice and J. Jortner, J. Chem. Phys. 43, 3336 (1965).

30. A. S. Davydov, Theory of Molecular Excitons (McGraw-Hill Book Co., New York, 1962).

31. S. Choi, J. Jortner, S. A. Rice, and R. Silbey, J. Chem. Phys. 41, 3294 (1964).

32. E. I. Rashba, Opt. Spektrosk. 2, 568 (1957); G. F. Koster and J. C. Slater, Phys. Rev. 95, 1167 (1954); R. E. Merrifield, J. Chem. Phys. 38, 920 (1963); S. Takeno, J. Chem. Phys. 44, 853 (1966); D. P. Craig and M. R. Philpott, Proc. Roy. Soc. (London) A290, 583 (1966); ibid. A293, 213 (1966); R. G. Body and I. G. Ross, Australian J. Chem. 19, 1 (1966); B. S. Sommer and J. Jortner, J. Chem. Phys. 50, 187 (1969).

33. D. M. Hanson, R. Kopelman, and G. W. Robinson, J. Chem. Phys. 51, 212 (1969).

34. S. D. Colson, J. Chem. Phys. 48, 3324 (1968).

35. G. N. Lewis and M. Kasha, J. Amer. Chem. Soc. 66, 2100 (1944).

36. H. Shull, J. Chem. Phys. 17, 295 (1949).

37. G. C. Nieman, J. Chem. Phys. 50, 1660, 1674 (1969).

B. SOME COMMENTS ON THE APPLICABILITY OF MIXED CRYSTAL THEORIES TO BENZENE AND ITS DEUTERATED ANALOGS

1. Introduction

Recently there has been much theoretical[1-6] and experimental[7-13] interest in isotopic mixed organic crystals. This interest arises at least in part from the possibility of obtaining detailed information on the host exciton band structure by using isotopic guests as probes. Hanson et al.[12] have shown that naphthalene isotopic mixed crystals can be completely understood in terms of existing mixed crystal theories. Isotopic mixed crystal studies of benzene, on the other hand, do not seem to conform to theoretical expectations. Impurity energy levels shift in the wrong direction[14] and average intermolecular interactions calculated from the experimental mixed crystal data are much larger than would be expected from independent measurements of these same interactions.[15] One might have expected these difficulties with benzene; as Rabalais et al.[16] have pointed out, "benzene is not a prototypical aromatic molecule...." Its high symmetry (D_{6h}) and its small size relative to other aromatics give rise to many unique spectroscopic features. The peculiar behavior of benzene mixed crystals is one of these unique features and will be the subject of the remainder of Part III.

2. Outline of Mixed Crystal Theory

Before we consider the specific application of the theory of mixed crystals to benzene and its deuterated analogs, we will review the theory itself in some detail. In this way all of the approximations made in the derivation of the expression for the electronic energy level of an isotopic impurity molecule in terms of the host exciton band structure will be apparent. We will use the Green's function approach developed by Lifshitz[17] and explicitly summarized for Wannier excitons by Izyumov.[18] The application of this method to Frenkel excitons and to crystals with more than one exciton band has recently been treated by Sommer and Jortner.[9] This approach yields exactly the same final result as an alternate method developed by Koster and Slater[19] and applied specifically to Frenkel excitons by Craig and Philpott.[2]

We will divide the remainder of this section into four parts:

(a) A derivation of the Green's function and the density of states for a pure crystal Frenkel exciton band.

(b) Using Dyson's equation, we obtain the mixed crystal Green's function in terms of the pure crystal function.

(c) A derivation of the mixed crystal density of states which yields an expression relating the pure crystal density of states, the impurity "trap depth" and the mixed crystal impurity energy levels.

(d) A discussion of the various types of solutions to the expression obtained in (c).

a. The Pure Crystal Green's Function and the Density of States

We will first obtain the pure crystal Green's function for Frenkel excitons. The pure crystal Hamiltonian may be written[20]

$$H_o = \sum_{n=1}^{N} \sum_{\alpha=1}^{\sigma} H^o_{n\alpha} + \sum_{n\alpha < m\beta} V_{n\alpha, m\beta} \tag{1}$$

for a crystal with N unit cells and σ molecules per unit cell. $H^o_{n\alpha}$ is not the free molecule Hamiltonian but rather the free-molecule Hamiltonian as modified by the static crystal interactions.[20] The excited eigenstates of the first term in Eq. (1) are

$$a^f_{n\alpha} = \hat{A}\, \phi^f_{n\alpha} \prod_{m\beta \neq n\alpha} \phi^o_{m\beta} \tag{2}$$

for the $f^{\underline{th}}$ excited state and for excitation localized on the $\alpha^{\underline{th}}$ molecule in the $n^{\underline{th}}$ unit cell. $\hat{A}$ is the electronic antisymmetrizing operator. The $\phi^f_{n\alpha}$ are not free-molecule wavefunctions but rather site-adapted molecular wavefunctions. This distinction is not important here but it will be crucial later when we must decide on what zero-order energy to use for the excited impurity molecule in the crystal. The $a^f_{n\alpha}$ are of course orthogonal so that

$$\langle a^f_{n\alpha} | a^{f'}_{n'\alpha'} \rangle = \delta_{nn'} \delta_{\alpha\alpha'} \delta_{ff'} \quad . \tag{3}$$

The second term in Eq. (1) allows for the delocalization of the excitation throughout the crystal so that the complete crystal wavefunction may be written in terms of either localized functions $a^f_{n\alpha}$ or delocalized functions $\Phi^f_\alpha(\vec{k})$ as

$$\psi_j^f(\vec{k}) = \sum_{\alpha=1}^{\sigma} B_{\alpha j}^f(\vec{k})\, \Phi_{\alpha}^f(\vec{k})$$

$$= \frac{1}{N^{1/2}} \sum_{n=1}^{N} \sum_{\alpha=1}^{\sigma} U_{\vec{k}j}(n\alpha f)\, a_{n\alpha}^f \qquad (4)$$

where the expansion parameters $B_{\alpha j}^f(\vec{k})$ and $U_{\vec{k}j}(n\alpha f)$ are related by

$$U_{\vec{k}j}(n\alpha f) = B_{\alpha j}^f(\vec{k}) \exp(i\vec{k}\cdot\vec{R}_{n\alpha}) \qquad (5)$$

and $j = 1, \ldots, \sigma$ corresponding to the σ branches of the exciton band. $\vec{k}$ is of course related to the crystal momentum vector. Charge transfer and double excitation states are ignored in writing Eqs. (4) and (5). $\psi_j^f(\vec{k})$ and $a_{n\alpha}^f$ are chosen to be orthonormal so that

$$\left.\begin{aligned} \frac{1}{N} \sum_{\vec{k}} \sum_{j} U_{\vec{k}j}^*(n\alpha f)\, U_{\vec{k}j}(n'\alpha' f') &= \delta_{nn'}\, \delta_{\alpha\alpha'}\, \delta_{ff'} \\ \frac{1}{N} \sum_{n} \sum_{\alpha} \sum_{f} U_{\vec{k}j}^*(n\alpha f)\, U_{\vec{k}'j'}(n\alpha f) &= \delta(\vec{k}-\vec{k}')\delta_{jj'} \end{aligned}\right\} \qquad (6)$$

We now will use the above information concerning the pure crystal wave functions to obtain the pure crystal Green's function. In general we define the Green's function G(E) for an energy E by

$$(E - H)G(E) = 1 \quad . \qquad (7)$$

This function G(E) has the interesting property that when written in matrix form with the eigenvectors of H, it is related to the normalized density of electronic states by

$$N\sigma g(E) = \frac{1}{\pi} \operatorname{Im} \operatorname{Tr} \underset{\sim}{G}(E - i\epsilon) \tag{8}$$

where $N\sigma$ is the total number of molecules in the crystal, Im means imaginary part, Tr indicates the trace of the matrix $\underset{\sim}{G}$ and ϵ tends to zero from positive values.

If H in Eq. (7) is replaced by the pure crystal Hamiltonian H_o, then in matrix form we have, using the localized basis functions $a^f_{n\alpha}$

$$\sum_{n'', \alpha'', f''} (E\,\delta_{nn''}\delta_{\alpha\alpha''}\delta_{ff''} - H^o_{n\alpha f, n''\alpha''f''})\, G^o_{n''\alpha''f'', n'\alpha'f'}(E)$$

$$= \delta_{nn'}\delta_{\alpha\alpha'}\delta_{ff'} \tag{9}$$

and where

$$H^o_{n\alpha f, n''\alpha''f''} = \int a^{f*}_{n\alpha} H_o\, a^{f''}_{n''\alpha''}\, d\vec{r} \quad . \tag{10}$$

Solving Eq. (4) for $a^f_{n\alpha}$ and using the orthogonality relationships Eq. (6), the pure crystal Green's function in matrix form becomes

$$G^o_{n\alpha f, n'\alpha'f'}(E) = \frac{1}{N} \sum_{\vec{k}} \sum_{j} \frac{U^*_{\vec{k}j}(n'\alpha'f')\, U_{\vec{k}j}(n\alpha f)}{E - E_j(\vec{k})} \quad . \tag{11}$$

From Eq. (5) for $U_{\vec{k}f}(n\alpha f)$, the pure crystal Green's function in the localized excitation representation is

$$G^o_{n\alpha f, n'\alpha'f'}(E)$$

$$= \frac{1}{N} \sum_{\vec{k}} \sum_{j} \frac{B^{f*}_{\alpha j}(\vec{k})\, B^{f'}_{\alpha' j}(\vec{k})\, \exp[i\vec{k}\cdot(\vec{R}_{n'\alpha'} - \vec{R}_{n\alpha})]}{E - E_j(\vec{k})} \quad . \tag{12}$$

The pure crystal density of states can be obtained from Eq. (12) making use of the general relationship given by Eq. (8).

$$g(E) = \frac{1}{N\sigma} \sum_{\vec{k}} \sum_{j} \left| B^{f}_{\alpha j}(\vec{k}) \right|^2 \delta(E - E_j(\vec{k})) \tag{13}$$

where use has been made of the identity[21]

$$\frac{1}{E-E'-i\epsilon} = \mathcal{P}\frac{1}{E-E'} + i\pi\delta(E-E') \quad . \tag{14}$$

Here $\mathcal{P}$ stands for the principal value. If the molecules in the unit cell are crystallographically inequivalent then Eq. (13) cannot be simplified further and one must know both $B^{f}_{\alpha j}$ and $E_j(\vec{k})$. This would be the case for tetracene for example.[22] If the molecules in the unit cell are crystallographically equivalent, that is if they are related to one another by factor group operations, then Eq. (13) can be simplified considerably to[2]

$$g(E) = \frac{1}{N\sigma} \sum_{\vec{k}} \sum_{j} \delta(E - E_j(\vec{k})) \quad . \tag{15}$$

In this case one only needs to know $E_j(\vec{k})$ to determine g(E).

b. Dyson's Equation and the Dilute Mixed Crystal Green's Function

If we replace the Hamiltonian H in Eq. (7) by $H_o + V$ and we note the simple algebraic identity

$$\frac{1}{E - H_o - V} = \frac{1}{E - H_o} + \frac{1}{E - H_o} V \frac{1}{E - H_o - V} \tag{16}$$

we can write the Green's function G(E) as follows

$$G(E) = \frac{1}{E - H_o - V} = G^0(E) + G^0(E)V\,G(E) \quad . \tag{17}$$

This is Dyson's equation. It can be solved directly for G(E) yielding

$$G(E) = \frac{1}{1 - G^0(E)V}\, G^0(E) \quad . \tag{18}$$

For the mixed crystal problem that we treat here, the zero-order Green's function $G^0(E)$ will be the pure crystal Green's function in the localized wave-function representation Eq. (12). Before we can proceed further, we must make some specific assumptions about the perturbing term V. We can write V exactly as

$$V = (H - H_o) \quad . \tag{19}$$

For isotopic mixed crystals it is generally assumed that the Coulomb terms are the same for both guest and host and that the major difference between H and H_o arises from changes in the nuclear kinetic energy

$$H - H_o = -\tfrac{1}{2} \sum_g \sum_h [(1/M_g - 1/M_h)]\, (\partial^2/\partial Q_{gh}^2) \tag{20}$$

where the subscripts g and h refer to guest and host nuclei, respectively.

One need not be so specific in defining V. In what follows we will assume that V is a one site operator acting only on functions centered at the impurity n = 0. We will also assume that there is only

one impurity molecule in the crystal. These are the only assumptions we make about V. V thus includes all of the static crystal Coulomb interactions as well as the nuclear kinetic energy contribution Eq. (20). In matrix form V thus becomes

$$V_{nm} = U_o \delta_{no} \delta_{mo} \quad . \tag{21}$$

U_o is of course the zero-order energy difference between guest and host molecules, i.e., the trap depth. It is also sometimes known as the ideal mixed crystal level[20] and is quite frequently assumed to be equal to the gas phase energy difference between guest and host molecules.[9] This would of course be true if Eq. (20) accurately represented V. But as we emphasized in the discussions following Eqs. (1) and (2), the one-site Hamiltonian contains static crystal interactions so that U_o is the energy difference between guest and host molecules in the crystal site.

The Green's function given by Eq. (17) thus becomes in matrix form

$$\begin{aligned} G_{nm} &= G^o_{nm} + \sum_{p\ell} G^o_{np} V_{p\ell} G_{\ell m} \\ &= G^o_{nm} + G^o_{no} U_o G_{om} \quad . \end{aligned} \tag{22}$$

Setting n = 0 in Eq. (22) gives

$$G_{om} = \frac{G^o_{om}}{1 - G^o_{oo} U_o} \tag{23}$$

and using this expression back in Eq. (22) we finally obtain the mixed crystal Green's function as

$$G_{nm} = G^{o}_{nm} + \frac{U_o G^{o}_{no} G^{o}_{om}}{1 - G^{o}_{oo} U_o} \quad . \tag{24}$$

The first term in Eq. (24) is the pure crystal Green's function given by Eq. (12) where for simplicity we have condensed the subscript $n\alpha f$ to $\underline{n}$ and $n'\alpha'f'$ to $\underline{m}$.

c. The Dilute Mixed Crystal Density of States

Using the expression Eq. (8) for the density of states with the mixed crystal Green's function Eq. (24), we have

$$g(E) = \frac{1}{N\rho} \operatorname{Im} \sum_{n} \left[G^{o}_{nn}(E') + \frac{U_o G^{o}_{no}(E') G^{o}_{on}(E')}{1 - G^{o}_{oo}(E') U_o} \right] \tag{25}$$

where $E' = E - i\epsilon$. With some algebraic manipulation and the definition

$$F_o(E) \equiv \mathrm{Re} G^{o}_{oo}(E - i\epsilon) \tag{26}$$

the mixed crystal density of states function can be shown to be[18]

$$g(E) = g_o(E) - \frac{1}{N} \frac{U_o^2 F'_o(E) g_o(E) + U_o(1 - U_o F_o(E)) g'_o(E)}{(1 - U_o F_o(E))^2 + (\pi U_o g_o(E))^2} \tag{27}$$

where the prime refers to differentiation with respect to E. The quantity $F_o(E)$ can be shown to be

$$F_o(E) = \mathcal{P} \frac{1}{N\sigma} \sum_{\vec{k}} \sum_{j} \frac{|B^f_{oj}(\vec{k})|^2}{E - E_j(\vec{k})} \tag{28}$$

for crystals with crystallographically inequivalent molecules and

$$F_o(E) = \mathcal{P} \frac{1}{N\sigma} \sum_{\vec{k}} \sum_{j} \frac{1}{E - E_j(\vec{k})} = \mathcal{P} \frac{1}{N\sigma} \sum_{E'} \frac{g_o(E')}{E - E'} \tag{29}$$

for all other crystals.

The density of states expression Eq. (27) has a maximum or minimum at E_o where

$$[1 - U_o F_o(E_o)] = 0 \quad . \tag{30}$$

The solutions of Eq. (30) thus represent the impurity level if g(E) is a maximum or an "anti-level" if g(E) is a minimum. Since the total number of states in the exciton band system must be constant the impurity maximum at one energy necessarily implies a decrease in g(E), that is an "anti-level," elsewhere. Equation (30) is exactly the same equation that Koster and Slater[19] and Craig and Philpott[2] obtained in a somewhat different way. It is this expression for the impurity energy level E_o in terms of the trap depth U_o and the function $F_o(E)$ that we will evaluate in Section 2 for benzene.

At this point it would perhaps be well to review all of the assumptions that are involved in the derivation of Eq. (27). Later we will want to examine these assumptions to see if they might explain the anomolous experimental results we obtain for benzene. These assumptions are:

(1) The effect of mixing of the single-excitation wavefunctions with crystal states such as charge-transfer and double-excitation states is completely ignored.

(2) Isotopic substitution changes only the one-site Hamiltonian $\sum_{n=1}^{N} \sum_{\alpha=1}^{\sigma} H^{o}_{n\alpha}$ and does not effect the interaction term $\sum_{n\alpha < m\beta}$ $V_{n\alpha, m\beta}$.

(3) Higher order effects of the one-site Hamiltonian, which would correspond to a distortion about the impurity site, are ignored.

(4) The crystal is considered to be infinitely dilute, that is guest-guest interactions are ignored.

d. Isolated Impurity Levels and Virtual States

Several different types of solutions to Eq. (30) are possible. If the trap depth is too small, there will of course be no solutions E_o for Eq. (30). In this case the impurity level is imbedded in the host exciton band and is indistinguishable from the host band.

If an E_o for which Eq. (17) is a maximum exists but lies within the host exciton band, one observes an increase in the density of states in the region of the impurity. An impurity state of this type is referred to as a virtual bound state. States of this type are familiar from the theory of alloys[23] and from scattering theory.[24] The excitation in a virtual state is not localized at the impurity center, but it is concentrated in the vicinity of the impurity in contrast to the case discussed in the preceding paragraph where the excitation is completely delocalized.

The third and final type of solution to Eq. (30) is the case where

U_o is large enough so that the impurity level is well outside the host exciton band. In this case, to a good approximation, the energy is localized at the impurity site. Solutions E_o of this type are referred to as isolated impurity levels.

3. Calculation of Impurity Energy Levels

To calculate the impurity energy level E_o for a given trap depth U_o from Eq. (30), we must know the functional form of $F_o(E)$. From Eq. (29) this means that we must know the complete pure crystal exciton band density of states $g_o(E)$ for the host molecule. In this section we will discuss the calculation of $g_o(E)$, $F_o(E)$ and E_o for isotopic mixed crystals of benzene. We will specifically treat the exciton bands formed from benzene's lowest singlet state $^1B_{2u}$ and from its lowest triplet state $^3B_{1u}$.

a. Density of States Calculation

We need an expression for the exciton band energy $E(\vec{k})$ as a function of $\vec{k}$ the wave-vector. Then by considering all possible values of $\vec{k}$ we can obtain the number of $\vec{k}$-states at each energy E which is just the density of states. The calculation of $E(\vec{k})$ for benzene has been discussed by Colson et al.[25] Benzene's crystallographic space group symmetry is D_{2h}^{15} with four molecules per unit cell.[26] All molecules in the unit cell are equivalent so that we do not need to know the $B_{\alpha j}^{f}(\vec{k})$ in subsequent calculations. There are four branches to the benzene $^3B_{1u}$ or $^1B_{2u}$ exciton bands. The energy for these branches indicated by superscript i may be written

$$E^i = \bar{\epsilon} + \Delta + L^i(\vec{k}) \tag{31}$$

where $\bar{\epsilon}$ is the gas phase excitation energy, Δ is the gas-to-ideal mixed crystal shift and $L^i(\vec{k})$ is the $\vec{k}$ dependent resonance term due to excitation exchange interactions between both translationally equivalent and translationally inequivalent molecules.[20] Note that in these terms the trap depth U_o may be written

$$U_o = (\bar{\epsilon}_{host} - \bar{\epsilon}_{guest}) + (\Delta_{host} - \Delta_{guest}) \quad . \tag{32}$$

The important term in Eq. (31) for the density of states calculation is the $\vec{k}$-dependent term $L^i(\vec{k})$.

Colson et al.[25] have pointed out that by ignoring only those interactions that occur between translationally equivalent molecules skew to the crystallographic axis and taking advantage of the centrosymmetric character of the benzene crystal space group, we can write this $\vec{k}$-dependent term as

$$\begin{aligned} L^i(\vec{k}) = {} & 2M_a \cos(k_a a) + 2M_b \cos(k_b b) \\ & + 2M_c \cos(k_c c) + 4a^i_{II} M_{I\,II} \cos(k_a \tfrac{1}{2} a) \cos(k_b \tfrac{1}{2} b) \\ & + 4a^i_{III} M_{I\,III} \cos(k_b \tfrac{1}{2} b) \cos(k_c \tfrac{1}{2} c) \\ & + 4a^i_{IV} M_{I\,IV} \cos(k_a \tfrac{1}{2} a) \cos(k_c \tfrac{1}{2} c) \quad . \end{aligned} \tag{33}$$

Here M_a, M_b and M_c are sums of excitation exchange interactions between translationally equivalent molecules along the crystallographic a, b and c axes, and the $M_{I\,II}$, $M_{I\,III}$ and $M_{I\,IV}$ are the corresponding

translationally inequivalent interactions. The values of a^i_{II}, a^i_{III}, a^i_{IV}, respectively are for the four values of $\underline{i}$

i =			
1	+1	+1	+1
2	+1	-1	-1
3	-1	+1	-1
4	-1	-1	+1

The quantities k_a, k_b and k_c are the projections of $\vec{k}$ on the crystallographic axes. The number of values of k_a for example is equal to the number of primitive unit cells along the a-axis. In calculating $E(\vec{k})$ we will thus have to consider a finite crystal. In the calculations presented below we have assumed that the crystal has 41 unit cells along all three crystal axes. This means that our crystal contains 275, 684 molecules.

The only additional parameters that we need for a calculation of $E(\vec{k})$ are the M's in Eq. (33). Colson et al.[25] have obtained the following values for the $^1B_{2u}$ state of benzene from an experimental investigation of band-band transitions:

$$M_a = M_b = M_c = 0$$
$$M_{III} = -1.55 \text{ cm}^{-1}$$
$$M_{IIII} = 3.93 \text{ cm}^{-1}$$
$$M_{IIIV} = 3.28 \text{ cm}^{-1}$$

These values are in good agreement with the experimentally observed position of the three spectroscopically allowed $\vec{k} = 0$ exciton components

and with independent estimates of the position of the fourth spectroscopically forbidden component.[14]

For the triplet state $^3B_{1u}$, we have no experimental information that would enable us to determine the translationally equivalent interactions M_a, M_b, M_c. We will make the very reasonable assumption that for the triplet, as for the singlet, they are zero. For three translationally inequivalent interactions can be determined from measurements of the exciton splitting in the $^3B_{1u} \leftarrow {}^1A_{1g}$ absorption.[15] Since we do not know the polarization of the various triplet exciton components in absorption, we cannot definitely assign the experimentally determined interaction energies to specific M's. We list them below by analogy to the singlet state:

$$M_{I\,II} = -0.270\ cm^{-1}$$
$$M_{I\,III} = 1.050\ cm^{-1}$$
$$M_{I\,IV} = 0.720\ cm^{-1}$$

The assignment of a given crystallographic interaction M_{ij} to a given experimentally determined interaction energy is done for convenience only. It does <u>not</u> effect the calculated density of states at all.

With these parameters the calculation of the pure crystal density of states $g_o(E)$ is merely a matter of calculating the energy given by Eq. (33) for each of the 375,684 values of $\vec{k}$ and then counting the number of k-states at each energy E. This calculation has been performed for both the $^3B_{1u}$ and $^1B_{2u}$ states. We calculated the number of k-states in $\frac{1}{4}\ cm^{-1}$ energy intervals using an IBM 360/75 computer.

The density of states function is plotted for the $^1B_{2u}$ state in Fig. 1 and for the $^3B_{1u}$ state in Fig. 2. Since the density of states function is the necessary starting point for calculations of impurity levels in benzene and the computer calculation of it takes a significant amount of time, we have listed the numerical values of $g_o(E)$ for future use in Appendix E.

b. Calculation of F(E)

Knowing $g_o(E)$ and the fact that all molecules in the benzene unit cell are crystallographically equivalent, F(E) can be calculated in a straightforward fashion from Eq. (29). Figure 3 is a plot of such a calculation for the $^1B_{2u}$ state. In Fig. 4 the function F(E) for the $^3B_{1u}$ state is indicated.

A great deal of information is contained in these F(E) functions. Recalling Eq. (30) we can see that if a point on the vertical axes is thought of as representing $1/U_o$, then a horizontal line drawn through that point intersects the curve of F(E) at two points E_o^{max} and E_o^{min}. The E_o^{max} is the position of the maximum in the $g_o(E)$ function and for the curves we have indicated in Figs. (3) and (4)

$$|E_o^{max}| > |E_o^{min}| \quad .$$

E_o^{min} of course is the energy of the corresponding anti-level.

For the $^1B_{2u}$ level, if the trap depth falls within the interval

$$-9.7\ cm^{-1} < U_o < +10.6\ cm^{-1}$$

the impurity level is completely engulfed in the host exciton band and

Figure 1. Density of states in the $^1B_{2u}$ exciton band of benzene. The four vertical lines indicate the position of the four $\vec{k} = 0$ exciton components.

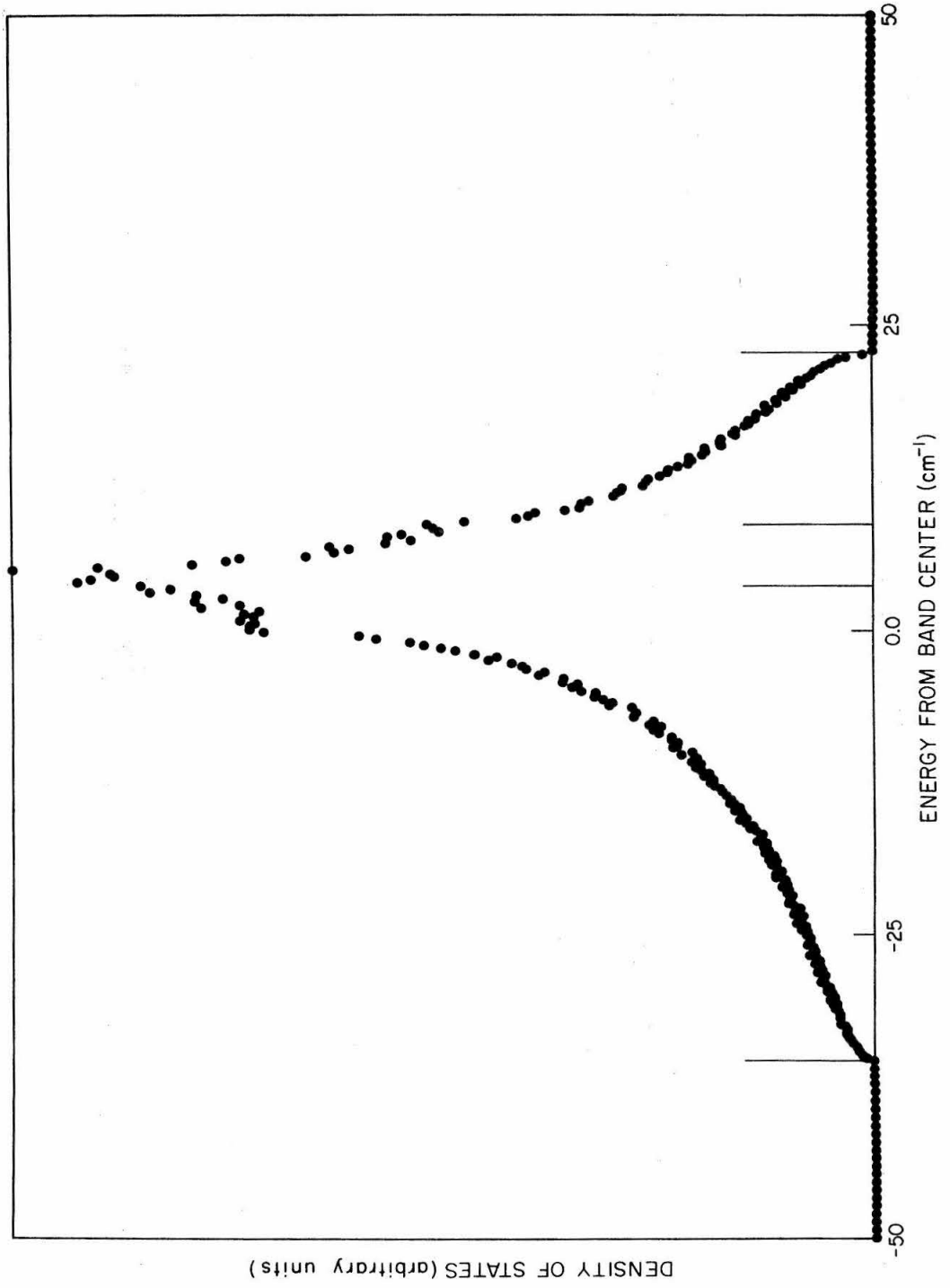
50
25
0.0
-25
-50
ENERGY FROM BAND CENTER (cm^{-1})
DENSITY OF STATES (arbitrary units)

Figure 2. Density of states in the $^3B_{1u}$ exciton band of benzene. The four vertical lines indicate the position of the four $\vec{k} = 0$ exciton components.

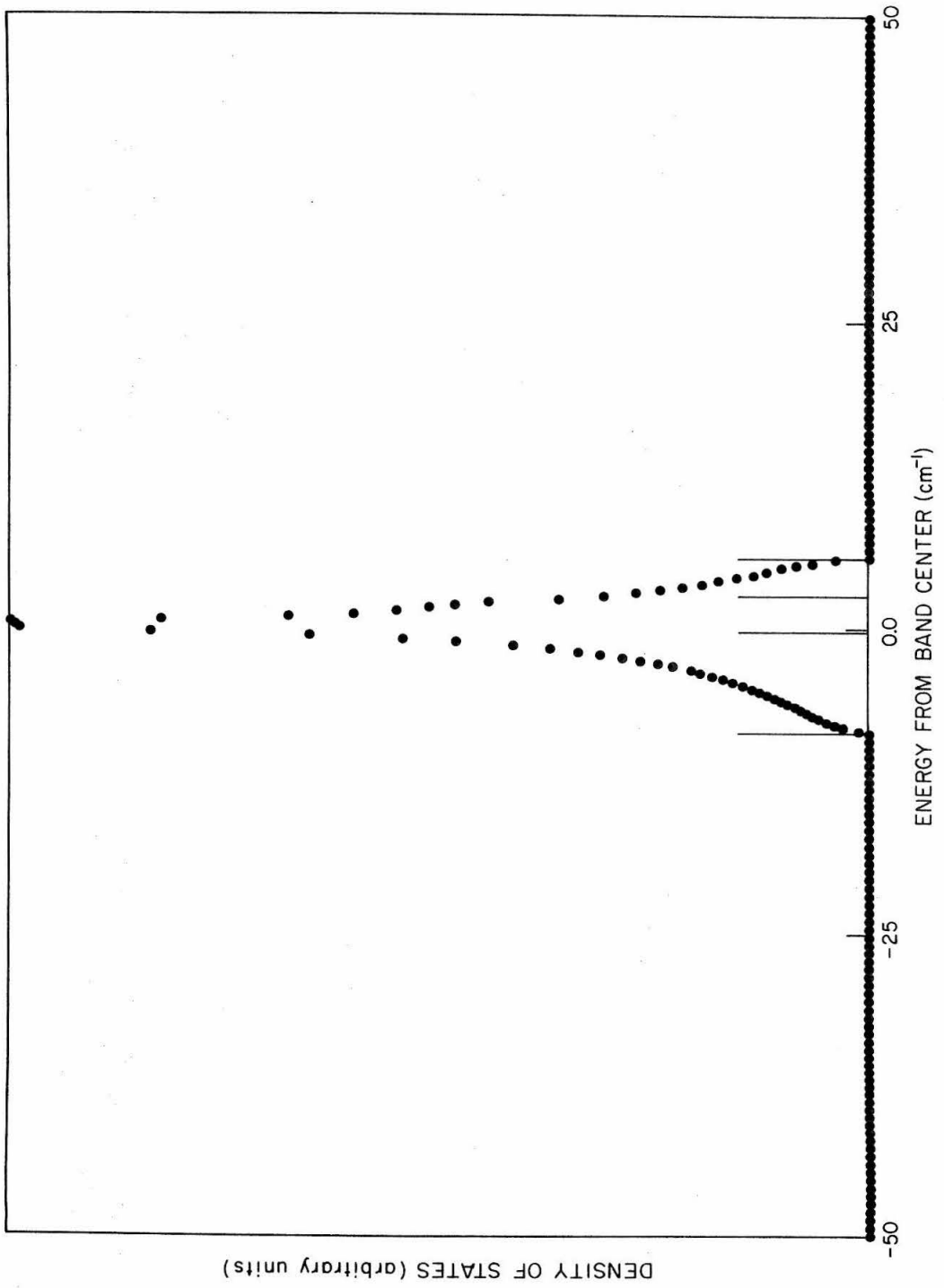
50
25
0.0
-25
-50
ENERGY FROM BAND CENTER (cm^{-1})
DENSITY OF STATES (arbitrary units)

Figure 3. F(E) for a C_6H_6 host in the $^1B_{2u}$ electronic state. The vertical lines indicate the boundaries of the host exciton band.

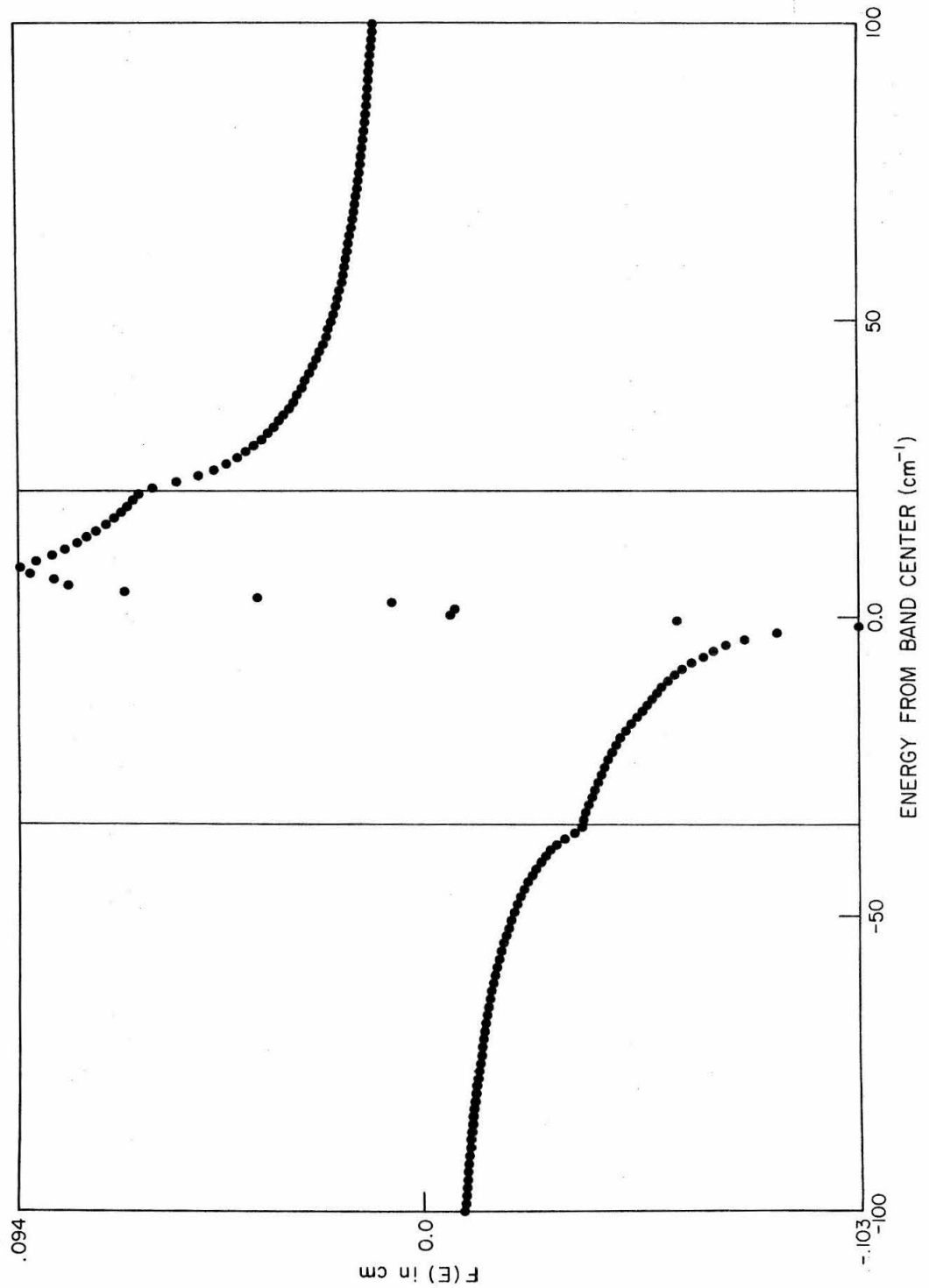
.094
0.0
-.103
F(E) in cm
-100
-50
0.0
50
100
ENERGY FROM BAND CENTER (cm⁻¹)

Figure 4. F(E) for a C_6H_6 host in the $^3B_{1u}$ electronic state. The vertical lines indicate the boundaries of the host exciton band.

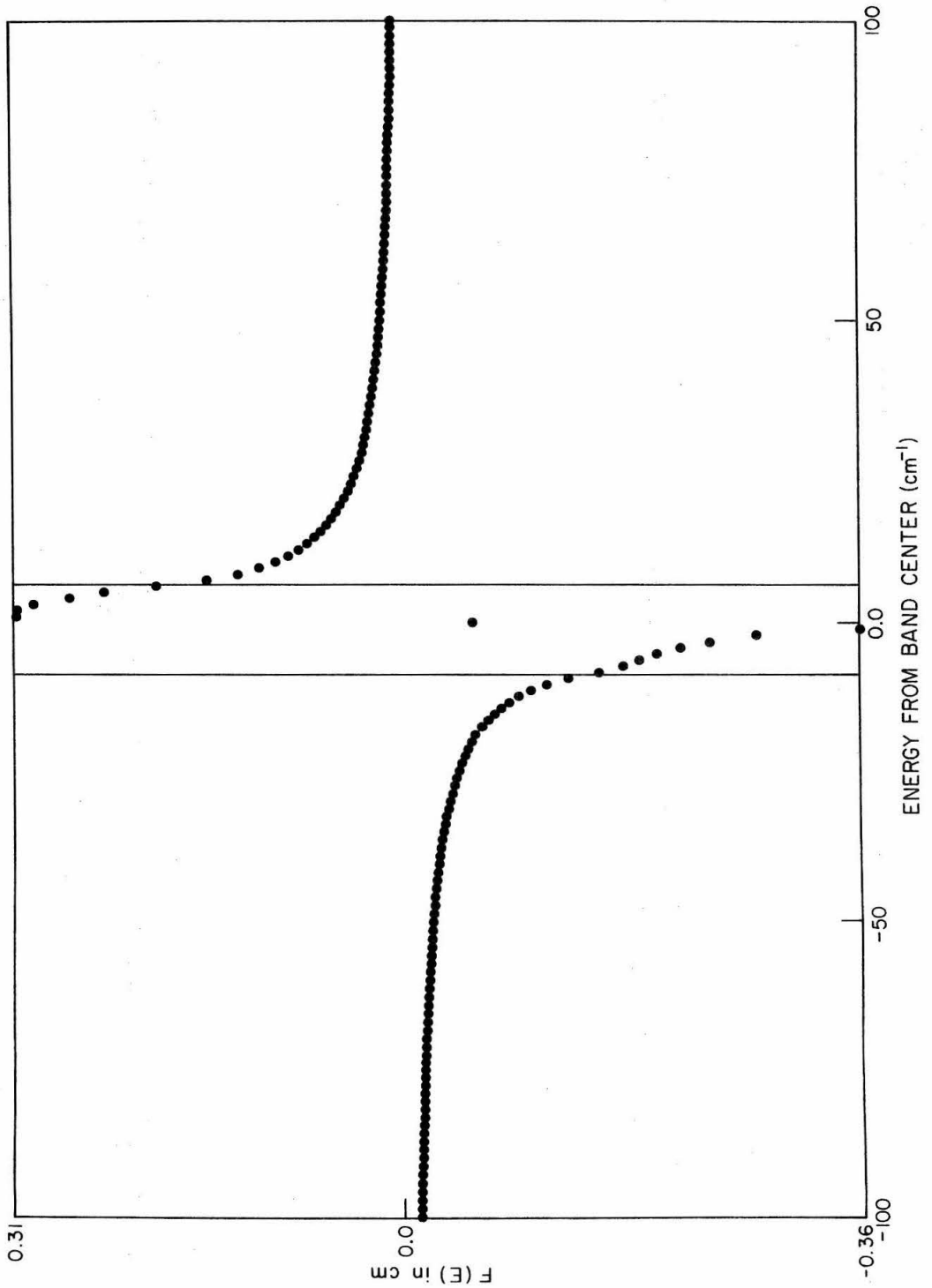
0.31
0.0
-0.36
F (E) in cm
-100
-50
0.0
50
100
ENERGY FROM BAND CENTER (cm⁻¹)

there is no solution E_o to Eq. (30). For U_o values in the range

$$-9.7\ cm^{-1} < U_o < -3.5\ cm^{-1}$$

$$+10.6\ cm^{-1} > U_o > +2.2\ cm^{-1}$$

the solutions E_o represent virtual bound states. Similarly for the $^3B_{1u}$ state we find no solutions for

$$-2.8\ cm^{-1} < U_o < +3.2\ cm^{-1}$$

and virtual bound states for

$$-2.8\ cm^{-1} > U_o > -8.1\ cm^{-1}$$

$$+3.2\ cm^{-1} < U_o < +6.0\ cm^{-1}$$

Outside of the energy intervals for U_o indicated above isolated localized impurity levels are found.

c. Position of Impurity Energy Levels

Once one knows F(E), it is a simple step to determine the impurity energy level E_o for a given U_o using Eq. (30). Because there may be and usually are two E_o's which satisfy Eq. (30), one representing the impurity level and the other the anti-level, it is easier to fix E_o and then to calculate the trap depth U_o giving rise to such an impurity level. This we have done for both the $^3B_{1u}$ and $^1B_{2u}$ states of benzene. The results are presented in Table I.

For the $^3B_{1u}$ state the shift in energy from U_o to E_o, known as the quasi-resonance shift,[20] is negligible ($< 1\ cm^{-1}$) for impurity levels deeper than $\pm 10\ cm^{-1}$. Measurements of $^3B_{1u}$ isotopic mixed crystal

TABLE I. Impurity levels for various trap depth values for the $^3B_{1u}$ and $^1B_{2u}$ states of C_6H_6.

Impurity Level E_o (cm^{-1})	Trap Depth U_o (cm^{-1})	
	$^3B_{1u}$	$^1B_{2u}$
-100.0	- 99.8	-98.6
- 95.0	- 94.8	-93.5
- 90.0	- 89.8	-88.4
- 85.0	- 84.8	-83.3
- 80.0	- 80.8	-78.2
- 75.0	- 74.8	-73.1
- 70.0	- 69.8	-67.9
- 65.0	- 64.8	-62.7
- 60.0	- 59.8	-57.4
- 55.0	- 54.7	-52.1
- 50.0	- 49.7	-46.7
- 45.0	- 44.7	-41.0
- 40.0	- 39.7	-34.9
- 35.0	- 34.7	-25.7
- 30.0	- 29.6	-24.6
- 25.0	- 24.6	-22.9
- 20.0	- 19.5	-21.3
- 15.0	- 14.3	-18.9
- 10.0	- 8.8	--

TABLE I. (Continued)

Impurity Level E_o (cm^{-1})	Trap Depth U_o (cm^{-1})	
	$^3B_{1u}$	$^1B_{2u}$
- 5.0	- 5.0	--
- 0.0	--	--
+ 5.0	+ 3.9	--
+ 10.0	+ 9.5	--
+ 15.0	+ 14.7	+12.8
+ 20.0	+ 19.8	+14.5
+ 25.0	+ 24.9	+20.1
+ 30.0	+ 29.9	+26.4
+ 35.0	+ 34.9	+32.0
+ 40.0	+ 40.0	+37.5
+ 45.0	+ 45.0	+42.8
+ 50.0	+ 50.0	+48.0
+ 55.0	+ 55.0	+53.2
+ 60.0	+ 60.0	+58.4
+ 65.0	+ 65.0	+63.5
+ 70.0	+ 70.0	+68.6
+ 75.0	+ 75.0	+73.7
+ 80.0	+ 80.0	+78.8
+ 85.0	+ 85.0	+83.9
+ 90.0	+ 90.0	+88.9
+ 95.0	+ 95.0	+94.0
+100.0	+100.0	+99.0

impurity levels therefore do not yield information on the host exciton bands; rather they yield only the ideal mixed crystal level defined by Eq. (32) and referred to the center of the host exciton band as the zero of energy.

The quasi-resonance shift in the benzene $^1B_{2u}$ state is not much larger ($< 5\ cm^{-1}$ for $U_o > 40\ cm^{-1}$). Since impurity line positions cannot be measured to much better than $\pm 1\ cm^{-1}$, the information on the singlet exciton band that can be gleaned from mixed crystal studies is also minimal. These comments are not meant to imply that mixed crystal studies on benzene are fruitless. In the next section we examine some of these experimental studies and the information regarding intermolecular interactions that can be obtained from them.

4. Experimental Results for Benzene Isotopic Mixed Crystals

a. The $^1B_{2u}$ Electronic State

The data presented here have been discussed before. Colson,[14] who obtained much of the data on the benzene singlet state himself, discussed it in terms of the failure of the Nieman and Robinson energy denominator method.[11] Sommer and Jortner[9] have recently reviewed these data using the mixed crystal theory outlined in Section 2. The present discussion deviates from these two earlier treatments in its emphasis on using the mixed crystal theory of Section 2 to obtain the ideal mixed crystal level U_o from the experimental data. We will not try to use the data to investigate the host exciton structure since this

information is already available from experimental measurements of $g_o(E)$[25] and since, as pointed out in Section 4, mixed crystal experiments yield very little information on the host exciton bands of benzene.

Our procedure in obtaining the ideal mixed crystal level will be to first make an "educated" guess of U_o that is accurate to within $\pm 10\ cm^{-1}$. From this value for U_o we can calculate a value of E_o, the real mixed crystal level using the results of Section 3. Then we obtain the quasiresonance shift δ by simply subtracting U_o from E_o. Since δ is a slowly varying function of U_o (see Table I), the calculated value for δ will be within $\pm 1\ cm^{-1}$ of the correct value provided our guess for U_o is as good as indicated and provided that U_o, referred to the exciton band center, is not too small. Knowing δ and determining E_o from experiment, we can obtain a value of U_o that is within $\pm 1\ cm^{-1}$ of the actual ideal mixed crystal level provided the theory of Section 3 is valid and provided the density of states function for C_6H_6 is also appropriate for other isotopic hosts.

The first order of business is to make an educated guess for U_o. This quantity is defined in Eq. (32). Colson[14] has shown that the guest mixed crystal energy minus its gas phase energy, given by

$$E_o - \bar{\epsilon} = \Delta + \delta \tag{34}$$

is for all mixed crystals studied $-246 \pm 13\ cm^{-1}$ which indicates that Δ may be nearly (within $13\ cm^{-1}$) equal for all isotopic benzenes. If this is true then to within $\pm 13\ cm^{-1}$ Eq. (32) may be approximated by

$$U_o \approx (\bar{\epsilon}_{host} - \bar{\epsilon}_{guest}) \quad . \tag{35}$$

Note, we do not assume that Δ is a constant, merely that it changes within a range of ± 13 cm^{-1}.

We can now approximate U_o by subtracting host and guest gas phase energy values. These gas phase energy values are listed in Table II. The ideal mixed crystal levels calculated from Eq. (35) are listed in Table III. In addition Table III contains the calculated values of E_o and δ. Finally in Table IV the actual value of U_o now referred to the benzene ground state as the zero of energy is obtained from the experimental E_o and δ from Table III.

It has been assumed in past studies of benzene isotopic mixed crystals[9,11] that U_o does not change with a change in the host molecule. But clearly from Table IV the ideal mixed crystal level for a given isotopic benzene seems to increase by about 2 cm^{-1} as deuteriums are added to the host. This is precisely the conclusion Colson[14] obtained from a less detailed inspection of the mixed crystal data. The only system that does not seem to conform to this 2 cm^{-1} shift per deuterium is C_6H_6 in C_6DH_5. The trap depth (Table III) for this system is -38 ± 10 cm^{-1} so that δ is -4 ± 7 cm^{-1}. The large margin of error for δ here is due to the proximity of the C_6H_6 level to the host C_6DH_5 band. In this region δ is no longer a slowly varying function of E_o.

Actually it would be helpful not to have to take such a roundabout approach in obtaining the ideal mixed crystal level U_o. If one assumes that translationally equivalent excitation exchange interactions are small, then U_o referred to the host exciton band center by Eq. (12) is merely the difference between the means of guest and host exciton

TABLE II. Gas phase singlet energies for isotopic benzenes.

Isotopic Benzene	Energy[a] (cm^{-1})
C_6H_6	38,086.1 ± .1
C_6H_5D	38,124 ± 5
p-$C_2D_2H_4$	38,155 ± 5
sym-$C_6D_3H_3$	38,186 ± 5
m-$C_6D_4H_2$	38,222 ± 5
C_6D_5H	38,260 ± 5
C_6D_6	38,289.1 ± .1

[a]V. L. Broude, Sov. Phys.-Uspekhi 4, 585 (1962) except C_6H_6 and C_6D_6 energies which are from J. H. Callomon, T. M. Dunn, and J. M. Mills, Phil. Trans. Roy. Soc. (London) 259A, 499 (1966).

TABLE III. Mixed crystal singlet levels for isotopic benzene.

Host	Guest	Calculated Mixed Crystal Level, E_o (cm^{-1})[a, b]	Ideal Mixed Crystal Level U_o (cm^{-1})[a, c]	Quasi-resonance Shift, δ (cm^{-1})
C_6D_6	C_6H_6	-204	-203	-1
C_6D_5H	C_6H_6	-175	-174	-1
m-$C_6D_4H_2$	C_6H_6	-137	-136	-1
sym-$C_6D_3H_3$	C_6H_6	-101	-100	-1
p-$C_6D_2H_4$	C_6H_6	- 71	- 69	-2
C_6DH_5	C_6H_6	- 42	- 38	-4
p-$C_6D_2H_4$	C_6D_6	+135	+134	+1
C_6DH_5	C_6D_6	+166	+165	+1
C_6H_6	C_6D_6	+203	+203	0
C_6H_6	C_6DH_5	+ 41	+ 38	+3
C_6D_6	C_6DH_5	-166	-165	-1
C_6H_6	m-$C_6D_4H_2$	+137	+136	+1
C_6D_6	m-$C_6D_4H_2$	- 69	- 67	-2
C_6H_6	C_6D_5H	+175	+174	+1
C_6D_6	C_6D_5H	- 36	- 29	-7

[a]The energies E_o and U_o are both referred to the center of the host exciton band.

[b]Calculated using the C_6H_6 host exciton band structure.

[c]Differences in gas phase energies. See Table I.

TABLE IV. Ideal mixed crystal level for isotopic benzene singlets in different hosts.

Host	Guest	Experimental Mixed Crystal Level, E_o (cm^{-1})	Ideal Mixed Crystal Level, U_o (cm^{-1})
C_6D_6	C_6H_6	37, 853 ± 1	37, 854
C_6D_5H	C_6H_6	37, 852	37, 853
m-$C_6D_4H_2$	C_6H_6	37, 850	37, 851
sym-$C_6D_3H_3$	C_6H_6	37, 846	37, 847
p-$C_6D_2H_4$	C_6H_6	37, 841	37, 843
C_6DH_5	C_6H_6	37, 830	37, 834
p-$C_6D_2H_4$	C_6D_6	38, 038	38, 037
C_6DH_5	C_6D_6	38, 035	38, 034
C_6H_6	C_6D_6	38, 033	38, 033
C_6H_6	C_6DH_5	37, 877	37, 874
C_6D_6	C_6DH_5	37, 884	37, 885
C_6H_6	m-$C_6D_4H_2$	37, 971	37, 970
C_6D_6	m-$C_6D_4H_2$	37, 981	37, 983
C_6H_6	C_6D_5H	38, 001	38, 000
C_6D_6	C_6D_5H	38, 003	38, 010

[a]S. D. Colson, J. Chem. Phys. 48, 3324 (1968).

bands. Or referred to the ground electronic state as the zero of energy, U_o is the mean of the exciton band of the benzene isotope in question. A more direct means of obtaining U_o is thus simply to measure the mean of the four benzene exciton components in absorption. For the benzene singlet however only three of the four Davydov components can be observed.[14, 20]

The means of the C_6H_6 and C_6D_6 $^1B_{2u}$ exciton bands have been indirectly determined by accurately measuring the position of a vibronic band in absorption and subtracting the appropriate vibrational frequency. The values obtained are 37, 838 cm^{-1} for C_6H_6[14] and 38, 046 cm^{-1} for C_6D_6.[27] No corresponding measurements for the other isotopic benzenes have been made. In the context of Table IV, these mean values correspond respectively to the position of a C_6H_6 guest in a C_6H_6 host and a C_6D_6 guest in a C_6D_6 host. Both values fit nicely into the 2 cm^{-1}/host deuterium shift of U_o.

b. The $^3B_{1u}$ Electronic State

The experimental information for the $^3B_{1u}$ state is much less abundent. In Section IIIA we have reported the measurement of all four factor group components for both C_6H_6 and C_6D_6. In addition the mean of the exciton band has been measured in the same way for sym-$C_6H_3D_3$ and C_6H_5D. These results are reported in Table V. In the table we also report the ideal mixed crystal level determined experimentally from mixed crystal phosphorescence measurements. Recall from Section 3(c) that E_o and U_o are practically (within .5 cm^{-1}) identical for the benzene triplet.

TABLE V. Mixed crystal energies for benzene triplet.

Host	Guest	Ideal Mixed Crystal Level (cm^{-1})	Mean of Guest Exciton Band[d] (cm^{-1})
C_6D_6	C_6H_6	29,658.2 ± .1 [a]	29,647 ± 1
$C_6H_3D_3$	C_6H_6	29,657 ± 5[b]	
C_6D_6	sym-$C_6H_3D_3$	29,753.8 ± .1[a]	29,754 ± 5
C_6D_6	C_6H_5D	29,690.5 ± .3 [c]	29,684 ± 5
		29,683.8 ± .3	

[a]E. R. Bernstein, S. D. Colson, D. S. Tinti, and G. W. Robinson, J. Chem. Phys. 48, 4632 (1968).

[b]G. C. Nieman and G. W. Robinson, J. Chem. Phys. 39, 1298 (1963).

[c]G. C. Nieman and D. S. Tinti, J. Chem. Phys. 46, 1432 (1967).

[d]This work.

The 2 cm^{-1}/host deuterium shift of U_o is again evident. The difference in energy, for example, between the C_6H_6 triplet in C_6D_6 and C_6H_6 hosts is 11 cm^{-1}. The other results are also consistent with the host dependence of U_o although the large error limits (± 5 cm^{-1}) in some cases obscure the details of the effect.

5. Discussion

In this section we will attempt to determine the source of the 2 cm^{-1}/host deuterium shift of the ideal mixed crystal level. The shift may be a real change in U_o with host isotopic composition or it may be an indication that the mixed crystal theory outlined in Section 2 breaks down for benzene in some systematic way. We will first examine this latter possibility by referring to the assumptions, listed at the end of Section 2c, that were made in deriving Eq. (30).

Equation (30) does not take into account any mixing of the electronic states that have free molecule origins (such as the $^3B_{1u}$ and $^1B_{2u}$ states) with those electronic states which are purely crystal states (charge-transfer and double-excitation states). Silbey et al.[28] have suggested that a charge transfer state located near the $^1B_{2u}$ exciton band origin might be responsible for some of the observed exciton splitting. These authors[29] have recently modified this suggestion however on the basis of work by Geacintov and Pope[30] which indicates that for anthracene and naphthalene and by implication benzene the charge-transfer state is near its position predicted from a classical analysis. This would place the benzene charge-transfer state some 10,000 cm^{-1} away from the $^1B_{2u}$ state. To explain the 2 cm^{-1} shift

on the basis of interaction with this distant charge transfer level, one would have to postulate a rather large effect of the level on the gas-crystal shift of the $^1B_{2u}$ state. Colson[14] has discussed the experimental evidence which argues against this large effect. In addition he has reported experimental results which indicate that the interaction of the $^1B_{2u}$ state with any purely crystal state is negligible. The $^3B_{1u}$ state being lower in energy than the $^1B_{2u}$ is expected to be even less susceptible to these types of interaction, unless of course one postulates an abnormally large energy difference between singlet and triplet charge transfer states. On balance then the bulk of available experimental evidence argues against the breakdown of the mixed crystal theory applied to benzene due to interaction with purely crystal states.

In our calculation of U_o we have also ignored any isotope effect on the interaction term $\sum_{n\alpha < m\beta} V_{n\alpha, m\beta}$. This means, according to Eq. (31) that $L^i(\vec{k})$ is independent of isotopic composition. We know that this is not quite true. The measured exciton splitting for the $^1B_{2u}$ states of C_6H_6 and C_6D_6 appear to be slightly different (Table VI). Using the C_6D_6 exciton splitting in Table VI, we have calculated $g_o(E)$ and values of U_o by the method discussed in the last section. In all cases the change in U_o due to this slight change in exciton band structure is negligible. The impurity level E_o for a given U_o is simply not very sensitive to the fine details of the host exciton band.

It is, of course, possible that the translationally equivalent interactions (M_a, M_b and M_c in Eq. (33)) are not zero as we have assumed. If this were true they might cause the observed 2 cm^{-1}

TABLE VI. Benzene exciton splitting-$^1B_{2u}$ state.

Molecule	Polarization	Exciton Level (cm^{-1})[a]
C_6H_6	$\vec{a}$	37, 803 ± 1
	$\vec{b}$	37, 842
	$\vec{c}$	37, 847
	-	(37, 860)
C_6D_6	$\vec{a}$	38, 012 ± 1
	$\vec{b}$	38, 046
	$\vec{c}$	38, 051
	-	(38, 075)[b]

[a]S. D. Colson, J. Chem. Phys. 48, 3324 (1968).

[b]Estimated from the mean of the exciton band determined by V. L. Broude, Sov. Phys. -Uspekhi 4, 584 (1962).

shift of U_o. The translationally inequivalent interactions are three times larger for the $^1B_{2u}$ state than for the $^3B_{1u}$ state. One would expect a comparable decrease in interaction strength for M_a, M_b and M_c. But the experimental results indicate that the shift of U_o due to host isotopic composition is very nearly the same for the $^1B_{2u}$ and $^3B_{1u}$ states. It thus does not seem likely that the isotope shift of U_o is due to changes of $\sum_{n\alpha < m\beta} V_{n\alpha, m\beta}$ with isotopic composition.

The final two approximations that we have made in deriving Eq. (30) seem entirely reasonable particularly when one looks at the very good results that the theory gives when applied to naphthalene mixed crystals.[9, 12] For naphthalene all interaction terms (translationally equivalent and inequivalent) are larger than the corresponding values for benzene. The gas-crystal shift is also much larger than for benzene. On this basis one would expect higher order effects of the one-site Hamiltonian and concentration effects to be much more of a problem for naphthalene than for benzene. The fact that they seem to be negligible for naphthalene has convinced us that they are also negligible for benzene.

It seems quite likely then that the isotope shift of U_o is really a shift in U_o and not a manifestation of the failure of the theory outlined in Section 2. Referring to the definition of U_o given by Eq. (32), this must mean that the static interaction term Δ_{guest} changes when deuteriums are substituted on the host molecule. This term Δ has been discussed in some detail by Bernstein et al.[20] It is basically the difference between the Coulomb interaction energies of excited state and ground state molecules in the crystal site. It is normally

assumed to be independent of host isotopic composition because H and D atoms produce very nearly identical Coulomb fields. This assumption seems to be quite good for naphthalene. But for naphthalene the H···· H intermolecular Coulomb interactions are not as important as they are for benzene.[31, 32] For benzene reasonable agreement can be obtained between experiment and theory if H···· H interactions alone are considered. Bernstein[32] has pointed out that C···· H and C···· C interactions cannot be entirely neglected however particularly when discussing some of the more subtle effects observed in infrared and ultraviolet spectroscopic studies.

Substitution of a deuterium for a hydrogen in both benzene and naphthalene is expected to reduce the C-H bond length (in CH_4, for example, the change is from 1.094 Å for C-H to 1.092 Å for C-D[33]; no comparable bond length measurements have been made for naphthalene or benzene) and in addition change the mean zero-point vibrational amplitude.[34] Both of these effects can cause a change in Δ by reducing the total H···· H repulsive interaction energy (they may also, of course, effect the C···· H interactions but this effect is expected to be smaller because of the larger interatomic distances involved). We suggest that the change in interatomic H··· H distance with host deuteration changes U_o by 2 cm^{-1}/host deuterium for benzene but does not effect the naphthalene U_o because of the smaller role played by H···· H interactions in naphthalene.

6. Conclusion

The theory of mixed crystals has been applied to isotopic mixed

benzene crystals. The agreement between theory and experiment is quite good if one assumes that the ideal mixed crystal level U_o increases by 2 cm^{-1} as deuterium molecules are added to the host. This shift in U_o is observed for both singlet and triplet mixed crystal levels. We attribute the change in U_o to a change in the H$\cdots$H intermolecular interaction energy as the intermolecular H$\cdots$H distance and the host zero-point vibrational amplitude change with isotopic substitution.

Previous calculations of intermolecular interactions in benzene crystals[31, 32] have all assumed that H$\cdots$H and H$\cdots$D interaction energies are equal. Isotope effects due to varying guest isotopic composition such as site splitting and the orientational effect[32] were adequately but not completely explained as being due solely to the mass difference between hydrogen and deuterium. The mass effect alone however cannot explain the host dependence of U_o. The shift in U_o is clearly due to changes in the static field set-up by the host molecules since its magnitude appears to be independent of guest isotopic composition.

As a final note we point out that the 2 cm^{-1}/host deuterium shift of U_o is observed in both the $^1B_{2u}$ and the $^3B_{1u}$ electronic states. This result is somewhat unexpected, particularly in view of the fact that the gas-crystal shift is positive for the triplet and negative for the singlet.

REFERENCES

1. R. G. Body and I. G. Ross, Australian J. Chem. 19, 1 (1966).
2. D. P. Craig, Adv. in Chem. Phys. 8, 27 (1964); D. P. Craig and M. R. Philpott, Proc. Roy. Soc. (London) A290, 583 (1966); A293, 213 (1966).
3. E. I. Rashba, Opt. i Spek. 2, 568 (1957); Sov. Phys. -Sol. State 4, 2417 (1963); V. I. Sugakov, Sov. Phys. -Sol. State 10, 2363 (1969).
4. R. E. Merrifield, J. Chem. Phys. 38, 920 (1963).
5. S. Takeno, J. Chem. Phys. 44, 853 (1966).
6. B. S. Sommer and J. Jortner, J. Chem. Phys. 50, 187 (1969).
7. V. L. Broude and M. I. Onoprienko, Opt. and Spec. 10, 333 (1961); E. F. Sheka, Opt. and Spec. 10, 360 (1961); E. F. Sheka, Akad. Nauk. SSR Isvestia Ser. Fiz. 27, 503 (1963); V. L. Broude, E. I. Rashba and E. F. Sheka, Sov. Phys. -Dokl. 6, 718 (1962); Phys. Stat. Sol. 19, 395 (1967).
8. D. P. Craig and T. Thirunamachandran, Proc. Roy. Soc. (London) A271, 207 (1963); D. P. Craig and M. R. Philpott, Proc. Roy. Soc. (London) A290, 602 (1966); C. D. Akon and D. P. Craig. Trans. Far. Soc. 63, 56 (1967).
9. B. S. Sommer and J. Jortner, J. Chem. Phys. 50, 822, 839 (1969).
10. M. A. El-Sayed, M. T. Wauk, and G. W. Robinson, Mol. Phys. 5, 205 (1962); G. C. Nieman and G. W. Robinson, J. Chem. Phys. 37, 2150 (1962).

11. G. C. Nieman and G. W. Robinson, J. Chem. Phys. 39, 1298 (1963).

12. D. M. Hanson, R. Kopelman, and G. W. Robinson, 51, 212 (1969).

13. D. M. Hanson, J. Chem. Phys. 51, 653 (1969).

14. S. D. Colson, J. Chem. Phys. 48, 3324 (1968).

15. D. M. Burland and G. Castro, J. Chem. Phys. 50, 4107 (1969) and Section IIIA of this thesis.

16. J. W. Rabalais, H. J. Maria, and S. P. McGlynn, J. Chem. Phys. 51, 2259 (1969).

17. I. M. Lifshitz, Adv. Phys. 13, 483 (1964).

18. Yu. A. Izyumov, Adv. Phys. 14, 569 (1965).

19. G. F. Koster and J. C. Slater, Phys. Rev. 95, 1167 (1954); 96, 1208 (1954).

20. E. R. Bernstein, S. D. Colson, R. Kopelman, and G. W. Robinson, J. Chem. Phys. 48, 5596 (1968).

21. J. Mathews and R. L. Walker, Mathematical Methods of Physics (W. A. Benjamin, Inc., New York, 1965), p. 456.

22. R. B. Campbell, J. M. Robertson, and J. Trotter, Acta Cryst. 15, 289 (1962).

23. C. Kittel, Quantum Theory of Solids (John Wiley and Sons, Inc., New York, 1963), Chap. 18.

24. M. L. Goldberger and K. M. Watson, Collision Theory (John Wiley and Sons, Inc., New York, 1964), pp. 498-508.

25. S. D. Colson, D. M. Hanson, R. Kopelman, and G. W. Robinson, J. Chem. Phys. 48, 2215 (1968).

26. E. G. Cox, D. W. J. Cruickshank, and J. A. S. Smith, Proc. Roy. Soc. A247, 1 (1958); E. G. Cox, Rev. Mod. Phys. 30, 159 (1958); G. E. Bacon, N. A. Curry, and S. A. Wilson, Proc. Roy. Soc. A279, 98 (1964).

27. V. L. Broude, Sov. Phys.-Uspekhi 4, 584 (1962).

28. R. Silbey, S. A. Rice, and J. Jortner, J. Chem. Phys. 43, 3336 (1965).

29. W. L. Greer, S. A. Rice, J. Jortner, and R. Silbey, J. Chem. Phys. 48, 5667 (1968).

30. N. Geacintov and M. Pope, J. Chem. Phys. 45, 3884 (1966).

31. I. Harada and T. Shimanouchi, J. Chem. Phys. 44, 2016 (1966); N. Rich and D. A. Dows, Mol. Cryst. 5, 111 (1968).

32. E. R. Bernstein, "Calculation of Ground State Vibrational Structure and Phonons of the Isotopic Benzene Crystals," (to be published).

33. Tables of Interatomic Distances and Configurations in Molecules and Ions, Supplement 1956-1959 (The Chemical Society, London, 1965).

34. S. J. Cyvin, Molecular Vibrations and Mean Square Amplitudes (Elsevier Publishing Co., Amsterdam, 1968), pp. 244-253.

PART IV

THE $^3E_{1u} \leftarrow {}^1A_{1g}$ ABSORPTION SPECTRA OF BENZENE AND PERDEUTEROBENZENE

A. INTRODUCTION

The position of the $^3E_{1u} \leftarrow {}^1A_{1g}$ absorption in benzene and benzene-d_6 has been observed by direct absorption[1] and by low energy electron impact techniques.[2] The direct absorption experiments were carried out with and without O_2 as a perturbing agent. In both cases the spectra were broad and structureless even at 4.2° K as might be expected from the discussion of line broadening in Section IIC. The low energy electron impact experiments measure the Franck-Condon maximum of the $^3E_{1u} \leftarrow {}^1A_{1g}$ transition, but do not have the resolution to distinguish any detailed structure that might be present. On the other hand, the direct absorption experiments have the resolution to distinguish structure in the spectra but are plagued with the problem of distinguishing a very small change due to absorption from random fluctuations in the light source.

In view of the low resolution of the electron impact spectra and the experimental difficulties involved in the direct absorption experiments, we decided to investigate the $^3E_{1u} \leftarrow {}^1A_{1g}$ absorption spectra for crystalline C_6H_6 and C_6D_6 at 4.2° K by a third technique, the method of phosphorescence photoexcitation.[3] It is important to pinpoint the position of the $^3E_{1u}$ level particularly because of the importance its position plays in semi-empirical calculations of the electronic energy level structure of benzene.[4] In addition the widths of the observed spectral lines provide a test of current theories of spectral line broadening.[5]

B. EXPERIMENTAL

1. Purification of the Benzene

In attempting to observe weak absorptions, impurity considerations become a real problem. Even a small amount of a strongly absorbing impurity such as phenol can completely mask the very weak $^3E_{1u} \leftarrow {}^1A_{1g}$ absorption of benzene. The purification problem for benzene has been discussed in some detail by Colson and Bernstein.[1] They developed a technique which involves refluxing thoroughly degassed Phillips research-grade benzene over Cs at 100° C for several hours. This technique removes all of the phenol, as far as we can tell spectroscopically, by the reaction

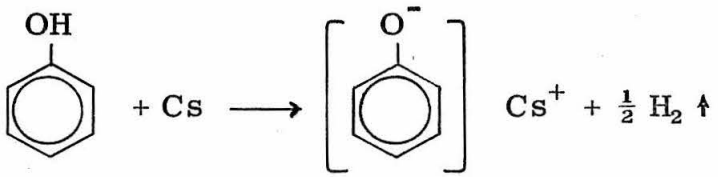

The reaction of Cs with toluene seems to occur much more slowly so that even after two separate refluxing stages and extensive zone-refining enough toluene remained to interfere seriously with the $^3E_{1u} \leftarrow {}^1A_{1g}$ absorption measurements. A detailed discussion of the impurity spectra of C_6H_6 is given in Appendix F. One other interesting point; the C_6D_6 deuterotoluene content was at least 10 times lower than the corresponding C_6H_6 toluene content. No impurities other than toluene and phenol were identified.

2. Apparatus

The experimental set-up used here was, but for one exception, identical to the set-up used in obtaining the $^3B_{1u} \leftarrow {}^1A_{1g}$ absorption spectrum and described in Section IIIA. Referring to Fig. 1 of that section, the only change made was to replace Pyrex Lenses C and D by fused quartz lenses. The wavelength resolution of the apparatus was never poorer than .3 Å and in most cases was as much as a factor of two better. Any detailed structure in the $^3E_{1u} \leftarrow {}^1A_{1g}$ spectra should thus have been detected. The impurity, whose emission was monitored as a function of exciting wavelength, was as before toluene for the C_6H_6 experiments and an isotopic impurity for the C_6D_6 experiments.

C. RESULTS

In Fig. 1 the $^3E_{1u} \leftarrow {}^1A_{1g}$ spectrum for C_6H_6 is presented. The benzene used in obtaining this spectrum had been double Cs-purified. Similar results were obtained with singly Cs-purified benzene and benzene that had been double Cs-purified and extensively zone-refined. In all cases the $^3E_{1u} \leftarrow {}^1A_{1g}$ transition appeared as a broad structureless maximum slightly to the low energy side of a much more intense absorption with a maximum at 2694 Å. The intense absorption was identified as the $^1B_1 \leftarrow {}^1A_1$ absorption of toluene.[6] We have not shown all of the intense impurity absorption in Fig. 1 because with the electrometer sensitivity used in obtaining this spectrum the toluene absorption was off scale.

Because of the interferring toluene absorption, we cannot unequivocally identify the broad spectral feature at 2705 Å as the

Figure 1. The $^3E_{1u} \leftarrow {}^1A_{1g}$ absorption spectrum of C_6H_6 at 4.2° K.

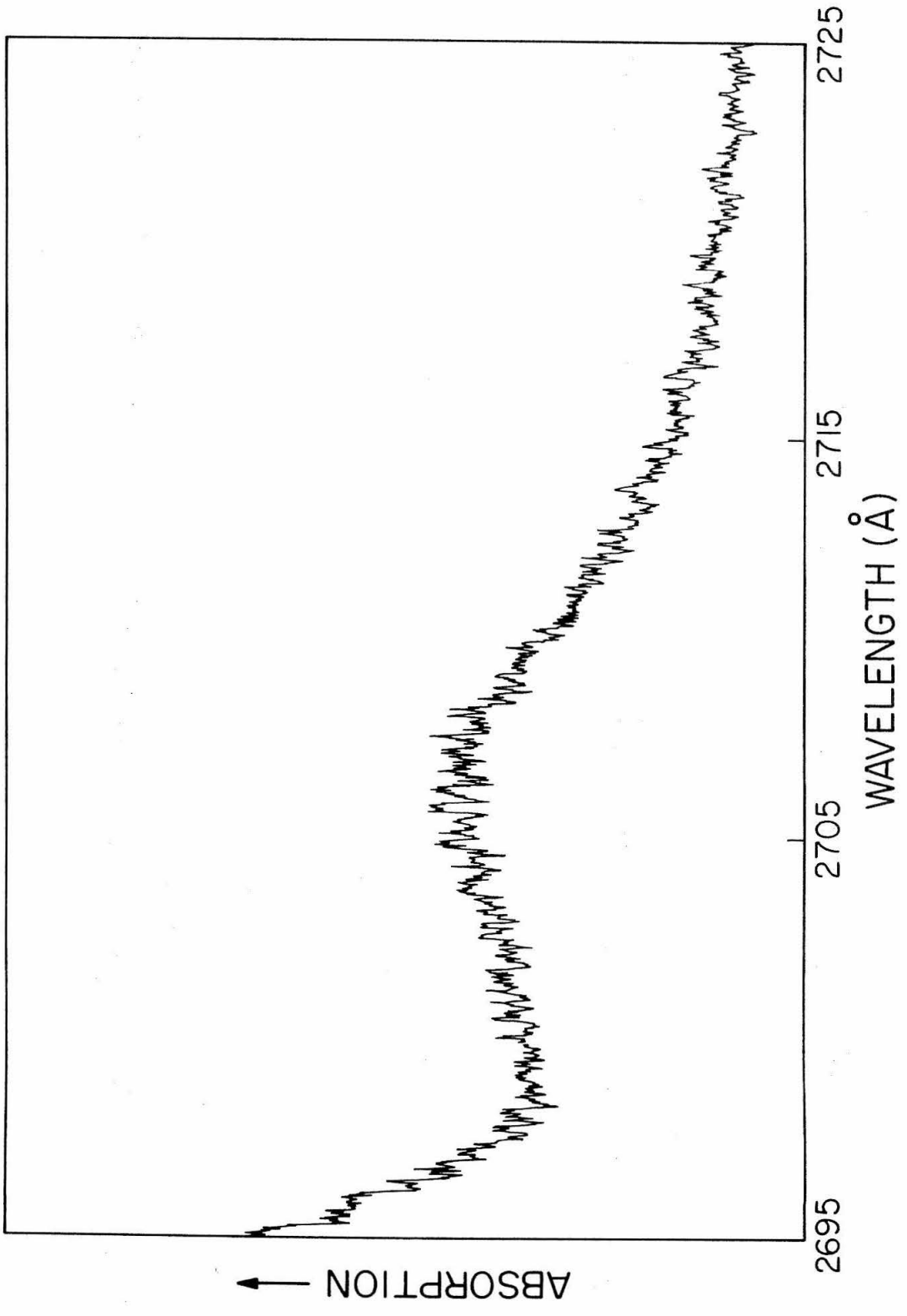
2695
2705
2715
2725
WAVELENGTH (Å)
ABSORPTION

$^3E_{1u} \leftarrow {}^1A_{1g}$ transition. We must still keep in mind the possibility that this feature may be related to the toluene impurity absorption system. The $^3E_{1u} \leftarrow {}^1A_{1g}$ assignment is strongly supported however by the C_6D_6 spectrum (vide infra) and the broad character of the features attributed to this transition. All of the clearly identifiable toluene impurity lines are quite sharp (< 10 Å halfwidth). The spectral feature at 2705 Å on the other hand is very broad (> 50 Å halfwidth) as would be expected on theoretical grounds for the second triplet (see Section IIC).

The C_6D_6 spectrum is displayed in Fig. 2. The most striking feature of this spectrum is the at least ten-fold reduction in the toluene impurity absorption. If the $^3E_{1u} \leftarrow {}^1A_{1g}$ peak (here at about 2790 Å) were due to toluene, one would expect a corresponding ten-fold reduction in the intensity of the 2790 Å peak. This would of course mean that in relative terms the C_6H_6 and C_6D_6 spectra would be quite similar. Instead we find that the sharp toluene impurity peaks have decreased in intensity with respect to the $^3E_{1u} \leftarrow {}^1A_{1g}$ peak.

The positions of the $^3E_{1u} \leftarrow {}^1A_{1g}$ absorption maxima are compared in Table I with the positions measured by Colson and Bernstein[1] in pure, O_2-perturbed and NO-perturbed benzene crystals. The agreement between the pure crystal values is quite good. The 400 cm^{-1} decrease in the absorption maxima of O_2-perturbed benzene is puzzling and may indicate the formation of some type of complex between O_2 and benzene in the condensed phase.[7] Because of the uncertainties surrounding the O_2 and NO perturbed results, we will restrict our discussion in the remainder of this section to the pure crystal results. In

Figure 2. The $^3E_{1u} \leftarrow {}^1A_{1g}$ absorption spectrum of C_6D_6 at 4.2° K.

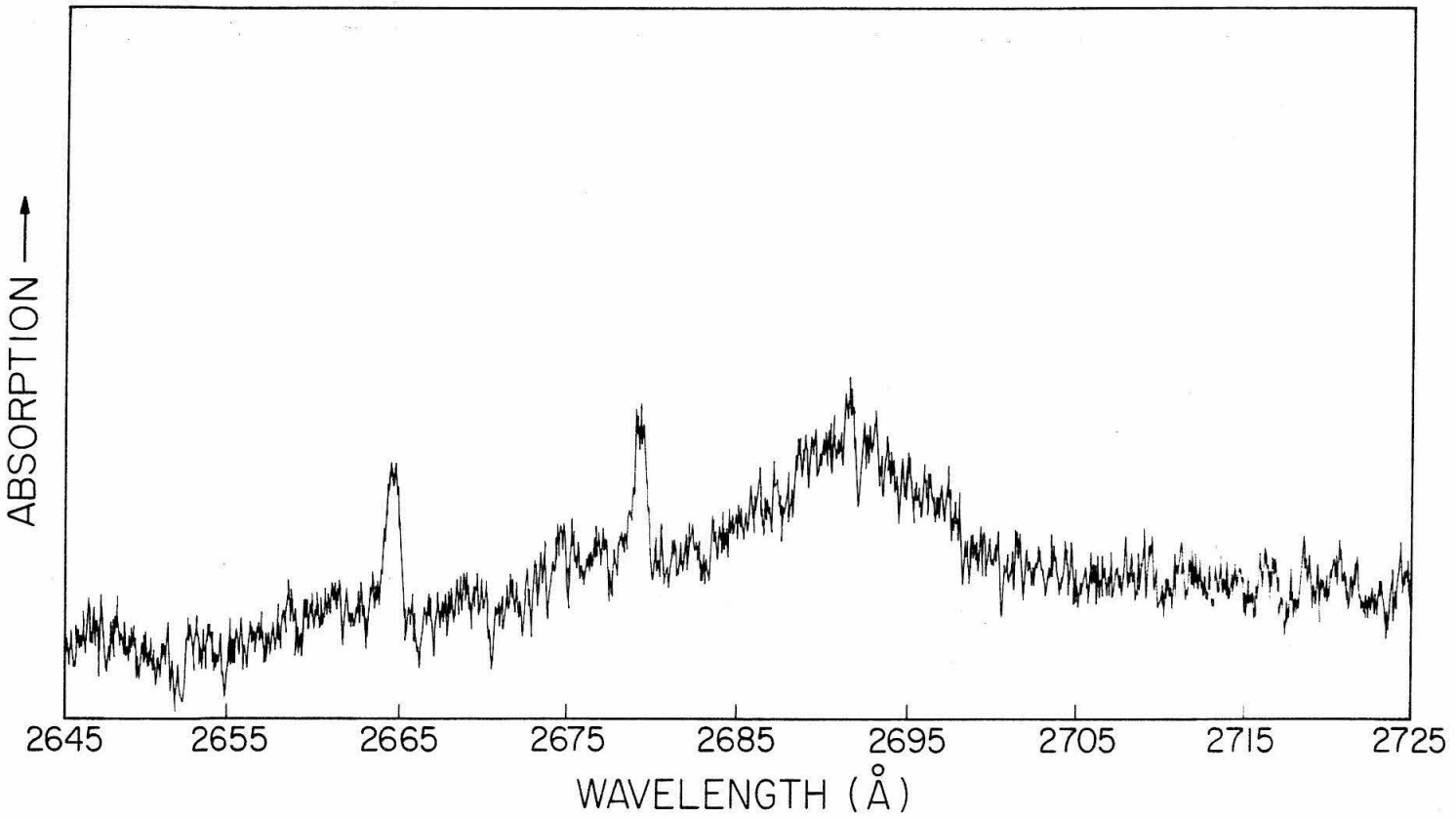
ABSORPTION
2645
2655
2665
2675
2685
2695
2705
2715
2725
WAVELENGTH (Å)

TABLE I. Position of the $^3E_{1u} \leftarrow {}^1A_{1g}$ absorption maximum for C_6H_6 and C_6D_6.

Experiment	C_6H_6		C_6D_6	
	Position (cm^{-1})	Halfwidth (cm^{-1})	Position (cm^{-1})	Halfwidth (cm^{-1})
Pure crystal[a]	36,947 ± 25	75 ± 10	37,142 ± 10	75 ± 10
Pure crystal[b]	36,947 ± 50	150	37,147 ± 50	--
O_2-perturbed[b]	36,560 ± 50	--	36,784 ± 50	--
NO-perturbed[c]	36,983 ± 50	--	--	--

[a]This work.

[b]S. D. Colson and E. R. Bernstein, J. Chem. Phys. 43, 2661 (1965).

[c]E. R. Bernstein and S. D. Colson, J. Chem. Phys. 45, 3873 (1966).

addition to the line positions we have also listed the spectral linewidths in Table I.

D. DISCUSSION

One puzzling aspect of the spectra presented in Figs. 1 and 2 is the apparent decrease in the toluene concentration in the C_6D_6 samples when compared to the toluene concentration of C_6H_6.[8] To see the explanation for this decrease we must look closely at the method used in preparing C_6D_6 from C_6H_6. The C_6H_6 starting material is shaken over D_2SO_4 and the following proton exchange process occurs:

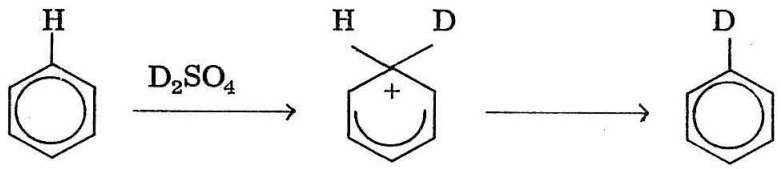

If the D_2SO_4 is present in excess, this exchange process eventually results in C_6D_6 as a final product.[9]

Any toluene that is present in the initial benzene starting material will undergo sulfonation[10]

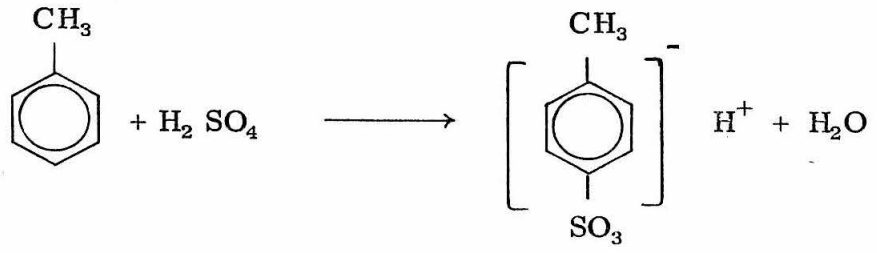

Some of the benzene may of course be sulfonated too but the rate of the sulfonation reaction for benzene is orders of magnitude smaller than for toluene. The toluene sulfonate is easily separated from the C_6D_6 and the C_6D_6 prepared in this way is thus reasonably free of toluene.

These results suggest a possible technique for further purification of C_6H_6. The benzene is shaken over H_2SO_4 and aqueous and non-aqueous phases separated. The benzene is then distilled from the non-aqueous phase, dried and refluxed over Cs as before. The toluene in the form of a water soluble sulfonate is left behind in the aqueous phase.

Colson and Bernstein[1] observed a second peak in pure crystal C_6H_6 at 37,496 cm^{-1} which they attributed to the $^3E_{1u} \leftarrow {}^1A_{1g}$ absorption system. They were unable however to see this same feature in C_6D_6. Our results suggest another interpretation for this second peak, namely that it is due to toluene impurity absorption. The C_6H_6 and C_6D_6 samples used to obtain the spectra in Figs. 1 and 2 were prepared in exactly the same manner as the samples used by Colson and Bernstein.[1] We observe absorption in the C_6H_6 samples in the 37,496 cm^{-1} spectral region as they did, but the absorption we observe is clearly attributable to toluene. We have also noted the absence of this absorption in C_6D_6 and have explained its absence as being due to the method of preparing the C_6D_6.

One of the drawbacks of the photoexcitation method is the difficulty in making intensity measurements. It is not clear that absorption and impurity emission intensities are directly proportional.

Nevertheless we can obtain a rough estimate of the relative intensity of the $^3B_{1u} \leftarrow {}^1A_{1g}$ absorption (Section IIIA) and the $^3E_{1u} \leftarrow {}^1A_{1g}$ absorption discussed in this section. We find by comparing phototube currents that the latter transition is at least 20 times stronger. This agrees qualitatively with a semi-empirical estimate that the second triplet absorption should be 12-75 times more intense.[1]

Finally we can compare the line half-width measurements with the calculated half-widths in Section IIC. The observed linewidth is 75 cm^{-1} and the calculated linewidth is 440 cm^{-1}. This is not particularly good agreement but two points should be kept in mind. First the theoretical values in Section IIC are good only to within an order of magnitude due to the approximations that have been made in order to make the calculations tractable. Second, the half-width we have measured is that due to the broad feature on the low energy side of the second triplet absorption spectrum. This feature may actually be composed of several broadened and thus indistinguishable absorption lines. Perhaps the safest conclusion that can be made concerning this aspect of the second triplet spectra is that as expected from the calculations both C_6H_6 and C_6D_6 spectra are broad. More quantitative comparisons are not particularly meaningful.

E. CONCLUSIONS

We have confirmed the position of the $^3E_{1u} \leftarrow {}^1A_{1g}$ absorption for pure crystalline benzene and deuterobenzene at 4.2° K initially measured by Colson and Bernstein.[1] In addition we have found, as they did, that the absorption spectra is broad and featureless.

A second line observed by Colson and Bernstein and attributed by them to the same $^3B_{1u} \leftarrow {}^1A_{1g}$ absorption system is assigned in the present work to a toluene impurity. The toluene impurity concentration in C_6D_6 is found to be an order of magnitude smaller than in C_6H_6. An examination of this result has suggested a new method of producing toluene free benzene by selective sulfonation of the toluene.

REFERENCES

1. S. D. Colson and E. R. Bernstein, J. Chem. Phys. 43, 2661 (1965); E. R. Bernstein and S. D. Colson, J. Chem. Phys. 45, 3873 (1966).
2. J. P. Doering, to be published.
3. P. Avakian, E. Abramson, R. G. Kepler, and J. C. Caris, J. Chem. Phys. 39, 1127 (1963); P. Avakian and E. Abramson, J. Chem. Phys. 43, 821 (1965); G. Castro and G. W. Robinson, J. Chem. Phys. 50, 1159 (1969).
4. R. Pariser and R. G. Parr, J. Chem. Phys. 21, 466, 767 (1953).
5. Section IIC of this thesis and R. M. Hochstrasser, Acct. Chem. Res. 1, 266 (1968).
6. The impurity absorption was identified as being due to toluene by comparing the impurity spectrum with a benzene crystal that had been artificially doped with toluene. See Appendix F for details.
7. The exact mechanism by which O_2 or NO enhances singlet-triplet absorptions has been the subject of some controversey. D. F. Evans, J. Chem. Soc. 1957, 1351, 3885 ; M. Tsubomura and R. S. Mullikan, J. Am. Chem. Soc. 82, 5966 (1960); G. J. Hoijtink, Mol. Phys. 3, 67 (1960); J. N. Murrell, Mol. Phys. 3, 319 (1960); C. Dijkgraaf and G. J. Hoijtink, Tetrahedron 19, 179 (1963); E. C. Lim and V. L. Kowalski, J. Chem. Phys. 36, 1729 (1962); G. W. King and E. H. Pinnington, J. Mol. Spec. 15, 394 (1965).
8. Actually the impurity species in C_6D_6 is probably $C_6D_5CH_3$. We

will refer to both deuterated and undeuterated species as toluene and it will be understood that when speaking of the C_6D_6 experiments we mean the deuterated toluene.

9. J. Hine, Physical Organic Chemistry (McGraw-Hill Book Co., Inc., New York, 1962), pp. 351-352; C. K. Ingold, C. G. Raisin, and C. L. Wilson, Nature 134, 734 (1934); J. Chem. Soc. 1936, 1637.

10. R. T. Morrison and R. N. Boyd, Organic Chemistry (Allyn and Bacon, Inc., Boston, 1959), pp. 502-507.

APPENDICES

APPENDIX A

BENZENE PHOSPHORESCENCE SPECTRUM

In Table I over 300 phosphorescence lines of crystalline benzene are listed from the origin at 3371 Å down to 4733 Å. Some of these lines have also been observed, measured and assigned by Bernstein et al.[1] and by Nieman.[2] In Table II the ground state vibrational frequencies that are a consequence of the phosphorescence line assignments in Table I are given. These frequencies should be compared with the ground state frequencies obtained from Raman[3] and infrared spectroscopic measurements on crystalline benzene.[4]

The method of purifying and growing the benzene crystals has been discussed in detail by Colson[5] and Colson and Bernstein[6] and is critically examined in Appendix F. The impurity noted by Colson[5] in the region of the first triplet was also observed in our experiments as a sharp line 500 cm^{-1} to low energy of the phosphorescence origin. This impurity does not correspond with any of the toluene in benzene phosphorescence lines (see Appendix F). It may be due to traces of phenol produced when the Pyrex crystal growing tube is sealed. It is known that heating the Pyrex tubes causes release of adsorbed oxygen[7] that can react with the benzene in the tube.

Of particular interest in the phosphorescence spectrum is the intensity of the $3 \cdot \nu_8$ line. van der Waals et al.[8] have predicted, assuming a non-hexagonal $^3B_{1u}$ state, that this line should be anomolously intense. We have measured the intensity of the ν_8 and $3 \cdot \nu_8$ lines

TABLE I. Phosphorescence lines of .4% C_6H_6 in C_6D_6 at 4.2° K.

Wavelength λ_{air} (Å)	Frequency ν_{vac} (cm^{-1})	Intensity[a]	Distance from 0-0 (cm^{-1})	Assignment[b]
3370.98	29656.5	M	0.0	0-0
3428.64	29157.7	M	500.4	Impurity
3441.44	29049.3	M	607.2	ν_6
3453.02	28951.9	S	704.6	ν_4
3465.43	28848.2	VW	808.3	
3466.57	28838.7	W	817.8	$2 \cdot \nu_{16}$
3467.64	28829.8	VW	826.7	
3471.93	28794.2	VW	862.3	
3472.88	28786.3	VVW	870.2	ν_{10}
3487.55	28665.2	S	991.3	ν_1
3488.28	28659.2	VVW	997.3	ν_5 - ^{13}C
3489.28	28651.0	S	1005.5	ν_5
3494.99	28604.2	VVW	1052.3	ν_5 + phonon
3497.99	28579.7	VVW	1076.8	ν_5 + phonon
3501.19	28553.6	VW	1102.9	$\nu_{16} + \nu_{11}$
3502.32	28544.3	VW	1112.2	
3504.01	28530.6	VVW	1125.9	
3505.86	28515.5	VVW	1141.0	
3506.58	28509.7	VVW	1146.8	
3509.05	28489.6	M	1166.9	ν_9 - ^{13}C
3510.13	28480.8	VS	1175.7	ν_9
3516.88	28426.2	VVWB	1230.3	ν_9 + phonon
3517.78	28418.9	VVWB	1237.6	ν_9 + phonon
3518.85	28410.3	MB	1246.2	ν_9 + phonon
3524.56	28364.2	VVW	1292.3	
3527.46	28340.9	VVW	1315.6	
3531.13	28311.5	VW	1345.0	
3534.37	28285.5	W	1371.0	

TABLE I. (Continued)

Wavelength λ_{air} (Å)	Frequency ν_{vac} (cm^{-1})	Intensity[a]	Distance from 0-0 (cm^{-1})	Assignment[b]
3535.88	28273.4	W	1383.1	
3536.61	28267.6	W	1388.9	$\nu_{16} + \nu_{17}$
3527.64	28259.3	VW	1397.2	
3539.25	28246.5	VVW	1410.0	
3540.15	28239.3	VVW	1417.2	
3545.87	28193.8	W	1462.7	
3547.81	28178.4	VWB	1478.1	$\nu_6 + \nu_{10}$
3551.19	28151.5	VVW	1505.0	
3553.80	28130.9	VVW	1525.6	
3556.00	28113.5	M	1543.0	
3556.91	28106.3	W	1550.2	
3558.11	28096.8	M	1559.7	
3559.06	28089.3	SB	1567.2	
3560.01	28081.8	W	1574.7	
3561.39	28070.9	VS	1585.6	ν_8
3562.93	28063.0	W	1593.5	$\nu_6 + \nu_1 - {}^{13}C$
3563.79	28052.0	VS	1604.5	$\nu_6 + \nu_1$
3564.32	28047.8	VW	1608.7	$\nu_6 + \nu_5$
3564.52	28046.2	VW	1609.3	
3570.34	28000.5	MB	1656.0	ν_8 + phonon
3572.96	27980.0	W	1676.5	$\nu_6 + \nu_1$ + phonon
3575.34	27961.4	S	1695.1	$\nu_4 + \nu_1$
3577.31	27946.0	VVW	1710.5	
3584.78	27887.8	VVW	1768.7	$\nu_9 + \nu_6$
3586.73	27872.6	VVW	1783.9	
3589.14	27853.9	W	1802.6	
3590.37	27844.3	M	1812.2	$2 \cdot \nu_{16} + \nu_1$
3591.54	27835.3	W	1821.2	

TABLE I. (Continued)

Wavelength λ_{air} (Å)	Frequency ν_{vac} (cm^{-1})	Intensity[a]	Distance from 0-0 (cm^{-1})	Assignment[b]
3594.61	27811.5	VVWB	1845.0	
3595.68	27803.2	W	1853.3	$\nu_{10} + \nu_1$
3596.69	27795.4	VW	1861.1	
3597.44	27789.6	W	1866.9	$\nu_5 + \nu_{10}$
3598.24	27783.4	W	1873.1	
3599.11	27776.7	W	1879.8	$\nu_9 + \nu_4$
3607.61	27711.3	VVW	1945.2	
3608.48	27704.6	VVW	1951.9	
3609.07	27700.1	VVW	1956.4	
3609.74	27694.9	VVW	1961.6	
3610.26	27690.9	VVW	1965.6	
3612.21	27676.0	M	1980.5	$2 \cdot \nu_1$
3612.82	27671.3	VVW	1985.2	
3614.10	27661.5	S	1995.0	$\nu_5 + \nu_1$
3619.75	27618.3	W	2038.2	
3620.68	27611.3	W	2045.2	$\nu_9 + \nu_{10}$
3621.50	27605.0	W	2051.5	
3623.29	27591.4	VWB	2065.1	$\nu_5 + \nu_1$ + phonon
3625.33	27575.8	W	2080.7	
3627.07	27562.6	W	2093.9	$\nu_{16} + \nu_{11} + \nu_1$
3628.37	27552.7	W	2103.8	
3629.88	27541.3	VVWB	2115.2	
3631.37	27530.0	VW	2126.5	
3634.26	27508.1	M	2148.4	$\nu_9 + \nu_1 - {}^{13}C$
3635.32	27500.0	VW	2156.5	$\nu_{12} + \nu_{15}$
3636.52	27491.0	VS	2165.5	$\nu_9 + \nu_1$
3638.20	27478.3	VW	2178.2	$\nu_9 + \nu_5$
3638.56	27475.6	W	2180.9	$\nu_{15} + \nu_{18}$
3639.27	27470.2	W	2186.3	

TABLE I. (Continued)

Wavelength λ_{air} (Å)	Frequency ν_{vac} (cm^{-1})	Intensity[a]	Distance from 0-0 (cm^{-1})	Assignment[b]
3642.92	27442.7	VWB	2213.8	
3644.71	27429.2	VVWB	2227.3	
3645.89	27420.3	MB	2236.2	$\nu_9 + \nu_1$ + phonon
3652.79	27368.5	W	2288.0	$\nu_8 + \nu_4$
3655.34	27349.5	VVW	2307.0	
3658.82	27323.4	VVW	2333.1	
3660.92	27307.8	VVW	2348.7	$\nu_{14} + \nu_{18}$
3661.31	27304.9	W	2351.6	
3664.23	27283.1	W	2373.4	
3664.96	27227.7	W	2378.8	$\nu_{16} + \nu_{17} + \nu_1$
3666.24	27268.1	VW	2388.4	$2 \cdot \nu_6 + \nu_9$
3666.83	27263.8	W	2392.7	
3667.66	27257.6	VVW	2398.9	
3669.57	27243.4	VWD	2413.1	
3674.09	27209.9	VW	2446.6	$\nu_8 + \nu_{10}$
3675.07	27202.6	VWB	2453.9	
3676.78	27190.0	VW	2466.5	$\nu_6 + \nu_{10} + \nu_1$
3677.67	27183.4	VW	2473.1	
3679.85	27167.3	VVW	2489.2	
3683.66	27144.2	W	2512.3	
3684.56	27132.6	W	2523.9	
3686.96	27114.9	MB	2541.6	
3687.66	27109.8	M	2546.7	^{13}C
3688.99	27100.0	M	2556.5	
3690.02	27092.4	M	2564.1	
3690.76	27087.0	VS	2569.5	$\nu_8 + \nu_1$
3692.70	27072.8	W	2583.7	$\nu_8 + \nu_5 - {}^{13}C$
3693.40	27067.6	W	2588.9	$\nu_8 + \nu_5$

TABLE I. (Continued)

Wavelength λ_{air} (Å)	Frequency ν_{vac} (cm^{-1})	Intensity[a]	Distance from 0-0 (cm^{-1})	Assignment[b]
3694.42	27060.2	VS	2596.3	$\nu_6 + 2 \cdot \nu_1$
3695.97	27048.8	VW	2607.7	$\nu_6 + \nu_1 + \nu_5$
3698.02	27033.8	VVW	2622.7	
3699.13	27025.7	VVW	2630.8	
3700.41	27016.4	MB	2640.1	$\nu_8 + \nu_1$ + phonon
3702.15	27003.7	VVW	2652.8	
3704.22	26988.6	VWD	2667.9	
3706.36	26973.0	M	2683.5	$\nu_4 + 2 \cdot \nu_1$
3708.58	26956.8	VW	2699.7	
3710.64	26941.9	VW	2714.6	
3712.71	26926.8	VW	2729.7	
3716.48	26899.5	W	2757.0	$\nu_8 + \nu_9$
3720.78	26868.4	VW	2788.1	
3721.70	26861.8	VW	2794.7	
3723.06	26859.2	W	2797.3	$2 \cdot \nu_{16} + 2 \cdot \nu_1$
3724.30	26843.1	VW	2813.5	
3728.33	26814.0	VW	2842.5	$\nu_{10} + 2 \cdot \nu_1$
3729.10	26808.5	VW	2848.0	
3730.19	26800.7	VW	2855.8	$\nu_{10} + \nu_5 + \nu_1$
3731.11	26794.1	VW	2862.4	
3732.01	26787.6	VW	2868.9	$\nu_9 + \nu_4 + \nu_1$
3734.29	26771.2	VW	2885.3	
3736.47	26755.6	VVW	2900.9	
3743.34	26706.5	VW	2950.0	
3744.62	26697.4	VWD	2959.1	
3746.05	26687.2	W	2969.3	$3 \cdot \nu_1$
3746.73	26682.4	VVW	2974.1	
3748.07	26672.8	M	2983.7	$\nu_5 + 2 \cdot \nu_1$
3749.07	26665.7	M	2990.8	

TABLE I. (Continued)

Wavelength λ_{air} (Å)	Frequency ν_{vac} (cm^{-1})	Intensity[a]	Distance from 0-0 (cm^{-1})	Assignment[b]
3751.88	26645.7	VW	3010.8	
3754.21	26629.2	VW	3027.3	
3755.31	26621.4	VVW	3035.1	$\nu_9 + \nu_{10} + \nu_1$
3756.02	26616.4	VVW	3040.1	
3758.06	26601.9	VW	3054.6	ν_7
3762.27	26572.2	VW	3084.3	
3763.71	26562.0	VW	3094.5	$\nu_{11} + \nu_{16} + 2 \cdot \nu_1$
3764.85	26553.9	VVW	3102.6	
3768.64	26527.2	W	3129.3	
3770.07	26517.2	VW	3139.3	$\nu_9 + 2 \cdot \nu_1 - {}^{13}C$
3772.20	26502.2	VS	3154.3	$\nu_9 + 2 \cdot \nu_1$
3773.57	26492.6	M	3163.9	$\nu_9 + \nu_5 + \nu_1$
3774.39	26486.8	W	3169.7	
3775.11	26481.8	VVW	3174.7	
3776.63	26471.1	VW	3185.4	$\nu_9 + 2 \cdot \nu_5$
3777.41	26465.7	VVW	3190.8	
3780.10	26446.8	VVW	3209.7	
3782.29	26431.5	VW	3225.0	$\nu_9 + 2 \cdot \nu_1$ + phonon
3788.98	26384.8	W	3271.7	$2 \cdot \nu_{15} + \nu_1$
3791.85	26364.9	W	3291.6	
3792.82	26358.1	VW	3298.4	
3794.19	26348.6	VW	3307.9	
3796.12	26335.2	VW	3321.3	
3798.11	26321.4	VVW	3335.1	
3798.88	26316.1	W	3340.4	
3801.68	26296.7	WB	3359.8	$\nu_8 + \nu_9 + \nu_6$
3802.96	26287.8	W	3368.7	
3804.53	26277.0	W	3379.5	$\nu_9 + 2 \cdot \nu_6 + \nu_1$
3807.56	26256.1	WD	3400.4	

TABLE I. (Continued)

Wavelength λ_{air} (Å)	Frequency ν_{vac} (cm^{-1})	Intensity[a]	Distance from 0-0 (cm^{-1})	Assignment[b]
3811.94	26225.9	VW	3430.6	
3812.90	26219.3	VW	3437.2	
3815.92	26198.6	W	3457.9	$\nu_6 + \nu_{10} + 2 \cdot \nu_1$
3816.82	26192.4	VW	3464.1	
3820.66	26166.1	VW	3490.4	
3829.31	26107.0	VS	3551.1	$\nu_8 + 2 \cdot \nu_1$
3831.24	26093.8	VW	3564.3	$\nu_6 + 3 \cdot \nu_1 - {}^{13}C$
3831.97	26088.8	W	2569.3	$\nu_8 + \nu_5 + \nu_1$
3833.99	26075.1	S	3583.0	$\nu_6 + 3 \cdot \nu_1$
3834.83	26069.4	W	3588.7	
3835.90	26062.1	VW	3596.0	$\nu_6 + \nu_5 + 2 \cdot \nu_1$
3837.55	26050.9	VW	3607.2	
3839.71	26036.3	VW	3621.8	$\nu_8 + 2 \cdot \nu_1$ + phonon
3844.40	26004.5	VW	3653.6	$\nu_6 + \nu_2$
3846.46	25990.6	VW	3667.5	$\nu_4 + 3 \cdot \nu_1$
3850.92	25960.5	VVW	3697.6	
3853.42	25943.6	VVW	3714.5	
3857.00	25919.5	VW	3738.6	$\nu_9 + \nu_8 + \nu_1$
3859.66	25901.7	M	3756.4	$\nu_6 + 2 \cdot \nu_8$
3860.11	25898.7	M	3759.4	
3864.56	25868.8	VVWB	3789.3	
3872.21	25817.7	VVW	3840.4	$\nu_{10} + 3 \cdot \nu_1$
3873.12	25811.7	VVW	3846.4	
3874.29	25803.9	VVW	3854.2	$\nu_5 + \nu_{10} + 2 \cdot \nu_1$
3875.47	25796.0	VVW	3862.1	
3876.67	25788.0	VVW	3870.1	$\nu_9 + \nu_4 + 2 \cdot \nu_1$
3878.61	25775.1	VVWB	3883.0	
3884.96	25733.0	S	3925.1	$\nu_8 + 2 \cdot \nu_9$
3890.61	25695.6	W	3962.5	

TABLE I. (Continued)

Wavelength λ_{air} (Å)	Frequency ν_{vac} (cm^{-1})	Intensity[a]	Distance from 0-0 (cm^{-1})	Assignment[b]
3891.62	25689.0	W	3969.1	$\nu_5 + 3 \cdot \nu_1$
3892.94	25680.3	VW	3877.8	
3895.83	25661.2	VW	3996.9	
3913.86	25543.0	VVW	4115.1	
3915.28	25533.7	VVW	4124.4	
3917.36	25520.2	S	4137.9	$\nu_9 + 3 \cdot \nu_1$
3917.81	25517.2	S	4140.9	
3919.95	25503.3	VVW	4154.8	$\nu_9 + \nu_5 + \nu_1$
3921.17	25495.4	W	4162.7	
3922.22	25488.6	VVW	4169.5	$\nu_5 + 2 \cdot \nu_8$
3924.24	25475.4	W	4182.7	$\nu_9 + 3 \cdot \nu_5$
3929.03	25444.4	VVW	4213.7	
3929.70	25440.0	VVW	4218.1	
3931.70	25427.1	VVW	4231.0	$\nu_9 + \nu_2$
3932.45	25422.2	VVW	4235.9	
3934.86	25406.7	VVW	4251.4	
3937.90	25387.1	W	4271.0	
3940.61	25369.6	VVW	4288.5	
3941.95	25361.0	VVW	4297.1	
3945.02	25341.2	VW	4316.9	
3946.37	25332.6	W	4325.5	$\nu_9 + 2 \cdot \nu_6 + 2 \cdot \nu_1$
3947.00	25328.5	S	4329.6	$\nu_9 + 2 \cdot \nu_8$
3950.19	25308.1	S	4350.0	$\nu_9 + \nu_8 + \nu_6 + \nu_1$
3952.35	25294.3	VVW	4363.8	
3963.97	25220.1	VVW	4438.0	$\nu_6 + \nu_{10} + 3 \cdot \nu_1$
3975.75	25145.4	W	4512.7	
3976.52	25140.5	W	4517.6	
3978.02	25131.0	W	4527.1	
3979.06	25124.5	S	4533.6	$\nu_8 + 3 \cdot \nu_1$

TABLE I. (Continued)

Wavelength λ_{air} (Å)	Frequency ν_{vac} (cm^{-1})	Intensity[a]	Distance from 0-0 (cm^{-1})	Assignment[b]
3980.79	25113.5	VVW	4544.6	$\nu_6 + 4 \cdot \nu_1 - {}^{13}C$
3982.33	25103.8	VVWB	4554.3	
3985.02	25086.9	S	4571.2	$\nu_6 + 4 \cdot \nu_1$
3994.13	25029.7	M	4628.4	$\nu_8 + \nu_2$
3996.37	25015.5	M	4642.6	$\nu_6 + \nu_1 + \nu_2$
4009.15	24935.9	VVW	4722.2	
4010.93	24924.8	S	4733.3	$2 \cdot \nu_8 + \nu_6 + \nu_1$
4011.80	24919.4	W	4738.7	$\nu_8 + 2 \cdot \nu_6 + 2 \cdot \nu_1$
4014.94	24899.9	S	4758.2	$3 \cdot \nu_8$
4018.67	24876.8	VW	4781.3	
4028.17	24818.2	VVW	4839.9	
4030.82	24801.8	VVW	4856.3	
4032.67	24790.5	VVW	4867.6	
4039.23	24750.2	S	4907.9	$\nu_8 + 2 \cdot \nu_9 + \nu_1$
4042.63	24729.4	VVWB	4928.7	
4044.19	24719.9	VVW	4938.2	
4045.35	24714.8	VVW	4943.3	
4046.46	24706.0	VVW	4952.1	$\nu_5 + 4 \cdot \nu_1$
4049.54	24687.2	VVW	4970.9	
4074.98	24533.1	M	5125.0	$\nu_9 + 4 \cdot \nu_1$
4077.43	24518.3	W	5139.8	
4080.16	24501.9	VW	5156.2	
4081.13	24496.1	VVW	5162.0	
4082.07	24490.5	VW	5167.6	
4090.64	24439.2	VVW	5218.9	
4091.50	24434.0	VW	5224.1	
4096.05	24406.9	VW	5251.2	
4099.32	24387.4	VW	5270.7	
4105.23	24352.3	S	5305.8	$\nu_9 + 2 \cdot \nu_8 + \nu_1$

TABLE I. (Continued)

Wavelength λ_{air} (Å)	Frequency ν_{vac} (cm^{-1})	Intensity[a]	Distance from 0-0 (cm^{-1})	Assignment[b]
4105.82	24348.8	W	5309.3	
4108.84	24330.9	W	5327.2	
4110.20	24322.9	S	5335.2	$\nu_9 + 2\cdot\nu_8 + \nu_6 + \nu_1$
4115.56	24291.2	VVWB	5366.9	
4117.12	24282.0	VVWB	5376.1	
4125.59	24232.1	W	5426.0	$\nu_6 + \nu_{10} + 4\cdot\nu_1$
4129.78	24207.5	VVW	5450.6	
4131.56	24197.1	VVW	5461.0	
4138.00	24159.5	VVW	5498.6	
4139.53	24150.5	VVW	5507.6	
4140.75	24143.4	M	5514.7	$\nu_8 + 4\cdot\nu_1$
4147.01	24107.0	VW	5551.1	
4147.92	24101.7	W	5556.4	$\nu_6 + 5\cdot\nu_1$
4150.40	24087.3	VVW	5570.8	$\nu_6 + \nu_5 + 3\cdot\nu_1$
4157.41	24046.7	W	5611.4	$\nu_8 + \nu_2 + 2\cdot\nu_1$
4159.95	24032.0	W	5626.1	$\nu_6 + \nu_2 + 2\cdot\nu_1$
4172.33	23960.7	W	5697.4	
4173.11	23956.2	M	5701.9	
4179.35	23920.4	S	5737.7	$3\cdot\nu_8 + \nu_1$
4180.07	23916.3	S	5741.8	
4182.86	23900.4	VW	5757.7	
4206.04	23768.6	M	5889.5	$\nu_8 + 2\cdot\nu_9 + 2\cdot\nu_1$
4207.86	23758.4	VVW	5899.7	
4210.08	23745.8	VVW	5912.3	
4212.99	23729.4	VVWB	5928.7	
4218.46	23698.7	VVW	5959.4	
4223.19	23672.1	VVW	5986.0	
4226.44	23653.9	VVWB	6004.2	
4229.31	23637.9	VVW	6020.2	

TABLE I. (Continued)

Wavelength λ_{air} (Å)	Frequency ν_{vac} (cm^{-1})	Intensity[a]	Distance from 0-0 (cm^{-1})	Assignment[b]
4237.41	23591.0	VW	6067.1	
4243.46	23559.0	VVWB	6099.1	
4245.36	23548.5	VVW	6109.6	
4276.01	23379.7	M	6278.4	$\nu_9 + 2 \cdot \nu_8 + 2 \cdot \nu_1$
4283.38	23339.5	M	6318.6	$\nu_9 + \nu_8 + \nu_6 + 3 \cdot \nu_1$
4295.44	23274.0	VVW	6384.1	
4334.44	23064.6	W	6593.6	$\nu_8 + \nu_2 + 2 \cdot \nu_1$
4337.08	23050.5	W	6607.7	$\nu_6 + \nu_2 + 3 \cdot \nu_1$
4341.04	23029.5	VVW	6628.7	
4343.73	23015.2	VVW	6643.0	
4348.04	22992.4	M	6665.8	
4350.79	22977.9	M	6680.3	
4351.70	22973.1	VVW	6685.1	
4357.64	22941.8	S	6716.4	$3 \cdot \nu_8 + 2 \cdot \nu_1$
4358.39	22937.8	VVW	6720.4	
4364.33	22906.6	W	6751.6	$\nu_8 + 2 \cdot \nu_9 + 3 \cdot \nu_1$
4388.45	22780.7	VVWB	6877.5	
4395.08	22746.3	VVW	6911.9	
4398.00	22731.2	VVW	6927.0	
4403.68	22701.9	VVW	6956.3	
4425.07	22592.2	WD	7066.0	
4429.10	22572.1	W	7086.1	$\nu_9 + 6 \cdot \nu_1$
4437.97	22526.5	VVW	7131.7	
4463.33	22398.5	W	7259.7	$\nu_9 + 2 \cdot \nu_8 + 3 \cdot \nu_1$
4471.40	22358.1	VW	7300.1	
4472.47	22352.7	VVW	7305.5	
4484.07	22294.9	VVW	7363.3	
4486.70	22281.9	VVW	7376.3	
4504.20	22195.3	VVW	7562.9	

TABLE I. (Continued)

Wavelength λ_{air} (Å)	Frequency ν_{vac} (cm^{-1})	Intensity[a]	Distance from 0-0 (cm^{-1})	Assignment[b]
4509.30	22170.2	VVW	7488.0	
4510.50	22164.3	VVW	7493.9	
4527.29	22082.1	VVW	7576.1	
4530.11	22068.3	VVW	7589.9	
4541.11	22014.9	VVW	7543.3	$\nu_8 + 2 \cdot \nu_2$
4543.40	22003.8	VVW	7654.4	$\nu_6 + \nu_1 + 2 \cdot \nu_{12}$
4551.82	21963.1	VVW	7695.1	
4560.00	21923.7	VVW	7734.5	
4593.74	21762.7	VVW	7895.5	
4604.33	21712.6	VVW	7945.6	$5 \cdot \nu_8$
4713.48	21209.8	VVW	8448.4	
4717.27	21192.7	VVW	8465.5	
4733.16	21121.6	VVW	8536.6	

[a]VS = very strong, S = strong, M = moderate, W = weak, VW = very weak, VVW = extremely weak, B = broad, D = barely resolved doublet.

[b]Numbering of the normal modes is due to E. B. Wilson, Phys. Rev. 45, 706 (1934).

TABLE II. Vibrational frequencies of C_6H_6 in C_6D_6 at 4.2° K.

Symmetry	Vibration[a]	Type[b]	Frequency (cm^{-1})
a_{1g}	1	C-St	991.3
	2	H-St	3060.2
a_{2g}	3	H-Bend	--
b_{2g}	4	Out of Pl	704.6
	5	Out of Pl	1005.5
e_{2g}	6	C-Bend	607.2
	7	H-St	3054.6
	8	C-St	1585.6
	9	H-Bend	1175.7
e_{1g}	10	Out of Pl	822.5
a_{2u}	11	Out of Pl	694.0
b_{1u}	12	C-Bend	1011.1
	13	H-St	--
b_{2u}	14	H-Bend	1309.9
	15	C-St	1143.2
e_{2u}	16	Out of Pl	408.9
	17	Out of Pl	974.2
e_{1u}	18	H-Bend	1040.4
	19	C-Def	--
	20	H-St	--

[a]Numbering is according to E. B. Wilson, Phys. Rev. 45, 706 (1934).

[b]C-St = carbon-stretching, H-St = hydrogen-stretching, H-Bend = hydrogen bending, Out of Pl = out of plane, C-Bend = carbon-bending, C-Def = carbon-deformation.

and these measurements corrected for phototube and spectrograph response are presented in Table III. The ν_8 line is in Fermi resonance with the $\nu_6 + \nu_1$ line and the $3 \cdot \nu_8$ with the $2 \cdot \nu_3 + \nu_6 + \nu_1$. Since the majority of the vibronic intensity is induced by the ν_8 mode,[9] the sum of the Fermi doublet intensities is the experimental value that should be compared with theory. To see if the $3 \cdot \nu_8$ line is really "anomolously" intense, we refer to the Franck-Condon factors for a doubly-degenerate carbon stretching mode (Table VII of Sec. IA). The Franck-Condon factor calculations indicate that for a hexagonal $^3B_{1u}$ state the ν_8 phosphorescence line should be 10^6 times stronger than the $3 \cdot \nu_8$ line. Table III of this section shows it to be only ten times stronger. This experimental result along with those discussed in Section IIIA provide additional evidence for the nonhexagonality of the $^3B_{1u}$ excited state of crystalline benzene.

TABLE III. Intensity of the $3 \cdot \nu_8$ phosphorescence.

Vibration	Distance from 0-0 (cm^{-1})	Intensity (arbitrary units)	Sum of Fermi doublet Intensity
ν_8	1586	163	170 ± 50
$\nu_6 + \nu_1$	1605	6.3	
$3 \cdot \nu_8$	4758	9.7	18 ± 5
$2 \cdot \nu_8 + \nu_6 + \nu_1$	4733	8.2	

REFERENCES

1. E. R. Bernstein, S. D. Colson, D. S. Tinti, and G. W. Robinson, J. Chem. Phys. 48, 4632 (1968).
2. G. C. Nieman, Ph. D. thesis, California Institute of Technology, 1965.
3. A. R. Gee and G. W. Robinson 46, 4847 (1967).
4. E. R. Bernstein and G. W. Robinson 49, 4962 (1968).
5. S. D. Colson, Ph. D. thesis, California Institute of Technology, 1968.
6. S. D. Colson and E. R. Bernstein, J. Chem. Phys. 43, 2661 (1965).
7. E. B. Priestley, Ph. D. thesis, California Institute of Technology, 1970.
8. J. H. van der Waals, A. M. D. Berghuis, and M. S. de Groot, Mol. Phys. 13, 301 (1967).
9. W. Moffitt, J. Chem. Phys. 22, 320 (1954).

APPENDIX B

FRANCK-CONDON FACTORS FOR BENZENE

In this appendix we complete the listing of Franck-Condon factors for benzene that was begun in Table III of Section IIA. The equations used for these calculations and the numerical values for the various parameters entering into the calculation can be found in Section IIA.

The dependence of the Franck-Condon factor on $\underline{f}$ the vibrational force constant change, δ the normal coordinate change and ν the vibrational frequency are graphically presented in Figs. 1-3, respectively. In Fig. 1 the discontinuity at f = 1.0 should be noted. At that point (referring to Eq. (10) of Sec. IIA) the overlap integral switches from the real to the imaginary axis and its absolute value squared, the Franck-Condon factor, is discontinuous. In Fig. 2 the Franck-Condon factor is zero for all odd quanta $\underline{n}$ provided $\delta = 0$. Again from Eq. (10) of Sec. IIA we see the reason immediately. The Hermite polynomial is an even function of δ for even values of $\underline{n}$ and an odd function for odd $\underline{n}$. When $\delta = 0$ only the constant term for even n-values is nonzero. For odd n-values all terms are zero.

From the figures we also note that the Franck-Condon factor is least sensitive to changes in $\underline{f}$ and most sensitive to changes in δ, particularly when δ is nearly zero (i.e., $\delta < .2$ amu$^{\frac{1}{2}}$ Å). Therefore in determining these two parameters from phosphorescence intensity data δ can be estimated more precisely than $\underline{f}$ (the ground state vibrational frequency ν is usually known).

Figure 1. Log_{10} [Franck-Condon Factor] as a function of the vibrational force constant change $\underline{f}$. The normal coordinate change δ and the vibrational frequency ν are held constant.

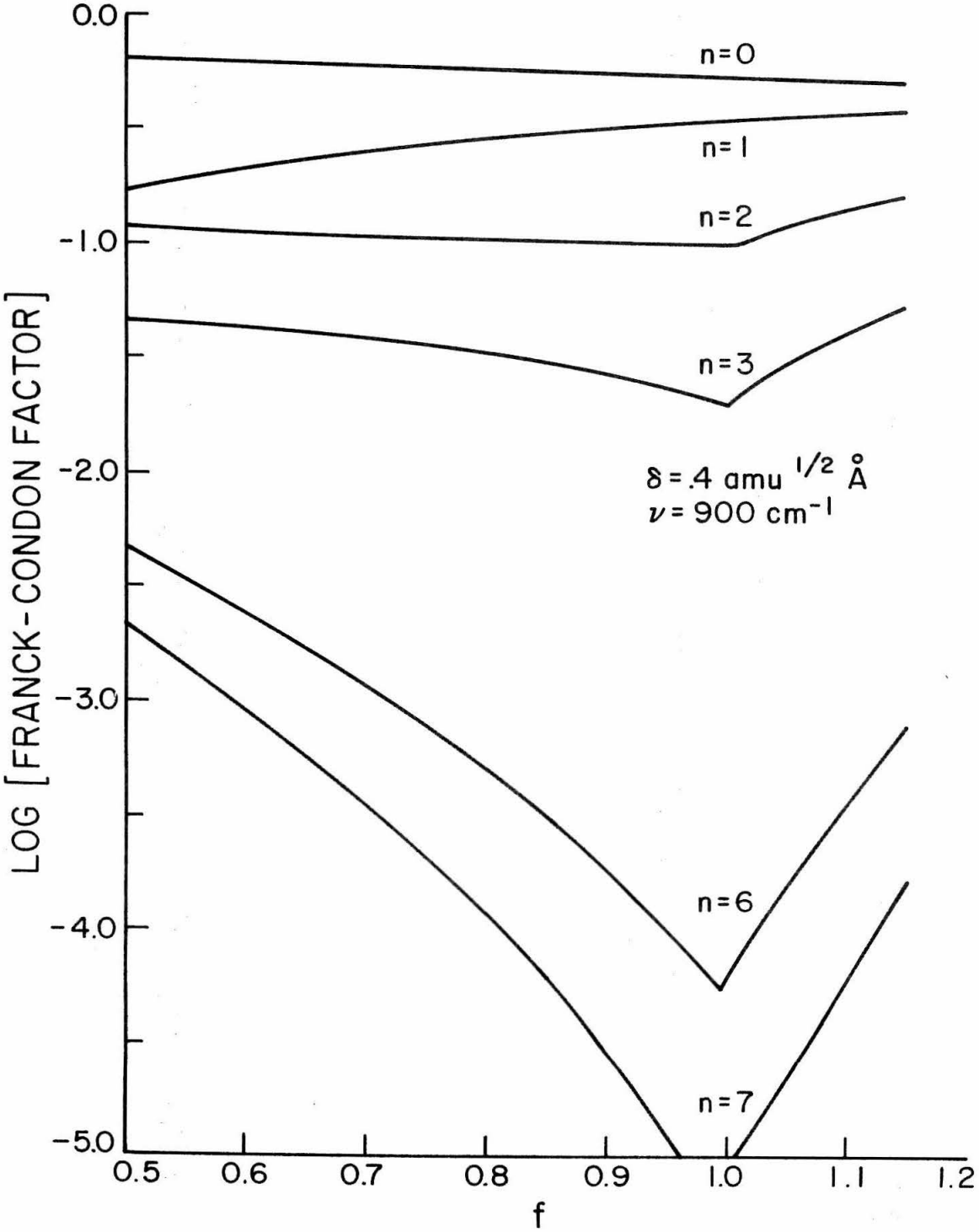
0.0
-1.0
-2.0
-3.0
-4.0
-5.0
LOG [FRANCK-CONDON FACTOR]
n=0
n=1
n=2
n=3
n=6
n=7
δ = .4 amu 1/2 Å
ν = 900 cm-1
0.5
0.6
0.7
0.8
0.9
1.0
1.1
1.2
f

Figure 2. Log_{10} [Franck-Condon Factor] as a function of the normal coordinate change δ. The vibrational frequency ν and the force constant change $\underline{f}$ are held constant.

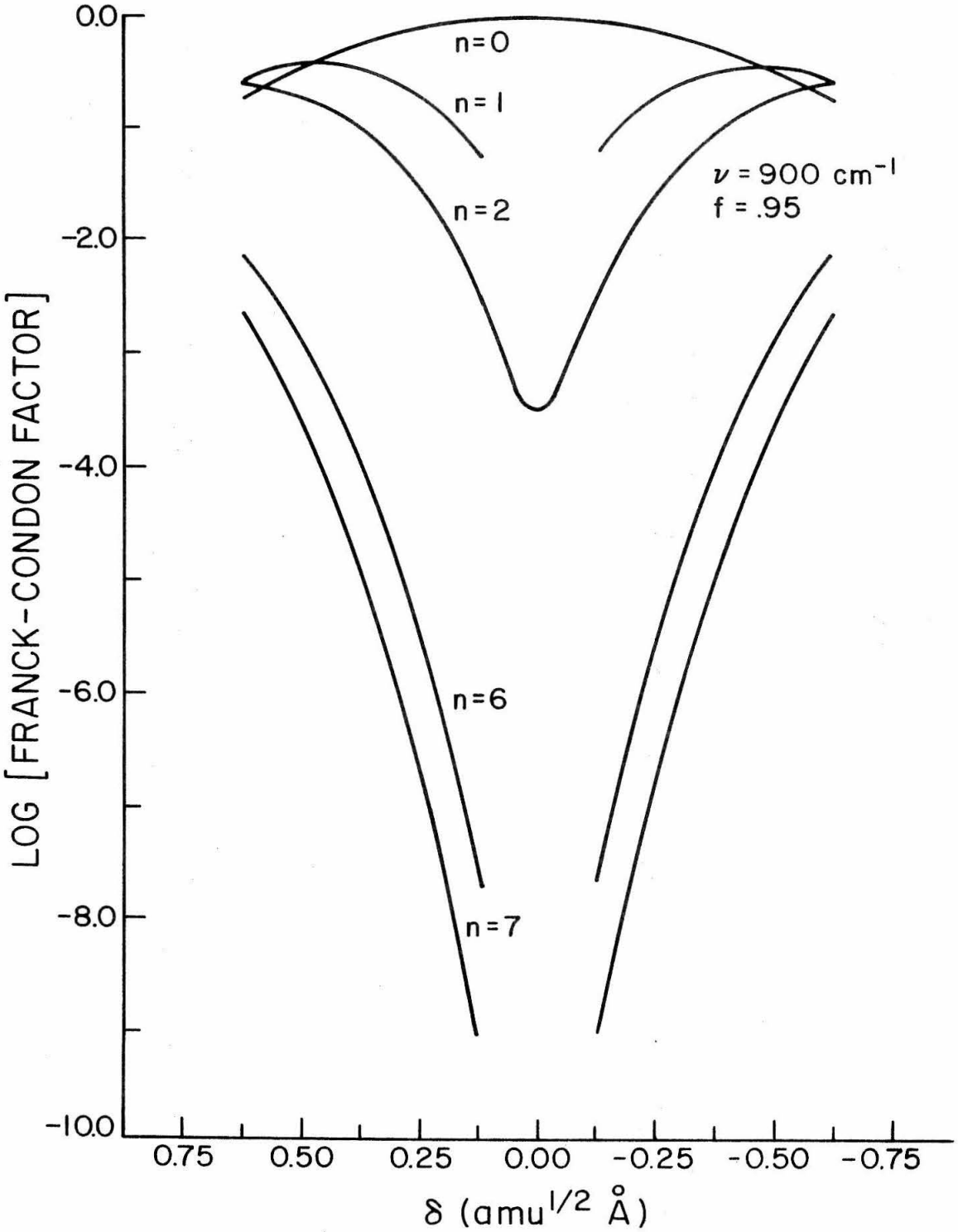
0.0
-2.0
-4.0
-6.0
-8.0
-10.0
LOG [FRANCK-CONDON FACTOR]
n=0
n=1
n=2
n=6
n=7
ν = 900 cm⁻¹
f = .95
0.75
0.50
0.25
0.00
-0.25
-0.50
-0.75
δ (amu^1/2 Å)

Figure 3. Log_{10} [Franck-Condon Factor] as a function of the vibrational frequency ν. The normal coordinate change δ and the force constant change $\underline{f}$ are held constant.

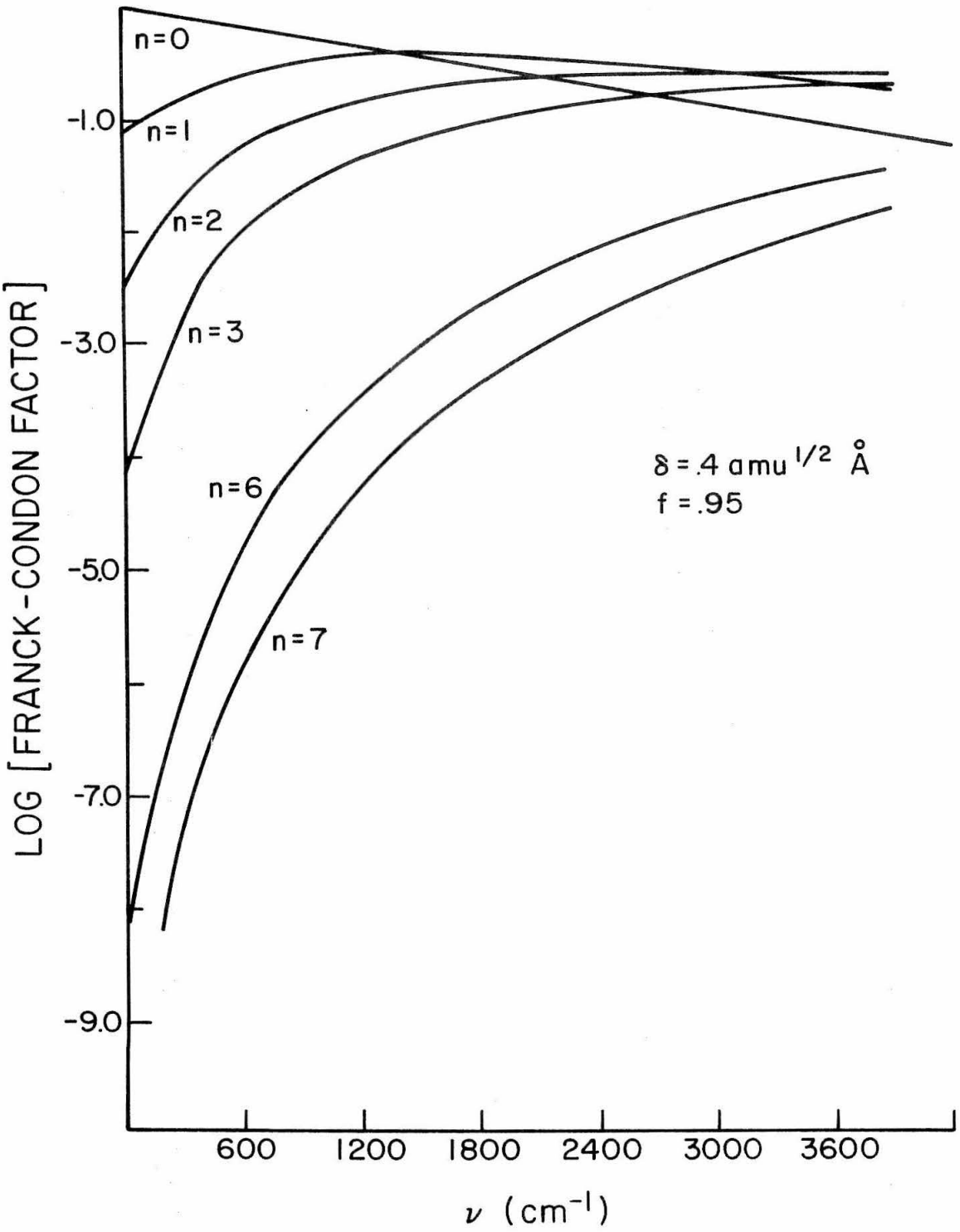
n=0
n=1
n=2
n=3
n=6
n=7
-1.0
-3.0
-5.0
-7.0
-9.0
LOG [FRANCK-CONDON FACTOR]
δ = .4 amu 1/2 Å
f = .95
600
1200
1800
2400
3000
3600
ν (cm-1)

TABLE I. Nondegenerate Franck-Condon factors for the $^3B_{1u} \rightarrow {}^1A_{1g}$ transition of C_6H_6.[a]

Ground State Vibrational Quantum No. n	Franck-Condon Factor[b]				
	C-St	H-St	H-Bend	C-Bend	C-Def
0	1.00	1.00	1.00	1.00	1.00
1	0.00	0.00	0.00	0.00	0.00
2	4.99×10^{-7}	3.98×10^{-5}	8.45×10^{-4}	1.44×10^{-3}	3.14×10^{-6}
3	0.00	0.00	0.00	0.00	0.00
4	3.74×10^{-13}	2.37×10^{-9}	1.01×10^{-6}	3.12×10^{-6}	1.48×10^{-11}
5	0.00	0.00	0.00	0.00	0.00
6	3.11×10^{-19}	1.57×10^{-13}	1.51×10^{-9}	7.52×10^{-9}	7.74×10^{-17}
7	0.00	0.00	0.00	0.00	0.00
8	2.7×10^{-25}	1.10×10^{-17}	2.24×10^{-12}	1.90×10^{-11}	4.26×10^{-22}
9	0.00	0.00	0.00	0.00	0.00
10	2.44×10^{-31}	7.85×10^{-22}	3.40×10^{-15}	4.94×10^{-14}	2.41×10^{-27}
11	0.00	0.00	0.00	0.00	0.00
12	2.23×10^{-37}	5.72×10^{-26}	5.27×10^{-18}	1.31×10^{-16}	1.39×10^{-32}
13	0.00	0.00	0.00	0.00	0.00
14	2.06×10^{-43}	4.23×10^{-30}	8.28×10^{-21}	3.50×10^{-19}	8.08×10^{-38}
15	0.00	0.00	0.00	0.00	0.00

[a]The parameters used in these calculations are listed in Table VI of Section IIA.

[b]C-ST = carbon stretching, H-St = hydrogen stretching, H-Bend = hydrogen bending, C-Bend = carbon bending, C-Def = carbon deformation.

TABLE II. Nondegenerate Franck-Condon factors for the $^3B_{1u} \rightarrow {}^1A_{1g}$ transition of C_6D_6.[a]

n	Franck-Condon Factor							
	C-St	H-St	H-Bend	O-Pl	C-Bend	C-Def	C-Ts	H-Ts
0	1.00	1.00	1.00	.983	1.00	1.00	.387	.974
1	0.00	0.00	0.00	0.00	0.00	0.00	.354	2.65×10^{-2}
2	1.01×10^{-4}	3.55×10^{-5}	8.45×10^{-4}	1.72×10^{-2}	1.44×10^{-3}	1.26×10^{-5}	.149	1.81×10^{-4}
3	0.00	0.00	0.00	0.00	0.00	0.00	3.82×10^{-2}	5.06×10^{-8}
4	1.53×10^{-8}	1.90×10^{-9}	1.07×10^{-6}	4.50×10^{-4}	3.12×10^{-6}	2.39×10^{-10}	6.61×10^{-3}	5.45×10^{-9}
5	0.00	0.00	0.00	0.00	0.00	0.00	7.96×10^{-4}	4.95×10^{-11}
6	2.56×10^{-12}	1.12×10^{-13}	1.51×10^{-9}	1.31×10^{-5}	7.52×10^{-9}	5.03×10^{-15}	7.05×10^{-5}	3.70×10^{-15}
7	0.00	0.00	0.00	0.00	0.00	0.00	4.33×10^{-6}	3.08×10^{-15}
8	4.51×10^{-16}	6.96×10^{-18}	2.23×10^{-12}	4.01×10^{-7}	1.90×10^{-11}	1.11×10^{-19}	1.75×10^{-7}	7.75×10^{-18}
9	0.00	0.00	0.00	0.00	0.00	0.00	3.85×10^{-9}	6.88×10^{-20}
10	8.20×10^{-20}	4.45×10^{-22}	3.40×10^{-15}	1.26×10^{-8}	4.94×10^{-14}	2.53×10^{-24}	1.92×10^{-11}	1.20×10^{-21}
11	0.00	0.00	0.00	0.00	0.00	0.00	7.82×10^{-13}	6.87×10^{-26}
12	1.52×10^{-23}	2.90×10^{-26}	5.28×10^{-18}	4.04×10^{-10}	1.31×10^{-16}	5.85×10^{-29}	1.57×10^{-13}	7.60×10^{-26}
13	0.00	0.00	0.00	0.00	0.00	0.00	5.51×10^{-15}	1.12×10^{-28}

TABLE II. (Continued)

n	Franck-Condon Factor							
	C-St	H-St	H-Bend	O-Pl	C-Bend	C-Def	C-Ts	H-Ts
14	2.83×10^{-27}	1.91×10^{-30}	8.28×10^{-21}	1.31×19^{-11}	3.51×10^{-19}	1.37×10^{-33}	2.61×10^{-17}	2.69×10^{-30}
15	0.00	0.00	0.00	0.00	0.00	0.00	1.79×10^{-18}	2.29×10^{-32}

[a]The parameters used in these calculations are listed in Table VI of Section IIA.

[b]C-St = carbon stretching, H-St = hydrogen stretching, H-Bend = hydrogen bending, O-Pl = out of plane, C-Bend = carbon bending, C-Def = carbon deformation, C-Ts = carbon totally symmetric, H-Ts = hydrogen totally symmetric.

TABLE III. Nondegenerate Franck-Condon factors for the $^1B_{2u} \rightarrow {}^1A_{1g}$ transition of C_6H_6.[a]

Ground State Vibrational Quantum No. n	Franck-Condon Factor	
	C-Ts	H-Ts
0	.265	.947
1	.340	5.23×10^{-2}
2	.205	9.29×10^{-4}
3	7.80×10^{-2}	4.45×10^{-6}
4	2.98×10^{-2}	1.58×10^{-9}
5	4.11×10^{-3}	6.10×10^{-10}
6	6.23×10^{-4}	3.90×10^{-12}
7	7.37×10^{-5}	5.38×10^{-15}
8	6.81×10^{-6}	6.86×10^{-16}
9	4.89×10^{-7}	1.69×10^{-18}
10	2.66×10^{-8}	3.02×10^{-20}
11	1.03×10^{-9}	6.66×10^{-22}
12	2.49×10^{-11}	3.60×10^{-27}
13	2.30×10^{-13}	7.49×10^{-26}
14	5.84×10^{-16}	2.74×10^{-28}
15	5.46×10^{-16}	3.50×10^{-30}

[a]The parameters used in these calculations are listed in Table VI of Section IIA.

[b]C-Ts = carbon totally symmetric, H-Ts = hydrogen totally symmetric.

TABLE IV. Degenerate Franck-Condon factors for the $^1B_{2u} \rightarrow {}^1A_{1g}$ or $^3B_{1u} \rightarrow {}^1A_{1g}$ transitions of C_6H_6.[a]

Ground State Vibrational Quantum No. n	Franck-Condon Factor[b]		
	H-Bend	C-Bend	C-Def
0	.957	1.00	1.00
1	4.11×10^{-2}	5.36×10^{-2}	2.51×10^{-3}
2	1.69×10^{-3}	2.88×10^{-3}	6.28×10^{-6}
3	6.94×10^{-5}	1.55×10^{-4}	1.57×10^{-8}
4	2.86×10^{-6}	8.32×10^{-6}	3.95×10^{-11}
5	1.17×10^{-7}	4.47×10^{-7}	9.89×10^{-14}
6	4.83×10^{-9}	2.40×10^{-8}	2.49×10^{-16}
7	1.99×10^{-10}	1.29×10^{-9}	6.21×10^{-19}
8	8.17×10^{-12}	6.94×10^{-11}	1.56×10^{-21}
9	3.36×10^{-13}	3.73×10^{-12}	3.90×10^{-24}
10	1.38×10^{-14}	2.00×10^{-13}	9.78×10^{-27}
11	5.68×10^{-16}	1.08×10^{-14}	2.45×10^{-29}
12	2.34×10^{-17}	5.79×10^{-16}	6.14×10^{-32}
13	9.61×10^{-19}	3.11×10^{-17}	1.54×10^{-34}
14	3.95×10^{-20}	1.67×10^{-18}	3.86×10^{-37}
15	1.62×10^{-21}	8.98×10^{-20}	9.67×10^{-40}

[a]The parameters used in these calculations are listed in Table VI of Section IIA.

[b]H-Bend = hydrogen bending, C-Bend = carbon bending, C-Def = carbon deformation.

TABLE V. Degenerate Franck-Condon factors for the $^1B_{2u} \rightarrow {}^1A_{1g}$ or $^3B_{1u} \rightarrow {}^1A_{1g}$ transitions of C_6D_6.[a]

Ground State Vibrational Quantum No. n	Franck-Condon Factor[b]					
	C-St	H-St	H-Bend	O-Pl	C-Bend	C-Def
0	1.00	1.00	.954	.879	.956	1.00
1	7.56×10^{-3}	7.44×10^{-3}	4.38×10^{-2}	.181	4.38×10^{-2}	5.03×10^{-3}
2	5.71×10^{-5}	5.54×10^{-5}	1.92×10^{-3}	3.40×10^{-2}	1.92×10^{-3}	2.53×10^{-5}
3	4.31×10^{-7}	4.33×10^{-7}	8.41×10^{-5}	6.37×10^{-3}	8.41×10^{-5}	1.27×10^{-7}
4	3.26×10^{-9}	3.07×10^{-9}	3.69×10^{-6}	1.19×10^{-3}	3.69×10^{-6}	6.38×10^{-10}
5	2.46×10^{-11}	2.29×10^{-11}	1.62×10^{-7}	2.24×10^{-4}	1.62×10^{-7}	3.20×10^{-12}
6	1.86×10^{-13}	1.70×10^{-13}	7.08×10^{-9}	4.21×10^{-5}	7.09×10^{-9}	1.61×10^{-14}
7	1.41×10^{-15}	1.26×10^{-15}	3.11×10^{-10}	7.90×10^{-6}	3.31×10^{-10}	8.09×10^{-17}
8	1.06×10^{-17}	9.43×10^{-18}	1.36×10^{-11}	1.48×10^{-6}	1.36×10^{-11}	4.07×10^{-19}
9	8.03×10^{-20}	7.02×10^{-20}	5.97×10^{-13}	2.78×10^{-7}	5.97×10^{-13}	2.04×10^{-21}
10	6.07×10^{-22}	5.23×10^{-22}	2.62×10^{-14}	5.22×10^{-8}	2.62×10^{-14}	1.03×10^{-23}
11	4.59×10^{-24}	3.89×10^{-24}	1.15×10^{-15}	9.80×10^{-9}	1.15×10^{-15}	5.36×10^{-26}

TABLE V. (Continued)

Ground State Vibrational Quantum No. n	Franck-Condon Factor[n]					
	C-St	H-St	H-Bend	O-Pl	C-Bend	C-Def
12	3.47×10^{-26}	2.90×10^{-26}	5.03×10^{-17}	1.84×10^{-9}	5.03×10^{-17}	2.59×10^{-28}
13	2.62×10^{-28}	2.36×10^{-28}	2.21×10^{-18}	3.45×10^{-10}	2.21×10^{-18}	1.30×10^{-30}
14	1.98×10^{-30}	1.60×10^{-30}	9.67×10^{-20}	6.48×10^{-11}	9.67×10^{-20}	6.55×10^{-33}
15	1.50×10^{-32}	1.39×10^{-32}	4.24×10^{-21}	1.22×10^{-11}	4.24×10^{-21}	3.29×10^{-35}

[a]The parameters used in these calculations are listed in Table VI of Section IIA.

[b]C-St = carbon stretching, H-St = hydrogen stretching, H-Bend = hydrogen bending, O-Pl = out of plane, C-Bend = carbon bending, C-Def = carbon deformation.

APPENDIX C

VIBRONIC DENSITY OF STATES CALCULATION

The calculation of the density of vibrational energy levels, $\rho(E)$, has received a considerable amount of attention primarily because of its importance in the theory of a variety of unimolecular reaction processes; for example, thermal unimolecular reactions, photoionization and electron impact phenomena, and decomposition of excited molecules and radicals.[1] Three distinct approaches have been taken to the calculation of $\rho(E)$: (1) semi-empirical modifications of classical formulae,[2] (2) exact counting[2] and (3) approximately exact counting.[1, 3, 4]

The exact counting method is obviously the most desirable one, but even with high speed computers this method becomes impractical for moderately sized molecules and energies greater than 5,000 cm^{-1}. For this reason several approximate methods have been proposed. The fastest method, from the point of view of computing time, involves a semi-empirical modification of the classical expression for the density of states. The classical expression is[5]

$$\rho(E) = \frac{E^{N-1}}{(N-1)! \prod_{i=1}^{N} h\nu_i} \quad . \tag{1}$$

This expression is valid for energies E much larger than the zero-point vibrational energy. In Eq. (1) N is the number of vibrational degrees of freedom and ν_i is the frequencies of the $i^{\underline{th}}$ vibrational mode. Since for most molecules the zero-point energy is quite large

(for benzene it is 21,384 cm^{-1}), the range of validity of Eq. (1) is quite often outside the range of E-values of interest. Whitten and Rabinovitch[2] have modified this classical expression to correct not only for the large zero-point energy but also for the spread in vibrational frequencies. Their equation is

$$\rho(E) = [E + (1 - \beta w)E_o]^{N-1}/(N-1)! \prod_{i}^{N} h\nu_i \qquad (2)$$

where E_o is the zero-point energy, β corrects for the spread in vibrational frequencies and is defined as

$$\beta = \frac{(N-1)}{N} \frac{\langle \nu^2 \rangle}{\langle \nu \rangle^2} \qquad (3)$$

and $\underline{w}$ is an empirical parameter that depends on E/E_o. Whitten and Rabinovitch have tabulated values of $\underline{w}$ for various values of E/E_o between .02 and 8.00. Equation (2) provides a formula for $\rho(E)$ that can be conveniently evaluated using only a desk calculator.

One disadvantage of this method for calculating $\rho(E)$ is that it is not possible to assess the importance of vibrational anharmonicity on the density of states. To calculate anharmonic densities one must resort to exact counting methods. Schlag and Sandsmark[3] have outlined a rapid exact count method, which also enables one to include the fact that the normal mode oscillators are anharmonic. This method makes use of the similarities between the density of states expression and the binomial series expansion of $\prod_{i=1}^{N} (1 - Z^{t_i})^{-g_i}$. A general term in the expansion is given by

$$\binom{n_1+g_1-1}{n_1}\binom{n_2+g_2-1}{n_2}\cdots Z^{(n_1t_1+n_2t_2+\cdots)} \quad . \qquad (4)$$

The exponent yields the energy E if t_i is defined as the vibrational frequency ν_i and n_i is the quantum number associated with the $i^{\underline{th}}$ oscillator. The coefficient then becomes the complexion sum, that is the total number of vibrational levels of energy E or lower. g_i is the degeneracy of the $i^{\underline{th}}$ mode. The density of states can be obtained from the complexion sum by subtracting sums for two different energies and dividing by the energy difference. Anharmonicities can be included if instead of associating the harmonic energy n_i (in units of $E/h\nu$) with the term

$$\binom{n_i+g_i-1}{n_i}$$

one uses the anharmonic energy

$$n_i(1 - x_i\{[2n_i/(g_i+1)] + 1\})$$

where x_i is the anharmonicity coefficient.

The exact count method outlined above involves an exponentially increasing amount of computer time as the energy E increases. For benzene with 30 vibrational degrees of freedom, even this rapid technique becomes prohibatively slow at energies greater than about $5,000\ cm^{-1}$. For higher energies one must resort to "approximately" exact counting approaches. One way of doing this is to write the

density of states $\rho(E)$ as an infinite sum and evaluate only the leading few terms.[1,3,4] Alternatively one can reduce the number of vibrational degrees of freedom by grouping them. This second approach is the one we have used in calculating the density of states in Secs. IIA and C. The 30 normal mode frequencies of benzene are grouped into five six-fold degenerate frequencies. These frequencies are 3055.8, 1462.4, 1093.9, 938.4 and 554.6 cm^{-1}. An "exact" count approach is then used with this reduced number of vibrational degrees of freedom.

In Fig. 1 we compare the approximately exact count calculations with calculations using Eq. (2). From the figure it can be seen that the density of states calculated using Eq. (2) is always lower than the more accurate approximately exact count method but it is well within a factor of two of this more accurate value. The anharmonic density of states is within 4% of the harmonic value for energies between 10,000 and 40,000 cm^{-1} and has not been indicated in Fig. 1. For higher energies the effect of anharmonicity becomes increasingly more pronounced.[3]

In addition to these density of states calculations, we have also used an exact count method for benzene which divided the number of vibrational states within a given energy interval $E \pm 50$ cm^{-1} into the different irreducible representations of the D_{6h} symmetry group. The vibrational frequencies used were those of Mair and Hornig.[6] The expression used to determine the number of states $n^{(\gamma)}(E)$ in the γth irreducible representation was[7]

$$n^{(\gamma)} = \frac{1}{g} \sum_R \chi_R^{(\gamma)*} \chi_R \qquad (5)$$

Figure 1. Comparison of the approximately exact count and semi-empirical methods for calculating the density of states ρ. The continuous line is drawn to fit the semi-empirical values.

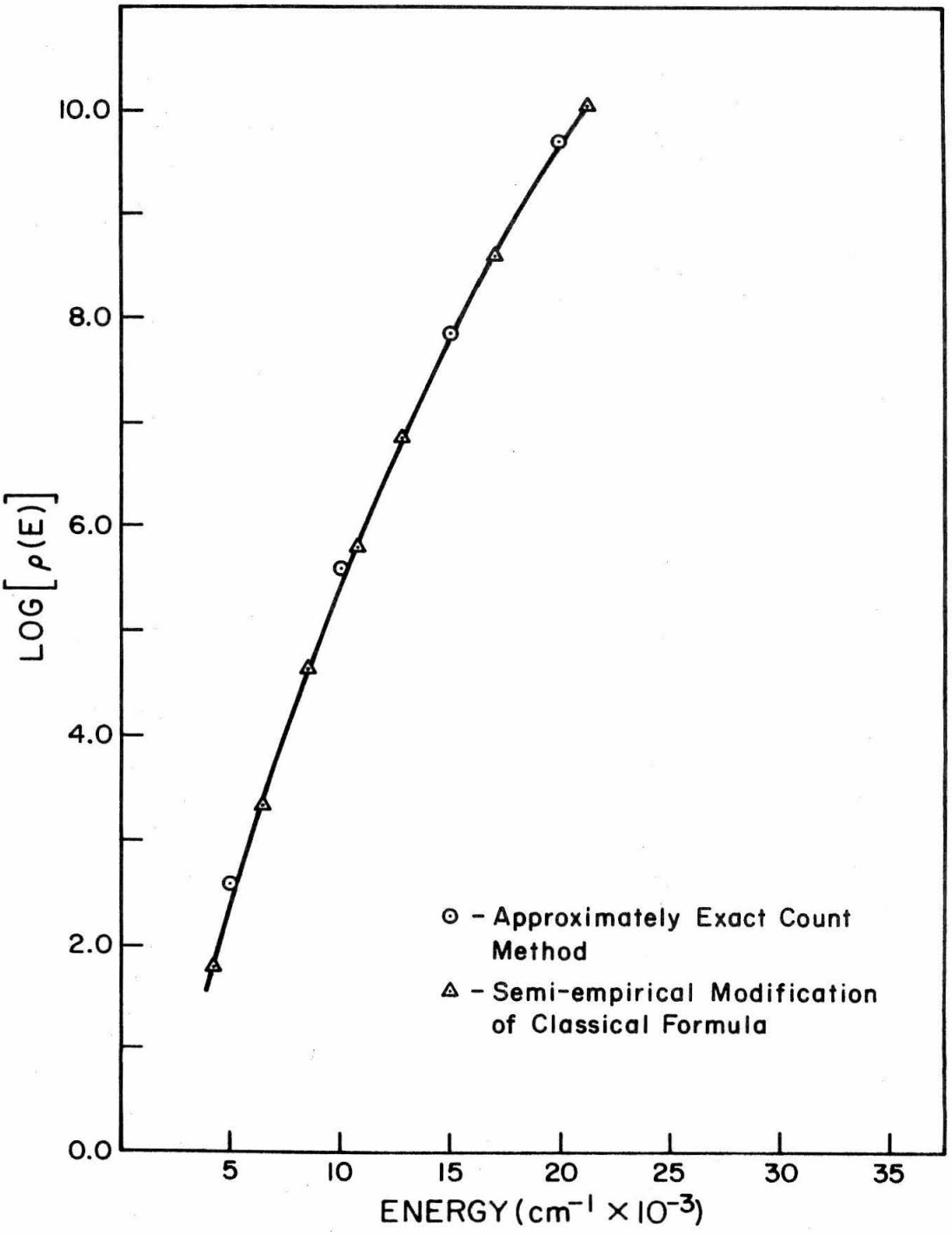
10.0
8.0
6.0
4.0
2.0
0.0
LOG[ρ(E)]
5
10
15
20
25
30
35
ENERGY (cm⁻¹ × 10⁻³)
⊙ – Approximately Exact Count Method
△ – Semi-empirical Modification of Classical Formula

where $\underline{g}$ is the number of operations in the group, χ_R is the character of the combination vibration for the group operator R and $\chi_R^{(\gamma)}$ is the character of operation R for the irreducible representation γ. The sum is over all of the operations of the symmetry group. Equation (5) is valid for combination levels only; it does not apply to overtone levels of degenerate fundamentals. We have nevertheless assumed, without serious loss of accuracy, that Eq. (5) can be used for overtones and combination levels. The results of this calculation for E = 5,000 cm^{-1} are listed in Table I. These results are discussed in Sec. IIA5.

TABLE I. Separation of the total density of states at $E = 5000 \pm 50\ cm^{-1}$ into the various irreducible representations of the D_{6h} symmetry group.

Representation	Density	Representation	Density
a_{1g}	3.75×10^3	a_{2g}	3.75×10^3
b_{1g}	3.64×10^3	b_{2g}	3.64×10^3
e_{1g}	7.28×10^3	e_{2g}	7.50×10^3
a_{1u}	3.90×10^3	a_{2u}	3.90×10^3
b_{1u}	3.42×10^3	b_{2u}	3.42×10^3
e_{1u}	6.83×10^3	e_{2u}	7.78×10^3

REFERENCES

1. For a detailed list of references on unimolecular reaction rate theory see P. C. Haarhoff, Mol. Phys. 7, 101 (1963).
2. G. Z. Whitten and B. S. Rabinovitch, J. Chem. Phys. 38, 2466 (1963).
3. E. W. Schlag and R. A. Sandsmark, J. Chem. Phys. 37, 168 (1962); E. W. Schlag, R. A. Sandsmark, and W. G. Valence, J. Chem. Phys. 40, 1461 (1964); J. Phys. Chem. 69, 1431 (1965).
4. E. Thiele, J. Chem. Phys. 39, 3258 (1963).
5. R. C. Tolman, The Principles of Statistical Mechanics (Oxford University Press, London, 1938), p. 492.
6. R. D. Mair and D. F. Hornig, J. Chem. Phys. 17, 1236 (1949).
7. E. B. Wilson, J. C. Decius, and P. C. Cross, Molecular Vibrations (McGraw-Hill Book Co., Inc., New York, 1955), p. 99.

APPENDIX D

DERIVATION OF VIBRATIONAL MATRIX ELEMENTS

A brief outline of the derivation of the two matrix elements given by Eqs. (19) and (20) of Sec. IIB is presented in this appendix. These matrix elements appear not only in theories of radiationless transitions but also in discussions of vibronic intensity enhancement of symmetry forbidden electronic transitions.[1]

The derivative matrix element is given by the expression

$$I_1^{n,m} = \langle x_\alpha^{kn} \left| \frac{\partial}{\partial Q_\alpha} \right| x_\alpha^{sm} \rangle = N_n N_m \int_{-\infty}^{\infty} e^{-\alpha^2 Q^2/2} H_n(\alpha Q) \left(\frac{\partial}{\partial Q} \right) e^{-\alpha'^2 Q'^2/2} H_m(\alpha' Q') dQ \tag{1}$$

where all symbols are defined in Sec. IIB. We will concentrate in this appendix on one normal mode so that the subscript α labeling the normal mode Q has been dropped. Also ground electronic state quantities are unprimed and excited state quantities are primed. We relate primed and unprimed quantities by

$$\alpha' = \sqrt{f}\ \alpha$$
$$Q' = Q + \delta$$

and define $y \equiv \alpha x$.

Equation (1) thus becomes

$$I_1^{n,m} = \alpha\sqrt{f}\ N_n N_m \int_{-\infty}^{\infty} e^{-y^2/2} H_n(y) \left[m\, H_{m-1}(y') - \frac{H_{m+1}(y')}{2} \right] e^{-y'^2/2} dQ \tag{2}$$

where we have made use of the following well-known properties of Hermite polynomials:[2]

$$y\, H_n(y) = \frac{H_{n+1}(y)}{2} + n\, H_{n-1}(y)$$

$$\frac{\partial H_n(y)}{\partial y} = 2n\, H_{n-1}(y) \quad .$$

The integral Eq. (2) can be evaluated in closed form by using Eq. (9) of Sec. IIA. The result for the specific case m = 0 is:

$$I_1^{n,o} = -N_n N_o \left(\frac{2\pi}{1+f}\right)^{\frac{1}{2}} \exp\left[\frac{-f\alpha^2\delta^2}{2(1+f)}\right] \left(\frac{f-1}{f+1}\right)^{n-1/2} \left\{\frac{1}{2}\left(\frac{f-1}{f+1}\right) H_{n+1}\left[\frac{-f\alpha\delta}{(f^2-1)^{1/2}}\right] + \left(\frac{3f-1}{f+1}\right) n\, H_{n-1}\left[\frac{-f\alpha\delta}{(f^2-1)^{1/2}}\right]\right\} \quad (3)$$

The coordinate matrix element is evaluated in a similar fashion:

$$I_2^{n,o} = \langle x_\alpha^{kn} | Q_\alpha | x_\alpha^{sm} \rangle$$

$$= N_n N_m \int_{-\infty}^{\infty} e^{-\alpha^2 Q^2/2} H_n(\alpha Q)\, Q e^{-\alpha'^2 Q'^2/2} H_m(\alpha' Q') dQ$$

$$= \frac{N_n N_m}{\alpha} \int_{-\infty}^{\infty} e^{-y^2/2} \left[\frac{H_{n+1}(y)}{2} + n H_{n-1}(y)\right] e^{-y'^2/2} H_m(y') dQ \quad (4)$$

For the special case m = 0, Eq. (4) becomes

$$I_2^{n,o} = \frac{N_n N_m}{\alpha^2}\left(\frac{2\pi}{1+f}\right)^{\frac{1}{2}} \exp\left[\frac{-f\alpha^2\delta^2}{2(1+f)}\right]\left\{\frac{1}{2}\left(\frac{f-1}{f+1}\right) H_{n+1}\left[\frac{-f\alpha\delta}{(f^2-1)^{1/2}}\right]\right.$$

$$\left. + n\, H_{n-1}\left[\frac{-f\alpha\delta}{(f^2-1)^{1/2}}\right]\right\}\left(\frac{f-1}{f+1}\right)^{n-1/2} \quad . \tag{5}$$

The ratio of $I_1^{n,o}$ to $I_2^{n,o}$ which is the quantity of interest in Sec. IIB may be written

$$\frac{I_1^{n,o}}{I_2^{n,o}} = \frac{-\alpha^2\left[\frac{(3f-1)}{(f+1)} + \left(\frac{f-1}{f+1}\right)\frac{H_{n+1}\left[\frac{-f\alpha\delta}{(f^2-1)^{1/2}}\right]}{2n\, H_{n-1}\left[\frac{-f\alpha\delta}{(f^2-1)^{1/2}}\right]}\right]}{1 + \frac{1}{2n}\left(\frac{f-1}{f+1}\right)\frac{H_{n+1}\left[\frac{-f\alpha\delta}{(f^2-1)^{1/2}}\right]}{H_{n-1}\left[\frac{-f\alpha\delta}{(f^2-1)^{1/2}}\right]}} \tag{6}$$

If $\delta = 0$, Eq. (6) takes a particularly simple form. Noting the fact that

$$H_{n+1}[0] = -2n\, H_{n-1}[0]$$

the ratio becomes

$$\frac{I_1^{n,o}}{I_2^{n,o}} = -\alpha^2 f \quad . \tag{7}$$

If $f = 1$, Eq. (6) is

$$\frac{I_1^{n,o}}{I_2^{n,o}} = -\alpha^2 \tag{8}$$

no matter what the value of δ.

For the special case $f = 1$ and $\delta = 0$, the two harmonic

oscillators x_α^{kn} and x_α^{sm} are solutions of the same Hamiltonian and the matrix elements $I_1^{n,m}$ and $I_2^{n,m}$ are more conveniently derived by using the commutation relations with the harmonic oscillator Hamiltonian.[3] (It will be noted that $\partial/\partial Q$ is related to the momentum of a harmonic oscillator.) In this case, m must equal $n \pm 1$ for the integrals to have nonzero values and Eq. (8) applies only when $n = 1$. We are normally interested in radiationless or radiative transitions between different electronic states and in general $f \neq 1$ and $\delta \neq 0$ although they are quite often very close to these values.

REFERENCES

1. G. Herzberg and E. Teller, Z. Physik Chem. B21, 410 (1933); A. C. Albrecht, J. Chem. Phys. 33, 156 (1960).
2. H. Margenau and G. M. Murphy, The Mathematics of Physics and Chemistry (D. Van Nostrand Co., Inc., Princeton, 1956), p. 123.
3. A. Yariv, Quantum Electronics (J. Wiley and Sons, Inc., New York, 1967), pp. 20-28.

APPENDIX E

THE EXCITON BAND STRUCTURE OF THE $^3B_{1u}$ AND $^1B_{2u}$ ELECTRONIC STATES OF BENZENE

In Table I we list the total number of exciton states within a $\frac{1}{4}$ cm^{-1} energy interval at various distance from the exciton band center. The calculations were performed as described in Sec. IIIB3 for a 275, 684 molecule benzene crystal. The density of states tabulated in Table I must be normalized by dividing by the total number of states in the exciton band, that is by 275, 684, when used in calculating the positions of isotopic impurity levels using Eq. (30) of Sec. IIIB.

TABLE I. Density of states in the $^3B_{1u}$ and $^1B_{2u}$ exciton bands of C_6H_6.

Distance from Band Center (cm^{-1})	No. of States	
	$^1B_{2u}$	$^3B_{1u}$
-36.00	0	0
-35.75	0	0
-35.50	0	0
-35.25	0	0
-35.00	7	0
-34.75	52	0
-34.50	69	0
-34.25	84	0
-34.00	102	0
-33.75	107	0
-33.50	122	0
-33.25	125	0
-33.00	141	0
-32.75	148	0
-32.50	149	0
-32.25	157	0
-32.00	174	0
-31.75	182	0
-31.50	182	0
-31.25	191	0
-31.00	193	0
-30.75	214	0
-30.50	198	0
-30.25	224	0
-30.00	231	0
-29.75	220	0
-29.50	236	0

TABLE I. (Continued)

Distance from Band Center (cm^{-1})	No. of States $^1B_{2u}$	$^3B_{1u}$
-29.25	249	0
-29.00	242	0
-28.75	259	0
-28.50	274	0
-28.25	261	0
-28.00	262	0
-27.75	299	0
-27.50	283	0
-27.25	295	0
-27.00	310	0
-26.75	291	0
-26.50	311	0
-26.25	341	0
-26.00	316	0
-25.75	328	0
-25.50	359	0
-25.25	341	0
-25.00	346	0
-24.75	359	0
-24.50	356	0
-24.25	384	0
-24.00	364	0
-23.75	409	0
-23.50	391	0
-23.25	391	0
-23.00	422	0
-22.75	421	0
-22.50	396	0

TABLE I. (Continued)

Distance from Band Center (cm^{-1})	No. of States $^1B_{2u}$	$^3B_{1u}$
-22.25	430	0
-22.00	452	0
-21.75	444	0
-21.50	437	0
-21.25	459	0
-21.00	460	0
-20.75	482	0
-20.50	471	0
-20.25	471	0
-20.00	517	0
-19.75	521	0
-19.50	490	0
-19.25	518	0
-19.00	540	0
-18.75	523	0
-18.50	554	0
-18.25	530	0
-18.00	587	0
-17.75	567	0
-17.50	581	0
-17.25	576	0
-17.00	622	0
-16.75	600	0
-16.50	596	0
-16.25	625	0
-16.00	657	0
-15.75	640	0
-15.50	678	0

TABLE I. (Continued)

Distance from Band Center (cm^{-1})	No. of States $^1B_{2u}$	$^3B_{1u}$
-15.25	708	0
-15.00	674	0
-14.75	704	0
-14.50	741	0
-14.25	709	0
-14.00	738	0
-13.75	758	0
-13.50	764	0
-13.25	780	0
-13.00	800	0
-12.75	805	0
-12.50	841	0
-12.25	862	0
-12.00	846	0
-11.75	899	0
-11.50	869	0
-11.25	917	0
-11.00	941	0
-10.75	914	0
-10.50	958	0
-10.25	947	0
-10.00	1017	0
- 9.75	959	0
- 9.50	1056	0
- 9.25	1042	0
- 9.00	1043	0
- 8.75	1067	0
- 8.50	1071	182

TABLE I. (Continued)

Distance from Band Center (cm^{-1})	No. of States $^1B_{2u}$	$^3B_{1u}$
- 8.25	1137	486
- 8.00	1162	655
- 7.75	1127	798
- 7.50	1189	929
- 7.25	1160	1060
- 7.00	1263	1173
- 6.75	1257	1290
- 6.50	1264	1392
- 6.25	1278	1554
- 6.00	1392	1662
- 5.75	1382	1785
- 5.50	1425	1942
- 5.25	1473	2079
- 5.00	1473	2209
- 4.75	1547	2397
- 4.50	1591	2588
- 4.25	1568	2772
- 4.00	1647	2992
- 3.75	1643	3217
- 3.50	1771	3390
- 3.25	1744	3745
- 3.00	1840	4037
- 2.75	1857	4366
- 2.50	1917	4714
- 2.25	2041	5136
- 2.00	1997	5565
- 1.75	2109	6103
- 1.50	2209	6827
- 1.25	2287	7912

TABLE I. (Continued)

Distance from Band Center (cm^{-1})	No. of States $^1B_{2u}$	$^3B_{1u}$
- 1.00	2382	8954
- 0.75	2456	10763
- 0.50	2635	13830
- 0.25	2725	16361
0.00	3238	16444
+ 0.25	3312	16527
+ 0.50	3310	13628
+ 0.75	3287	11166
+ 1.00	3361	9913
+ 1.25	3288	9074
+ 1.50	3341	8425
+ 1.75	3256	7932
+ 2.00	3569	7300
+ 2.25	3361	5937
+ 2.50	3599	5082
+ 2.75	3453	4449
+ 3.00	3592	3978
+ 3.25	3844	3556
+ 3.50	3733	3175
+ 3.75	3890	2866
+ 4.00	4226	2517
+ 4.25	4153	2201
+ 4.50	4034	1946
+ 4.75	4049	1658
+ 5.00	4568	1370
+ 5.25	4120	1056
+ 5.50	3616	619
+ 5.75	3433	0

TABLE I. (Continued)

Distance from Band Center (cm^{-1})	No. of States $^1B_{2u}$	$^3B_{1u}$
+ 6.00	3361	0
+ 6.25	3009	0
+ 6.50	2862	0
+ 6.75	2779	0
+ 7.00	2879	0
+ 7.25	1580	0
+ 7.50	2446	0
+ 7.75	2578	0
+ 8.00	2501	0
+ 8.25	2301	0
+ 8.50	2328	0
+ 8.75	2360	0
+ 9.00	2162	0
+ 9.25	1888	0
+ 9.50	1827	0
+ 9.75	1787	0
+10.00	1629	0
+10.25	1548	0
+10.50	1544	0
+10.75	1507	0
+11.00	1369	0
+11.25	1360	0
+11.50	1325	0
+11.75	1318	0
+12.00	1215	0
+12.25	1199	0
+12.50	1187	0
+12.75	1124	0
+13.00	1081	0

TABLE I. (Continued)

Distance from Band Center (cm^{-1})	No. of States $^1B_{2u}$	$^3B_{1u}$
+13.25	1078	0
+13.50	1029	0
+13.75	973	0
+14.00	953	0
+14.25	968	0
+14.50	897	0
+14.75	884	0
+15.00	884	0
+15.25	803	0
+15.50	810	0
+15.75	804	0
+16.00	720	0
+16.25	738	0
+16.50	725	0
+16.75	660	0
+17.00	659	0
+17.25	650	0
+17.50	612	0
+17.75	614	0
+18.00	566	0
+18.25	548	0
+18.50	563	0
+18.75	504	0
+19.00	509	0
+19.25	462	0
+19.50	476	0
+19.75	424	0
+20.00	432	0

TABLE I. (Continued)

Distance from Band Center (cm^{-1})	No. of States $^1B_{2u}$	$^3B_{1u}$
+20.25	381	0
+20.50	391	0
+20.75	345	0
+21.00	330	0
+21.25	312	0
+21.50	273	0
+21.75	255	0
+22.00	217	0
+22.25	189	0
+22.50	142	0
+22.75	53	0
+23.00	0	0

APPENDIX F

SPECTROSCOPIC INVESTIGATION OF IMPURITIES IN Cs-PURIFIED C_6H_6 AND C_6D_6

In Sections IIIA and IV we have referred to the impurities present in Cs-purified C_6H_6 and C_6D_6. In this appendix we discuss several experiments performed in an attempt to positively identify these impurities.

The "pure" benzene used here was prepared in a manner similar to the method developed by Colson and Bernstein.[1] The benzene was first thoroughly degassed by at least four freeze-pump-thaw cycles. This degassed benzene was then dried over K and finally extensively refluxed over Cs for 2-4 hours at 90-95° C. The "pure" benzene was then degassed again and finally transferred under vacuum to a crystal growing tube. Both the C_6H_6 and C_6D_6 samples were prepared in this way.

To assess the effect of more extensive purification techniques on the impurity content, one C_6H_6 sample was doubly Cs-purified. After the initial Cs-refluxing step, the benzene was degassed and transferred to another tube containing fresh Cs metal. The refluxing step was then repeated and the benzene subsequently transferred to a crystal growing tube after thorough degassing.

A third C_6H_6 sample was Cs-purified once and then extensively zone-refined. This particular purification procedure thus closely resembled the one used to prepare β-methylnaphthalene-free naphthalene.[2] No discernable difference was found in the impurity spectra of

C_6H_6 prepared in the three ways just described. It was thus concluded that single-refluxing over Cs was as effective as any more extensive techniques at purifying benzene.

Since toluene was expected to be the major impurity in the Cs-purified samples,[3] a Cs-purified sample doped with about 1% toluene was also prepared. The toluene was degassed and allowed to sit over K at room temperature for several hours before being added to the Cs-purified benzene. At no time after degassing was the toluene or benzene exposed to the atmosphere.

The phosphorescence spectra from both the Cs-purified and toluene doped C_6H_6 samples at 4.2° K are reported in Table I. The Cs-purified benzene spectrum was obtained photoelectrically using an intense 4000 watt xenon lamp and a $\frac{1}{2}$ m Jarrel-Ash grating spectrometer. We also used a rotating sector apparatus which exposed the sample alternately to the light source and the phototube. The toluene doped benzene emission spectrum was obtained photographically using a 2 m spectrograph built in our laboratory and a 150 watt xenon light source. Corning glass and Kasha[4] liquid filters were used to isolate the appropriate spectral region.

All lines observed in the toluene doped sample were easily correlated with the stronger features in the pure benzene spectrum. The weaker features of the pure crystal spectrum were not observed for the toluene doped sample. This is simply because of the much lower sensitivity of the photographic set-up used in the toluene doped benzene experiments. From these results we conclude that toluene is the major emitting species in Cs-purified benzene at 4.2° K. We cannot,

TABLE I. Emission from toluene in benzene at 4.2° K.

Cs-purified		Toluene doped		Strength[a]
λ_{air} (Å)	ν_{vac} (cm^{-1})	λ_{air} (Å)	ν_{vac}[b] (cm^{-1})	
3448.2	28,992 ± 5	3448.9	28,987	VS
3453.5	28,948			W
3464.7	28,854			VW
3477.2	28,751	3476.0	28,761	M
3482.2	28,709			VW
3502.8	28,540			W
3526.2	28,351			W
3531.9	28,305			VW
3535.2	28,279			W
3540.2	28,239			VW
3546.5	28,189	3546.6	28,196	M
3552.9	28,138			W
3558.2	28,096			VW
3563.4	28,055			VW
3573.2	27,978	3571.3	27,993	M
3577.4	27,945	3572.8	27,981	M
3584.3	27,891			W
3594.6	27,812	3593.0	27,824	M
3601.2	27,761	3595.5	27,805	M
3604.8	27,733			W
3612.6	27,673			W
3625.5	27,575			W
3632.2	27,524			M
3636.1	27,494			W
3648.6	27,400	3648.8	27,398	VVS
3651.5	27,378	3651.0	27,382	VVS
3676.6	27,191			M
3679.1	27,173			M

TABLE I. (Continued)

Cs-purified		Toluene doped		Strength[a]
λ_{air} (Å)	ν_{vac} (cm^{-1})	λ_{air} (Å)	ν_{vac}[b] (cm^{-1})	
3683.2	27,143	3682.6	27,147	M
3701.4	27,009			M
3708.1	26,960			M
3712.9	26,925			M
3730.8	26,796			M
3734.7	26,757			M
3757.5	26,606	3758.0	26,602	S
3761.3	26,579	3761.5	26,578	S
3765.5	26,542			M
3787.4	26,396	3787.5	26,395	S
3791.3	26,369	3791.0	26,371	VS
3793.9	26,351	3794.6	26,347	S

[a]VW = very weak, W = weak, M = moderate, S = strong, VS = very strong, VVS = very, very strong.

[b]The accuracy of these measurements is ± 3 cm^{-1} for VVS, VS and S lines. For lines of moderate strength (M) the energy measurements may be in error by as much as 50 cm^{-1}. Weak and very weak lines were not observed in the toluene doped samples.

however, conclude on the basis of the results summarized in Table I that it is the only species which contributes to the emission. It may be that some of the weaker features are due to other impurities although at the moment we consider this possibility unlikely.

The 4.2° K absorption spectrum of the toluene doped samples in the region of toluene's first singlet state[5] was obtained using the same photographic set-up. This spectrum was compared with the pure crystal absorption obtained and described in Part IV. The results of this comparison are tabulated in Table II. The toluene doped benzene absorption spectrum was broad with very little structure. The absorption edge began at 36,990 cm^{-1} and reached a peak at 37,110 cm^{-1} after which the absorption declined to zero at 37,340 cm^{-1}. One small peak to longer wavelength was observed at 37,440 cm^{-1}. The C_6H_6 absorption began at 37,520 cm^{-1}. These doped benzene results agree very well with the pure crystal results. Both observed peaks in the doped benzene spectrum agree in energy with two quite strong features of the pure benzene spectrum. And the general envelop of the doped benzene spectrum agrees with the overall character of the pure crystal spectrum.

No phenol absorption was observed. Broude[6] has obtained the absorption spectrum of phenol in benzene at 20° K. His results show quite strong absorption peaks at 35,598 cm^{-1}, 36,542 cm^{-1} and 37,329 cm^{-1}. None of these features are observed in the Cs-purified benzene spectrum reported in Table II.

From these results for C_6H_6, we conclude that toluene is the major spectroscopically active impurity in Cs-purified C_6H_6. The

TABLE II. Absorption of toluene in benzene at 4.2° K.

Cs-purified		Toluene doped		Strength[a]
λ_{air} (Å)	ν_{vac} (cm^{-1})	λ_{air} (Å)	ν_{vac} (cm^{-1})	
2693.7	37,113 ± 5	2694.1	37,110 ± 10	VS
2690.3	37,160			S
2689.9	37,165			S
2688.7	37,182			S
2685.0	37,233			W
2681.6	37,280			S
2675.6	37,364			M
2669.6	37,448	2670.0	37,440	S
2660.9	37,570			S
2660.6	37,574			S
2657.4	37,620			M
2656.1	37,638			S
2647.7	37,757			M

[a]VS = very strong, S = strong, M = moderate, W = weak.

extent of Cs-purification has little effect on the toluene concentration. No evidence of phenol was found.

The emission spectrum of Cs-purified C_6D_6 is dominated by isotopic impurities. Colson and Robinson,[7] from an examination of the absorption spectrum in the region of benzene's first singlet, have obtained the isotopic composition of the C_6D_6 we used. They found the following impurity concentrations in mole fractions:

.02	C_6HD_5
.005	$C_6H_2D_4$
.0005	$C_6H_3D_3$
10^{-5}	C_6H_5D
10^{-5}	C_6H_6

The phosphorescence spectrum we have obtained from Cs-purified C_6D_6 is presented in Table III. The spectrum is quite complicated but can be interpreted as being due primarily to $C_6H_2D_4$ and $C_6H_3D_3$. There are three different forms for each of these isotopic modifications and for some of these six different isotopic benzenes there are several orientations within the crystal site.[8] It is no wonder that the spectrum is quite complicated.

The presence of $C_6H_3D_3$ is inferred from the two lines at 28, 187 and 28, 182 cm^{-1} which agree quite well with the strong ν_8 line observed in sym-$C_6H_3D_3$ by Bernstein et al.[8] The two lines at 28, 204 and 28, 197 are assigned to the corresponding ν_8 vibration of $C_6H_2D_4$. If we take the $C_6H_2D_4$ 0-0 as 29, 783 cm^{-1}[9] and assume that the ν_8 vibration has a frequency of 1581 cm^{-1},[10] we obtain good agreement

TABLE III. Impurity emission spectrum of Cs-purified C_6D_6 at 4.2° K.

λ_{air} (Å)	ν_{vac} (cm^{-1})	Intensity[a]
3428.4	29,160 ± 3	S
3452.3	28,958	W
3457.9	28,911	VVW
3458.9	28,903	VVW
3460.3	28,891	VVW
3476.6	28,755	VVW
3494.4	28,609	VVW
3500.3	28,561	VVW
3501.9	28,548	VVW
3509.8	28,484	W
3516.5	28,430	VVW
3532.7	28,299	W
3534.1	28,288	S
3541.5	28,229	M
3542.8	28,219	W
3543.9	28,210	W
3544.6	28,204	VS
3545.5	28,197	VS
3546.7	28,187	M
3547.4	28,182	M
3561.0	28,074	S
3621.0	27,609	VS
3624.9	27,579	VS
3636.1	27,494	S

[a]VS = very strong, S = strong, M = moderate, W = weak, VW = very weak, VVW = very, very weak.

with the positions of the two observed lines. No corresponding evidence for the presence of C_6D_5H was found in the phosphorescence spectrum. This is not unexpected since the C_6D_5H impurity is quite near the host exciton band, and its excited states are much more delocalized than the corresponding states of other isotopic impurities. Energy can thus be transferred from the shallow C_6D_5H trap to deeper isotopic traps.[7] The strong line in the C_6D_6 emission spectrum at 29,160 cm^{-1} has been discussed in Appendix A.

The impurity absorption spectrum in the region of the C_6D_6 singlet has been previously presented (Fig. 2 of Sec. IV). Three sharp but weak impurity lines are observed at 37,142 cm^{-1}, 37,315 cm^{-1} and 37,524 cm^{-1}. These lines are attributed to absorption into the deuterotoluene lowest singlet state although no specific experiments to verify this assignment were performed.

These experimental results for C_6D_6 indicate that the major spectroscopic impurities in Cs-purified C_6D_6 are the isotopic species $C_6H_3D_3$ and $C_6H_2D_4$. Evidence for traces of deuterotoluene have also been found. It should be emphasized that the spectroscopic technique used here to assess the purity of both C_6D_6 and C_6H_6 is not sensitive to impurities with electronic states higher than 38,000 cm^{-1} in energy. Thus cyclohexane-d_{12} which is definitely present in the C_6D_6 samples we used[11] was not observed in our experiments.

Several people have helped in the experiments described in this Appendix. I am indebted to Dr. George Castro for supplying me with the zone-refined benzene samples and to Dr. E. B. Priestley for providing some of the doubly Cs-purified benzene used here. It is also a

pleasure to acknowledge a fruitful collaboration with Dr. J. H. Smith on the pure C_6H_6 emission experiments. Dr. Smith designed and built the rotating sector apparatus used in these experiments.

REFERENCES

1. S. D. Colson and E. R. Bernstein, J. Chem. Phys. 43, 2661 (1965).
2. E. B. Priestley, Ph. D. thesis, California Institute of Technology, 1970.
3. The manufacturers (Phillips Petroleum Company) claim that the major impurity present in their research grade C_6H_6 is toluene.
4. M. Kasha, J. Opt. Soc. 38, 929 (1948).
5. C. S. Burton and W. A. Noyes, J. Chem. Phys. 49, 1705 (1968).
6. V. L. Broude, Sov. Phys. -Usp. 4, 584 (1962).
7. S. D. Colson and G. W. Robinson, J. Chem. Phys. 48, 2550 (1968).
8. E. R. Bernstein, S. D. Colson, D. S. Tinti, and G. W. Robinson, J. Chem. Phys. 48, 4632 (1968).
9. G. C. Nieman and D. S. Tinti, J. Chem. Phys. 46, 1432 (1967).
10. S. Brodersen and A. Langseth, Mat. Fys. Skr. Dan. Vid. Selsk. 1, No. 7, 1 (1959).
11. The only nonisotopic chemical impurity that the manufacturers (Merck, Sharp and Dohme, Ltd. of Montreal, Canada) have been able to detect is cyclohexane-d_{12}.

PROPOSITIONS

PROPOSITION 1

OPTICAL ABSORPTION SPECTRUM OF ANTIFERROMAGNETIC α-Fe_2O_3

Transition metal cations have highly localized inner d-shell electronic transitions. For this reason the optical excitation of these cations in a crystal can be described in terms of tight-binding or Frenkel excitons.[1] The theoretical apparatus which has been developed to describe electronic transitions in molecular crystals[2] can thus be adapted for use in treating electronic transitions in crystals containing transition metal cations. This adaptation has only recently been outlined in detail by Louden.[3]

Many crystals containing transition metal cations are antiferromagnetic and this fact leads to some interesting differences between the electronic states of molecular crystals and those of magnetic insulators. For molecular crystals one quite frequently observes, in addition to pure excitonic optical transitions, transitions involving the simultaneous excitation of an exciton and a lattice mode or phonon. Both of these types of transitions are also observed in magnetic insulators. A third type of optical transition is possible in antiferromagnetic crystals, a magnon-exciton transition, which involves simultaneous excitation of an exciton and a spin deviation or spin wave. Both exciton-phonon and exciton-magnon transitions are experimentally observed as sidebands in the region of the pure exciton transitions of magnetic insulators.

Much of the previous work on excitons in magnetic insulators

has been done on antiferromagnetic crystals having the rutile (TiO_2) structure.[4] These crystals include MnF_2, CoF_2, FeF_2 and NiF_2.[5] All of these crystals have fairly low antiferromagnetic Neel temperatures ($T_N < 80°$ K),[6] indicating that the transition metal electron exchange interactions are small. The antiferromagnetic ordering in all four cases is of the first kind; that is the crystal lattice may be divided into two interpenetrating lattices, one with spin up and the other with spin down. Each of the inter-penetrating sublattices has only one molecule per unit cell and since the interaction between ions on different sublattices is small the Davydov splitting is small (< 10 cm^{-1}).[7] In addition to the small Davydov splittings, the pure $\underline{d} \rightarrow \underline{d}$ exciton transitions are very weak being both spin and parity forbidden[4] in the centrosymmetric rutile-type crystals.

It is obviously desirable to examine the optical properties of magnetic insulators with stronger exchange interactions not only to further test the applicability of Frenkel exciton theory to these systems, but also to extract more detailed information about the interion coupling. Allen et al.[8] have recently completed an investigation of the optical absorption spectrum of Cr_2O_3 with these goals in mind. Cr_2O_3, which crystallizes in the corundum (Al_2O_3) structure, has a very high Neel temperature ($T_N = 308°$ K).[9] There is no center of symmetry at the Cr^{+3} site so that optical transitions are spin but not parity forbidden. Like the rutile-type antiferromagnets the ordering is of the first kind. As would be expected for a material with a high Neel temperature the observed Davydov splitting is as large as 180 cm^{-1}.[8]

A logical next candidate in this series of increasingly more complicated antiferromagnetic crystals is α-Fe_2O_3 (hematite). This

crystal has a Neel temperature of 950° K[10] indicating even stronger interion interactions than Cr_2O_3. It, too, has the corundum crystal structure but unlike Cr_2O_3 its magnetic ordering is of the second kind.[11] One can visualize the difference between the magnetic ordering in Cr_2O_3 and α-Fe_2O_3 by imagining four ions placed uniformily along the body diagonal of a rhombohedron. For Cr_2O_3 the spins alternate in sign (up, down, up, down) and for α-Fe_2O_3 the middle two ions have the same spin direction (up, down, down, up).

Previous work on α-Fe_2O_3 has been primarily concerned with its non-spectroscopic magnetic properties. In this vein α-Fe_2O_3 has been investigated using the Mössbauer effect, neutron diffraction and antiferromagnetic resonance techniques.[12] The only optical absorption experiments reported to date were low resolution (100 Å) measurements on .00025 inch thick crystals at room and at liquid nitrogen temperatures.[13] In these low resolution experiments the lowest energy peak near 12,000 cm^{-1} showed some signs of structure. There is reason to hope that at higher resolution this structure can be resolved and analyzed.

It is proposed that the optical absorption spectrum of α-Fe_2O_3 be investigated at temperatures below 250° K[10] and at moderately high resolution ($\sim$1 Å). The hematite crystals can be grown from Bi_2O_3-Na_2CO_3[14] or $Pb_2P_2O_7$-MgO[15] melts. Polarization measurements should be made so that the observed exciton levels can be associated with specific intermolecular interactions. In addition, the magnetic field dependence of the spectrum would be useful in separating exciton levels from magnon sidebands.[4]

REFERENCES

1. R. S. Knox, Theory of Excitons, (Academic Press, New York, 1963), pp. 21-37.
2. A. S. Davydov, Theory of Molecular Excitons (McGraw-Hill Book Co., New York, 1962).
3. R. Louden, Advan. Phys. 17, 243 (1968).
4. D. S. McClure in Excitions, Magnons and Phonons in Molecular Crystals (Ed: A. B. Zahlan, Cambridge University Press, Cambridge, 1968), p. 135.
5. The magnetic structure of NiF_2 is a bit more complicated than the other three antiferromagnetic fluorides. For this reason it has not yet been theoretically treated in detail.
6. D. H. Martin, Magnetism in Solids (The M. I. T. Press, Cambridge, Mass., 1967), p. 51.
7. J. P. van der Ziel, Phys. Rev. 161, 483 (1967).
8. J. W. Allen, R. M. Macfarlane, and R. L. White, Phys. Rev. 179, 523 (1969).
9. J. P. van der Ziel, Phys. Rev. Letters 18, 237 (1967).
10. C. G. Shull, W. A. Strauser, and E. O. Wollan, Phys. Rev. 83, 333 (1951); I. E. Dzyaloshinskii, Sov. Phys. -JETP 5, 1259 (1957). Below the Neel temperature α-Fe_2O_3 is antiferromagnetic and weakly ferromagnetic. At $T \approx 250^\circ$ K, however, α-Fe_2O_3 assumes a different antiferromagnetic state, one in which no ferromagnetism is possible. We will only be concerned with this lower temperature modification.

11. Crystallographic structure: F. Bertaut, C. R. Acad. Sci. (France) 246, 3335 (1958). Magnetic structure: C. G. Shull, W. A. Strauser, and E. O. Wollan, Phys. Rev. 83, 333 (1951).

12. For a list of previous nonspectroscopic work on α-Fe_2O_3 see F. van der Woude, Phys. Stat. Sol. 17, 417 (1966).

13. P. C. Bailey, J. Appl. Phys. 31 Supplement, 39S (1960); Reflection measurements in the region 3600-7000 Å have been reported by R. C. Vernon, J. Appl. Phys. 33, 2140 (1962).

14. R. A. Voskanyan and I. S. Zheludev, Sov. Phys. -Cryst. 12, 473 (1967).

15. D. G. Wickham, J. Appl. Phys. 33, 3597 (1962).

PROPOSITION 2

THE VACUUM ULTRAVIOLET REFLECTION SPECTRUM OF SOLID H_2

Measurements in the spectral region which has come to be known as the rocket ultraviolet have revealed an apparent deficiency in stellar fluxes in the wavelength region below 1215 Å.[1] This deficiency remains even after corrections for interstellar reddening and line blanketing have been made. Duley[2] attempted to explain these spectroscopic observations by attributing the absorption to hydrogen atoms trapped at or near the surface of dielectric interstellar grains. McIntyre and Williams[3] have pointed out the inadequacy of Duley's calculation if the interstellar grains are assumed to be conducting graphite particles.[4,5] The most recent evidence[6] indicates that the interstellar grains may be a mixture of graphite and a refractory dielectric such as $MgSiO_3$, $(Mg, Fe)SiO_3$. If this model is correct then it is quite possible that the interstellar grains assume a temperature very near the 2.7° K background temperature determined from microwave measurements.[7] In this case H, which is 1000 times more abundant in the universe than any other element,[8] will begin to condense as H_2 on the surface of the interstellar particles. We suggest that the stellar flux deficiency below 1215 Å is due to absorption by this H_2 outer layer and not to adsorbed H atoms as Duley proposed.

The lowest allowed transition for the free H_2 molecule occurs at 91, 690 cm^{-1} (1090 Å) and has been assigned to the $^1\Sigma_u^+ - {}^1\Sigma_g^+$ transition.[9] The position of this transition in the solid has never been

determined but it does not seem unreasonable for it to be "solvent" shifted to the low frequency side of its gas phase value. The stellar flux measurements exhibit an apparent minimum at 1180 Å but this value is subject to quite large error limits and should be considered only approximate.

To see what kinds of experimental measurements would be necessary to test our hypothesis concerning the source of the far ultraviolet flux deficiency, we must first consider more precisely the details of the absorption of light by interstellar grains. First note that when an astronomer speaks of absorption, he does not always mean quite the same thing that a spectroscopist does. When he speaks of the absorption or more properly extinction of starlight by interstellar grains, the astronomer includes all of the processes which attenuate the starlight. The total extinction cross-section is thus a sum of absorption (in its spectroscopic sense) and scattering, that is:

$$C_{ext} = C_{abs} + C_{sca} \tag{1}$$

where the C's are cross-sections. If the radius of the particle $\underline{r}$ obeys the inequality

$$r \ll \frac{\lambda}{2\pi}$$

as interstellar grains appear to do then the extinction cross-section per unit area may be written[10]

$$Q_{ext}(r,\lambda) = \frac{C_{ext}}{\pi r^2} = \frac{8\pi r}{\lambda} \operatorname{Im} \frac{(1-m^2)}{(2+m^2)} \tag{2}$$

where Im indicates the imaginary part of a complex expression and m^2 is the complex index of refraction

$$m^2 = n - ik \quad . \tag{3}$$

Here $\underline{n}$ is the real index of refraxtion and $\underline{k}$ is the extinction coefficient. $\underline{k}$ is related to the decadic molar extinction coefficient ϵ by

$$\epsilon = \frac{(4\pi k)}{(2.303\ \lambda C)} \tag{4}$$

where C is the concentration of absorbers.

Apparently then, we need to obtain values for $\underline{n}$ and $\underline{k}$ as a function of wavelength for solid H_2 in the 1200 Å region in order to test our hypothesis. The first method that comes to mind is the determination of $\underline{k}$ directly by measuring the absorption spectrum and the determination of $\underline{n}$ by interferometric techniques.[11] The oscillator strength for the H_2 transition of interest $^1\Sigma_u^+ \leftarrow {}^1\Sigma_g^+$ is .26.[12] If we assume a Gaussian line shape and a half-width of 1000-10,000 cm^{-1} for the transition, then in order to obtain $\underline{k}$ directly from absorption measurements, we would have to use crystals of 1-10 μ thickness. It is hard enough to obtain crystals of this thickness for substances that are easily handled at room temperature. It would seem almost impossible to obtain H_2 crystals of a reliable thickness in the range 1-10 μ, since these crystals must be grown and handled below 20° K.

An experimental technique which yields both $\underline{n}$ and $\underline{k}$ and is ideally suited for use on highly absorbing materials is specular reflection spectroscopy.[13,14] In this technique the reflectivity at

normal incidence $\underline{R}$ is measured as a function of wavelength. $\underline{R}$ can be expressed in terms of $\underline{n}$ and $\underline{k}$ as

$$R = \frac{(n-1)^2 + k^2}{(n+1)^2 + k^2} \quad . \tag{5}$$

This expression can be inverted to obtain $\underline{n}$ and $\underline{k}$ in terms of $\underline{R}$ and a phase angle θ. ℓnR and θ are related by the Kramers-Kronig relationship, so that in principle knowing $R(\lambda)$ one can extract the optical constants $\underline{n}$ and $\underline{k}$. One problem with this technique for highly absorbing crystals is that it measures $\underline{n}$ and $\underline{k}$ only for molecules at or near the surface. One is normally interested in bulk crystal properties and it is never clear whether $\underline{k}$ measured by reflection spectroscopy reflects the absorption of the bulk of the crystal or just those molecules near the surface. In the case of an H_2-crystal layer on the surface of an interstellar grain, however, it is just these surface values for $\underline{n}$ and $\underline{k}$ that we need to use in Eq. (2).

In light of the preceding discussion, it is proposed that the vacuum ultraviolet reflection spectrum of solid H_2 crystals near 1200 Å be determined preferably at or near 3° K and that this spectrum be used to obtain both $\underline{n}$ and $\underline{k}$ as a function of wavelength. These optical parameters can then be used in Eq. (2) to obtain $Q_{ext}(r, \lambda)$ which can be compared with the observed stellar flux deficiency in this spectral region. The experimental details of reflection spectroscopy[13, 14] and the particular experimental problems encountered in the vacuum ultraviolet[15] have been discussed elsewhere. There seem to be no particular problems involved in the growth and storage of good hydrogen crystals.[16]

REFERENCES

1. E. T. Byram, T. A. Chubb, and M. W. Werner, Ann. d. Astrophys. 28, 594 (1965); C. B. Opal, H. W. Moos, W. G. Fastie, M. Bottema, and R. C. Henry, Astrophys. J. 153, L179 (1968); G. R. Carruthers, Astrophys. J. 151, 269 (1968).
2. W. W. Duley, Nature 222, 361 (1969).
3. H. A. J. McIntyre and D. A. Williams, Nature 223, 488 (1969).
4. N. H. Dieter and W. M. Goss, Rev. Mod. Phys. 38, 256 (1966).
5. F. Hoyle and N. C. Wickramasinghe, Roy. Astro. Soc. -Monthly Notices 124, 417 (1962).
6. F. Hoyle and N. C. Wickramasinghe, Nature 223, 459 (1969).
7. Graphite grains being conductors would absorb a considerable amount of the incident starlight and would thus assume a temperature well above 3° K. Solid hydrogen could not form on the surface of such grains. Low conductivity dielectric grains scatter starlight but hardly absorb it at all. They thus can assume the temperature of the thermal background 2.7° K.
8. L. Goldberg, E. Müller, and L. H. Aller, Ap. J. Suppl. 5, No. 45 (1960).
9. G. Herzberg, Spectra of Diatomic Molecules (D van Nostrand Co., Inc., Princeton, 1950), p. 532.
10. H. C. van de Hulst, Light Scattering by Small Particles (John Wiley and Sons, Inc., New York, 1957), p. 270.
11. D. E. Diller, J. Chem. Phys. 49, 3096 (1968).
12. J. Geiger, Z. Physik. 181, 413 (1964).

13. B. G. Anex, Mol. Cryst. 1, 1 (1966).

14. W. W. Wendlandt and H. G. Hecht, Reflectance Spectroscopy (Interscience Publishers, New York, 1966).

15. J. C. Boyce, Rev. Mod. Phys. 13, 1 (1941); W. R. S. Garton, Adv. At. and Mol. Phys. 2, 93 (1966).

16. W. H. Keesom, J. de Smedt, and H. H. Mooy, Comm. Kam. Onnes Lab (Leiden) 19, 209d (1930).

PROPOSITION 3

EPR INVESTIGATION OF THE REACTION BETWEEN TOLUENE AND Cs METAL

The reaction of an alkali metal with any of a number of aromatic hydrocarbons to produce the corresponding hydrocarbon radical anion has been known for quite some time.[1] In fact this reaction is very commonly used as a means of producing such radical anions for EPR investigations.[2] More recently the reactions of Cs with benzene[3] and K with naphthalene[4] have been discussed as means of purifying these compounds. It has been shown that Cs quite effectively removes phenol from benzene[3] and that K very efficiently removes β-methylnaphthalene from naphthalene.[4] However a significant amount of the toluene impurity in benzene seems to be unaffected even when the benzene is refluxed for several hours over Cs.[5] This result is indeed puzzling. If K can react with β-methylnaphthalene why does Cs not react with toluene? Perhaps Cs does react with toluene but the alkali metal mirror used in the purification procedure very quickly becomes coated and rendered inactive, or perhaps there is insufficient contact between the Cs and toluene.

Quite clearly one of the first steps towards unraveling this is a detailed investigation of the nature of the reaction of toluene with Cs in a benzene solvent. Three possible reactions are suggested. They are in order of decreasing plausability.

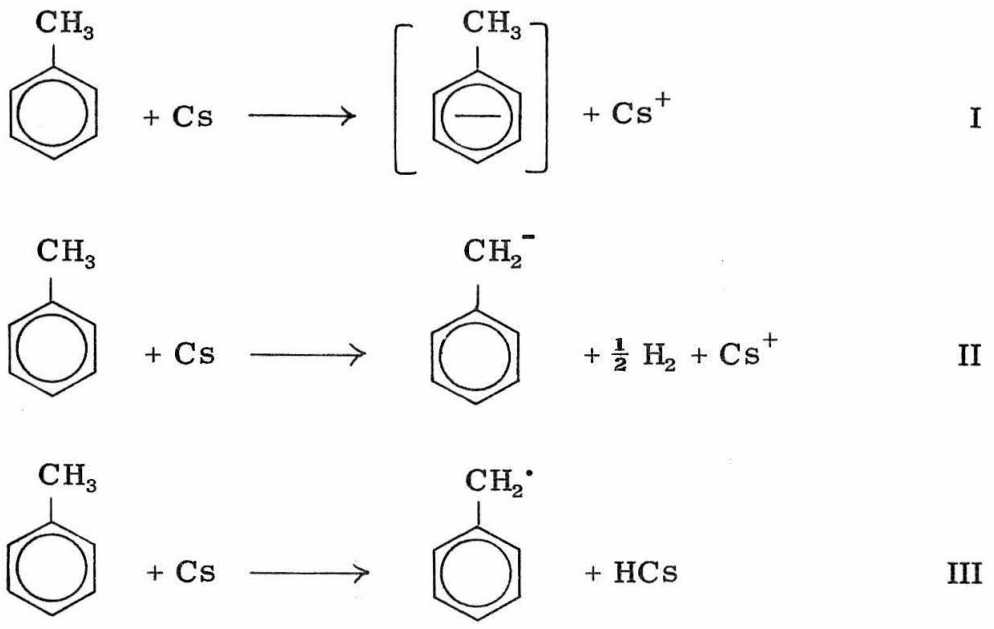

Reaction I is known to occur in solvents such as tetrahydrofuran and 1, 2 dimethoxyethane.[2, 6] One would expect benzene to be converted to its radical anion by mechanism I also.[2] In fact, one would expect benzene to be even more reactive than toluene since the $-CH_3$ substituent destabilizes the radical anion. There is some experimental evidence suggesting that the toluene radical anion does in fact form less rapidly. If a mixture of benzene and an alkylbenzene is reduced by potassium in methylamine, benzene is more extensively converted than the alkylbenzene.[7] If Reaction I occurs in a benzene solvent, one might then expect that the relative concentration of toluene would slightly increase rather than decrease.

Reaction II is analogous to the reaction of Cs with phenol. For phenol it is a very efficient reaction as indicated before. If we assume

that the ease of removal of an acidic proton is related to the corresponding pK_a, then we can see from the table below that toluene and benzene are both overwhelmingly less reactive than phenol:

Compound	pK_a[8]
phenol	9.99
toluene	39
benzene	41

We can also see from the table that toluene is about 100 times more reactive than benzene. If Reaction II is the dominant reaction pathway, then reaction with Cs will purify the benzene by more efficiently removing the toluene.

Reaction III is not considered a very likely possibility because of the instability of the alkali metal hydride that is formed. The insolubility of CsH in nonpolar benzene may, however, remove it from solution before it has a chance to decompose. In any case we cannot definitely rule out this reaction and we include it here for completeness.

An obvious way of distinguishing between the three suggested reactions is to examine the EPR spectrum of a solution of toluene in benzene. Both Reactions I and III produce free radicals which can be detected by EPR. To avoid any complications that might arise from interfering free radicals produced by reaction of Cs with the benzene solvent, it is proposed that the reaction be studied in C_6D_6. The hyperfine splitting due to the deuteron in the C_6D_6 radical anion is a factor of seven smaller than that due to the proton in the C_6H_6 radical anion.[9]

Hyperfine splittings due to the protonated solvent can thus easily be distinguished from splittings due to the deuterated solvent. The hyperfine patterns for the toluene radical anion (Reaction I)[10] and the benzil radical (Reaction III)[11] are well known and can easily be distinguished. Thus Reactions I and III can easily be detected in an EPR experiment.

The EPR technique is really quite sensitive to small free radical concentrations. The smallest sample that the best EPR spectrometer can see is about 10^{-14} moles of unpaired electrons per gauss of line width and line widths in solution are typically less than 1 gauss.[12] Any reaction between Cs metal and toluene that could be described as useful at all for purifying benzene would thus be observed in EPR provided free radicals were produced in the process.

If no EPR signal at all were observed, one of two possibilities would be suggested; either the reaction proceeds via mechanism III and no free radicals are produced or no reaction occurs at all. To distinguish between these two possibilities we can measure the electrical conductivity of the reaction mixture.[13] No conductivity increase in the presence of Cs obviously indicates no reaction.

To summarize then, it is proposed to determine the precise nature of the reaction of Cs metal with toluene in a deuterobenzene solvent by studying the EPR spectrum of the free radicals produced. If no EPR spectrum is detected, then electrical conductivity measurements are suggested.

REFERENCES

1. W. Schlenk, J. Appenrodt, A. Michael and A. Thal, Ber. D. D. Chem. Ges. 47, 473 (1914); N. D. Scott, J. F. Walker, and V. L. Hansley, J. Am. Chem. Soc. 58, 2442 (1936); G. J. Hoijtink, E. De Boer, P. H. van der Meij, and W. P. Weijland, Rec. Trav. Chim. 74, 277 (1955), 75, 487 (1956); P. Balk, G. J. Hoijtink, and J. W. H. Schreurs, Rec. Trav. Chim. 76, 813 (1957).
2. T. R. Tuttle and S. I. Weissman, J. Am. Chem. Soc. 80, 5342 (1958); M. G. Townsend and S. I. Weissman, J. Chem. Phys. 32, 309 (1960).
3. S. D. Colson and E. R. Bernstein, J. Chem. Phys. 43, 2661 (1965).
4. D. M. Hanson and G. W. Robinson, J. Chem. Phys. 43, 4174 (1965); E. B. Priestley, Ph. D. thesis, California Institute of Technology, 1970.
5. Appendix F of this thesis.
6. J. R. Bolton, Mol. Phys. 6, 219 (1963).
7. L. H. Slaugh and J. H. Raley, J. Org. Chem. 32, 2861 (1967).
8. E. M. Kosower, An Introduction to Physical Organic Chemistry (John Wiley and Sons, Inc., New York, 1968), p. 27.
9. R. G. Lawler and G. K. Fraenkel, J. Chem. Phys. 49, 1126 (1968).
10. J. R. Bolton, A. Carrington, A. Forman, and L. E. Orgel, Mol. Phys. 5, 43 (1962).
11. A. Carrington and I. C. P. Smith, Mol. Phys. 9, 137 (1965).

12. M. Bersohn and J. C. Baird, An Introduction to Electron Paramagnetic Resonance (W. A. Benjamin, Inc., New York, 1966), p. 76.

13. R. M. Fuoss and F. Accascina, Electrolytic Conductance (Interscience Publishers, Inc., New York, 1959).

PROPOSITION 4

THE MECHANISM OF ENERGY TRANSFER IN CHLOROPHYLL-a MONOLAYERS

The chlorophyll-bearing grana in chloroplasts are known from electron microscopy studies to have a lamellar structure. If we compare the chlorophyll concentration in these grana with the available lamellar surface area, there appears to be just enough room to accommodate the chlorophyll molecules in a close-packed monomolecular layer.[1] This has led many workers to attempt to duplicate the *in vivo* environmental conditions of the chlorophyll molecules by studying their properties on artificially produced monomolecular layers.[2] The majority of the chlorophyll molecules in the grana are presumed to be involved in gathering light and transferring energy to the photosynthetic centers where the actual chemical processes occur.[3] The exact nature of the energy transfer process between monolayer chlorophyll molecules is thus of great importance for an overall understanding of photosynthesis.

Before the nature of the transfer process can be understood, one must first decide whether the transfer involves singlet or triplet electronic states. The possible involvement of triplet states in the energy transfer phase of photosynthesis has recently been discussed in some detail by Robinson.[4] Indirect experimental evidence[5] however seems to rule out triplet state energy transfer as an important part of the photosynthetic process. Therefore, with the reservation that triplet-triplet transfer has not as yet been completely *ruled out*, we

will assume in the remaining discussion that singlet excitation transfer is the dominant method by which light energy is conveyed to the photosynthetic reaction center.

There are three distinctly different ways that singlet energy can be transferred from a light gathering molecule (or donor) to an excitation trap (or acceptor) at the reaction center. The most commonly discussed method is known as Förster-type transfer or transfer by inductive resonance.[6] This process is essentially a one step dipole-dipole (or multipole-multipole) process between donor and acceptor. Another type of excitation transfer that is receiving an increasing amount of theoretical and experimental attention in connection with photosynthesis is excitonic transfer.[7] In this process from one point of view the excitation hops from donor to donor until it is finally trapped at an acceptor molecule. The excitation is thus undergoing a two dimensional random-walk.[8]

A third excitation process that can occur when the donor emission and acceptor absorption overlap is sometimes called trivial transfer. The acceptor molecules in this process merely absorb the donor emission. For the experiments discussed here the overlap between donor emission and acceptor absorption is small and the trivial process will consequently be ignored.

One can think of several ways of distinguishing between Förster and excitonic transfer. Excitonic transfer which occurs only when there is short range molecular order is characterized by polarization and Davydov splitting in absorption.[9] In this regard there is some evidence of <u>in vivo</u> polarized chlorophyll absorption although the

polarization is very slight and difficult to interpret.[10] Any Davydov splitting which might be present would probably be obscured by the broad linewidths in absorption.

Perhaps the best method for deciding between the two different types of transfer is to examine the donor emission characteristics in the presence of a suitable excitation trap. This method has been used extensively in investigations of energy transfer in three dimensional systems[11] but its use in studies of monolayer energy transfer has been limited.[12]

It is suggested that the emission properties of chlorophyll-a monolayers be investigated using bacteriochlorophyll as a low energy excitation trap. Bacteriochlorophyll has two properties which make it ideally suited for the suggested experiments. First its lowest singlet is about 4000 cm^{-1} lower in energy than the chlorophyll-a singlet.[13] Second, it differs from chlorophyll-a in chemical structure only by the replacement in the porphyrin part of the molecule of a $-CHCH_2$ group with a $-COCH_2$ group and the saturation of a double bond. One might thus reasonably expect bacteriochlorophyll to fit substitutionally into an ordered chlorophyll-a monolayer without disturbing the monolayer structure. This is important because one is interested in energy transfer in ordered chlorophyll-a monolayers not in monolayers which have been significantly disturbed by the presence of excitation traps.

Early work on the preparation and properties of chlorophyll monolayers has been reviewed by Ke.[2] The particular monolayer suggested for these experiments has recently been described by Sperling and Ke.[14] Basically it consists of a five layer barium arachidate

($n-C_{20}$ acid) smooth lipid background deposited on glass microscope slides. Chlorophyll layers are deposited by moving the glass slides through a liquid surface monolayer of chlorophyll under controlled surface pressure. The monolayers prepared in this way have the distinct advantage of being mechanically stable and thus not subject to the noise problems of monolayers on shimmering water surfaces.[12]

It is suggested that the fluorescence from these chlorophyll-a monolayers be then measured as a function of the bacteriochlorophyll concentration. If Förster type transfer is involved and the interaction energy is assumed to vary as $(1/R^{l})$ where R is the donor-acceptor distance and l is greater than 2 then the relative fluorescence yield η/η_0 may be written[15]

$$\frac{\eta}{\eta_0} = \frac{1}{\tau_0} \int_0^{\infty} \exp\left[-\frac{t}{\tau_0} - b\frac{c}{c_0}\left(\frac{t}{\tau_0}\right)^{2/l}\right] dt \quad . \tag{1}$$

Here η_0 is the fluorescence yield in the absence of trapping, $b = \Gamma(1 - 2/l)$, τ_0 is the donor fluorescence lifetime and c_0 is a constant related to the trapping efficiency. Alternatively one can measure the fluorescence decay curve after flash excitation. In this case the fluorescence intensity as a function of time may be represented as

$$I(t) = I_0 \exp\left[-\frac{t}{\tau_0} - b\frac{c}{c_0}\left(\frac{t}{\tau_0}\right)^{2/l}\right] \quad . \tag{2}$$

For excitonic energy transfer the interaction energy is independent of R and the expressions for η/η_0 and I(t) become

$$\frac{\eta}{\eta_0} = (1 + c/c_0)^{-1} \tag{3}$$

and

$$I(t) = I_0 \exp\left[- \frac{(1 + c/c_0)}{\tau_0} t \right] \quad . \tag{4}$$

Thus by determining both η/η_0 and I(t) experimentally one can distinguish between Förster and excitonic energy transfer. If Föster type transfer is involved, one can also determine the exact form of the interaction by fitting the experimental results to Eqs. (1) or (2) and in this way obtain 1 .

REFERENCES

1. J. B. Thomas, K. Minnaert, and P. F. Elbers, Acta Botan. Neerl. 5, 315 (1956).
2. B. Ke in The Chlorophylls (Ed: L. P. Vernon and G. R. Seely, Academic Press, New York, 1966), p. 253.
3. G. W. Robinson, Ann. Rev. Phys. Chem. 15, 311 (1964).
4. G. W. Robinson, Proc. Nat. Acad. Sci. 49, 521 (1963).
5. R. K. Clayton, Photochem. and Photobiol. 5, 807 (1966).
6. Th. Förster, Ann. Physik. 2, 55 (1948).
7. A. S. Davydov, Sov. Phys. -Usp. 7, 145 (1964).
8. E. W. Montrall, J. Math. Phys. 10, 753 (1969).
9. R. M. Hochstrasser and M. Kasha, Photochem. and Photobiol. 3, 317 (1964).
10. J. B. Thomas, J. H. van Lierop and M. Ten Ham, Biochim. et Biophys. Acta 143, 204 (1967); K. Sauer, E. A. Dratz, and L. Coyne, Proc. Nat. Acad. Sci. 61, 17 (1968).
11. R. G. Bennett and R. E. Kellogg, Photochem. and Photobiol. 7, 571 (1968); W. Klopffer, J. Chem. Phys. 50, 1689 (1969).
12. A. G. Tweet, G. L. Gaines, and W. D. Bellamy, J. Chem. Phys. 40, 2596 (1964); 41, 538 (1964); 41, 2069 (1964); T. Trosper, R. B. Park, and K. Sauer, Photochem. and Photobiol. 7, 451 (1968).
13. R. K. Clayton, Molecular Physics in Photosynthesis (Blaisdell Publishing Co., New York, 1965), p. 4.
14. W. Sperling and B. Ke, Photochem. and Photobiol. 5, 857 (1966).

15. Equations (1) and (2) have been modified for the two-dimensional case of interest here. The corresponding three-dimensional equations are given in M. Inokuti and F. Hirayama, J. Chem. Phys. 43, 1978 (1965).

PROPOSITION 5

FLUORESCENCE RISE TIMES OF EUROPIUM CHELATES IN THE NANOSECOND TIME RANGE

It has been known for quite some time that organic bidentate coordination complexes of europium, terbium and samarium exhibit emission characteristic of the rare-earth ions when excited into the π-system of the organic ligand.[1] Recently these complexes have been extensively investigated since it has been found that in solution they can be used as liquid lasers.[2,3] Despite extensive investigation, however, the exact nature of the transfer of energy from the organic ligand to the metal ion is still in some question. Two distinct mechanisms have been proposed. The energy may be transferred directly from the ligand singlet state to the rare-earth ion[4] or it may go directly[5] or indirectly[6] from ligand singlet to ligand triplet state and thence to the rare-earth ion levels. The bulk of the experimental evidence seems to indicate that the triplet state is the one that is involved in the ligand-ion transfer step although the singlet state has not been unequivocally ruled out. For example, Crosby et al.[5,7] found that rare-earth emission from a given chelate is observed only when "the lowest triplet state energy level of a complex [is] nearly equal to or . . . above the resonance energy level of the rare-earth ion." Crosby et al. interpreted this experimental result as proof that energy transfer occurs via the lowest triplet state to the rare-earth ion level. In this case the emission would be quenched by a lower lying ligand triplet. Other experimental investigations that tend to support ligand-ion energy transfer from the

triplet state, such as O_2 quenching[8] and EPR[9] experiments, are equally inconclusive.

Clearly more quantitative evidence is needed in order to determine the exact nature of the process that transfers energy from the organic ligand to the central rare-earth ion in these chelate complexes. Bhaumik and Nugent[10] have begun this quantitative investigation by examining the fluorescence rise and decay times of several europium chelates at 77° and 300° K in microcrystalline samples and from EPA and ethanol-methanol solutions. Eu^{+3} in these chelates has a $4f^6$ electronic configuration and the fluorescence transitions observed are $^5D_0 \rightarrow {}^7F_2$ (613 mμ) and $^5D_1 \rightarrow {}^7F_1$ (535 mμ). The energies of these transitions are not significantly affected by the detailed nature of the organic ligands. Bhaumik and Nugent investigated the fluorescence properties of seven different chelates. For clarity we will here discuss the results they obtained for only two of these complexes. All of the other chelates investigated behave in a manner qualitatively similar to the behavior of one or the other of these two complexes.

The europium chelates we will discuss are EuB_4HP (B = benzoylacetonate, P = piperidine) and $Eu(BP)_3 \cdot 2H_2O$ (BP = o-hydroxybenzophenone). The ligand triplet level of EuB_4HP lies above both the $^5D_0$ and $^5D_1$ levels of the rare-earth ion. Emission from both levels was observed as expected and decay times were measured for both transitions. However, the rise time of the $^5D_1 \rightarrow {}^7F_1$ transition was faster than the .2 μsec minimum time resolution of the experiment. $Eu(BP)_3 \cdot 2H_2O$ on the other hand has its ligand triplet level between the $^5D_0$ and $^5D_1$ ion levels. In this case only the low energy

$^5D_0 \rightarrow {}^7F_2$ transition is observed and its rise time is too fast to be measured with the apparatus used by Bhaumik and Nugent. Note that in both cases the rise time of the rare-earth transition that is directly involved in the ligand-ion energy transfer process is too rapid to be detected by these experiments. This is indeed unfortunate since it is the ligand-ion process that we hope to illucidate in these investigations.

It is proposed that the work of Bhaumik and Nugent[10] be extended into the nanosecond region using the technique of pulse fluorometry.[11] In this technique a repetitively pulsed hydrogen flash lamp is used to excite the organic rare-earth chelate. The fluorescence emission is then converted into an electric pulse using a high gain, small transit time spread photomultiplier. Each pulse is then sampled sequentially by a sampling oscilloscope. The pulse height from the oscilloscope is next converted to digital form and stored in a multichannel analyzer. Two separate measurements are made, one with the sample in place and the other without the sample. With the sample in place the curve is shifted in position and the pulse shape is modified according to the value of the fluorescence decay constant. The fluorescence decay curve is then synthesized by means of a convolution integral from the two experimental curves.[12] Systems of this type have resolutions of less than a nanosecond.[11] These systems have the added advantage of allowing analysis of the decay curves without any assumptions as to the particular mathematical form of the curves. This is not true, for example, of phase fluorometry techniques.[11]

Measurements of the fluorescence rise times of various rare-earth chelates by the method described above can be used to investigate

the organic ligand-rare-earth ion energy transfer process. The observed transfer rates can also be compared with theoretical calculations of the rates.[13] In addition the experimental energy transfer rates can be used to suggest ways of reducing the pumping power needed to make rare-earth chelates lase.[14]

REFERENCES

1. S. I. Weissman, J. Chem. Phys. 10, 214 (1942).
2. G. A. Crosby, Mol. Cryst. 1, 37 (1966).
3. L. D. Derkacheva, G. V. Peregudov, and A. I. Sokolovskaya, Sov. Phys.-Usp. 10, 91 (1967).
4. M. Kleinerman, Bull. Am. Phys. Soc. 9, 265 (1964).
5. G. A. Crosby, R. E. Whan, and R. M. Alire, J. Chem. Phys. 34, 743 (1964).
6. M. L. Bhaumik and M. A. El-Sayed, J. Chem. Phys. 42, 787 (1965).
7. G. A. Crosby and R. E. Whan, J. Chem. Phys. 32, 614 (1960); Naturwiss. 47, 276 (1960).
8. V. L. Ermolaev, E. B. Sveshnikova, and E. A. Saenko, Opt. and Spec. 22, 86 (1967).
9. R. F. Riley and J. Rosenthal, Spec. Letters 1, 391 (1968).
10. M. L. Bhaumik and L. J. Nugent, J. Chem. Phys. 43, 1681 (1965).
11. I. B. Berlman, Handbook of Fluorescence Spectra of Aromatic Molecules (Academis Press, New York, 1965), p. 25; I. H. Munro in Luminescence in Chemistry (Ed: E. J. Bowen, D. Van Nostrand Co., Ltd. London, 1968), p. 16.
12. I. H. Munro and I. A. Ramsay, J. Phys. E 1, 147 (1968).
13. V. L. Ermolaev, E. A. Saenko, G. A. Domrachev, Yu. K. Khudenskii, and V. G. Aleshin, Opt. and Spec. 22, 466 (1967).
14. A. Yariv, Quantum Electronics (John Wiley and Sons, Inc., New York, 1968), Ch. 15.